Atomic Force Microscopy to evaluate the effect of concentration and reciprocal position on ZDDP tribofilm topography and an assessment of its ability to determine tribofilm durability

Rachel Frances Bingley Cunningham

Submitted in accordance with the requirements
for the degree of Doctor of Philosophy

The University of Leeds

Institute of Functional Surfaces

School of Mechanical Engineering

Faculty of Engineering

June 2020

The candidate confirms that the work submitted is her own and that appropriate credit has been given where reference has been made to the work of others.

Acknowledgements

During my research I have received support and input from numerous places. I would like to take the opportunity to thank some of these people now.

Firstly, I would like to thank Prof. Anne Neville, for guiding me through what was sometimes a confusing transition to tribological research. I am aware that I was often difficult to wrangle, and I appreciate the determined effort with which you kept me on track.

I would also like to thank my other supervisors, Prof. A. Morina and Dr. C. Wang, both of whom challenged and engaged me, even when the research seemed to be making no real progress.

I'd like to thank the entire CDT community, my friends at the university, and particularly Kimberley Matthews, who absorbed a number of the administrative headaches which usually eat up researchers' time, allowing me to make progress. Thank you, Kim!

My thanks also go to my colleagues at ESR Technology, whose support and encouragement enabled me to face the final uphill battle to completion.

Thank you to my parents, sister and all our family. You have tried hard to keep me sane, and managed to convince me that throwing the towel in was not an acceptable response to extreme stress, and that I wouldn't be able to live with myself if I didn't complete the "darn book". You were, as usual, completely right.

Last, but definitely not least, I would like to thank my wonderful husband, Oscar, for his ongoing and unfailing support. He has kept me going, particularly when the going got extremely tough, and he never let me face the terror of the write up alone. He was by my side; feeding me, keeping me in clean clothes, comforting me in moments of extreme self-doubt, acting as a sounding board (particularly when de-bugging annoying MATLAB codes!) and generally keeping our lives moving whilst I panicked my way to the end of the road. Without you this PhD would not have happened. Thank you Darling!

Abstract

ZDDP has been used in most vehicles since the early 1950s; however, it has been proven to reduce the efficiency of catalytic converters. The incoming Euro 6 legislation introduces a stricter restriction on harmful emissions, increasing the importance of achieving maximum efficiency from catalytic converters. Therefore, it is necessary to remove ZDDP from cars. However, ZDDP is an effective anti-wear additive, without which modern cars, with tight design tolerances, are unable to function. Previous work has shown that the morphology of ZDDP tribofilms can relate to their anti-wear efficacy; however, no previous work has undertaken a robust characterisation, considering both the topography and durability, of ZDDP tribofilms.

This research activity has shown that the concentration of ZDDP within a base oil affects the resultant pad topography in the tribofilm, with higher concentrations resulting in smaller but more evenly distributed pads. It has also shown that for lower concentrations the position along a reciprocating stroke influences the topography, with regions that experience lower lambda ratios displaying topography similar to that seen for higher concentrations. This effect is understood to occur as a result of increased shearing of the ZDDP resulting in the adherence of more, but shorter, polyphosphate chains to the surface and a hypothesis for how this occurs is presented.

This thesis also demonstrates the potential of AFM for use in assessing the durability of ZDDP tribofilms. It has been shown that the AFM can be used to conduct a semi-quantitative assessment, with the potential for further improvements to be developed. It has also been shown that there can be an effect of the ZDDP concentration used to form a ZDDP tribofilm on its durability. The upper layer of the ZDDP tribofilm can be easily manipulated by the AFM tip, and two hypotheses are presented to explain this phenomenon.

Table of Contents

Table of Figures

Table of Tables

List of Abbreviations

AFM	Atomic Force Microscope/Microscopy
DDP	DialkylDithioPhosphate
DLC	Diamond Like Carbon
EDS	Energy-Dispersive X-ray Spectroscopy
EDTA	EthyleneDiamineTetraAcetic acid
GPS	Geometrical Product Specifications
HFRR	High Frequency Reciprocating Rig
IFM	Interfacial Force Microscopy
ISO	International Organisation for Standardisation
MODTC	Molybdenum DialkyldiThioCarbamate
MTM	Mini Traction Machine
NO	Nitrous Oxide
PAO	PolyAlphaOlefin
SEM	Scanning Electron Microscope
SLIM	Spacer Layer Imaging Method
SPM	Scanning Probe Microscopy
TCP	Tricresyl Phosphate
XPS	X-ray Photoelectron Spectroscopy
ZDDP	Zinc DialkylDithioPhosphate
ZDTP	Zinc DialkyldiThioPhosphate

Chapter 1: Introduction

1.1 Rationale for Research

One of the most prominent challenges currently facing the automotive industry is compliance with the Euro 6 emissions legislation [1,2]. Compliance requires a drastic reduction in the emissions released from internal combustion engines [1]. The need to reduce emissions necessitates an improvement in the efficiency of catalytic converters, that remove the harmful chemicals from exhaust fumes, that are the undesirable constituents in such emissions [1]. Unfortunately, catalytic converters are effectively poisoned by the presence of phosphorus and sulphur within the engine. Phosphorus and sulphur are present as by-products created by the decomposition of an essential additive within most engine oil formulations, Zinc DialkylDithioPhosphate (ZDDP) [3].

Oil additives have been essential in improving engine efficiency, with additives being used to modify friction, reduce wear and prevent surface oxidation, amongst many other functions. The additives that have been developed to modify friction (most commonly the additive Molybdenum DialkyldiThioCarbamate, (MoDTC)) have been tailored to reduce the surface friction between sliding components. Others, such as ZDDP, have been specifically used to reduce the surface wear [4].

ZDDP can be found in most of the engine oil formulations currently in use in the majority of commercially available passenger cars [4]. It was developed in the 1950s for use as an anti-oxidative additive, to protect the steel surfaces within the engine from chemical degradation; however, it was rapidly discovered that the additive was also effective at reducing wear [5]. Over the past fifty years the success of ZDDP as an antiwear additive has resulted in reductions in tolerances within engines, such that the friction experienced in the absence of ZDDP is believed to result in catastrophic seizure [5]. The additive is decomposed during the shearing motion within the contact (such as the sliding motion between a piston

and a piston ring) and the decomposed molecules then chemisorb onto the exposed surfaces [4]. The chemisorbed molecules form a protective layer, referred to as a tribofilm. The tribofilm is formed of pads (which appear as hills on a landscape) that distribute the applied load, such that the contact pressure is reduced, and they can be worn sacrificially. The pads are formed of different chemical layers, which can slide relative to each other, in-situ, and are generally understood to be solid in structure [5].

In order to comply with the incoming Euro 6 legislation, it has become necessary to remove ZDDP from engines [1]. Unfortunately, as the efficacy of ZDDP as an anti-wear additive was discovered accidently identifying a replacement is difficult. Therefore, how ZDDP works, particularly how it forms tribofilms, has been focus of extensive research. Previous research avenues have included a focus on understanding the effect of ZDDP tribofilms on friction and considering the effect of contaminants or conditions on the effectiveness of the tribofilm at reducing wear [5,6]. However, work conducted by Gosvami et al [3,7], has utilised an Atomic Force Microscope (AFM, which is also the abbreviation for Atomic Force Microscopy) to generate and analyse ZDDP tribofilms in-situ. AFM has previously been used to analyse the topography of ZDDP tribofilms; however, this has typically been a secondary analysis, with single images included in academic papers as a “representative” topography [8].

The novel use of the AFM, in 2015 [3], showed that as a technique AFM can be used to do much more than just provide comparisons in topography, with ongoing research expanding its use as a nano-tribometer. In addition to expanding the techniques used in tribological research the major 2015 paper by Gosvami et al [3] introduced questions regarding the uniformity of tribofilms. They showed that in a reciprocating tribometer the tribofilm thickness is dependent on position within the stroke, with the current research considering whether such a position dependence is also present in macro-scale tribofilms. An increased understanding of the nature of ZDDP tribofilms will aid researchers in

determining appropriate replacement additives, that will enable compliance with emissions legislation.

An improved understanding of the durability of ZDDP tribofilms would enable researchers to better comprehend their sacrificial nature [5]. This would increase the likelihood of identifying, or synthesising, a non-phosphorus based additive to replace ZDDP. Work, in 2019, by Professor Spikes has shown that there is an increased interest it quantifying the durability of such tribofilms and has suggested that this might be linked to crystallinity [9].

1.2 Aims and Objectives

The current research is biphasic. Phase 1 aims to use the atomic force microscope to assess whether there is a difference in tribofilm topography as a result of a non-uniform lambda ratio across a wear track length. Phase 2 aims to consider whether the atomic force microscope can be used to manipulate an existing tribofilm, and to characterise any differences in the durability of tribofilms formed from different concentrations of oil additive.

1.2.1 Phase 1

The first phase of the research investigates whether the morphology of a ZDDP tribofilm is influenced by the specific lambda ratio in the area of generation. In addition, phase 1 compares the morphology of tribofilms generated from different concentrations of ZDDP and determines whether there is a resultant difference in the anti-wear properties.

Objectives:

- To generate tribofilms formed from three different concentrations of ZDDP, as recommended by an industrial advisor (Akzo Nobel).
- To utilise the atomic force microscope to characterise the morphology of these ZDDP tribofilms, at different locations along the length of the wear scar.
- To conduct a comparison between different morphologies, such as between the topography towards the end of the stroke in a lower concentration tribofilm and the topography towards the middle of the stroke in a higher concentration tribofilm.
- To explore the use of the atomic force microscope to determine the extent to which the surface has been worn, for each concentration and at each location.

- To understand whether there is a difference in either the tribofilm topography or the efficacy of the additive to protect against wear as a result of the location.

1.2.2 Phase 2

The second phase of the research consists of the development of a method which uses the atomic force microscope to investigate the durability of a ZDDP tribofilm. As well as manipulating the tribofilm, the method needs to permit the in-situ analysis of any resultant deformation of the pad structure, whilst producing high quality semi-quantitative image-based results.

Objectives:

- To define a method by which ZDDP tribofilm pads could be manipulated and any resultant deformations could be assessed, using a commercially available AFM.
- To develop and implement an analysis technique to quantify any resultant deformation of the tribofilm
- To assess whether the concentration of additive in the original oil has any influence on the extent of deformation of the tribofilm.
- To investigate whether the load applied by the AFM tip influences the behaviour of any such deformation.
- To attempt a comparison between the volume of removed material and the predicted wear, using Archard's Wear Law.

1.3 Report Outline

This report will have nine primary sections, these are ordered below.

2. **Fundamentals of Tribology**

   This section introduces the subject of tribology, including details of friction, lubrication and wear mechanisms.

3. **Surface Parameters**

   This section introduces different surface parameters, and gives definitions, for use in understanding AFM scans.

4. **Literature Review of ZDDP**

   This section details previously conducted research into ZDDP and tribofilms.

5. **Literature Review of Atomic Force Microscopy**

   This section details analyses previously conducted using an AFM, across different disciplines.

6. **Characterisation of ZDDP Tribofilms**

   This section details the test activity conducted to determine whether there were any differences between ZDDP tribofilms formed in oils with differing concentrations of ZDDP.

7. **Durability of ZDDP tribofilms**

   This section details the test activity conducted to determine whether the AFM could be used to manipulate pre-existing ZDDP tribofilms.

8. **Conclusions, Impact to industry and Future works**

   This section summarises the key findings of the research activity, its significance and details possible avenues of future research.

Chapter 2: Fundamentals of Tribology

2.1 What is Tribology?

Tribology is the "science and technology of interacting surfaces in relative motion and of related subjects and practices" [10]. The topic was first identified as a discipline and defined in 1966 in what is colloquially referred to as the "Jost report" [11]. The "Jost report" was the outcome of a government sponsored meeting between a collection of researchers and industrial engineers. This collection were able to determine that a better understanding of tribology as it related to engine and bearing design would save developing countries approximately 1.4% Gross Domestic Product [12]. Tribology is a multi-disciplinary subject, with significance and overlap with many other aspects of science and engineering.

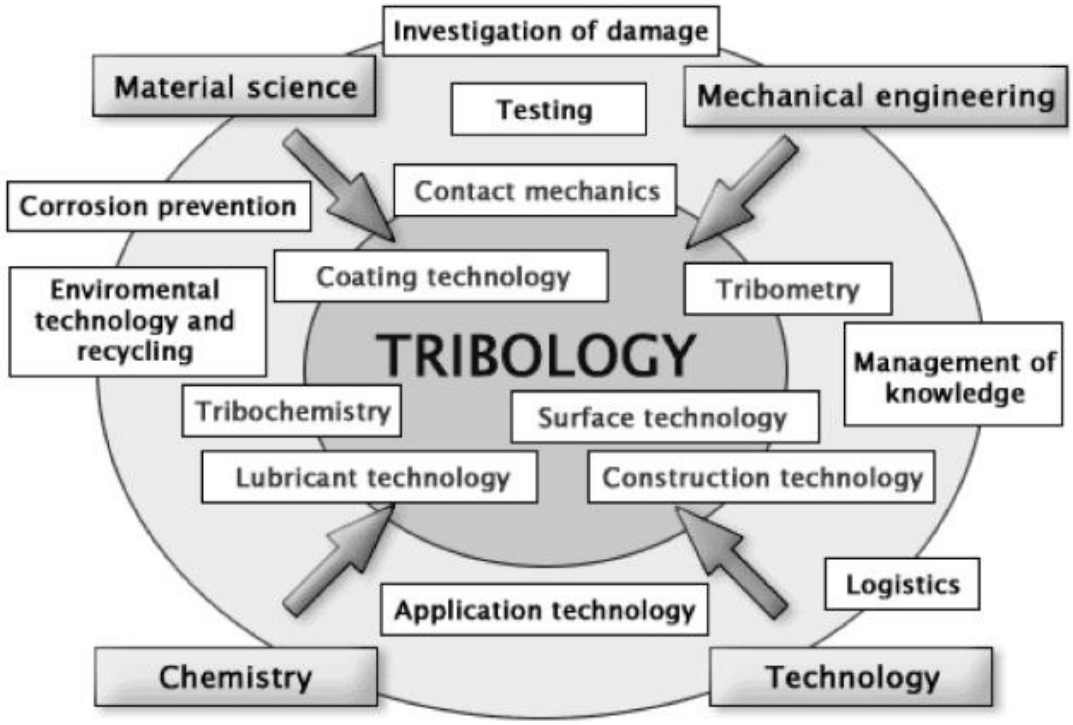

Figure 2-1: How tribology interacts with other sciences [13]***.***

Tribology is best understood through its primary components of friction, lubrication and wear.

2.2 The Mechanics of Friction

Friction is defined as "the resistance to relative motion of contacting bodies" [14]. There are three basic methods by which dry friction occurs. These are adhesion, ploughing and the synergistic effect of both. Friction can also occur when surfaces are fully separated by a fluid film, as a result of the viscous properties of the lubricant.

2.2.1 Adhesion

The simple model of adhesion is most commonly credited to the work of Bowden and Tabor [15,16]. Adhesion is the theory that asperities from contacting surfaces plastically adhere to each other at the tips and thus prevent the surfaces moving relative to one another. The adhesion theory is explained, at its simplest, in the following diagram, Figure 2-2.

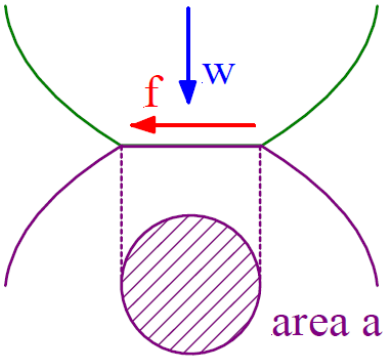

Figure 2-2: Adhesive asperity contact [15]**.**

In the above schematic the load applied to the interface, via the top asperity, is denoted as w; the frictional force applied, via the motion, is denoted by f and the actual contact surface area is denoted by a. This phenomenon occurs across the interface until the surface area has been increased and an equilibrium achieved, such that the interface is capable of supporting the load in an elastic way. Adhesion theory is governed by the following sets of equations where p_o is the material yield pressure, s_o is the shear stress, w is the total normal applied load, f is the total friction force and μ is the coefficient of friction [15,17].

$$\boldsymbol{w = p_o a}$$ ***(Equation 1)*** [15]

This represents the applied load as a function of the contact area using the material yield pressure.

$$\boldsymbol{f = s_o a}$$ ***(Equation 2)*** [15]

Bowden and Tabor [17] theorised that the asperity contacts suffered from strong adhesion resulting in the cold welding of the junctions. The above equation was predicted to show the friction force on an asperity during motion, it relies on the shear stress required to separate the adhered junction as well as the contact area.

These basic equations are then used to find the total normal applied load (W) and the total friction force (F):

$$\boldsymbol{W = \sum p_o a}$$ ***(Equation 3)*** [15]

$$\boldsymbol{F = \sum s_o a}$$ ***(Equation 4)*** [15]

Assuming that the shear stress and yield pressure are properties of the material, and hence do not vary between asperities, we can determine the coefficient of friction is:

$$\boldsymbol{\mu = \frac{s_o}{p_o}}$$ ***(Equation 5)*** [15]

In most materials the yield pressure is approximately the Vickers hardness and so these are often substituted. For metals the coefficient of friction calculated via this method is 0.17, which is not the same as the experimental results seen by Leonardo da Vinci (0.25) or Amontons (0.33) [15,18]; therefore, this cannot be the only mechanism.

As stated above adhesion is a fundamental concept of friction as few scenarios are governed solely by material. Friction is environmentally dependent with the specific mechanism driving the effect. Other parameters which affect friction include speed, temperature and energy distribution [19].

2.2.2 Ploughing

As the name suggests this theory of friction is simply that the resistance to motion experienced during sliding is due to a harder surface penetrating the opposing softer surface and "ploughing out a grove" [20]. As with the description of adhesion a simplistic diagram can be used to represent the fundamental concept.

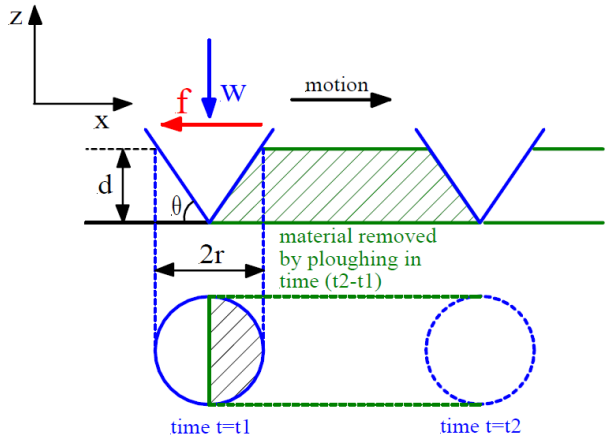

Figure 2-3: A schematic representation of a ploughing contact [15]***.***

Figure 2-3, explains that a hard asperity, with a side inclination angle of θ, that has penetrated a depth, d, into the opposing surface and has created an indentation with diameter $2r$, will plough out a section of the opposing surface when initiated to slide against a counterface. This mechanism is similar to adhesion, in that it does not fully explain the experimental results, further confirming that a synergy between ploughing and adhesion typically exists, dependent on the larger mechanism [15].

2.3 Wear

Wear is the removal of material from a surface during relative motion between two contacts. This wear occurs through five primary mechanisms, which will be expanded on in this section. These mechanisms are; adhesive wear, abrasive wear, erosive wear, corrosive wear and fatigue wear [19].

2.3.1 Adhesive

Adhesive wear occurs when asperities from opposing surfaces undergo cold welding. This results in a single, joined asperity, similar to adhesion in friction; however, instead of them separating at the junction they separate elsewhere, effectively wearing one surface. Adhesive wear is believed to be the most likely and least preventable form of wear [21].

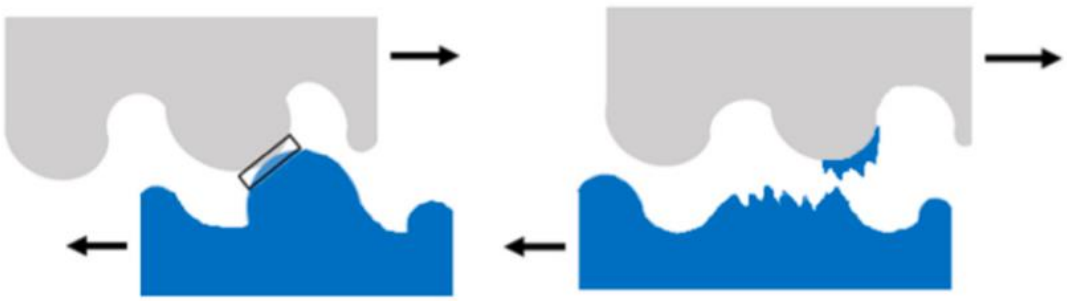

Figure 2-4: Adhesive wear.

2.3.2 Abrasive

Abrasive wear is similar to ploughing, in that one surface penetrates the other. The material is ploughed out and typically congregates at the end of the ploughed section, or along the banks of the gulley. Abrasive wear can also occur as a result of wear particles abrading (ploughing) the surface. This is referred to as third body abrasion and can be an escalating phenomenon, i.e. the more wear there is, the more particles that interact in the contact and thus the more abrasive wear that occurs [21]. Third-body abrasion can occur as a result of a hard particle becoming embedded into one substrate and then damaging the counterface, or as a result of wear debris being contained within the contact and abrading both surfaces equally [21].

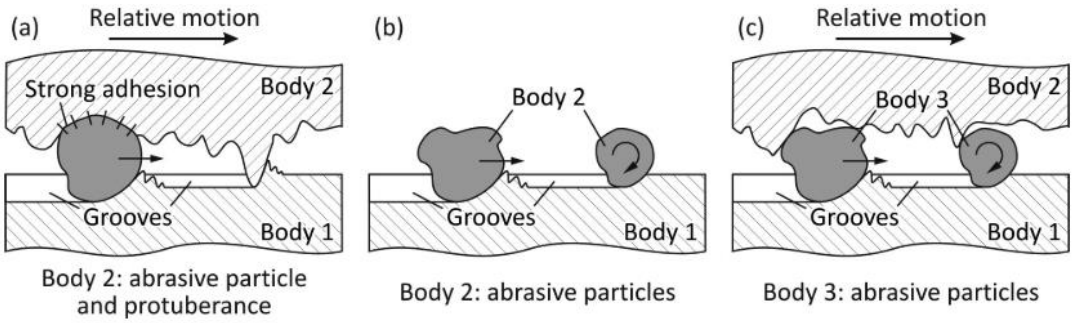

Figure 2-5: Abrasive wear processes (a), (b) two-body abrasion, (c) third-body abrasion [22]**.**

2.3.3 Erosive

Erosion is generally considered as the wear of one surface by the repeat impingement of a particle carried by a fluid. For more ductile surfaces this can induce fatigue wear, whereas for more brittle surfaces it can cause surface cracks, which can then propagate into the surface to form a wear particle. There are three additional methods of erosion, fluid erosion, cavitation erosion and spark erosion. Fluid erosion occurs when instead of a solid particle it is a micro-droplet of water, moving at extreme speeds, which impinges upon the surface. Cavitation erosion occurs when a vapour bubble within the fluid implodes, due to increased pressure, in close proximity to the surface. Spark erosion occurs when a small electrical charge is generated between two surfaces, resulting in material decomposition [15,21].

2.3.4 Corrosive

Corrosion is when a surface is worn as a result of chemical interactions. A common example of corrosive wear is “rust”, the formation of brittle iron oxide on steel surfaces. This reaction alters the material properties of the surface making it more susceptible to other forms of wear. Corrosion will stabilise and the reaction rate will reduce if motion (rubbing) ceases as the reaction product becomes thick enough to act as a protective layer, stopping the lower layers of the surface from being exposed to the corrosive chemical [14,15].

2.3.5 Fatigue

Fatigue wear occurs when a part is cyclically loaded past a specific point of failure. This is often caused (or at least precipitated) by micro-cracks and increased porosity on the surface. Fatigue wear is particularly prevalent in scenarios where the surfaces have low conformity, as this results in the maximum shear stress being experienced below the surface (assuming a friction coefficient of less than 0.27), which can cause unseen flaws (such as micro-cracks). Once these flaws exist, the recurring high contact pressures can induce crack propagation within the substrate, until such time as multiple cracks join and breach the surface. At this point the newly formed wear particle is often moved away as part of the motion [15].

2.3.6 Archard's Wear Law

There exists a formula to determine the volume of wear, V, that may occur within a contact. This formula is often referred to as the Archard's wear law and includes a dimensionless parameter, k, which is the wear coefficient. To predict the amount of wear it is necessary to first know the sliding distance, x, the maximum contact pressure, P_0, and the total normal load W [15].

$$\boldsymbol{V = k\frac{Wx}{3P_o}} \qquad \textit{(Equation 6)} \text{ [15]}$$

The dimensionless wear coefficient can depend on many factors. These include the surface material mechanical properties, such as the yield strength, and the material structure, for example a granular or lamellar structure. The adhesion between the asperities will also be considerable; however, the friction and wear volume are not always linked [15].

2.4 Hertzian Contact Mechanics

Hertzian contact mechanics is a simplistic model to determine the contact geometries and maximum contact pressures experienced in a contact. Assuming a contact between two surfaces each with a rounded surface (i.e. two balls) the following contact mechanics can be utilised. If one of the surfaces is a flat plane then the same equations can be applied; however, the radius for the plane can be considered to be infinite [14,21].

Initially it is necessary to calculate the summated radius of curvature, R. This is completed using the following equations, where the parameters r_{Ax} and r_{By} (etc.) are determined as shown in Figure 2-6 [15].

$$\frac{1}{R_x} = \frac{1}{r_{Ax}} + \frac{1}{r_{Bx}} \qquad \textit{(Equation 7)} \text{ [23]}$$

$$\frac{1}{R_y} = \frac{1}{r_{Ay}} + \frac{1}{r_{By}} \qquad \textit{(Equation 8)} \text{ [23]}$$

$$\frac{1}{R} = \frac{1}{R_x} + \frac{1}{R_y} \qquad \textit{(Equation 9)} \text{ [23]}$$

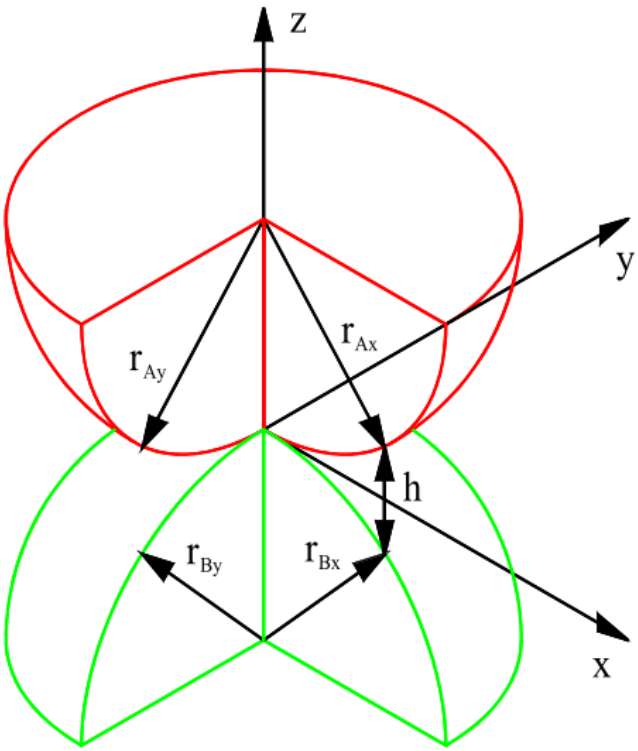

Figure 2-6:A schematic to show the radii in a ball on ball contact [15]**.**

In order to determine the maximum contact pressure, it is necessary to calculate the exact contact geometry, referred to in terms of the semi-major (a) and semi-minor (b) axes of the ellipsoidal shape. In order to determine a and b, one must determine: the load (W), the summed radius (R), the equivalent modulus (E') and the ellipticity ratio (k). The summed radius (R) has previously been calculated (in Equation 9). It is also possible to calculate the deformation in the contact (Equation 16) [15].

The ellipticity ratio (k) is calculated thus:

$$\boldsymbol{k = 1.0339\left(\frac{R_x}{R_y}\right)^{0.6360}} \quad \textbf{\textit{(Equation 10)}} \text{ [24]}$$

The equivalent modulus is calculated:

$$\boldsymbol{\frac{1}{E'} = \frac{1}{2}\left(\frac{1-\nu_a{}^2}{E_a} + \frac{1-\nu_b{}^2}{E_b}\right)} \quad \textbf{\textit{(Equation 11)}} \text{ [23,24]}$$

The first and second complete elliptic integrals are defined as:

$$\boldsymbol{\psi = 1.5277 + 0.6023\, ln\left(\frac{R_x}{R_y}\right)} \quad \textbf{\textit{(Equation 12)}} \text{ [24]}$$

$$\boldsymbol{\xi = 1.0003 + \frac{0.5968}{\frac{R_x}{R_y}}} \quad \textbf{\textit{(Equation 13)}} \text{ [24]}$$

These can then be used to calculate a and b:

$$\boldsymbol{a = \left(\frac{6k^2\xi WR}{\pi E'}\right)^{\frac{1}{3}}} \quad \textbf{\textit{(Equation 14)}} \text{ [24]}$$

$$\boldsymbol{b = \left(\frac{6\xi WR}{\pi kE'}\right)^{\frac{1}{3}}} \quad \textbf{\textit{(Equation 15)}}\text{[24]}$$

The deformation at the centre of the contact is:

$$\boldsymbol{\delta = \psi\left[\left(\frac{9}{2\xi R}\right)\left(\frac{W}{\pi kE'}\right)^2\right]^{\frac{1}{3}}} \quad \textbf{\textit{(Equation 16)}}\text{[24]}$$

The maximum Hertzian contact pressure is:

$$\boldsymbol{Pmax = \frac{3W}{2\pi ab}} \quad \textbf{\textit{(Equation 17)}}\text{[24]}$$

2.5 Lubrication

Lubrication is the addition of a tertiary substance (often a liquid) into a contact to reduce the friction, wear or commonly both. The most common automotive lubricants are mineral oils, usually blended with various additives which improve the effectiveness in controlling specific phenomena. In tribology there are four classifications for lubrication, these correspond to four surface separation regimes. These lubrication regimes are; elastohydrodynamic, hydrodynamic, boundary and mixed [19].

- Elastohydrodynamic lubrication is when low conformity in a contact results in high contact pressure, which causes local elastic deformation of the surface (into a more favourable conformity) and the fluid lubricant experiences an increase in viscosity [21].
- Hydrodynamic lubrication is when the surfaces are completely separated, such that there is no (or negligible) asperity contact, due to a sufficiently full lubricant film [21].
- Boundary lubrication is when the surfaces are barely separated, such that there is considerable asperity contact, due to a very sparse lubricant film [21].
- Mixed lubrication is often-considered the primary regime, with most mechanisms operating in this regime at some stage, as it covers the substantial gap between the extremes of hydrodynamic lubrication and boundary lubrication. Mixed lubrication is a regime with both areas which are well lubricated (acting in hydrodynamic lubrication) and areas which are poorly lubricated (acting in boundary lubrication) [21].

2.5.1 Lambda Ratio and Stribeck Curves

The mathematical means of determining which regime a component will operate in, for specific conditions, is termed the lambda ratio. This is the function which combines

minimum film thickness and surface roughness. If the lambda ratio is less than one it can be assumed that the system is entirely in boundary lubrication, if the lambda ratio is greater than or equal to one, or is less than three the system is likely to operate in mixed lubrication and if the lambda ratio is equal to or greater that three the system can be assumed to be in hydrodynamic lubrication [20].

The lambda ratio, in the viscous-elastic regime, is calculated thusly:

$$\boldsymbol{\lambda = \frac{h_{min}}{R_a}} \qquad \textit{(Equation 18)} \text{ [25]}$$

$$\boldsymbol{h_{min} = 3.63U^{0.68}G^{0.49}W^{-0.073}(1 - e^{-0.68k})} \qquad \textit{(Equation 19)} \text{ [26]}$$

$$\boldsymbol{R_a = \left({R_{a1}}^2 + {R_{a2}}^2\right)^{\frac{1}{2}}} \qquad \textit{(Equation 20)} \text{ [25]}$$

$$\boldsymbol{U = \frac{\eta u}{E\prime R_x}} \qquad \textit{(Equation 21)} \text{ [26]}$$

$$\boldsymbol{W = \frac{F}{E\prime {R_x}^2}} \qquad \textit{(Equation 22)} \text{ [26]}$$

$$\boldsymbol{G = \alpha E'} \qquad \textit{(Equation 23)} \text{ [26]}$$

Where the equivalent modulus (E') is calculated as in equation 11 and the summed radius of curvature (R) is calculated as in equation 9. The values denoted as U, W and G are dimensionless parameters, these are used in several equations to calculate the minimum film thickness, the value calculated using equation 19 is specifically for determining the film thickness when the fluid is in the viscous-elastic regime [26]. The value denoted as U is the dimensionless speed equation, this is calculated from u, the linear velocity; η, the viscosity; E' and R_x. The value denoted as W is the dimensionless load parameter which is calculated using: F, the applied force; E' and R_x. The value denoted as G is the dimensionless material parameter, which is calculated using α, the pressure-viscosity coefficient and E'. The pressure-viscosity coefficient is an additional property, this is distinct from the viscosity.

Equation 19 has been used extensively in tribology, particularly as applies to the TE77 and was confirmed as the correct equation for use by Professor Duncan Dowson, who conducted the initial experiments to determine the exponents used in this equation [26].

The lambda ratio also corresponds to the Stribeck diagram, a pictorial means of determining the lubrication regime. Stribeck diagrams connect the coefficient of friction with the minimum film thickness (h_{min}), as shown in Figure 2-7 [27].

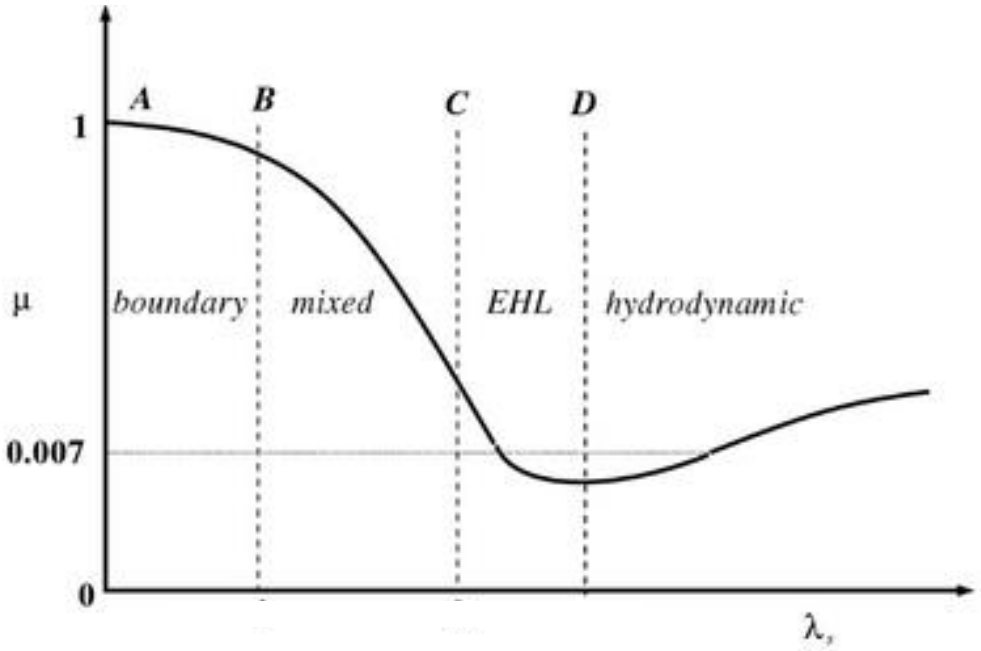

Figure 2-7: A Stribeck curve (not to scale) with the different lubrication regimes marked on it [23]**.**

2.5.2 Boundary Lubrication

As has been stated above, boundary lubrication occurs when there is very little lubricating film as to allow substantial asperity contact and the principles of dry friction apply, this is represented in the schematic in Figure 2-8. In boundary lubrication the properties of a bulk fluid lubricant do not govern the interaction and the behaviour is essentially independent of viscosity [21].

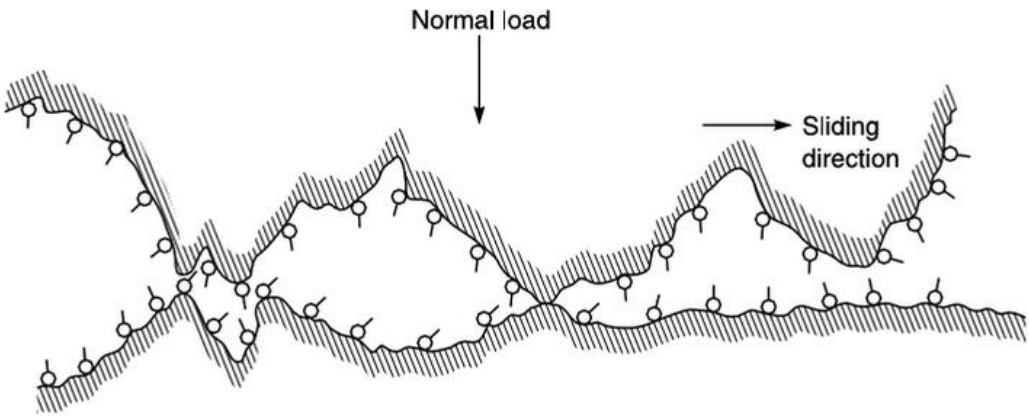

Figure 2-8: A schematic to show asperity contact during boundary lubrication [21]***.***

Due to the asperity-asperity contact in this regime the molecular interactions become more important. Molecules from a fluid lubricant (shown in Figure 2-8 as attached to the surfaces) can become chemisorbed onto the surface and form a boundary layer. The components of this layer are dependent on any additives included in the lubricant. In tribology this chemisorbed layer is referred to as a tribofilm [21]. Boundary lubrication often occurs as result of decreased tolerances between moving surfaces, for example between the piston and a piston ring, in such situations the components are unable to sufficiently separate precluding the existence of hydrodynamic or mixed lubrication [28].

2.5.3 Mixed Lubrication

Mixed lubrication is potentially the most common form of lubrication within an engine. It encompasses all lubrication regimes which do not result in complete separation of the surfaces (as in hydrodynamic lubrication) nor which abide by the rules of dry friction (as in boundary lubrication). This means that there are some sections with extensive asperity-asperity contact (and the formation of chemisorbed layers) and others where there is sufficient fluid film lubrication as to permit lubrication on the bulk fluid level, Figure 2-9. Most components will operate in this regime, at some point in their life span [21].

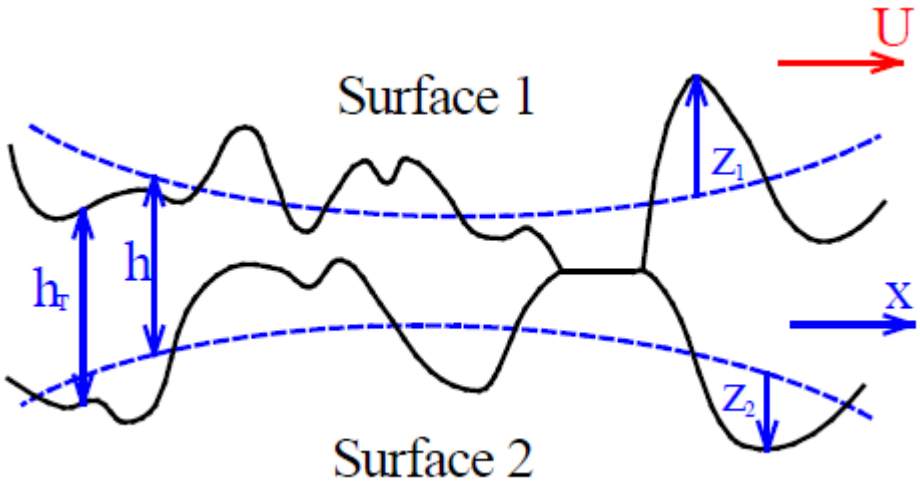

Figure 2-9: Schematic to represent a potential mixed lubrication scenario. Z indicates the difference between the surface geometry and the nominal radius of curvature, h represents the separation between the nominal radii of curvature and h_r indicates a complete separation of the surfaces [27]***.***

The amount of hydrodynamic lubrication versus boundary lubrication within a contact is a result of the magnitude of the film thickness and the roughness of the two surfaces (the lambda ratio). In mixed lubrication both the physical properties (such as viscosity) and the chemical properties (such as the presence of elements which can chemisorb) are important [19].

2.5.4 Elastohydrodynamic Lubrication

In some low conformity applications (such as rolling element bearings) the effects of hydrodynamic lubrication can persist into the region when boundary lubrication should occur. This is caused by local elastic deformation of the contacting surfaces and a substantial viscosity increase. These phenomena occur as a result of the high contact pressures which such applications experience. In this lubrication regime the shape of the surface is favourably altered (to reduce the prominence of asperities, Figure 2-10) and the physical properties of the lubricant are enhanced (for example, in a gear the viscosity may rise to several thousand times the typical atmospheric value) [27].

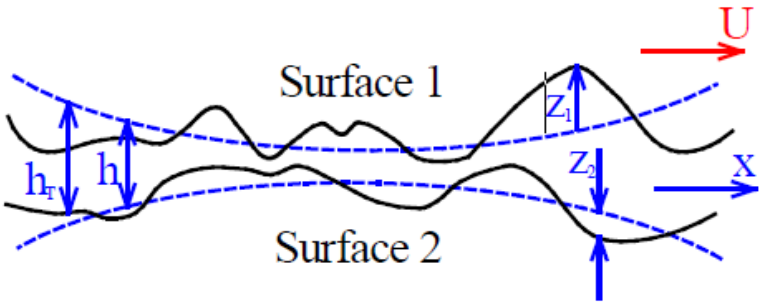

Figure 2-10: Schematic to represent a hydrodynamic lubrication scenario. Z indicates the difference between the surface geometry and the nominal radius of curvature, h represents the separation between the nominal radii of curvature and h_r indicates a complete separation of the surfaces [27]***.***

2.5.5 Hydrodynamic Lubrication

Hydrodynamic lubrication is the form of lubrication when the interacting surfaces are completely separated. In this lubrication regime the bulk properties of the lubricating fluid dominate, and the chemical properties of the fluid are negligible. Therefore, the characteristics of lubrication and friction can be ascertained through conventional fluid mechanics. Typically, the minimum separation between the two surfaces will be greater than 1µm [27].

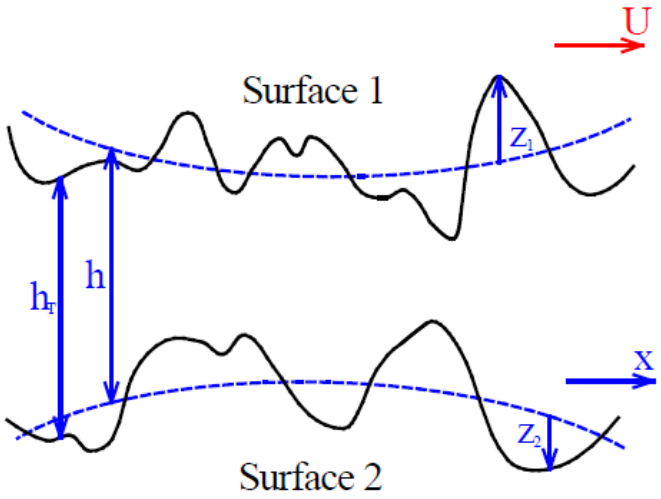

Figure 2-11: Schematic to represent a hydrodynamic lubrication scenario. Z indicates the difference between the surface geometry and the nominal radius of curvature, h represents the separation between the nominal radii of curvature and h_r indicates a complete separation of the surfaces [27]***.***

2.5.6 Additives

Additives are chemical compounds which are specifically added to the oil to provide a given benefit, often for use within the boundary and mixed lubrication regimes. Some form tribofilms, to aid in lubrication during boundary lubrication, whilst others provide a benefit as part of the bulk fluid, such as altering the viscosity. Often oil additives have been synthesised to work synergistically within the system, resulting in highly complex fully formulated oils. Typically a traditional fully formulated oil will include additives to modify (reduce) the friction; to reduce the wear; to mitigate against oxidation; to alleviate, or activate under, extreme pressure situations; to disperse contaminants; to clean impurities and prevent deposits; to reduce the pour point; and to improve the viscosity index [27].

According to a leading oil manufacturer, Total [29], up to 30% of a commercially sold engine oil can be additive. Another source [30] indicates that the minimum quantity of a commercial oil that consists entirely of additives is usually 10%, indicating that all engines require additives. The quantity of each specific additive is carefully controlled and can vary depending on the other additives present within the oil. Prominent additives, such as ZDDP (an anti-wear additive) and MoDTC (a friction modifier), can be used in larger concentrations, with the provider of the oil for use in the present study indicating that the ideal quantity of ZDDP in a commercial oil is approximately 0.5wt%.

2.5.6.1 Anti-Wear Additives

In this investigation the additive to be considered, ZDDP, is an anti-wear additive. Anti-wear additives act to either separate the surfaces or to protect the surfaces by wearing sacrificially. ZDDP contains phosphorus, which is the functional part of the molecule, as does tricresyl phosphate (TCP), another anti-wear additive. TCP is very prominent in aerospace propulsion systems but is far less so in the automotive industry [31]. Whilst TCP is an effective anti-wear additive there are severe health risks associated with this chemical and so it is

primarily used in small quantities and for industries which either have no alternative or, as with the aerospace industry, have limited contact with humans [32]. Another anti-wear additive type is ashless DialkylDithioPhosphate (DDP). Additives of this type are novel alternatives to ZDDP and contain different core elements (not zinc). These are becoming more prominent with ongoing research indicating these additives are very effective whilst being less polluting than the process to create ZDDP[33]. All three of the mentioned anti-wear additives protect their underlying surfaces by forming a tribofilm, a shear induced chemically absorbed layer, on one or both of the contacting surfaces. The tribofilm is then worn sacrificially, and can have the ability to be replenished if sheared in the presence of sufficient fluid. There are many research activities focussing on tribofilm forming anti-wear additives [32,34,35], with a focus on determining a replacement for ZDDP, the additive of concern in this research activity.

2.5.6.2 Zinc DialkylDithioPhosphate

ZDDP is an additive that has been used extensively in the automotive industry for many years. It is composed of zinc, sulphur and phosphorus and forms a protective tribofilm on the surfaces within a contact [4].

When heated ZDDP will form a thermal film, with the film formation being vastly improved when formed whilst the lubricant is being sheared. This tribofilm is primarily made up of phosphate pads, “bumps” across the surface, which have a distinctive glassy appearance [36]. The presence of a film, even in the absence of shear, indicates that the formation process is not exclusively motion driven; however, motion does influence the structure [37]. The prevalent theory is that the ZDDP molecule decomposes, such that the zinc, sulphur and phosphate atoms separate, and the three elements adhere to the surface. This is supported by EDS (Energy Dispersive X-ray Spectroscopy) and Raman investigations carried out in the past, which find distinctive peaks identifying the three elements [38]. It is

hypothesised that the functional tribofilm pads are those that primarily consist of polyphosphates, which is the largest portion of ZDDP tribofilms [39].

ZDDP was initially intended as an antioxidant additive; however, its use as an anti-wear additive has greatly increased its popularity. Unfortunately, there may be a positive correlation between the concentration of the ZDDP additive and the amount of friction within the system [4]. This means that ZDDP is often coupled with a friction modifier, even when a friction modifier would not otherwise be necessary. There is some inconsistency in the literature as to the true effects of ZDDP on friction with most papers claiming that ZDDP does cause this increase [40]. However, some claim that it may have no effect [41] or even that it could potentially decrease the friction [42].

2.6 Types of tribometer

Small scale tribological testing is typically conducted using test equipment referred to as tribometers. These simulate either rolling or sliding contacts and are chosen to best replicate the contact scenario experienced within a component or a mechanism. The primary function of tribometers is to create the sliding motion necessary to produce wear, friction and tribofilms [43]. There are two main methods by which this motion can be created; reciprocal motion (as in a piston) or unidirectional motion (as in a camshaft). Unidirectional motion means that one contacting surface is moving in a single direction, tracing a circular wear scar. The counter-surface can either be a ball, a pin or a smaller plate. Figure 2-12 shows both a unidirectional contact (with a stationary pin and a rotating plate) and a reciprocating contact (with a stationary plate and a sliding pin) [16].

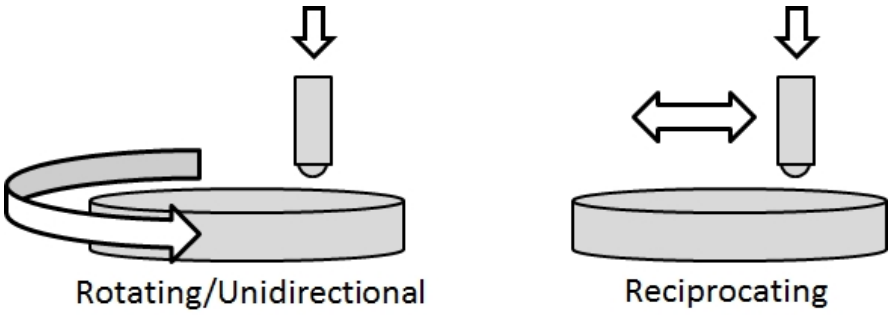

Figure 2-12: A schematic diagram to explain different Tribometer types [16]***.***

Tribometers usually have an internal (or at least electronically controlled) mechanism for controlling the speed of the motion; however, several mechanically controlled tribometers do not have an internal mechanism of loading the pin. Numerous tribometers load the pin using an elongated arm (mounted either directly beneath the contact (as in a TE77) or perpendicular to the contact (as in a pin-on-disc)) as shown in Figure 2-13. It is also necessary to control the temperature and thus in both pictures there are small thermocouples mounted inside the oil tray [16,44].

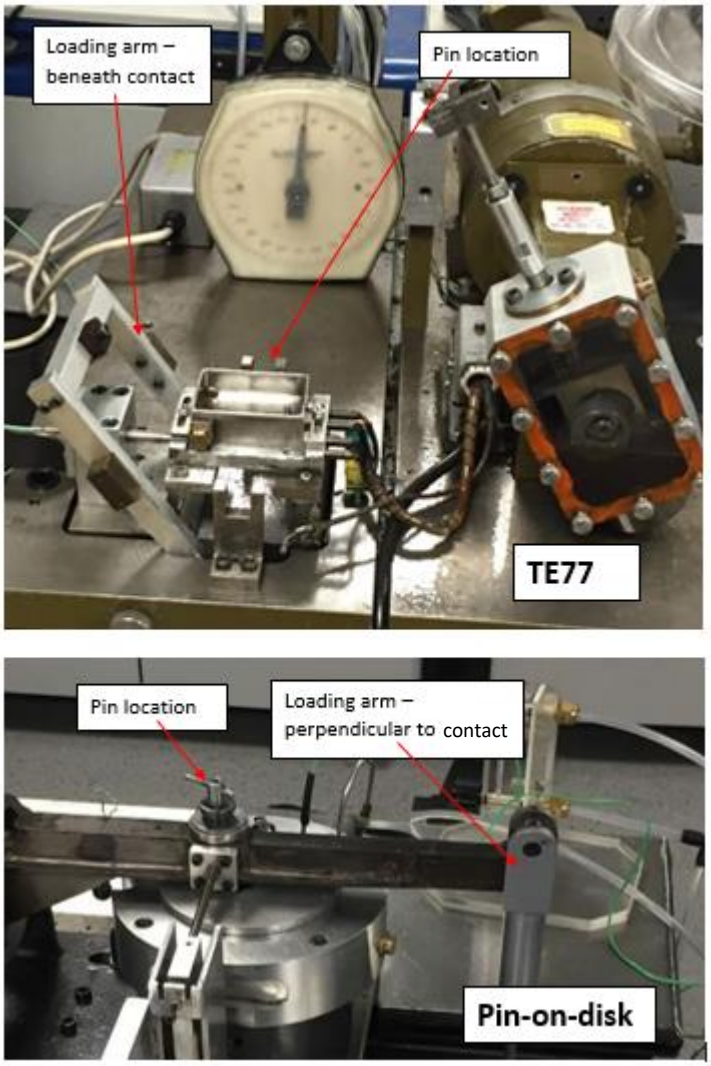

Figure 2-13: The large TE77 and single station pin-on-disc tribometers as found at the University of Leeds [45]**.**

2.6.1 Unidirectional Tribometers

The University of Leeds has several custom-made tribometers; however, it is accepted that most unidirectional tribometers will have a pin on disc set-up. This means that there is a circular plate, often with a hole in the centre, which is rotated about its central axis [19]. The pin is then held in a single location with the load applied, as shown in Figure 2-12. The contact is usually made in a closed container, as the centripetal force of the rotating disc can cause any lubricant to be dispersed away from the contact [46]. A commercially available unidirectional tribometer is the PCS Instruments Mini Traction Machine (MTM). This is an electronically controlled machine, where the load is applied through an arm onto which a

ball is inserted. The oil temperature is controlled, as is the speed. The lid mechanism ensures that no lubricant is lost due to centripetal acceleration [47].

Unidirectional tribometers are often employed to be representative of conditions within a single direction sliding contact, such as a cam, with most modern research using a MTM or a simple single station pin-on-disc [48,49]. Advantages and disadvantages of these tribometer types are detailed in Table 2-1.

Table 2-1: Advantages and disadvantages of unidirectional tribometers

Advantages	Disadvantages
Simple to operate, meaning multiple tests can be set up identically for comparison.	Limited relevance to industry as there is a general focus on the contact between the piston and the piston ring, which is reciprocating.
There is abundant literature using the MTM with the spacer layer imaging method (SLIM) attachment for verification of in-situ monitoring results.	The sample baths for these tribometers required a large quantity of oil to submerge the samples and this can be expensive.
Some variants (not the MTM) can be used to run multiple tracks on a single sample set, permitting consistency between tests.	Can typically only be used with a limited number of possible surface radii on the countersurface.
Once the tribometer has achieved the running speed (finished accelerating) this speed is maintained for the entirety of the test.	

2.6.2 Reciprocal Motion Tribometers

As with unidirectional tribometers some reciprocating tribometers are made in-house for use in a given research group; however, most are (or have previously been) available commercially as well. Some of the commercially available tribometers are: PCS Instruments High Frequency Reciprocating Rig (HFRR) [50]: the Cameron Plint TE77 [44] and the Plint TE99 (typically known as the Biceri Reciprocating tribometer) [51]. The PCS Instruments HFRR is an electronically controlled machine, with similar controls to those in the PCS Instrument MTM [50]. The Cameron Plint TE77 is a simplistic mechanical design, as shown in Figure 2-13,

with a mechanical loading method and manual controls [44]. The Plint TE99 is considered a universal wear tester and is capable of producing both reciprocating and unidirectional motion [51]. For this research the TE77 shall be employed as this has been used extensively to produce ZDDP tribofilms in literature [52,53]. Examples of the conditions employed in some of these investigations are summarised in Table 2-2 and some advantages and disadvantages of reciprocating tribometers is presented in Table 2-3.

Table 2-2: Experimental conditions used for the TE77 in the literature.

Paper	Load [N] (Contact Pressure [GPa])	Temperature [°C]	Frequency [Hz]	Stroke length [mm]	Sliding distance [m] (Duration [minutes])
Qu et al [54]	100	100	10	10	1000
Landauer et al [52]	100	100	10	10	1000
Barnhill et al [55]	100	100	10	10	1000
Wright et al [56]	100	100	10	10	1000
Yang et al [57]	(0.7)	100		5	(120)
Patel et al [53]	220N (0.5GPa)	75	50	11	(60)

Table 2-3: Advantages and disadvantages of reciprocating tribometers

Advantages	Disadvantages
Simple to operate, meaning multiple tests can be set up identically for comparison.	Can only be used to generate a single wear scar on each sample set.
Highly relevant to a key industrial research focus, the contact between a piston and piston ring.	Cannot be used with a single stated lambda ratio, meaning comparisons between tests can be more complicated.
Small sample baths, requiring lower quantities of oil per test.	Susceptible to surface gradient of the flat plate (can affect a measurement of friction).
The countersurface can be varied a lot, both material and surface radius.	Cannot be used to determine lubricant life, only to assess wear and friction for a fixed amount of time.

The TE77 has been also been selected due to its prominence in the tribological research community, increasing the repeatability of this work. The University of Leeds has two TE77 tribometers in-house, which means that more tests could be conducted as a result of the increased availability. The TE77 has a large enough stroke length to permit a true range of velocities to be experienced, with an appropriately large nominal velocity to ensure the validity of the lambda ratio calculations.

Chapter 3: Surface Parameters

In tribology, as with much of engineering, a focus is placed on the surface parameter R_a; however, R_a is a linear parameter and does not consider the entire surface. Important other surface parameters are typically the areal surface parameters, including S_a, S_{sk} and S_{ku} but can also include textural parameters such as isotropy. This chapter will introduce these other parameters, as well as give details of how they are calculated.

3.1 ISO 25178 - 2

There exists an International Organisation for Standardisation (ISO) standard to define the various Areal surface texture parameters that can be employed to describe and quantify a surface; this standard is ISO 25178 – 2, "Geometrical product specifications (GPS) — Surface texture: Areal — Part 2: Terms, definitions and surface texture parameters" [58]

Within the standard there exist definitions for the surface roughness (S_a), surface skewness (S_{sk}), surface kurtosis (S_{ku}) and the texture direction (S_{td}, which relates to the surface isotropy). These parameters are useful in tribology as they permit a true understanding of the surface morphology, beyond the traditional R_a [58].

To determine the surface parameters, it is necessary to remove plane bias from a scan. This is done by calculating the best fit, up to a 6^{th} order polynomial, and removing this from the scan. If too much processing is done on the data set prior to analysis then the data can become meaningless; therefore, it can be difficult to ensure that scan artefacts (such as noise) are removed whilst maintaining confidence in the calculations [59].

3.2 Arithmetic Mean Height

In a 2-dimensional profile a common roughness parameter is the R_a. R_a is calculated using Equation 24, which determines the arithmetical mean deviation of all the measured values in the assessed profile [58].

$$R_a = \frac{1}{n}\sum_{i=1}^{n}|y_i|$$

(Equation 24) [58]

This is calculated by considering the absolute distance from the mean line of each point along the profile (assuming a discrete set of data points). The R_a is the average value of these, as indicated in Figure 3-1. The R_a simply gives an understanding of the variation in the

height parameter of the profile, it does not differenetiate between peaks and valleys and so is of limited use in the true analysis of topography, despite its prevalence in engineering [58].

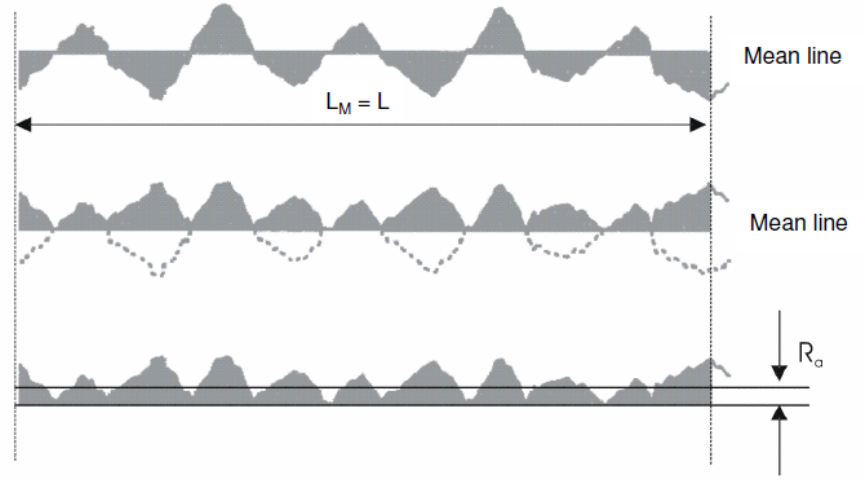

Figure 3-1: Arithmetic mean roughness – profile.

An additional parameter exists to describe the roughness of a 2-dimensional profile, the surface root mean square deviation R_q, which is similar to the standard deviation in statistics. The R_q is more sensitive to the distribution of valleys and peaks across the surface but still does not distinguish specific morphology. The R_q is calculated using Equation 25 [58].

$$R_q = \sqrt[2]{\frac{1}{l}\int_0^l Z^2 ds} = RMS = \sigma$$

(Equation 25) [58]

The equivalent parameter for analysing a surface is the S_a. S_a is similar to R_a, in that it determines the arithmetical mean height; however, this is calculated across three dimensions (as shown in Figure 3-2). The S_a parameter is calculated using Equation 26 [58].

$$S_a = \frac{1}{A}\iint_A |Z(x,y)|dxdy$$

(Equation 26) [58]

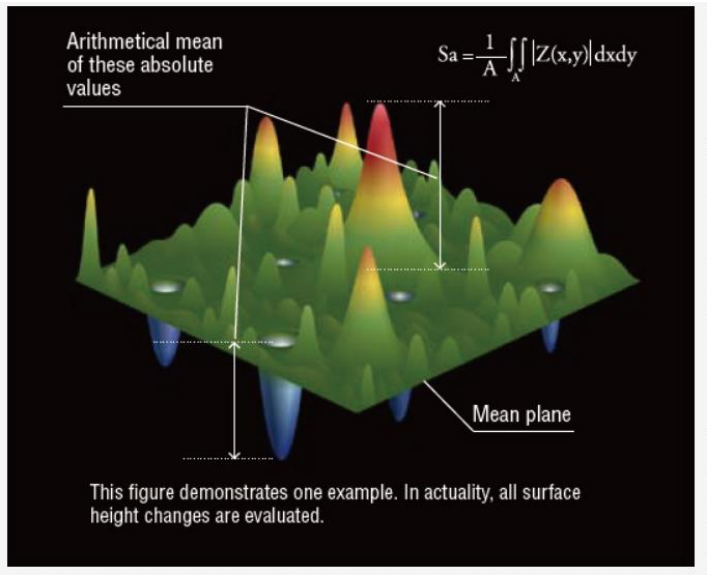

Figure 3-2: Example surface for S_a calculation [60]***.***

3.3 Surface Skewness

The skewness of a surface is a measure of asymmetry within the profiles. If the peaks and valleys are distributed symmetrically about the mean line then the skewness is equal to 0; however, if there are more peaks than valleys then the surface has a negative skew [58].

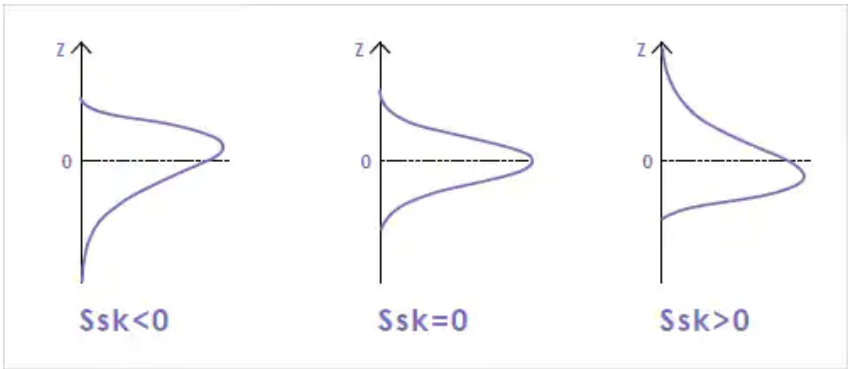

Figure 3-3: Surface skewness [60]***.***

The skewness can be calculated using Equation 27.

$$S_{sk} = \frac{1}{{S_q}^3}\frac{1}{A}\iint_A Z^3\,(x,y)dxdy$$

(Equation 27) [58]

The surface skewness is an additional parameter to determine the shape of the asperities on a surface. This can be related to the way the lubricant is sheared and degraded and may relate to the formation and topography of a tribofilm. If more of the surface is above the mean line then the lubricant will be sheared less by the asperities whilst having a few deep valleys, within which the lubricant can become pooled. If more of the surface is below the mean line then the lubricant is sheared by a few tall and sharp asperities, with the load being primarily supported by these asperities [61].

3.4 Surface Kurtosis

Kurtosis is a measure of the "sharpness" of the surface. The kurtosis is calculated using Equation 28. If the kurtosis value is equal to three then the height distribution has both sharp regions and indented regions. If the kurtosis is less than three then asperities are smoother, whilst if the kurtosis is greater than three the asperities are very spiky [58].

$$S_{ku} = \frac{1}{{S_q}^4}\left(\frac{1}{A}\iint_A Z^4(x,y)dxdy\right)$$

(Equation 28) [58]

Kurtosis can be used to infer the nature of the asperities and can be used to consider the real area of contact. If the surface has a kurtosis of less than three then it can be assumed that the applied load is distributed evenly across the surface; however, if the kurtosis is greater than three then it can be expected that the contact pressure will increase. Also, if the surface has a number of very sharp asperities the lubricant will be sheared in a different manner to if the surface has smooth asperities. This effect is enough that it can affect the degradation mechanism of lubricants [61].

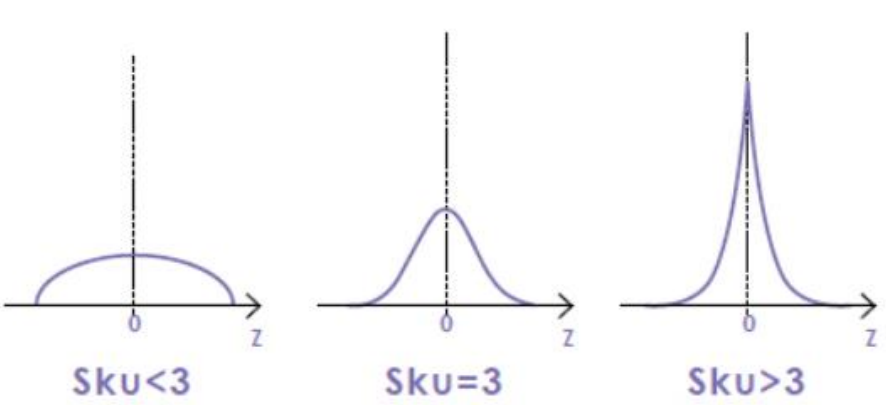

Figure 3-4: Relationship between kurtosis and the height distribution [60]***.***

3.5 Texture Direction

In addition to determining the distribution of material and the sharpness of asperities it is possible to determine and quantify the directionality of the surface. A surface is considered to be isotropic if the surface characteristics are identical independent of direction. A completely isotropic surface is rare, with most machining processes resulting in some remnant surface texturing. A surface which is not completely isotropic is considered to be anisotropic. The extent of the anisotropy is determined using the Fourier transform and the autocorrelation function. These calculations are often conducted as part of the surface scan and can be used to determine a polar spectrum of the directionality. From the polar spectrum it is possible to determine the texture direction (Std) which is expressed in degrees and corresponds to the most prominent lay direction [58,60].

Chapter 4: Literature Review of ZDDP

ZDDP has been the subject of extensive tribological research for many years. The requirement to replace ZDDP in the automotive industry has resulted in an increased research effort since 1980. Research avenues have included the effect of ZDDP tribofilm on the friction and wear performance of various surfaces, as well as investigations into the chemical formation mechanisms of the tribofilm itself. Investigations in the 2000s have considered in-situ analyses of the film formation (such as by using an MTM SLIM attachment) and the effect of contaminants on the tribofilm efficacy.

4.1 Tribochemistry and Structure

As stated in section 2.5.6.2, ZDDP is a decomposable additive that chemically bonds with the surfaces in the contact. This means that the covalent bonds between the zinc, sulphur and phosphorus are somehow broken, this results in the three elements being able to join with the surface [4].

The additive structure is represented in Figure 4-1. It is necessary to understand this chemical structure to comprehend the method by which a ZDDP tribofilm can form.

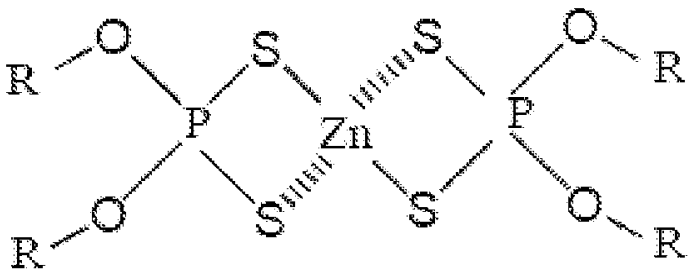

Figure 4-1: A chemical diagram of ZDDP [62]**.**

This structure has a core zinc atom with two covalent and two partial (hydrogen) bonds between it and sulphur atoms. The sulphur atoms are each covalently bonded to a phosphate, such that there are two sulphur atoms to each phosphorus atom. To complete the phosphate molecule, with a stable core structure, there are four oxygen atoms, also two for each phosphorus. These oxygen bonds provide the link between the core structure and the varying reaction groups. These reaction groups are represented as 'R' as these can be different depending on the specific formulation of ZDDP [63].

The reaction groups that are present are either aryl or alkyl hydrocarbon chains. Aryl hydrocarbons are aromatic, meaning they form ring structures instead of linear structures, with a single hydrogen missing, permitting their attachment to a larger structure (in the case of ZDDP this hydrogen is replaced by the oxygen). Alkyl reaction groups are linear hydrocarbon chains, which also have a hydrogen replaced by the oxygen of the core ZDDP molecule. These reaction groups can have any hydrocarbon chain length; however, if an alkyl

carbon chain contains fewer than four carbon atoms then a pure ZDDP molecule will be solid at ambient temperature and will not dissolve in petroleum base stocks. If the molecule contains carbon chains of five carbon atoms or longer then it is likely to be liquid at room temperature. Alkyl reaction groups can also be branched or straight chain hydrocarbons, meaning that they can either consist of middle carbons bonded to two carbons and two hydrogens (straight) or have a middle carbon that is instead bonded to three carbons and only one hydrogen, with the third carbon forming a perpendicular hydrocarbon chain (branched) [64].

The reaction groups are added to the ZDDP molecule using an alcohol, either an aromatic or traditional alcohol (such as phenol or ethanol), and rely on a substitution reaction, with the ZDDP molecule and water being the reaction products [64]. While the molecule is suspended within the oil solution there are few polymerisation reactions. However, when the molecule is sheared the phosphate chains begin to polymerise. Therefore, it is unknown how long the reaction groups typically are [4].

There are also molecular structure differences between different alkyl ZDDPs, namely primary and secondary alkyl ZDDP. The primary alkyl ZDDP consists of a reaction group bonded to the oxygen at the end of a chain, such that the attached carbon is only attached to one other carbon and two hydrogens. Secondary alkyl ZDDP consists of a reaction group bonded to the oxygen from the middle of a chain, such that the attached carbon is attached to two other carbons and only one hydrogen. Secondary alkyl ZDDP is weaker than primary alkyl ZDDP (which is in turn weaker than aryl ZDDP), as the carbon-oxygen bond is affected by the number of hydrogen bonds the carbon has, which has been shown to affect the rate of tribofilm growth. The stronger the carbon-oxygen bond is then the slower the tribofilm will form, resulting a reduced efficacy as an anti-wear additive [65].

The exact method of ZDDP decomposition is unclear, although much research has been conducted to discover it [55,56]. The three primary methods proposed included thermal decomposition [67] and both hydrolytic and oxidative mechanisms [4]. The bonds between the core elements, the zinc, phosphorus and sulphur are commonly believed to decompose as a result of the temperature within the contact, both the operating temperature and the natural increase in temperature due to friction [63].

Naveira-Suarez et al [68] have speculated on the exact method of tribofilm adsorption based on other literature and their own experimental research. They state that the initial mechanism is for separate reactions to occur (on the asperity level) forming unique and isolated pads. This occurs very rapidly, as shown in the SLIM images in Figure 4-2, with clear dark regions being visible from as early as 30 minutes. This increased rate of reaction implies a catalysed series of reactions occurring, such that the ZDDP is decomposed with the aid of chemicals either created or increased during the rubbing process [37]. Naveira-Suarez also proposes the use of ligand exchange as the second stage decomposition method [68]. This is validated by Piras et al [67] who found evidence of zinc and iron orthophosphates, in the tribofilm, implying an exchange of zinc phosphate into iron phosphate.

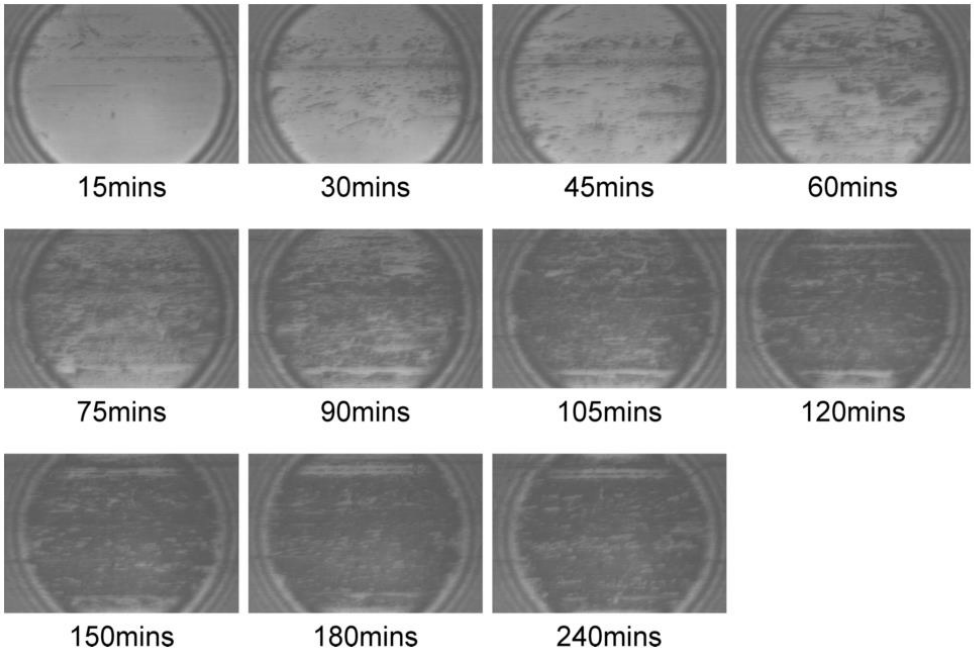

Figure 4-2: SLIM images to show the speed of tribofilm pad formation [69]**.**

4.2 Mechanical Properties

Assessing the mechanical properties of ZDDP tribofilms has been an area of substantial interest over the last few decades. There have been multiple studies investigating these characteristics using a variety of techniques. AFM, Interfacial Force Microscopy (IFM), Scanning Electron Microscopy (SEM) and nano-indenters have all been used to characterise tribofilms [8,70–72].

Nicholls et al [72] performed a comprehensive review of the available literature in 2005 and have shown the development in the understanding of ZDDP tribofilms over the previous twenty years (since 1985). The paper describes how tests have been done to compare the characteristics of thermal films and those of tribofilms. It has previously been shown that the characteristics of thermal films are similar to those of tribofilms and it was speculated that this meant the easier to produce thermal films could be used as a substitute for tribofilms [73]. However, multiple papers show distinct differences between the two [8,71]. These differences can include topographic differences, when a ZDDP is tested within an MTM there is some evidence of a film prior to motion (a thermal film) which then evolves and changes as the tribofilm grows, and mechanical differences, with the thermal film demonstrating a lower protection against wear [69].

It must be noted that most analyses of ZDDP tribofilms are conducted ex-situ [8,74] and that this means that any properties that may be different in motion are not considered; thus, any values found can be considered only a snapshot of the potential properties. This is a limiting factor in most (non-MTM) tribofilm analyses, with later work by Gosvami et al [3,7] initialising a series of research activities that focus on in-situ analyses.

Graham et al [8] investigated the moduli of aryl and alkyl ZDDP tribofilms using IFM. They found that the moduli varied across the topography. They determined that the aryl ZDDP film had a much lower strength (~50GPa) than the alkyl film which also had larger pads

(>70GPa). It was also discovered that the larger alkyl pads had a varying modulus within its own structure. The central location demonstrated a high modulus of 209 ± 38GPa, which is similar to the bulk steel substrate (220GPa), whereas the edge of the pads had a lower modulus of 87 ± 23GPa. The smaller alkyl pads had a lower modulus again, 74 ± 20GPa, and the area between pads had a very low modulus, comparatively, 37 ± 7.3GPa. This low inter-pad modulus is similar to the trough indentation modulus reported, also using IFM, of 25GPa by Warren et al [73]. The method used to determine these moduli appears to have focussed on a single location within the tribofilm, indicating an assumption that the tribofilm is uniform. It is possible that the variation in modulus observed within the larger alkyl pads is due to the increased area measured, as opposed to a true difference between the aryl and alkyl structures. The assumption of tribofilm uniformity is a common limitation in several pieces of tribological research, indicating the need to determine whether the tribofilm is truly uniform throughout.

Other work was conducted to determine the mechanical properties of ZDDP tribofilms by Bec et al [75]. A key finding of this paper showed that the top layer of the tribofilm is a "thick organic overlayer of ZDTP [Zinc DialkyldiThioPhosphate] degradation precipitates". The overlayer consists of alkyl phosphate precipitates, to a thickness of a few hundreds of nanometres, which is mobile under a probe. The thick soft layer is easily removed during a solvent wipe, and thus is not typically considered in indentation testing. This paper, also, explained the different elastic moduli present for the different layers within the tribofilm, with modulus values ranging from 15GPa to 90GPa, and the possibility for localised film flow in the type one and type two polyphosphate layers (the long chain polyphosphates). In addition, this activity showed a localised displacement of the tribofilm through the application of a small load (Figure 4-3). The friction coefficient for each layer of the tribofilm was measured during the "nano-machining" process, with mean values from 0.24 to 0.31. The work in this study has shown that a scanning force apparatus can be used to both

conduct a topographic analysis and to manipulate (machine) the tribofilm. However, the tribofilm in this activity was generated under a bespoke rolling contact tribometer. This is not a commonly used tribometer and so there is merit in attempting to repeat such a method on a more conventionally formed tribofilm. Additionally this paper specifies that "special care was taken with regard to the choice of the areas tested on the patchy films" [75]. This indicates a bias, whilst it also acknowledges that the general topography of the tribofilm is non-uniform. The inherent bias in the selection of the locations for testing means that the true repeatability of this method is uncertain; however, this does indicate that such a method can be employed successfully.

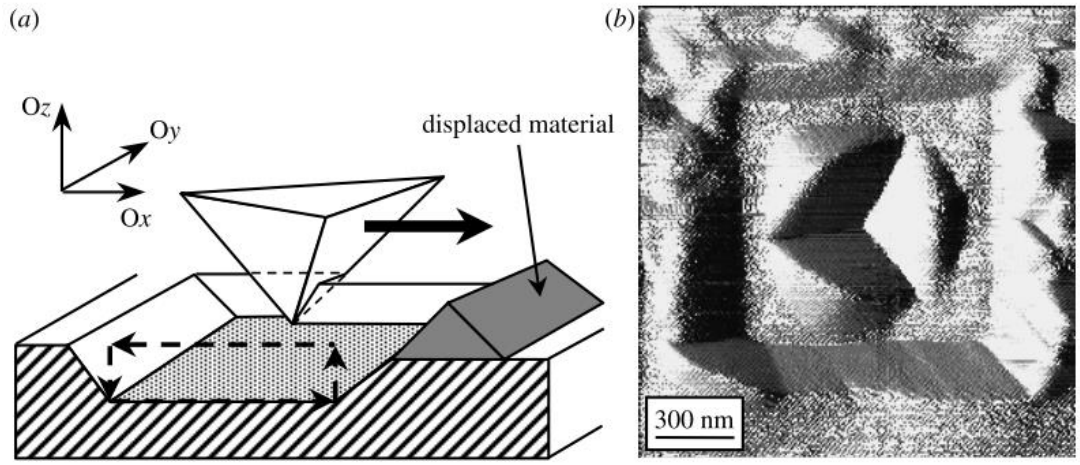

Figure 4-3: (a) a schematic for the motion used to displace the tribofilm, (b) the resultant topography after nano-machining [75]***.***

4.3 Morphology

Several papers have compared the morphology and mechanical properties of alkyl ZDDPs with aryl ZDDPs [8,76]. Graham et al [8] analysed tribofilms, of aryl and alkyl ZDDP, generated in a Cameron Plint reciprocating wear tester (this was unspecified but could have been the TE77) with a frequency of 25Hz and a normal load of 225N (to give a maximum contact pressure of 600MPa) The test was conducted over 1 hour at 100°C. The tribofilm characterisation was conducted in a static manner, ex-situ, although the author notes that the mechanical properties may involve a dynamic component and thus are different under shear. By comparing the different films using AFM it was shown that alkyl ZDDP tribofilms include elongated large pads, which Graham et al conclude are an agglomeration of smaller pads, and that these elongated pads are thicker and preferential to the direction of sliding (as shown in Figure 4-4). Also, in Figure 4-4 it can be seen that the aryl ZDDP tribofilms are "streaky" and are all elongated in the sliding direction. Graham et al hypothesise that the elongated thicker pads in the alkyl tribofilms bear the majority of the normal and tangential forces and that this is the reason for the preferential directionality, whereas the aryl tribofilms are more uniformly loaded and thus the preferential directionality is apparent in all the pads.

The work conducted by Graham et al [8] used a reciprocating tribometer; however, the hypothesis as to the reason for the unusual morphology observed within the tribofilms formed from the alkyl ZDDP does not take into consideration the relative position of each part of the scan within the larger tribofilm. There is also no indication of the initial topography, to determine whether the unusual topography is a reflection of the topography of the underlying substrate.

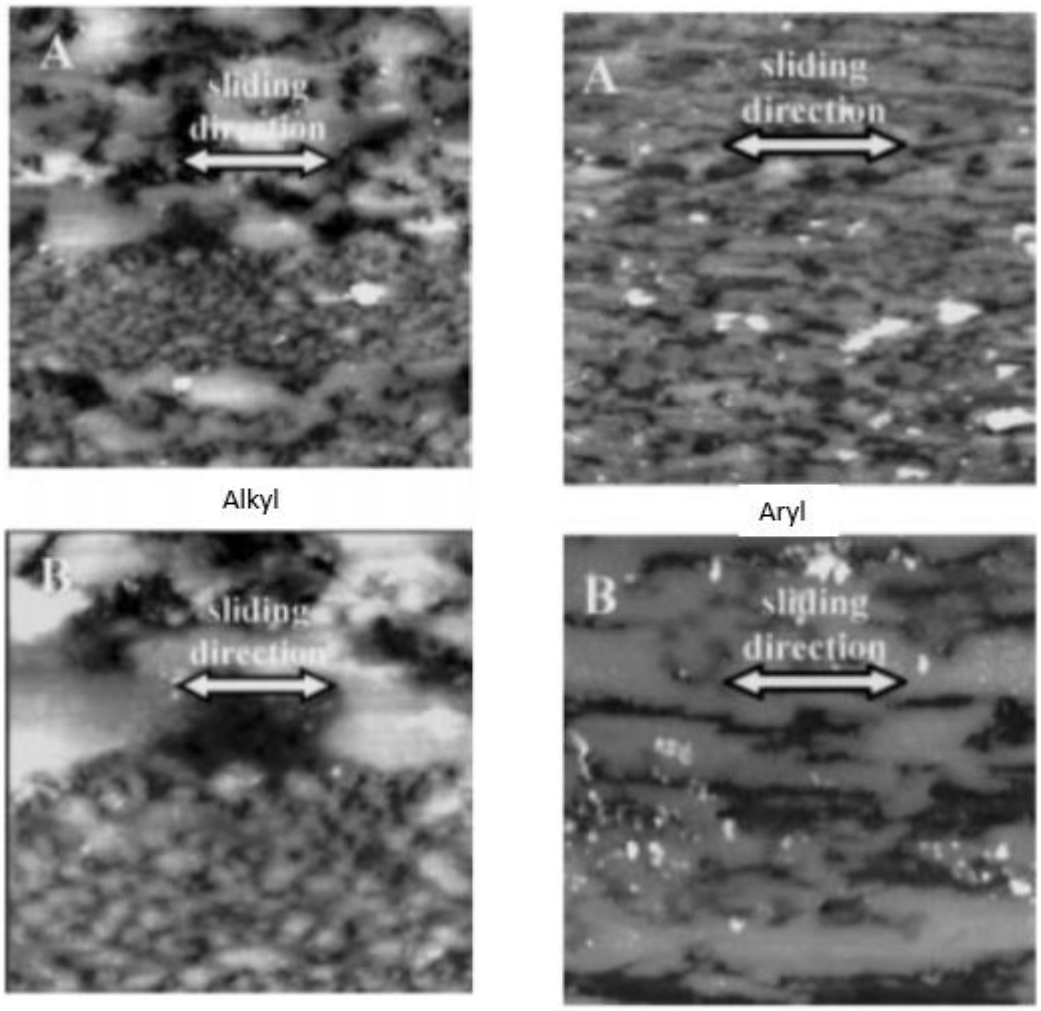

Figure 4-4: A comparison of AFM images taken for alkyl and aryl ZDDP tribofilms. (A) 50 x 50 µm area (x=250nm). (B) 25 x25µm area (x=250nm) [8]***.***

Narita and Priest [76] also investigated the difference between secondary alkyl ZDDP and aryl ZDDP. The tribofilms were formed in a ball on plate reciprocating tribometer with a varying contact pressure (between 0.8 and 1.4GPa), a 3 minute step load, a temperature of 200°C and a frequency of 22Hz. They found that the alkyl ZDDP tribofilm indeed forms non-heterogenous larger pads, 5-30µm, preferentially in the sliding direction. They speculate that this could be due to the pads bearing a larger load and thus decomposing at a faster rate than other forms of tribofilm. They also found streaked pads for the aryl tribofilm, as well as an area of indentifiable ploughing. The streaked nature of the aryl pads are heterogenous and have small pads, approximately 4µm in length. These differences can be clearly seen in Figure 4-5.

The preferential direction of the tribofilm is very apparent and has a similar topography to a ground surface. The journal article [76] does not specify the finishing method used to prepare the tribological test samples and so the extreme directionality may be due to an anisotropic surface that has been tested with the sliding direction aligned to the lay direction. In addition, the ploughed channel within the aryl tribofilm occurs next to a raised region. The raised region extends beyond the edges of the scan, indicating a length in excess of 50µm. Whilst a ploughed region next to an apparent long pad can be expected when it occurs in the sliding direction, the perpendicular nature of this phenomenon is unexpected. The streaked structure is reminiscent of scan artefacts and the absence of any information pertaining to the scan direction means this morphology cannot be confirmed to be a true representation of the tribofilm structure.

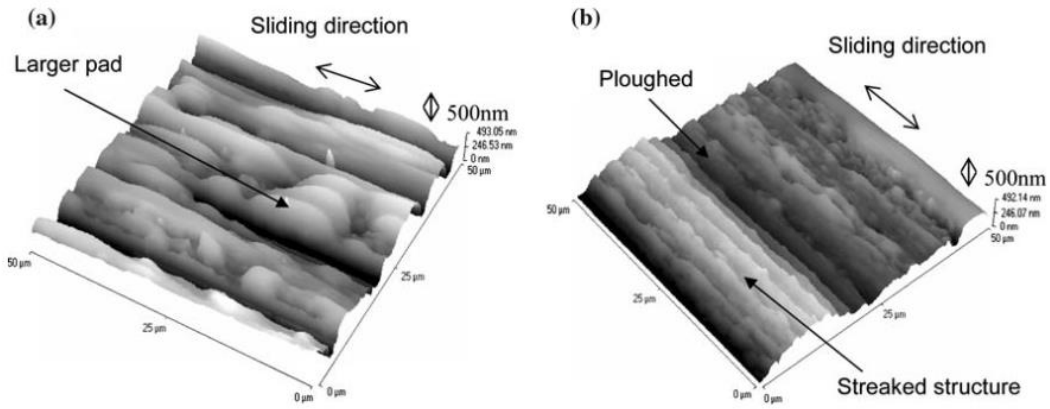

Figure 4-5: AFM topography images of tribofilms formed of a. sec. alkyl ZnDTP and b. aryl ZnDTP [76]***.***

There is evidence of tribofilm morphology altering over time. This has been shown by Naveira-Suarez et al [68] where they use an MTM SLIM and an AFM to investigate the evolution of the tribofilm over time. The SLIM images shown in Figure 4-6 clearly show that the tribofilm (shown here as a blue-purple colour) increases over time with a full film being present from approximately 30minutes. This is explained as being due to a maximum thickness being achieved, with the pads acting in a self-limiting manner. They also explain that the rapid initial decomposition is catalysed by chemicals that may be released (or

created) during rubbing, this effect has also been shown by Fujita and Spikes [37] as shown in Figure 4-7.

Figure 4-6 shows that whilst there is a full coverage by thirty minutes, with the image being covered with ZDDP (showing as blue), the specific topography changes during the test, with a more “patchy” morphology being present after sixty minutes and evidence of a reduction in thickness by 180 minutes into the test [68]. This effect is not replicated in the similar experiment shown in Figure 4-7, where the topography changes little after the test has run for twenty minutes [37]. This indicates that the spacer layer interferometry does not necessarily capture the full evolution of the tribofilm topography, which supports the concept that the slight changes in film thickness, caused either by a differing contact pressure (such as across the slight contacting diameter of a rolling ball) or speed , can affect this evolution. Therefore, whilst the MTM SLIM can provide some insight into the in-situ topography of a tribofilm further methods are required to capture more information on this morphology.

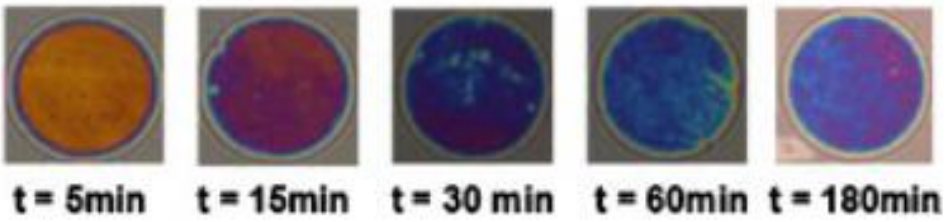

Figure 4-6: Spacer layer interferometry images over time for tribofilms formed of PolyAlphaOlefin (PAO) and ZDDP [68]**.**

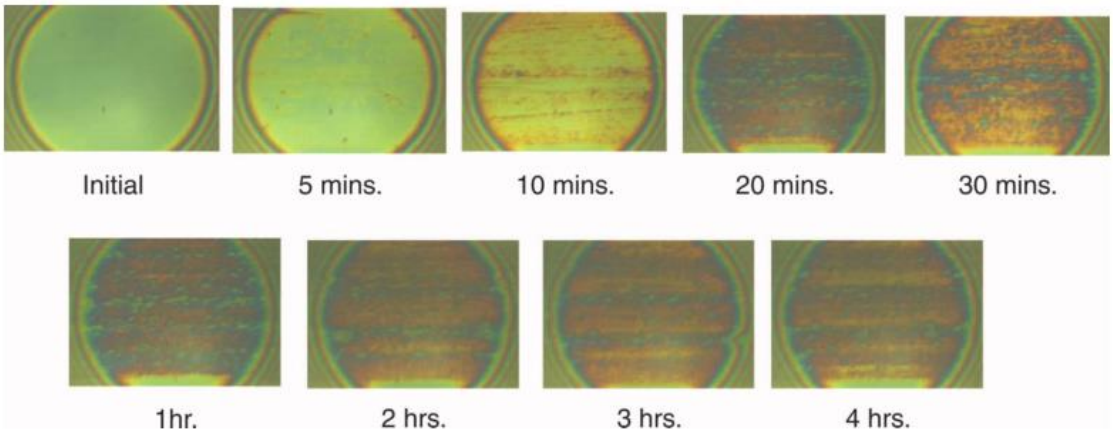

Figure 4-7: Spacer layer interferometry images for 1.2wt% ZDDP in mineral oil [37]**.**

4.4 Use as an anti-wear Additive

ZDDP has been used as an anti-wear additive since 1952 and has been much researched over this time [5,37]. As with other phosphorus containing anti-wear additives ZDDP is effective as it forms a protective layer (the tribofilm) which wears sacrificially instead of the surface. This layer is comprised of various compounds, including zinc phosphates, iron phosphates and an outer layer of zinc polyphosphates and orthophosphates, as seen in Figure 4-8 [5].

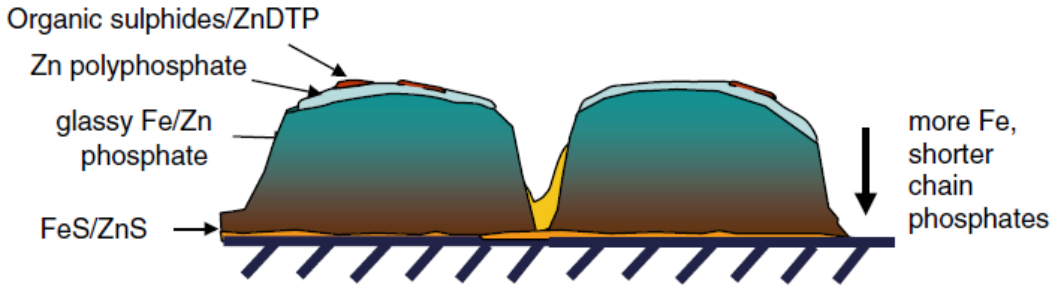

Figure 4-8: A schematic to show the approximate locations of compounds within ZDDP pads [5]***.***

These phosphate layers, particularly those made up of long and short chain polyphosphates, are specifically suited to use as an anti-wear additive, whereas the surface organic sulphides, whilst useful as an anti-wear additive are more utilised when ZDDP acts as an extreme pressure additive [4].

ZDDP has also been used as an anti-oxidative additive by disrupting the essential chain propagation sections of the oxidation reaction by acting as a free radical trap [77]. This same report states that ZDDP can also be an effective corrosion additive, this is because the tribofilm causes a protective layer over the surface and, therefore, the surface then cannot corrode. However, this has not been as extensively researched as the use of ZDDP as an anti-wear additive, as this has been found to be extremely effective and invaluable to the automotive industry [5].

As previously stated, ZDDP has been much researched as an anti-wear additive, with Hugh Spikes [5] stating that early research (conducted in the 1950s) included investigating the thickness of ZDDP films and the discovery of a thermal film. They also performed some initial chemical analysis, using sulphur radio tracing, to determine that the amount the phosphorus appears to increase, relative to sulphur, during the tribofilm formation process [78]. This research was followed by investigations into the chemistry of ZDDP in the 1960s and a furthering of this using newer methods, X-ray Photoelectron Spectroscopy (XPS) and Auger Electron Spectroscopy, in the 1970s. The 1980s saw investigations into adsorption and the true nature of the ZDDP phosphate pads whilst the 1990s saw the advent of in-situ analysis techniques, including in-contact and in-lubro techniques [5]. Whilst much research has previously been conducted, the full mechanisms for how ZDDP tribofilms form and how those tribofilms are capable of preventing wear are still not fully understood, necessitating further studies using emerging and developing techniques.

Such research, conducted since 2000, has taken advantage of the more modern analysis techniques available, including AFM, Secondary Ion Mass Spectrometry, nano-indentation and Raman spectroscopy [5]. In the 2010s, anti-wear investigations included Costa and Spikes [79] using the MTM SLIM to investigate the effect of ethanol on the formation of ZDDP tribofilms and Austin et al [80] who used AFM and XPS methods to investigate whether ZDDP tribofilms could form in diamond like carbon coatings from fully formulated oils. Austin et al's [80] results are shown in the AFM images in Figure 4-9, these show that the ZDDP tribofilm has been formed and has provided a higher layer to cover the surface, this will then be worn instead of the surface. They also performed XPS results, which showed phosphorus and sulphur present on the surface from six hours, which is supported by the appearance of small pads in Figure 4-9(c). Research conducted since the publication of Spikes' literature summary [5] includes advances in in-situ formation techniques, using bespoke and commercial AFMs [3,7] and combining tribometers with existing chemical

analysis techniques, such as using a small pin-on-disc unidirectional tribometer within a Raman spectrometer, ongoing at the University of Leeds.

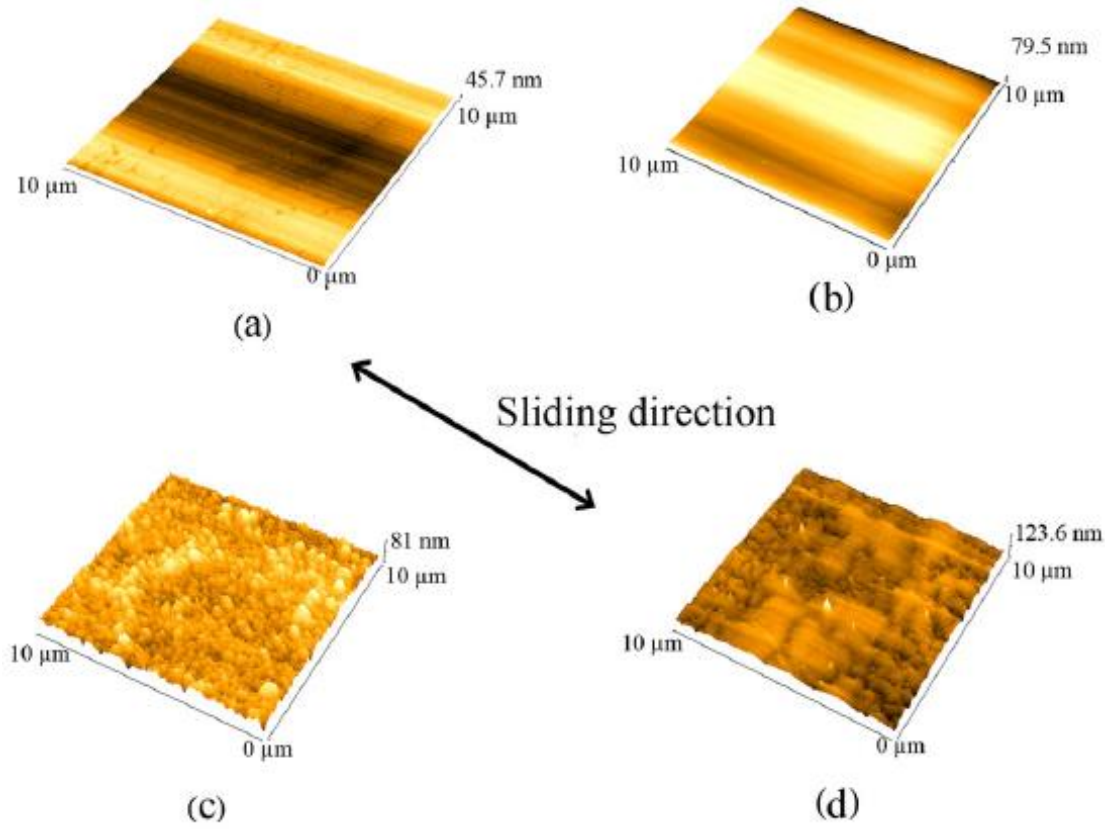

Figure 4-9: AFM images of a diamond like carbon (DLC) coating after being tested in a reciprocating pin on plate set up for (a) six hours in a base oil, (b) twenty hours in a base oil, (c) six hours in fully formulated oil and (d) twenty hours in fully formulated oil [80]**.**

Figure 4-9 also shows the increase in pad size for a longer test. This indicates that the tribofilm formation is stimulated over time, and also that the pad height increases as more time passes. The scan denoted as (d) also shows that the increased pads are smoother and are likely to have a lower R_a than the pads in the scan denoted as (c). This implies the sacrificial nature of the polyphosphate chains is functioning as the tribofilm is being worn, resulting in the smoother morphology. This means that the tribofilm is protecting the surface and thus limiting the effect of wear and also the effect of corrosion [80].

This study [80] considered both the surface after testing with base oil alone and the surface after testing with fully formulated oil. The base oil tests show evidence of a partially

lubricated contact (as would be expected) with some evidence of tilt within the scan but not obvious artefacts. There are artefacts present in the scan taken after the longer duration testing with fully formulated oil; however, these do not appear to detract from the general morphology. In addition to the large pads that are present in this image remnant small pads can also be observed, indicating that the topography is not uniform; however, no explanation is proffered for this. The indication of a non-uniformity within the tribofilm merits further study of such morphology, which was not the primary focus in this activity.

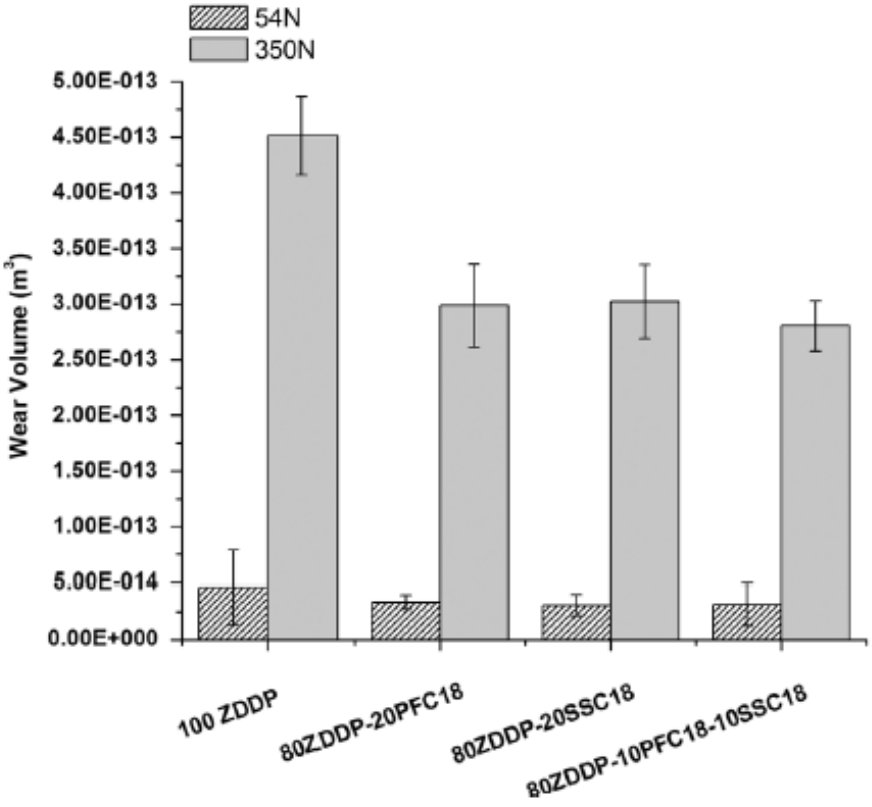

Figure 4-10: The wear volumes for different oil formulations, at different loads [81]**.**

Sharma et al [81] investigated the effect of additional anti-wear additives when used in conjunction with ZDDP. Using optical interferometry they determined the results shown in Figure 4-10, these show the exact wear volumes for ZDDP, $4.5x10^{-13}m^3$ (for a load of 350N) and $5x10^{-14}m^3$ (for a load of 54N). They then used nano-indentation to determine some nano-mechanical properties of the tribofilm, Figure 4-11. This shows the hardness for both loads considered in Figure 4-10, it can be seen from the Scanning Probe Microscopy (SPM) images

that the tribofilm pads formed for a load of 350N are more pronounced, this implies more polyphosphate chains, with these having likely grown after an initial run-in period.

This work [81] shows that the presence of other additives within a fully formulated oil can have a detrimental effect on the efficacy of ZDDP; however, this can also be accounted for simply by the reduction in ZDDP present. There is little difference in the anti-wear performance of the tests conducted with other additives present, indicating that the additional additives do not contribute to the anti-wear performance, with the ZDDP being the primary additive active. The pad morphology observed in Figure 4-11 (cb) is often considered to be “typical” of a ZDDP tribofilm; however, this has evolved within the fully formulated oil. The difference between this scan and the equivalent scan showing a tribofilm formed within a ZDDP only oil relates primarily to the pad size. This difference could be caused by the scans being taken as a “representative” image, with no consideration of the potential influence of relative position on the possible topography. The topographies shown in the scans for the different loads applied in ZDDP only oil are very similar, with little evidence that this is much affected by the load.

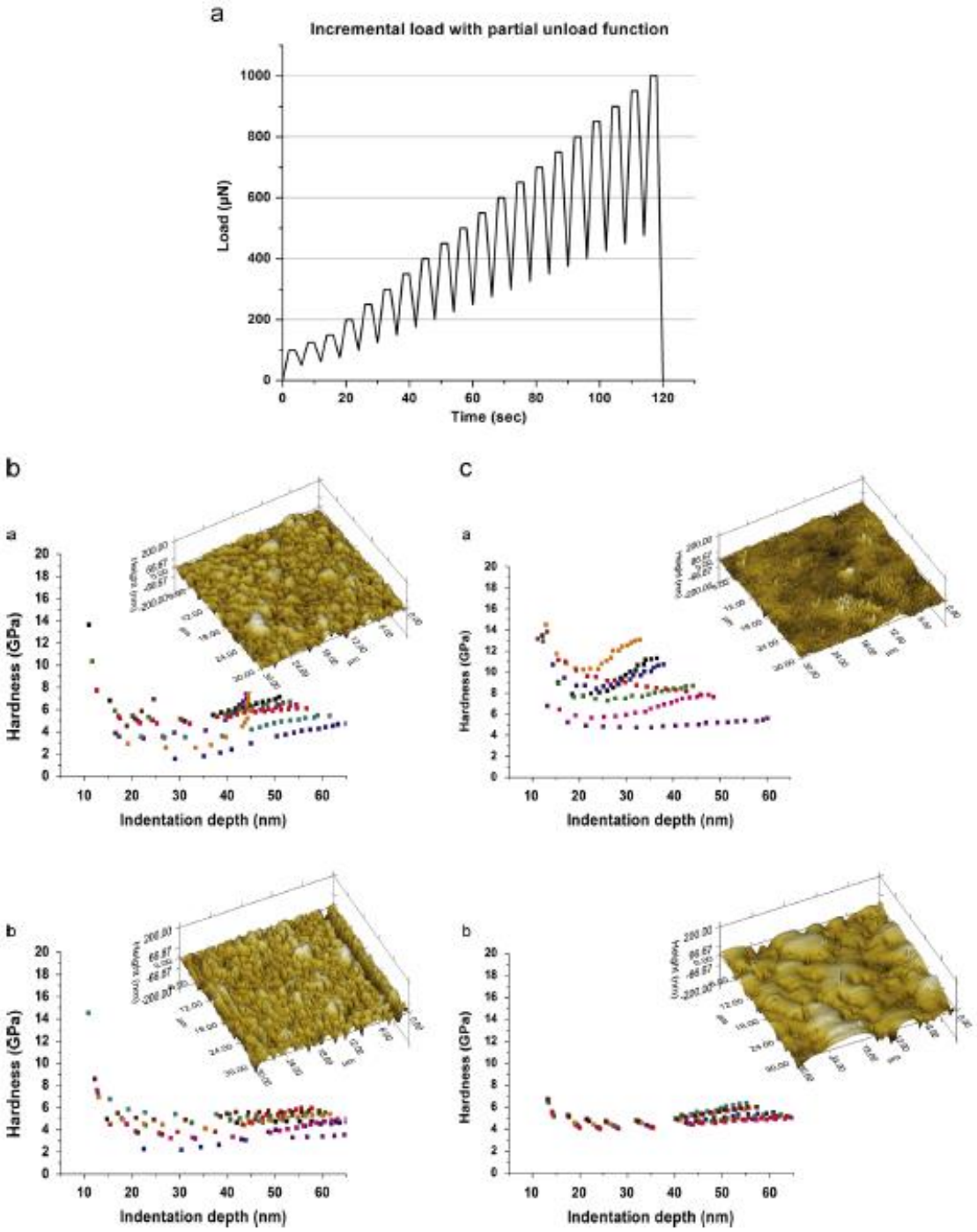

Figure 4-11: Tribofilm nano-mechanical properties from nano-indentation using cyclic loading, with a partial unloading load function (shown as a). Nano-hardness of ZDDP (ba and bb) and 80%ZDDP +20%PFC (ca and cb) as a function of indention depth of 54N and 350N, respectively with corresponding 3-D SPM images [81]***.***

4.5 ZDDP Tribofilm durability and growth

A 2015 study by Gosvami et al [3] has utilised an atomic force microscope to investigate the evolution of ZDDP tribofilms. They generated tribofilms in-situ using a single asperity nanocontacts to provide the sliding motion necessary. They report that there exists a thickness maximum, a point at which the thickness stabilises and the tribofilm is unlikely to grow thicker. This supports the concept of tribofilms being sacrificial and renewable, with the top layer of the tribofilm being simultaneously worn away and re-formed. Figure 4-12 shows the tribofilm morphology over the test span, with the clear increase in height shown in the graph. Whilst the article states that a thickness plateau was achieved this did not occur within the number of sliding cycles presented in this figure; therefore, the stabilisation cannot be verified by a reader. The initial evolution of the tribofilm occurs at a slower rate, before the thickness appears to increase at a rate that can be approximated by a power law. The volume graph includes error bars. The error bars indicate that the results are comprehensive and have been statistically validated; however, these bars relate to an average volume observed over the same scan area. There is little evidence that this method has been repeated. Whilst it is acknowledged and accepted that AFM testing is difficult to conduct exhaustively the misleading nature of the error bars may undermine the conclusion that the tribofilm achieves stability.

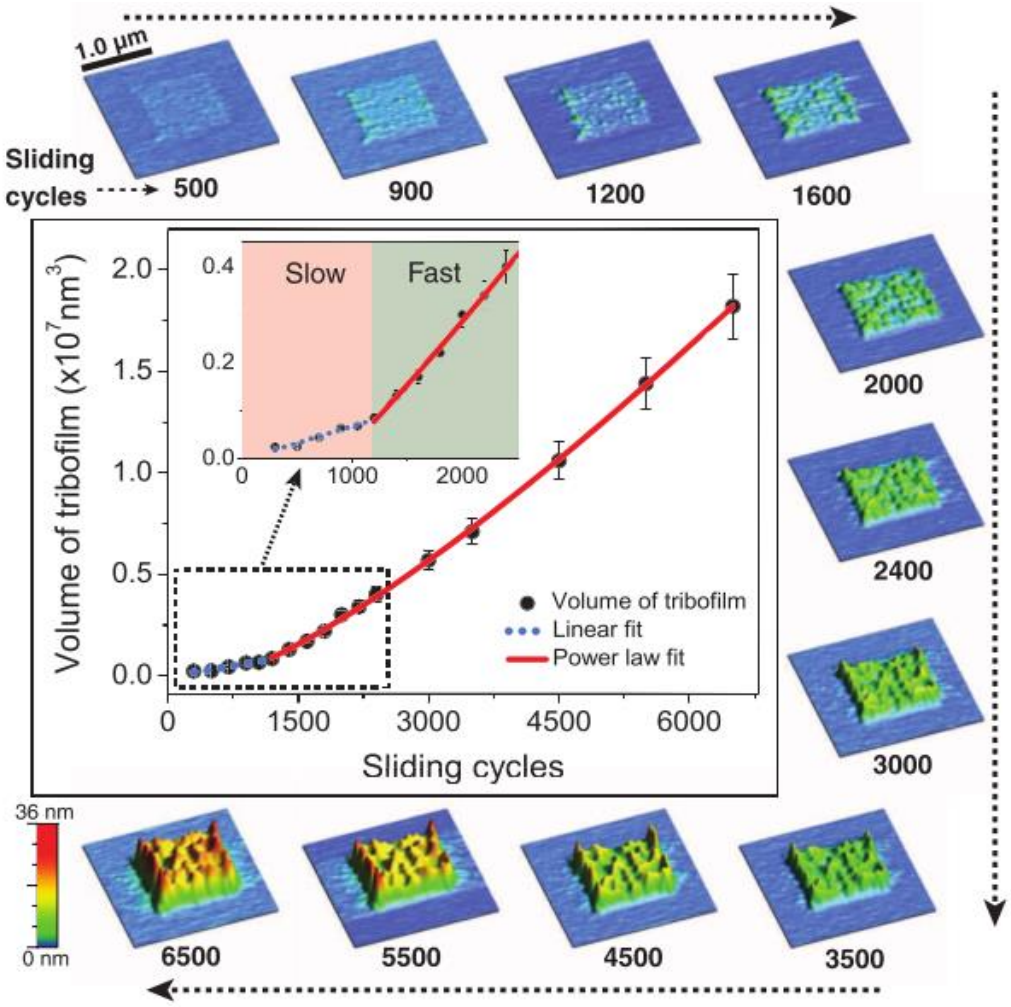

Figure 4-12: Morphology and volumetric growth of a ZDDP tribofilm, formed in-situ within an AFM [3]**.**

In the same paper [3] Gosvami et al also noted that the growth rate for the tribofilm is exponentially increased with contact pressure, until 5GPa at which point it is much more stable, as shown in Figure 4-13. They hypothesise that this is due to the increased pressure causing the tip to wear away the top layers of the tribofilm whilst stimulating further growth. This supports the concept of tribofilms being sacrificial. Also, in Figure 4-13 it can be seen that increased temperature causes an exponentially increasing growth rate. They also found evidence of thermal films in the initial scans which provides support to the widely accepted theory of thermal decomposition. This graph provides more evidence to support their statements, with the reported plateau being clearly observable.

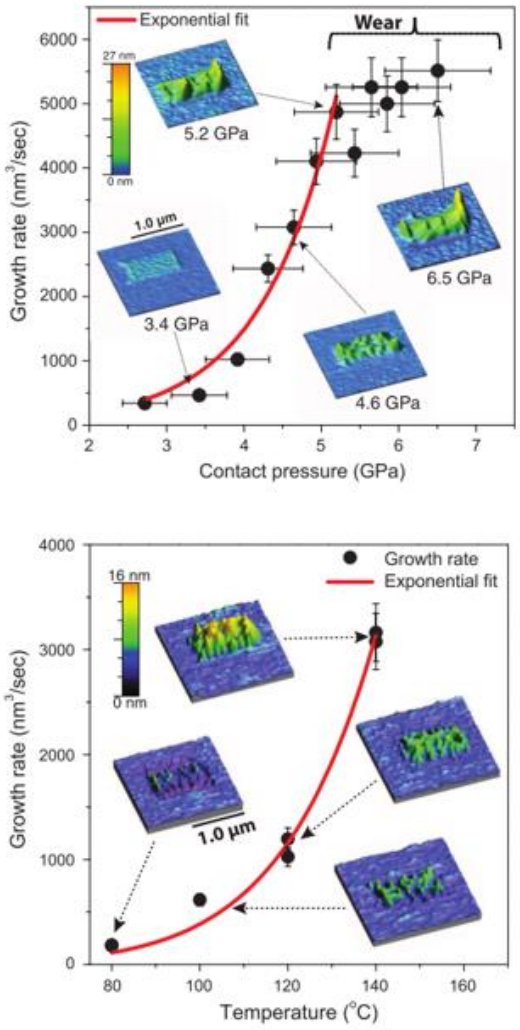

Figure 4-13: Graphs to determine the effect of contact pressure and temperature on tribofilm growth rate. The contact pressure test was conducted at 100°C and the temperature test was conducted at an initial contact pressure of ~4.4GPa [3]***.***

Another study, by Ghanbarzadeh et al [6], compared an analytical wear model (that takes into consideration the alterations to the Archard's wear law caused by the presence of a ZDDP tribofilm) to experimental results, obtained using an MTM SLIM. A component of these results included comparing the tribofilm thickness formed in tests of differing durations. These results are summarised in Figure 4-14, it can be seen that the tribofilm thickness has stabilised in each test by 30 minutes; however, most MTM tests occur over a time span of at least 2 hours [82–84]. This stabilised thickness supports the MTM SLIM observations reported by Naveira-Suarez et al [68]; however, this may simply be due to the same in-situ observation technique being employed in the validation of the analytical model.

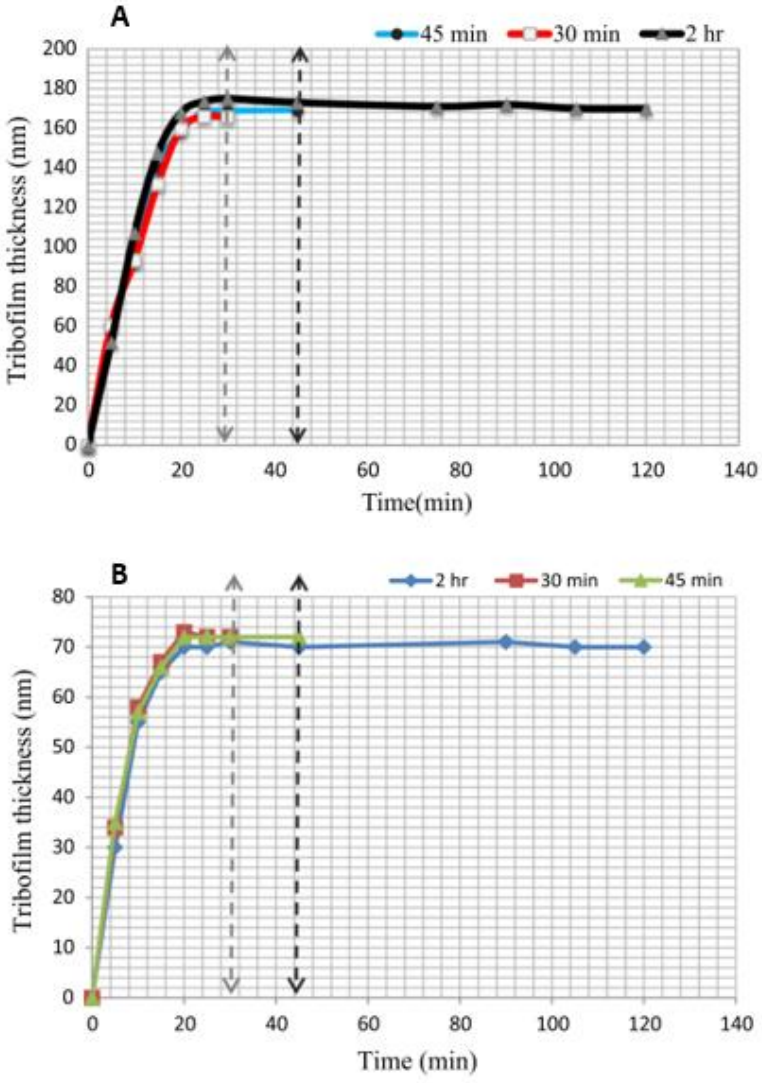

Figure 4-14: Tribofilm thickness against time for different test durations. (A) test conducted at 100°C, (B) test conducted at 60°C [6]***.***

Building on the work conducted within the Ghanbarzadeh et al study [6], Parsaeian et al [85] investigated the effect of water on formation of ZDDP tribofilms, and the efficacy of the films. This study used the analytical model validated in the previous work as well as new experimental tests, also conducted using an MTM SLIM. Some of their results, specifically those related to tribofilm thickness, are shown in Figure 4-15. It can be seen that the effect of water contamination reduces the tribofilm thickness and thus the durability and stability of the film. It is also clear that the effect of water increases over time, with the tribofilms peaking in thickness between 40 and 80 minutes at 80°C and between 30 and 50 minutes at 100°C.

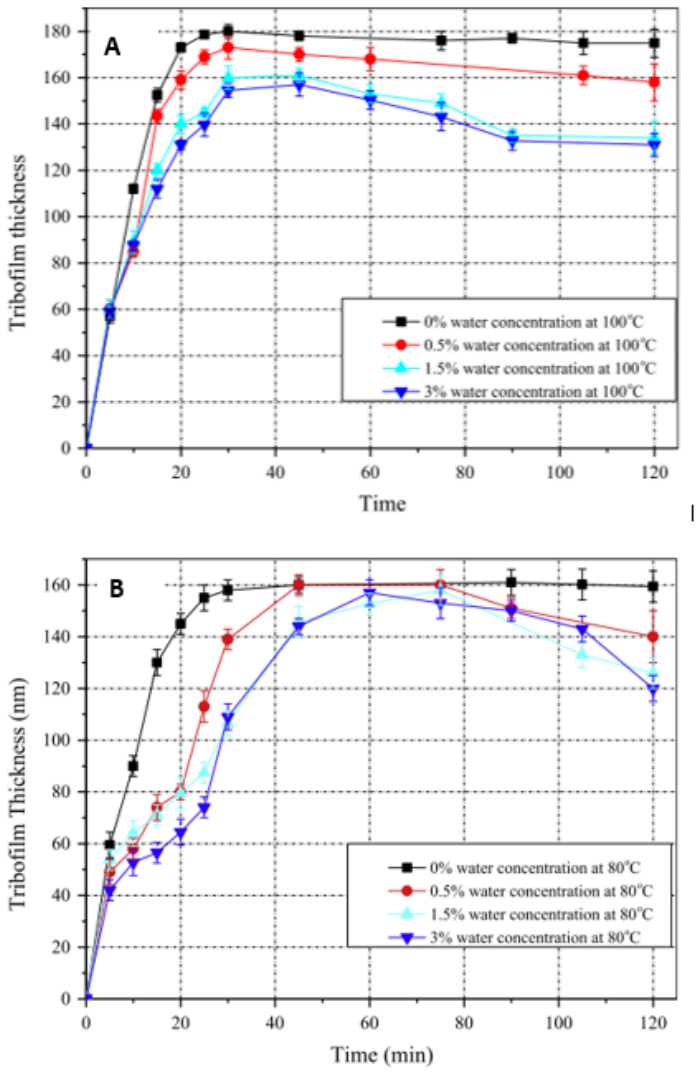

Figure 4-15: Tribofilm thickness measurements with varying water concentrations. (A) test was conducted at 100°C (B) test was conducted at 80°C [85]***.***

Both the Ghanbarzadeh et al [6] and Parsaeian et al [85] studies are validated against a single value of thickness, determined from the spacer layer interferometer. The SLIM attachment is only capable of observing the topography of the region of the ball that is pressed against the glass lens, which can only be considered a snapshot of the topography on the countersurface. In addition, an assumption is made that the topography on both the flat disc and the curved ball are comparable, which indicates that the topography would not be dependent on the contact geometry. This assumption is inherently flawed, as the radius of the two surfaces is considered important in determining the minimum film thickness and thus the extent of the asperity contacts and, therefore, cannot be callously ignored.

4.6 Environmental Concerns

It has been well documented in the literature that the decomposition of ZDDP can detrimentally affect the function of catalytic converters [77,86,87]. The washcoat of a catalytic converter is a carrier for the catalytic materials; it has a mottled surface to increase the surface area and to maximise the emission reduction. The tribo-induced breakdown of ZDDP into its constituent elements (or more stable associated compounds) can cause absorption, as shown in Figure 4-16, of crystalline Zinc, Calcium and Magnesium phosphates onto the washcoat surface, as well as Aluminium phosphate inside the washcoat. There is also possible evidence of cerium (III) phosphates in the washcoat layer as well as the phosphorus compounds which further decreases the effectiveness of the catalyst [88].

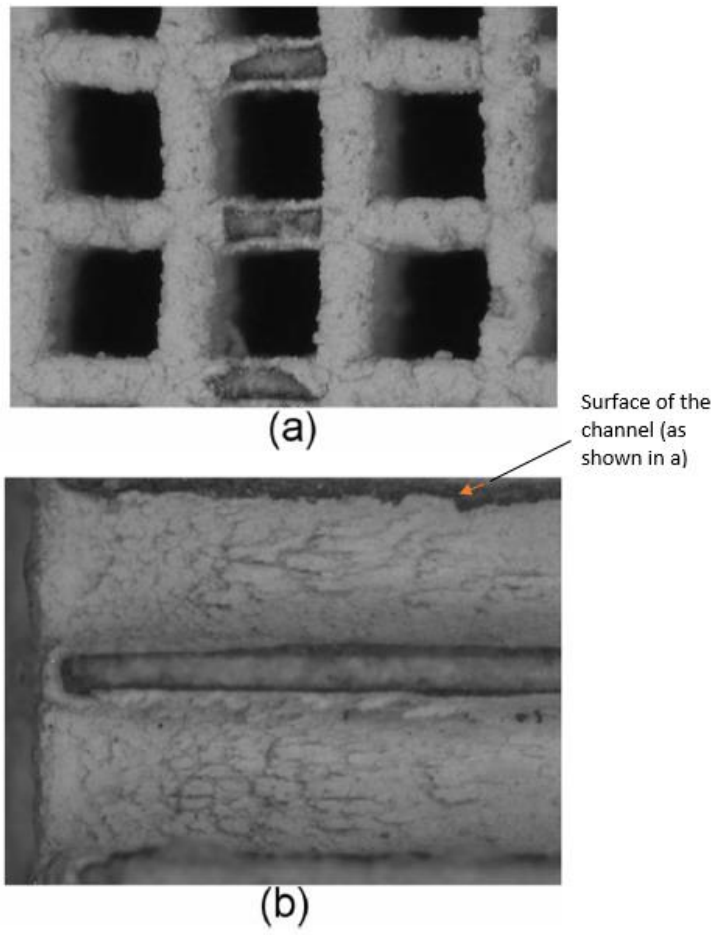

Figure 4-16: Low power optical images of the inlet section of an unaged catalytic converter (a) and the cleaved section along the length of the channels (b) [88]***.***

An increased phosphorus build-up negatively affects the functionality of the catalytic converter with the toxic overlayer specifically preventing the exhaust compounds reacting with the catalyst. This means that the reduction and oxidation reactions needed to breakdown exhaust compounds, such as Nitrous Oxide (NO) into Nitrogen (N_2) and Oxygen (O_2), do not occur. This results in harmful chemicals, including NO and Carbon Monoxide (chemically noted as CO), being released into the atmosphere [87,89]. These chemicals have been shown to be harmful, both to humans [1] and the environment. An ongoing initiative attempts to control the quantities of these harmful chemicals, making catalytic converters a legal requirement in cars produced in Europe, since the Euro 1 legislation was created in 1992 [90]. However, the current Euro 6 legislation further reduces the permissible amount of released exhaust emissions, necessitating the need for a further improvement in the efficacy of catalytic converters [1,2].

The presence of phosphorus has been demonstrated to cause a reduction in the efficiency of the catalytic converters and, therefore, as part of the ongoing effort to further improve this efficiency it is vital that phosphorus be removed from the engine [4]. In order to remove the phosphorus an improved understanding of the behaviour of ZDDP is required, with the ultimate intention of synthesising a non-phosphorus containing additive to replace it.

4.7 Summary of ZDDP focussed Literature

Numerous papers have been presented that demonstrate the state-of-the-art understanding of ZDDP tribofilms. These have shown that whilst extensive work has been conducted to determine the means by which ZDDP tribofilms are formed and how they function under different scenarios there is still much work to be conducted [3–5].

The chemical structure of ZDDP molecules varies depending on the process used to synthesise them and this has been shown to affect the topography of the resultant tribofilm [8]. Therefore, the specific formulation of the additive to be used in this research activity will be an overbased primary ZDDP, provided by (and at the suggestion of) Afton Chemical. This has been recommended as it is being used extensively within the British automotive industry and provides a “middle of the road” performance, being worse than a secondary alkyl ZDDP but better than an aryl ZDDP.

The use of AFM, and related technologies, has been found to be much utilised in determining the mechanical properties and morphology of ZDDP tribofilms; however, the morphology is often considered to be a secondary analysis [91]. This indicates the relevance of using such techniques to better understand these tribofilms. Work conducted to determine the mechanical properties of a ZDDP tribofilm showed that scanning force microscopy could even be used to machine a tribofilm [75] but did not present a comprehensive overview of the tribofilm topography, even stating that care was taken to select ideal portions of the topography. This indicates that whilst much work has been conducted that considers the morphology of ZDDP tribofilms no research has been conducted to confirm fundamental assumptions, such as determining whether the topography is uniform, this will be a consideration in the current research activity.

ZDDP tribofilms have been generated and analysed in-situ using both MTM SLIMs and AFMs; however, these studies have focussed on the thickness of the tribofilm and the effect

of altering test conditions on the rate of formation [3,69]. In most of these studies the evolution of the tribofilm has been considered separately from the more fundamental pad morphology, with research using the MTM SLIM relying on the presence of pads to confirm the complete coverage of the surface imaged, with a tribofilm, but with no reference to the specific pad structure itself. Work conducted by Gosvami et al [3] actually demonstrated the non-uniformity of the tribofilm topography, with a notable difference in pad thickness towards the end of the reciprocating stroke, but did not make this the subject of the study, nor has it been considered in any subsequent papers [7]go.

The state-of-the-art understanding of the evolution of ZDDP tribofilms has advanced using techniques that rely on the tribofilm topography; however, no studies have been focussed entirely on this feature, leaving fundamental question still unanswered. The current work will focus entirely on the morphology (both topography and manipulability) of ZDDP tribofilms to further advance this understanding.

Chapter 5: Literature Review of Atomic Force Microscopy

Atomic force microscopy has been used in tribology for many years and has been considered "...the most widely used tool for nanoscale single-asperity studies" [92]. It was initially proposed by Binnig and Quate [93] as an improvement on the scanning capacitance microscope proposed by Matey and Blanc [94]. Advances in the use of atomic force microscopy include Gosvami et al's [3] work in in-situ tribofilm analysis and by Oblak et al, who used AFM to thoroughly characterise tribofilms formed on a DLC coating [70].

This chapter provides details of how to use the AFM as well as instances when it has been used within the literature. The AFM is used extensively in biology and so reference is made to studies from other disciplines in order to show the versatility of the apparatus and to facilitate cross-pollination between these fields.

5.1 Background and Functions

AFMs have been well utilised as means of taking topography images on the nanometre scale [93,95]. This means that the topography images taken using the AFM have the highest resolution of all the possible topography methods available. However, the current state of the art and advanced models are capable of many other functions [59].

The AFM requires a small cantilever, approximately 100µm in length, that has a very small tip attached to the end, often made from silicon and approximately 10nm in length shown in Figure 5-1 [59]. This cantilever is controlled using a piezoelectric method and has to be carefully maintained. The cantilever is deflected towards the surface and the piezoelectric system is aided by the natural attraction of the tip to the surface. Once contact has been made the interaction forces become repulsive, as the weak Van der Waals forces are less than the repulsive Coulomb forces and thus the cantilever deflects back to a resting position. The piezoelectric system is able to measure the force distance curve required, an example is shown in Figure 5-2 [59]. The exact deflection is measured using a laser beam reflected off the end on the cantilever, above the tip, and a photodetector mounted within the AFM. The angle of deflection gives the height of the cantilever, and thus an accurate topography [59].

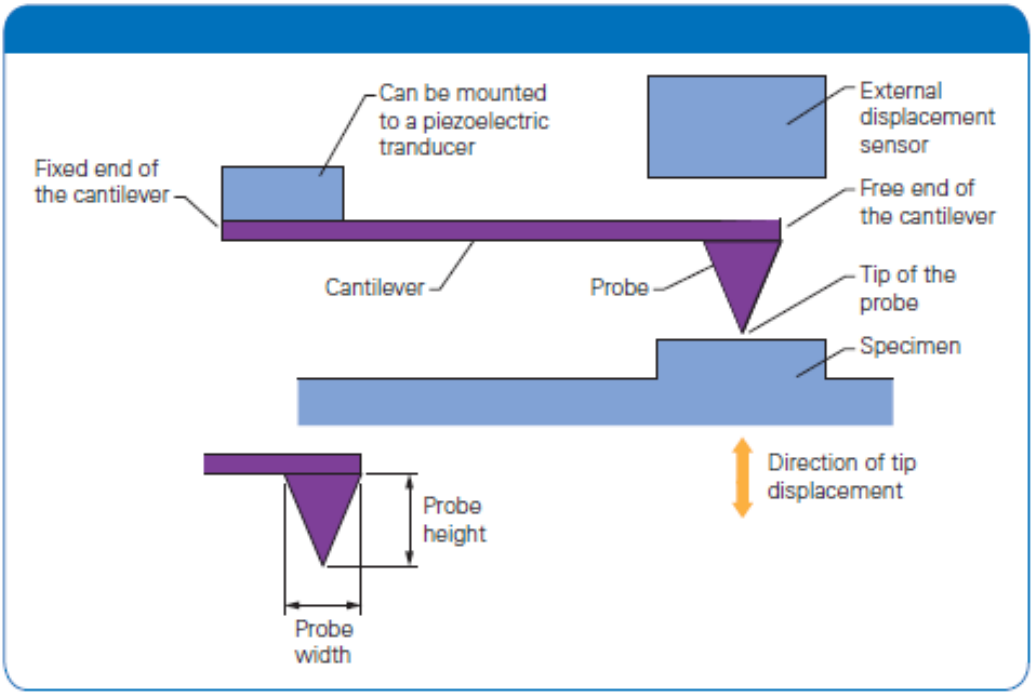

Figure 5-1: An annotated schematic of the cantilever system within an AFM [59]***.***

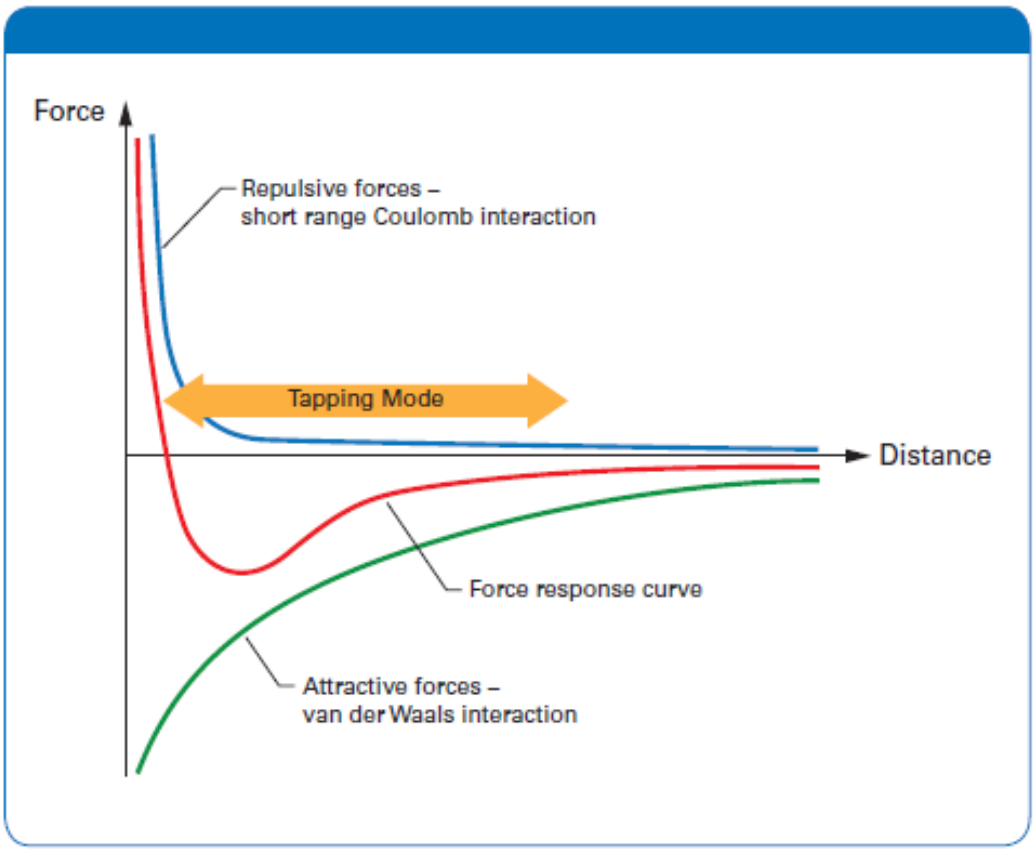

Figure 5-2: An annotated force distance curve to show the relative forces encountered by a cantilever during tapping mode [59]***.***

The piezoelectric system is governed by a feedback loop, which registers the laser deflection and adjusts the piezoelectric control of the cantilever accordingly. This system has to be carefully maintained, as any damage to the control system will result in a weakened feedback loop and the accuracy of the AFM will be affected [59,96].

There are two traditional and one relatively novel method for using the AFM. The traditional methods are the contact mode and the tapping mode, the novel mode is referred to as the peak force tapping mode. The contact mode, as the name suggests, involves constant contact between the tip and the surface. Tapping mode, which is the most common method for topography, involves a slight alteration of force and only short periods of direct contact. Peak force tapping mode is similar to tapping mode; however, the force is well below the resonant frequency of the cantilever, giving the operator more control over the system [59,97].

5.1.1 Contact Mode

As stated above the contact mode is aptly named, as the primary difference between this and other modes is that the tip remains in contact with the surface throughout the scanning. A fixed deflection of the cantilever is set, and this is maintained by the piezoelectric system. The tip is then moved in a raster motion, linearly, across the sample. This results in the tip being deflected, in a manner not controlled by the piezo electrics and the resultant laser deflection being different to the base line. It is then possible to create a three dimensional map of the surface, with the base line deflection used to zero the system [59].

An unfortunate consequence of the constant contact is that the tip experiences high lateral forces during motion. This can cause damage both to the sample and to the tip. It can also cause erroneous data if used with loosely bonded surfaces, such as removing elements of the tribofilm. A combination of these issues could result in the cantilever becoming misaligned (twisted) and base line value altering during a scan [59].

5.1.2 Tapping Mode

Tapping mode is similar to contact mode, in that it still forms contact with the surface; however, to reduce the effects of the lateral forces the contact is of short duration and also discrete. This means that the cantilever is moved laterally a small amount whilst the tip is not in contact with the surface, and then contact is resumed. A benefit of this method is that the lateral forces are limited; however, the tapping is conducted at a near resonant frequency, resulting in an unstable system. The force curve shown in Figure 5-2 is representative of the system; however, there is no means of determining a truly quantitative force measure for each interaction. It is possible to calculate an average value, as is shown in Figure 5-2, this is sufficient for high resolution topography images; however, it is insufficient for mechanical property determination [59].

Other issues with the tapping mode include that the amplitude must be set to guarantee clearance of all the peaks, which is difficult to determine prior to testing, and thus incorrectly assessed amplitude values are a leading cause of tip damage. This is also possible in cases where there is high surface flexibility and adhesion. If the surface adheres to the tip, the contact may not be broken when the amplitude is set too low [59].

5.1.3 Peak Force Tapping Mode

Therefore, whilst the tapping mode is less affected by the lateral forces, and thus could be perceived as better than the contact mode, the effects of the near resonant frequency could damage the feedback system, which would not be the case in contact mode. If these were the only two operating options available the mechanical properties of a tribofilm could not be determined; however, the peak force tapping mode is a more novel technique that has been developed. Peak force tapping mode combines the low lateral forces of the tapping mode with the high force control of the contact mode [59].

The primary difference between the force control curves in the contact and peak force tapping modes, is that the triangular curve in the contact mode is softened into a sine curve in peak force tapping. The system also resonates at frequencies far below the resonant frequency, resulting in a more accurate system due to the reduction in the instability of the controls [59].

An additional benefit of the peak force tapping mode is that the AFM is able to determine the peak force on a case by case basis. There is no fixed force that the contact must produce to initiate retraction. In standard tapping mode once the contact has been initiated the force continues to ramp until such time as a pre-set force is reached, this means that regions of softer material within the sample area may be plastically deformed during contact, resulting in a less accurate result. In the peak force tapping mode the peak force is decided for each contact, internally by the control system. Resulting in a more reliably accurate topography result. This method also increases the resolution of the force curves, which enables the systems use in mechanical property determinations [59].

For the Bruker Dimension Icon, it is possible to couple peak force tapping mode with the proprietary Scan Asyst function. This function minimises errors within the feedback loop of the peak force mode and ensures high-quality image resolution, without additional operator input. The function detects feedback oscillations and adjusts the gain to compensate. This is an improvement over traditional AFM techniques, which use a single gain value for an entire scan, independent of the localised surface topography [59].

5.2 General Uses

Atomic force microscopy is much utilised across the sciences, from cell topography to tribofilm characterisation. It is necessary to continue advancing our understanding of how the AFM can be applied in order to advance all disciplines. The biological applications have been studied to provide a complete understanding of the methodologies used with AFM.

5.2.1 Biology

AFM is much applied in biology for determining the topography of in-vitro cells. These are imaged either in solution (aqueous or not) or dry [98]. By utilising AFM to investigate cell morphology, biological researchers have been able to detect discrepancies between malignant tissue transformation (initial cancer formation) and healthy control tissue [99]; however, a limitation of the technique has been identified. This limitation is related to the soft and delicate nature of living cells and the ease by which damage can be caused when using a scanning probe [98].

Guz et al [99] comprehensively describe the types of analysis, in biology, for which AFM has been deemed suitable. They specifically refer to the use of AFM to determine the mechanical properties of cells, which can then be utilised in the identification and diagnosis of disease. The use of AFM to investigate the cell morphology and the adhesion (caused by alterations in the cytoskeleton and extracellular matrix) has been theorised for use in identifying differences between healthy, precancerous and cancerous cells. Some typical results of this analysis are shown in Figure 5-3 [99]. From this it can be seen that clear AFM images can be taken of cells, and that there is a distinct difference (in all three parameters) between normal, immortal (precancerous) and cancerous cells. They then utilised fractal dimensions to determine a more quantitative difference between the results [100].

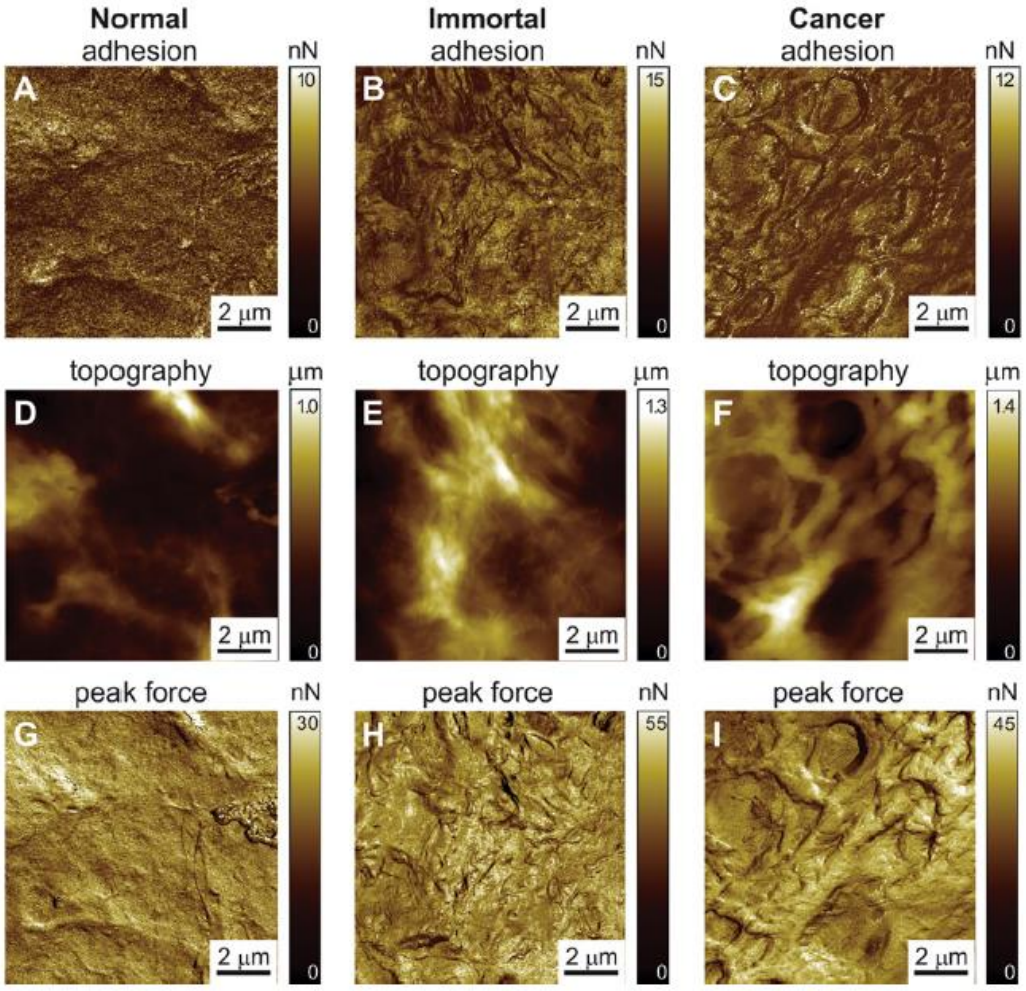

Figure 5-3: 2D AFM 10µm x 10µm images to compare normal, immortal and cancerous cells [99]**.**

The above figure shows the clarity of the images obtained using AFM; however, another paper describes AFM as being too slow and the cell morphology changing during the acquisition time [101]. The advances in using the AFM to image and characterise biological samples were improved by the arrival of the peak force tapping technology. This was designed and optimised for use in biology but can be applied to image any surface.

5.2.2 Tribology

AFM use in tribology has traditionally been focussed on tribofilm characterisation; specifically, topography and thickness. However, many studies have also been conducted investigating the lateral force of tribofilms and several have been conducted using the AFM to determine the hardness and Young's modulus [70,75,102].

Lateral force microscopy is commonly used both to determine the small scale morphology, as a typical AFM, and to investigate the interfacial forces [103]. Lateral force is found using a contact mode scanning method to create a hysteresis loop, as in Figure 5-4b. The quantity shown as ΔV_L is proportional to the friction; however, the exact relationship is dependent on the system and the calibration. Lateral force can also be coupled with topography, to provide an increased understanding of a surface [104].

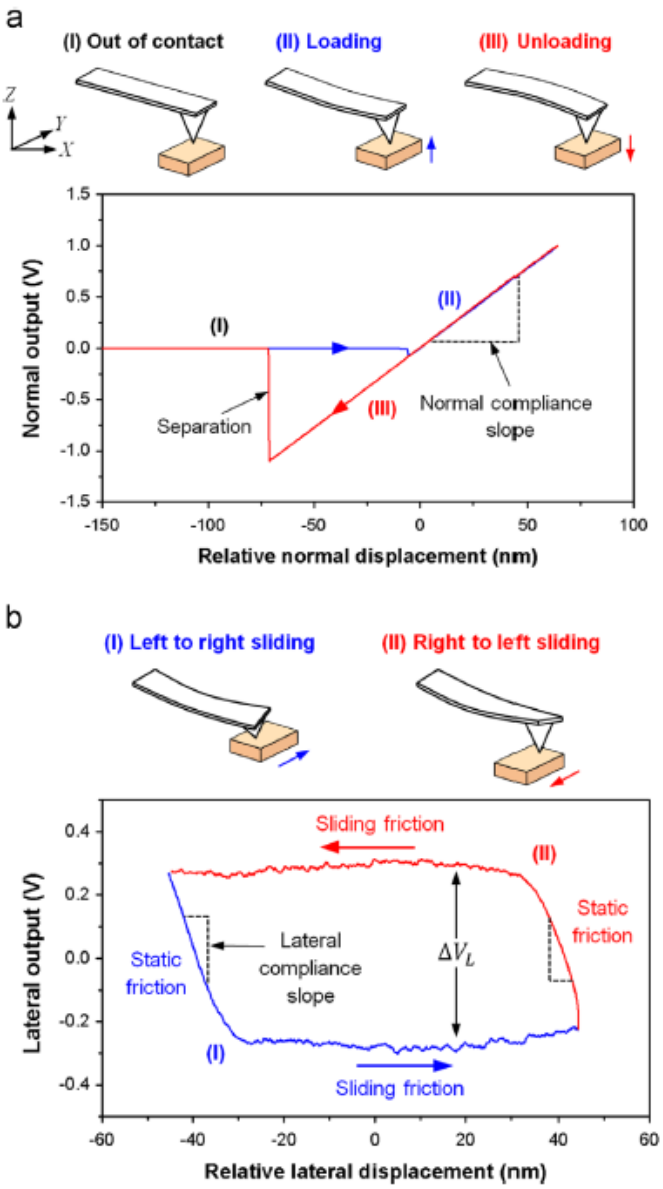

Figure 5-4: Graphs and cantilever position schematics to compare tapping (a) and contact mode (b) AFM [104]***.***

Lateral force calibration is inherently difficult and there are many different methods for calculating this, a paper by Khac and Chung [104] includes a summary of these. The two methods most easily implemented are from Le et al [105] (a diamagnetic levitation spring system) and Varenberg et al [106] (wedge calibration method).

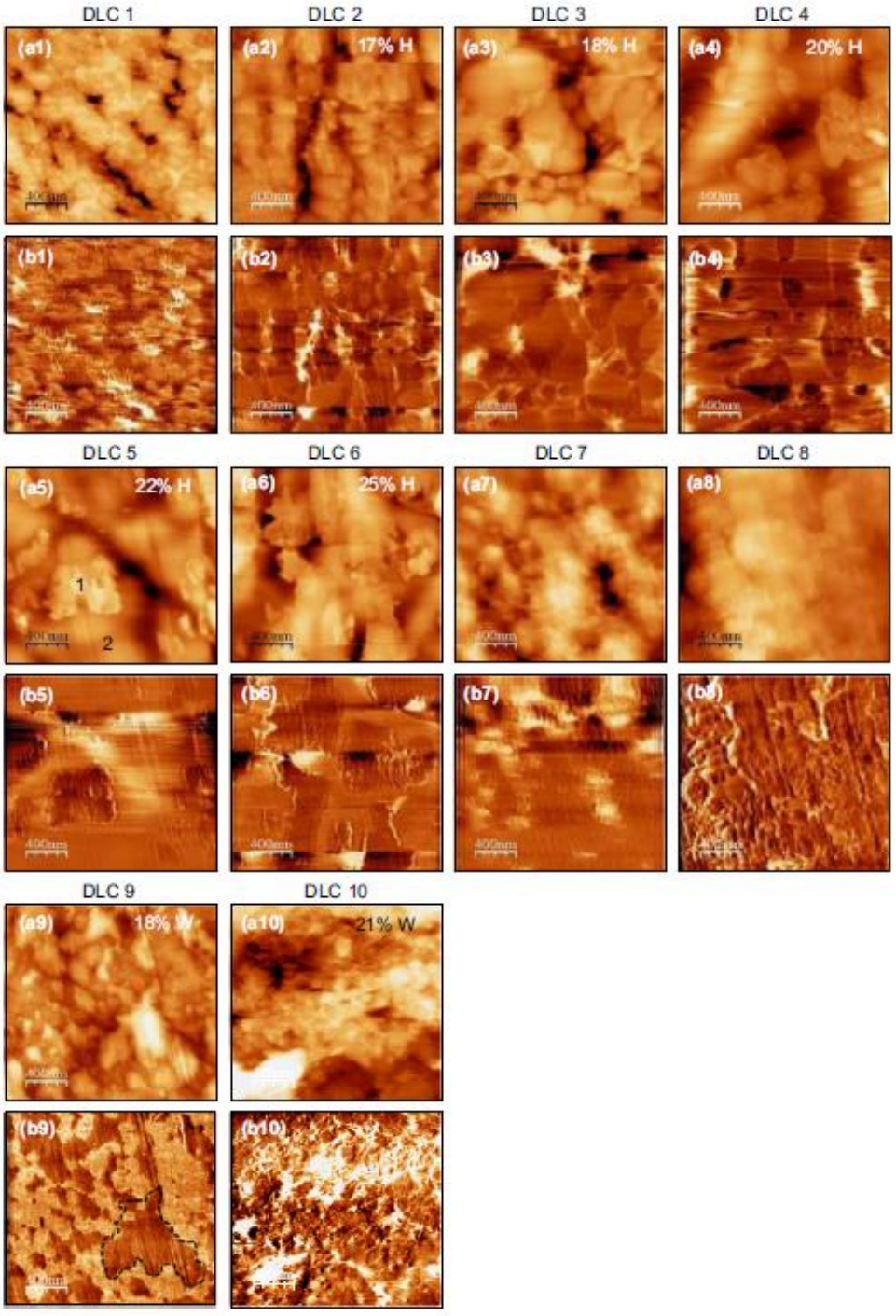

Figure 5-5: 2µm x 2µm AFM topography (a) and lateral force (b) images of different DLC surfaces after 2hr of rubbing in ZDDP solution [82]***.***

Examples of lateral force images, as taken by the AFM, [82] are shown in Figure 5-5 (the sections marked as b). It can be seen that there is an increased amount of error in these images which is due to the increased sensitivity and resolution. In these images the lighter sections correspond to areas of higher lateral force (as is typical for AFM scales) and usually correspond to areas with low topography. For DLC 8 it can been seen that the lateral force image gives a clearer idea of the potential pads forming, when compared to the topography image for the same sample. This may be due to the topography appearing as one consistent pad but the lateral force being more distinct.

Whilst the lateral force is able to provide additional information about the tribofilm, the combination of the difficulties in accurately calibrating the system and the increased risk of damage to the analysis machine mean that this technique is less routinely used. The bespoke nature of lateral force analyses (specifically the calibration) mean that this technique would not be well suited to the current activity as any proposed methodology for tribofilm durability is intended to be repeatable and to make use of commercially available pieces of kit, namely the Bruker Dimension Icon.

5.3 Use in Tribofilm Characterisation

Having considered the general applications of AFM in tribology a more detailed investigation will now be completed to determine the extent to which certain aspects of tribofilm characterisation have been previously attempted.

5.3.1 Topography of a tribofilm

AFM has long been established as an ideal method for analysing surface topography. The nanometre resolution makes it ideal for accurate thin film analysis. In tribology it has been much utilised for analysis of the tribofilm, with some studies even succeeding in analysing the topography during different stages of the film production [3].

Studies which have used AFM topography as an ex-situ analysis include Burkinshaw et al [107] and Tasdemir et al [108]. In both studies the AFM was used to see the tribofilm at a higher resolution. In Burkinshaw et al they compared the AFM topography images with SEM images, as shown in Figure 5-6, and mass spectrometry images. These show that for a similar magnification the resolution of the AFM provides a clearer image than the SEM; however, the SEM is capable of performing EDS and thus may be more useful in some instances.

This study [107] demonstrated that the AFM is capable of producing topographic analyses of ZDDP tribofilms; however, this was not the focus of the study and no additional information (such as the relative location of the scan) was provided. In addition, the surface scans of the tribofilms appeared to show very small pads (which may have been elongated in the scan direction, although this information was also not provided) with clear gaps between them. This is not the topography that has been demonstrated in the previous work by Graham et al [73], further supporting that the topography of a tribofilm can vary, even within a single sample.

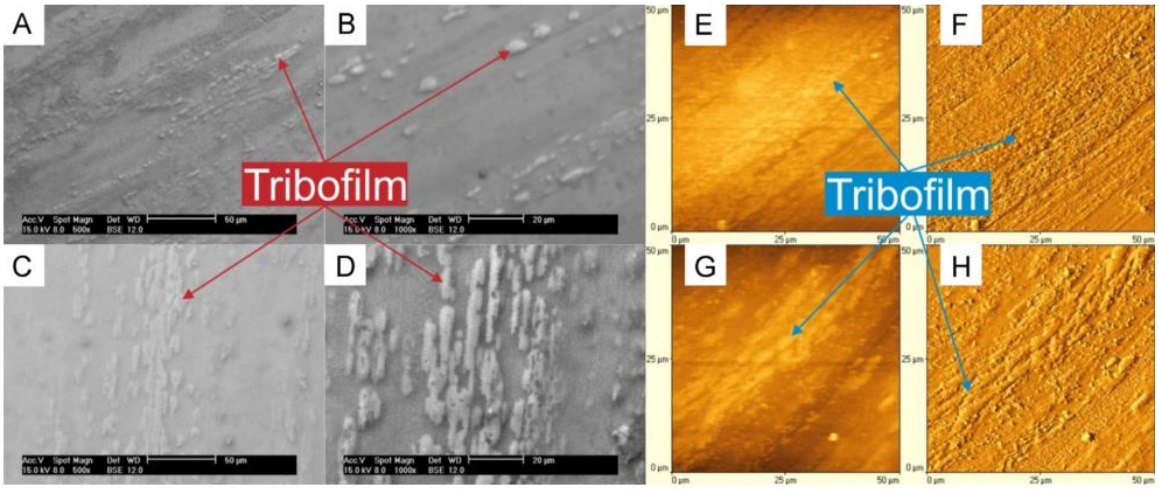

Figure 5-6: "SEM (A and B) and AFM (E and F) images of a silicon crystal lubricated with ZDDP, SEM (C and D) and AFM (G and H) images of silicon crystal lubricated with ZDDP + an Organic Antiwear Additive" [107]***.***

Tasdemir et al [108] compared the topography and lateral force, amongst other things, of ZDDP tribofilms formed on various types of DLC coatings. It can be seen that there are clear topography images; however, there are noticeable errors on the lateral force images. There are small pads apparent on the topography image (a) which indicate potential phosphate pads, these correspond with areas of increased lateral force. However, there is no similar increase in lateral force for the peak identified in topography (e). This may indicate that the peak in the topography is a particle or other artefact on the surface, which will have influenced the scale of that topography.

This study [108] shows, again, the difficulties in using lateral force microscopy, with obvious artefacts present in several of the scans. The more important observation is the apparent presence of the phosphate pads within the tribofilm, with some being validated by the lateral force analyses and others negated. This study again presents a single scan location and posits that the different substrates result in different tribofilms, this ignores the possibility that the tribofilm morphology may naturally vary from test to test, and indeed within tests.

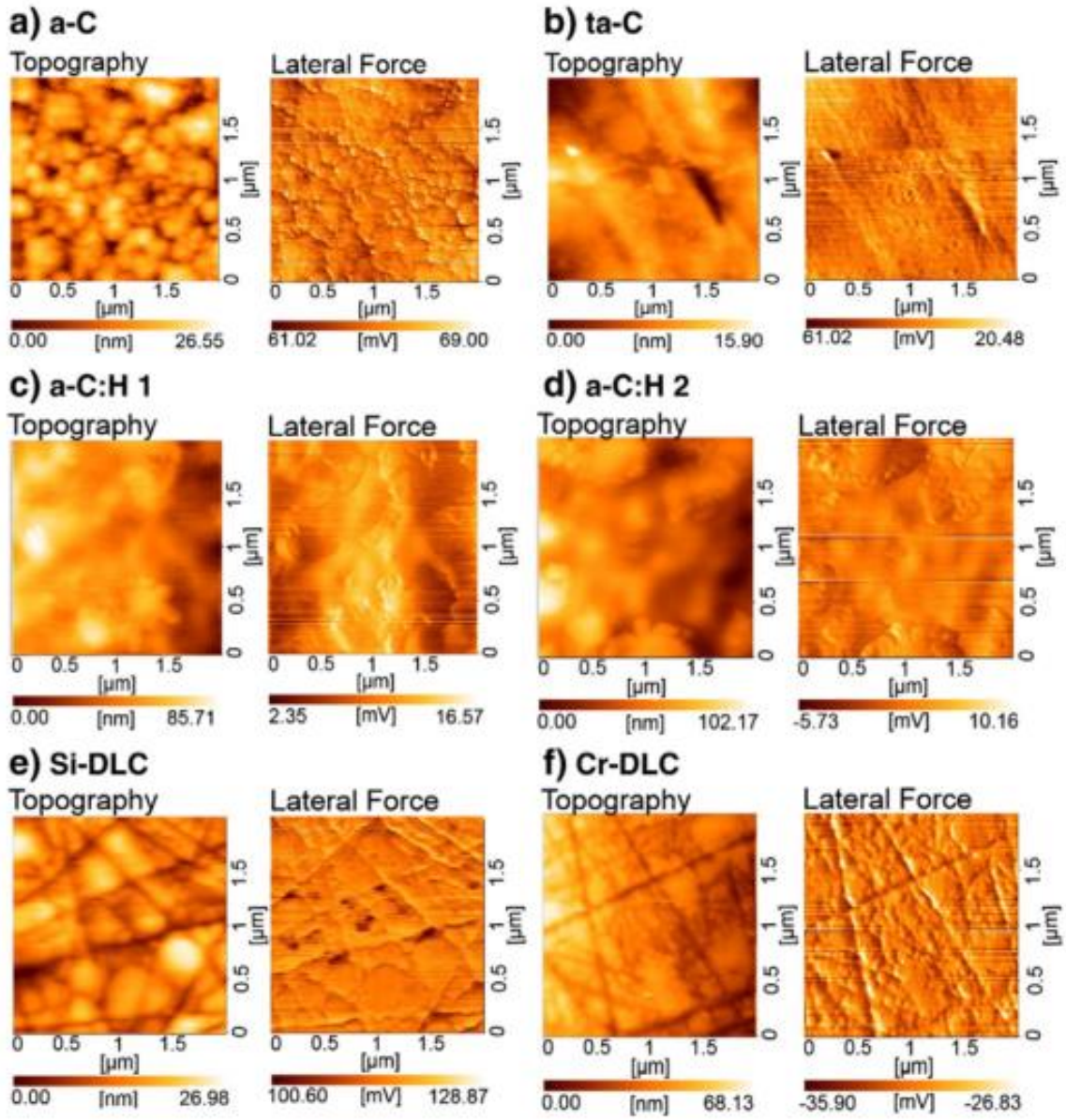

Figure 5-7: AFM topography (left) and lateral force (right) images for different DLC surfaces after two hours of rubbing in a ZDDP solution [108]**.**

Ozkan et al [109], also used AFM topography images. They used AFM to expand on chemical analysis, which was conducted at a lower resolution, to better characterise the tribofilm. They presented the results as a comparison between optical microscopy, AFM topography (in both two dimensions and in three) and a cross-section, as shown in Figure 5-8. The investigation aimed to determine the efficacy of a protective additive layer for use with an engine cylinder. The AFM topography results were used to validate the SEM results as well as to determine the width and depth of the wear scar.

The study by Ozkan et al [109] demonstrates the use of AFM as a secondary analysis, in this case as a means of validating a primary analysis. They also show a single AFM topography image for a small section of the presented SEM image, making the assumption that the tribofilm will be uniform across the surface. The scan that has been shown is only 10µm by 10µm, which is smaller than the size most pads are assumed to be [4]. Therefore, it is not possible to confirm if the evident scratch has been created during the test, occuring on a forming or existing tribofilm, or if it was residual from the polishing technique, in which case there will be an absence of tribofilm to the sides of it.

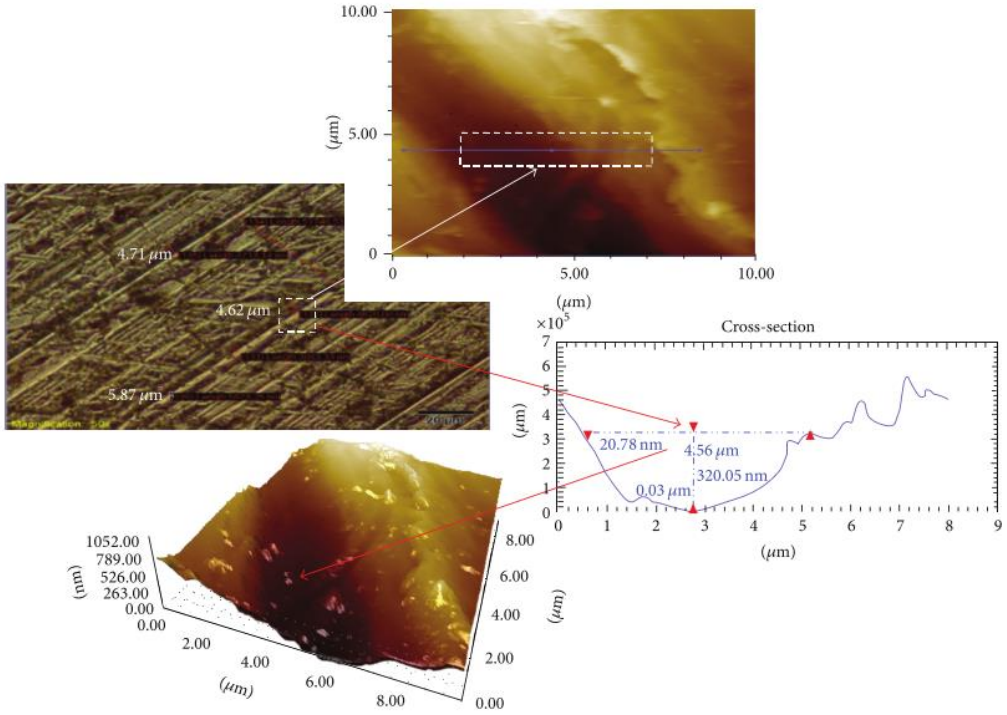

Figure 5-8: Optical microscopy and AFM topography images of honing marks of a new cylinder liner [109]**.**

5.3.2 Thickness of a tribofilm

The AFM has previously been used to determine the thickness of the tribofilm. The studies investigated used the same fundamental method, washing a portion of the surface with EthyleneDiamineTetraAcetic acid (EDTA) [102]. This compound is believed to remove the tribofilm phosphate pads, by breaking the covalent bonds between the steel and the initial layer of the tribofilm. This “bond breaking” process is caused by the chelation of the

tribofilm by the EDTA. EDTA is a chelator, which is designed to form coordination complexes with metal cations, specifically those with two or three electrons missing, such as Fe^{3+} and Zn^{2+}, both of which are present in a ZDDP tribofilm on a ferrous metal [102].

Topolovec-Miklozic et al [102], to this authors knowledge, developed this method (as no papers dated prior to this have been identified as using it) and Figure 5-9 shows that they have had a measure of success in utilising it for thickness measurements on the AFM. Once the tribofilm has been cleared this is shown by the darker brown patch in comparison to the tribofilm shown by the lighter yellow patches, as shown in Figure 5-9. Once the topography images have been taken a section was utilised in ten discrete locations and the height drop caused by the tribofilm removal was measured. The ten height drops were then averaged to determine the approximate tribofilm thickness.

This study does not assume a single location is representative of all tribofilms, with several topography scans included within the wider analyses. However, there is no indication that care was taken to monitor the specific locations of these scans within the wider tribofilm nor is it apparent if the four presented scans were taken from the same tribofilm or from multiple repeats. In addition, an assumption is made that all of the tribofilm has been removed, despite the scan in the top right showing evidence of residual tribofilm even after cleaning.

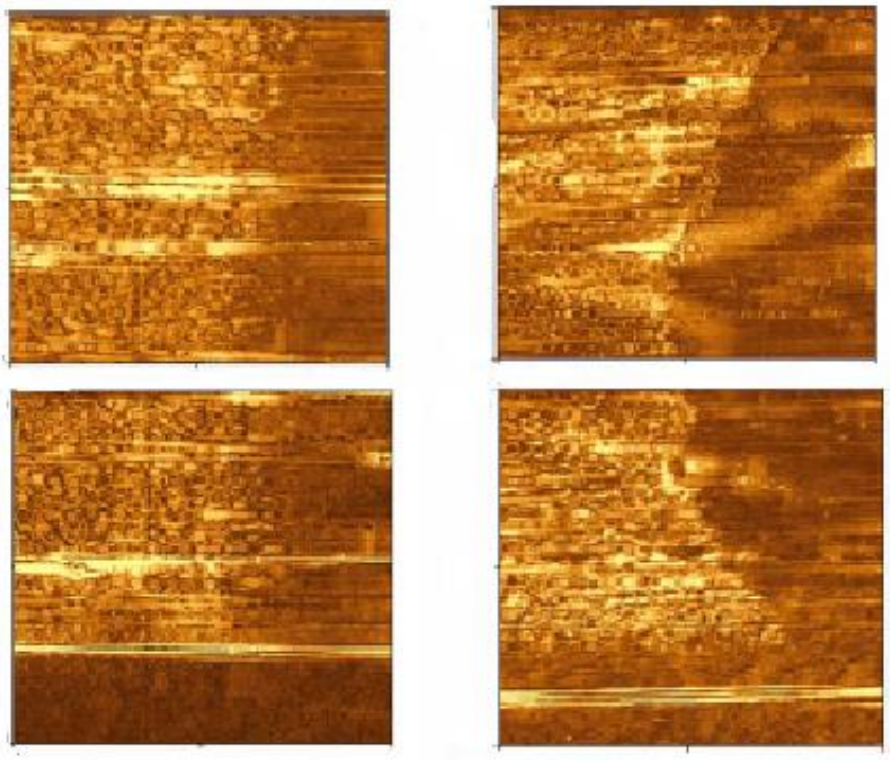

Figure 5-9: AFM images after partial cleaning with EDTA, originally published by Topolovec-Miklozic in Tribology Letters [102]**.**

The specific method involves using 0.05M of EDTA in distilled water pipetted onto the surface. This droplet was then left on the surface for 60 seconds, before being wiped off using a paper towel.

Other studies which have used this method include Burkinshaw et al [107] and Burkinshaw et al [110]. In both studies they use the exact method outlined above.

An alternative method, also conceived by Topolovec-Miklozic et al [111], is to assume that the thermal film, caused simply by the presence of the hot oil and not a product of the tribofilm [3], is not present at the end of the test, once the sample has cooled and been washed in hexadecane. This then enables the edge of the wear track to be used as a height drop at the edge of the tribofilm, as in Figure 5-10. Another, potentially more important, assumption of this method is that the additive, in this case calcium carbonate, has been completely effective as an anti-wear additive [111].

The assumption that there is no thermal film present is extremely flawed with several papers showing that any steel heated in the presence of ZDDP will form at least a minimal thermal film [72]. The invalidity of this assumption is further supported by the presented cross-section, with some rounded surface features being present outside of the wear scar, this would not be the case for a polished surface in the absence of a thermal film. The assumption that no wear occurs outside of the wear scar is more acceptable, as long as care is taken to ensure the true width of the wear scar is considered, as appears to have been the case for this work [111].

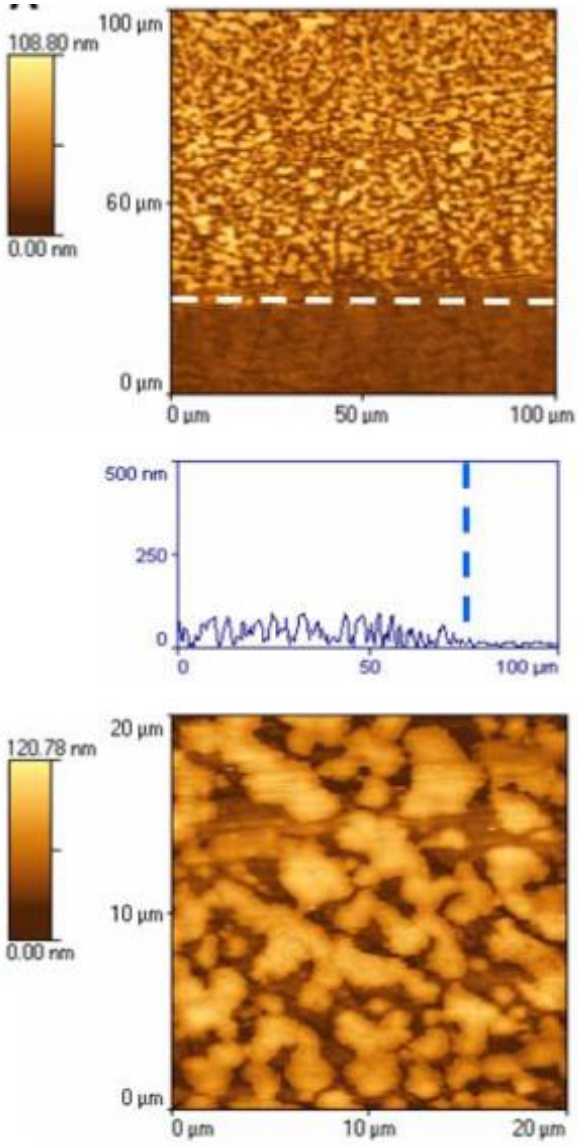

Figure 5-10: AFM topography images and a profile for a detergent film formed in a 2hr test. The region beneath the line in the top image is outside of the wear scar. The profile has been taken from the top to the bottom of the image at the top [111]***.***

5.4 In-Situ Testing of Tribofilms

Gosvami et al [3] showed that it was possible to generate ZDDP tribofilms in-situ, using the AFM. The study used a DLC coated silicon AFM tip immersed in 100°C ZDDP containing oil, sliding across a 2µm x 2µm area, whilst loaded to 100nN. The resultant tribofilms were 36nm in height at the ends of the reciprocating stroke, after 6500 sliding cycles (Figure 5-11). The same study [3] also determined that an increase in contact pressure resulted in an increase in tribofilm growth rate, as did an increase in oil temperature.

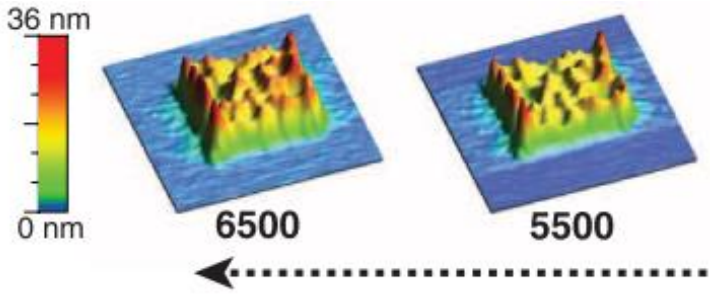

Figure 5-11: Tribofilm growth with sliding cycles [3]**.**

A subsequent study, also by Gosvami et al [7], used a multi-asperity probe, to more accurately represent a tribological contact, instead of a sharp tip. The multi-asperity probe was created by adhering a steel colloid to the end of the cantilever, alongside the existing sharp tip. The experimental set up allowed for repeatable scan locations, even when replacing the modified cantilever with a traditional sharp asperity tip to accurately image the resultant tribofilm formation. The test set up used is shown in Figure 5-12 and used both a commercially available AFM and commercial cantilevers.

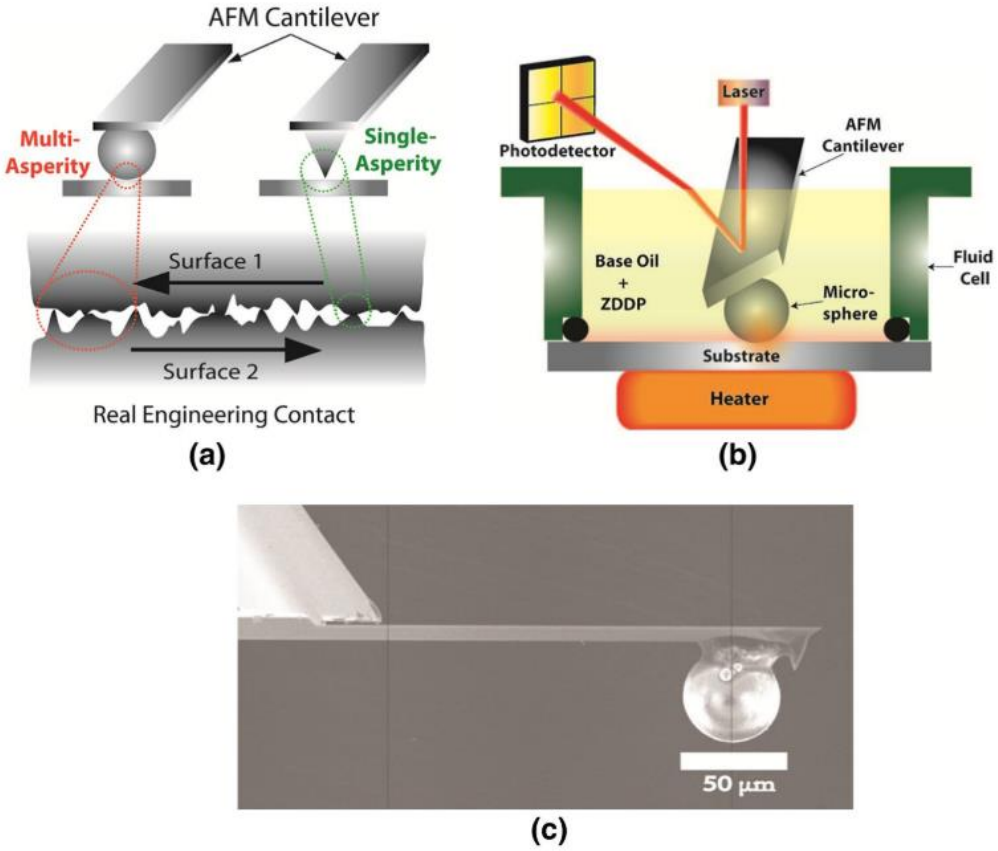

Figure 5-12: (a) The difference between a multi-asperity probe and a sharp tip (b) the test set up used to generate the tribofilms (c) an SEM image of the modified probe [7]**.**

Gosvami et al [7] describe the method used to accurately calibrate the frictional force for the modified probe, when used in lateral force mode. The paper then demonstrates that the modified probe provides similar initial topography image resolution as a more traditional tip. The dual-probe method presented (to use a modified multi-asperity colloid probe to generate tribofilms and a sharp tip to analyse the topography) reveals an increased resolution of the formed tribofilm, when analysed with the sharp tip, as opposed to the colloid, Figure 5-13. This indicates that the specific tribofilm features (pads) are smaller in magnitude than the initial topography features (surface scratches).

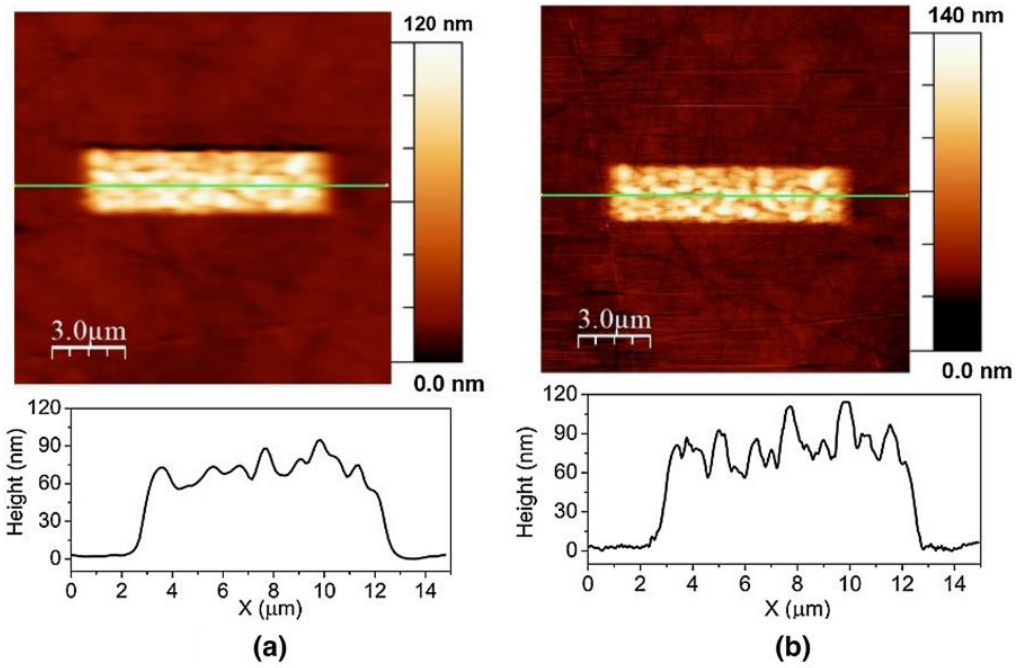

Figure 5-13: (a) The tribofilm, as imaged using the multi-asperity colloidal probe, (b) the tribofilm, as imaged using a sharp tip [7]***.***

The authors of this study [7] note that limitations of using the AFM in this manner include the slow sliding speeds, which are in the order of a few µm/s, and the small contact size. The multi-asperity probe, whilst providing a more realistic representative contact surface, is still orders of magnitude different to a component level application.

Both of the studies by Gosvami et al [3,7] demonstrate the versatility of the AFM as well as its capability in generating ZDDP tribofilms. The different methodologies employed for the two papers show that the AFM can be used in more varied manners and is robust enough to be used in conjunction with modified probes and in unintended contacts. These activities used either entirely bespoke or highly modified equipment, meaning these cannot be easily repeated; it is unknown, from this work, whether a commercially available AFM can also be used to manipulate or grow ZDDP tribofilms. Despite these studies having limitations, including the use of a bespoke AFM, the earlier of these activities (2015) was revolutionary in highlighting the increased capabilities of this technology, specifically within tribological studies.

Work by Dorgham et al [33,112] has shown that it is possible to also generate ZDDP and DDP tribofilms in situ in a commercially-available AFM, using “off-the-shelf” AFM probes (RTespa 300). The focus of this research was to determine the reaction kinetics for ZDDP tribofilms and to assess the dependence of these with the contact pressure and temperature. Figure 5-14 shows a schematic of the AFM set up used in Dorgham et al’s investigation, as well as representations of the growth mechanisms for the formation of ZDDP and DDP tribofilms.

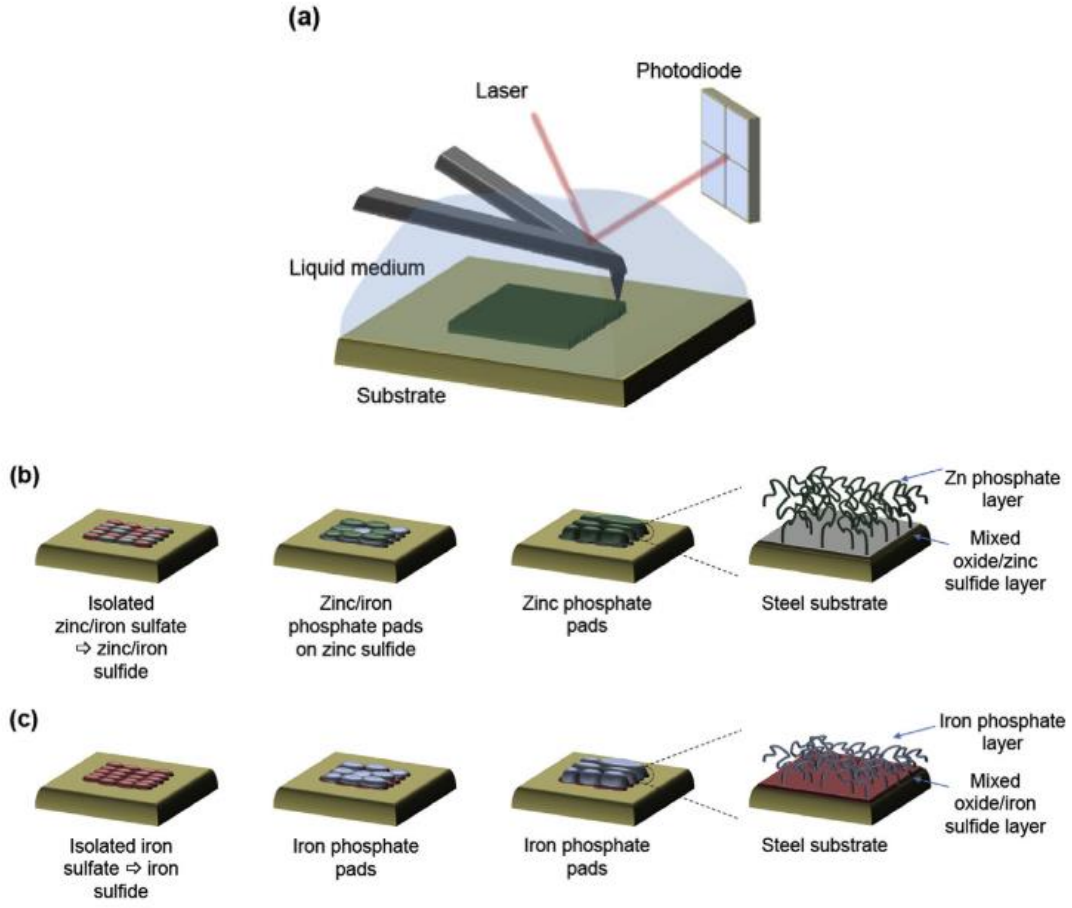

Figure 5-14: In-situ formation of ZDDP and DDP triboreactive films using single asperity AFM tests. a) The in-situ AFM setup, showing that the probe and steel substrate are fully submerged in oil, b) the growth steps of a ZDDP film, c) the growth steps of a DDP film [33]**.**

This activity [33] included an assessment of the wear behaviour of the AFM tip (which was a silicon variety, with a nominal initial radius of 8nm) by scanning a titanium substrate with a large roughness for different sliding distances. They observed that a large increase in

the tip radius (as a result of wear) can result in the flattening of rough features They conclude that the alteration to the tip results in an overestimation of any features with a size smaller than the tip radius. This research notes that the measured initial radius was approximately 15nm, almost double the nominal value, and rationalises this discrepancy as being a result of the initial tip engagement with the surface and the wear caused during the calibration of the cantilever deflection sensitivity. The maximum load applied to the tip was set to be greater than 150nN (which represented the larger normal loads experienced during in-situ tribofilm generation) for which the tip radius increased to approximately 80nm before achieving a steady state. After achieving steady state there appears to be no further increase in the tip radius. In addition to the maximum load, the minimum load was considered, representing the load applied through pure adhesion. This lower load also resulted in a steady state tip radius, however, at a value between 40nm and 50nm. For both loads (maximum and minimum) the tip radius steady state appears to have been reached after the first 50mm of sliding, with little effect caused by the subsequent 150mm.

This activity also presents some key observations of the growth of the tribofilm itself, with a note that tribofilms with a smoother surface displayed less evidence of experiencing sacrificial wear, compared to the rougher tribofilms. This is then expanded to indicate that the rougher the surface the faster the thickness growth occurs, suggesting that the rougher the tribofilm the more easily the remnant ZDDP molecules can be decomposed.

A related activity, also by Dorgham et al [113], refers to the concept of tribofilm growth using a single asperity mechanism (an AFM) as tribo-nanoprinting and indicates the potential use of this technique in further understanding tribofilms. Specifically, they demonstrate how controlled such a method is, presenting examples, such as Figure 5-15, where the tribofilm can be grown into recognisable shapes.

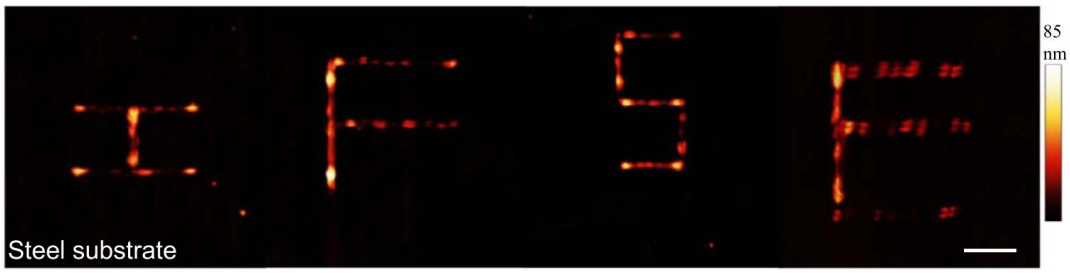

Figure 5-15: An example of the accuracy of in-situ tribofilm generation [113]**.**

The work conducted by Dorgham et al [25,104] has demonstrated that it is possible to replicate the in-situ growth of ZDDP tribofilms, previously demonstrated by Gosvami et al [3], using a commercially available AFM. They have shown that commercially available companion tips can be used, negating the need for customised tips, and have made assessments of the wear of these. The specific AFM used in their work is the same model that shall be used in the current research activity and the current work will also be utilising commercially available tips, therefore the characterisation work shall be considered when defining the test parameters.

The second of Dorgham et al's activities [113] highlighted the extent to which the AFM can be used to govern the formation of a tribofilm. This activity focussed on the triboprinting of the film onto a surface, resulting in recognisable patterns on the substrate. This indicates that the AFM can be considered to be more versatile than had been demonstrated in the work by Gosvami et al [7] and suggests that the technology could be used to manipulate a tribofilm in other manners, this was pivotal in the decision to ascertain whether an AFM can be used to assess the durability of a ZDDP tribofilm.

5.5 Summary of AFM focussed literature

There has been a lot of work conducted using the AFM, with many of the state-of-the-art technologies being dominant in the biological sciences community [100]. Advances include the initial addition of tapping mode, which reduces the amount of tip wear during testing and the subsequent invention of peak force tapping mode [59]. The latter is prevalent in the biological sciences as it can be employed to conduct high resolution topography scans on soft substrates, this technique can be translated for use in tribology to analyse soft tribofilms.

Work has been conducted to use the AFM to analyse tribofilms, with a focus on determining the specific surface morphology (using both lateral force microscopy and more traditional topography scans) and the tribofilm thickness [8,102]. A key limitation in much of the previous work is the assumption that a single location can be considered to be representative of an entire tribofilm [109]. The current research activity will consider the validity of this assumption by conducting topography scans in varying locations across the length of a reciprocating wear scar.

The current state of the art in AFM and ZDDP tribofilms is the ability to generate and analyse the tribofilm in-situ. Work, in 2015 [3] and 2018 [7], shows that the AFM can be used to both replicate a single asperity contact and a more representative multi-asperity contact, with accurate topography images shown for each. This work supports the idea that the tribofilm is not homogeneous and that a single location cannot be representative of a larger tribofilm. A similar in-situ generation technique [113] has been used to grow ZDDP tribofilms to create specific shapes, demonstrating that there is much that can still be determined about both the nature of ZDDP tribofilms (the morphology can be dictated) and the utility of AFM (its ability to analyse the durability of ZDDP tribofilms). The current research activity will build on this discovery by attempting to ascertain whether a commercially available AFM

can be used to assess tribofilm durability, to provide a secondary means of manipulating ZDDP tribofilms.

Chapter 6: Characterisation of ZDDP Tribofilms – Phase 1

This phase of the research shall focus on characterising the morphology of ZDDP tribofilms. Tribofilms were formed in oil containing differing concentrations of the additive ZDDP, such that comparisons could be made and any differences in topography investigated. In addition, a study was undertaken to assess whether all positions within a reciprocating stroke formed tribofilm pads with the same morphology and distribution.

An explanation for differences in the morphology is presented and this is then applied to tribofilm morphology as presented in literature.

6.1 Introduction

Whilst many topographic results have been presented in previous works it is rare to see a topographic analysis as the primary motivation for a research project. As such whilst research is being conducted to determine the extent to which the AFM can be used to aid in tribological research, it is necessary to take a step back to determine the validity of the current results which are typically displayed. In this research the first phase aims to determine whether there is any variation in the topography of a single sample and thus whether it is possible to include a single "snapshot" of topography as a valid result to non-topographic focussed research.

For future research to compare tribofilms formed in an AFM (as in the work by Gosvami et al [3] and Dorgham et al [112]) with those formed using more traditional tribometers it is necessary to have first conducted a thorough analysis of traditional tribofilms.

In this first phase of the research a thorough topographic analysis has been conducted to determine whether there is any variation in the topography of tribofilms formed in a TE77 reciprocating tribometer with position. The nature of a reciprocating system is such that the speed is necessarily variable resulting in a variable lambda ratio. Therefore, it is possible to observe the topographic results for a lambda ratio profile on a sample; which, if being greatly variable, would indicate that stating a single topographic result for such samples would be a misrepresentation. In order to be a comprehensive study these comparisons are conducted for samples exposed to differing concentrations of ZDDP, enabling any potential correlation to be determined between the importance of concentration and lambda ratio.

This phase of the research was structured to resolve the following research conundrums:

- Is there a difference in tribofilm pad morphology as a result of a differing lambda ratio across the length of the wear scar?
- Does the ZDDP concentration in the oil used to initially generate the tribofilm affect the tribofilm pad morphology?
- Do lower lambda ratio regions of a tribofilm produced from a lower ZDDP content oil result in a pad morphology similar to the pad morphology of higher lambda ratio regions of a tribofilm produced from a high ZDDP content oil?

6.2 Method

This first phase of the research included generating ZDDP tribofilms using a TE77 reciprocating pin on plate tribometer and then analysing these using a Bruker Dimension Icon, Scan Asyst enabled, AFM. To enable a true wear scar roughness (R_a) to be determined the samples were first polished to an average surface roughness of 3.207nm and representative scans were taken using the AFM prior to tribofilm generation.

6.2.1 Sample and Tribofilm Preparation

6.2.1.1 Sample Preparation

The samples were 7mm x 7mm EN31 steel plates which were mounted in batches into an epoxy resin such that their surfaces were all horizontal and exposed. Once the resin had set the resultant cylindrical mount was used to hand load the surface against grinding pads with grit grades 600, 800 and 1200. The exposed surfaces of the samples were washed with distilled water between each grit stage. Once the surfaces were ground, they were then polished using diamond pastes, with grain sizes of 9µm, 3µm and 0.25µm, this resulted in a "mirror finish". After the polishing process was completed the resin cylinders were wrapped securely in laboratory paper and the resin was broken to retrieve the undamaged samples. The polished surfaces could then be measured in the AFM to quantify "mirror finish" which resulted in an average surface roughness of 3.207nm and a standard deviation of 1.26nm. An example of the topography produced using this method can be found in Figure 6-1.

6.2.1.2 Tribofilm Generation

The counter-surface was provided by an EN31 steel cylinder, with an end radius of 10mm and a nominal R_a of 10nm. The TE77 was set up to provide a 7mm stroke length, diagonally across the samples. The operating conditions for these tests were non-varying.

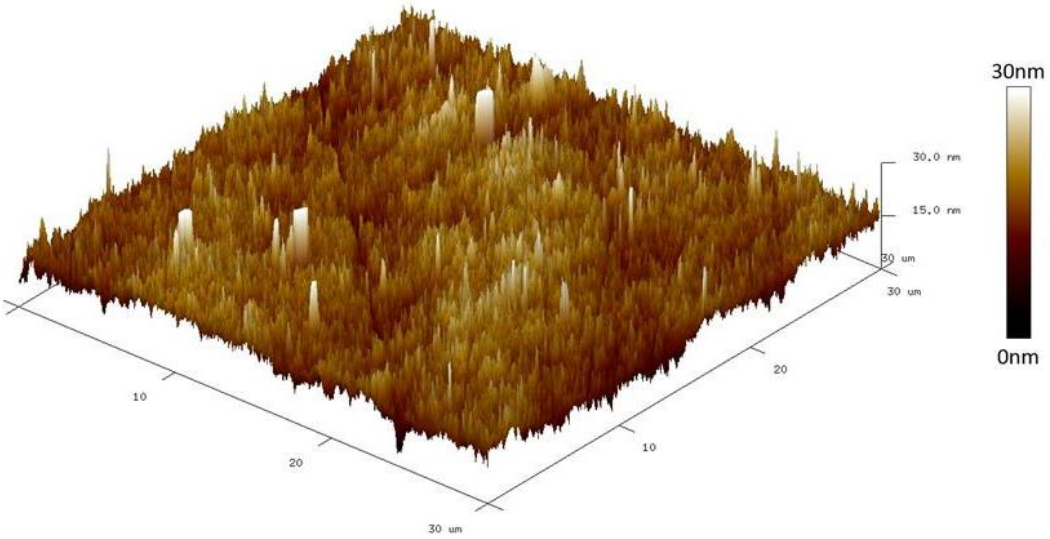

Figure 6-1: A representative image of the topography produced by the initial polishing method, as determined by the AFM.

The temperature was set to 100°C, the frequency was 25Hz (in a reciprocating manner, which for the prescribed stroke length gives a representative speed of 0.35m/s) and the load was 65N (which for the sample geometries corresponds to a maximum Hertzian contact pressure of 1.14GPa). The duration was set to last for one hour, corresponding to 180,000 strokes, with no dwell periods. The test was conducted under ambient conditions, within a standard laboratory environment.

The base oil used was a PAO provided by Afton Chemical and the additive included was an over-based primary ZDDP, also provided by Afton Chemical. The oil was provided pre-blended with concentrations of 0.275wt%, 0.55wt% and 1.1wt%. Using the Hamrock, Dowson Equation (1977) [21,114,115] it was possible to determine the representative lambda ratio values (for the representative speed 0.35m/s) for each of the given concentrations as 0.0220, 0.0227 and 0.0239 respectively. It is necessary to note that each of these lambda ratios can only be representative as the velocity has a sinusoidal profile (with a maximum of 0.550m/s) not a fixed speed and thus the actual lambda ratio is also a profile, Figure 6-2. The lambda ratios for each of these tests were similar as the only property altered was the concentration of oil, which is only considered within the pressure-viscosity

coefficient, with all other parameters kept consistent between tests. The other conditions were selected to be representative of those observed in the literature and to ensure the tests remained within the boundary region throughout.

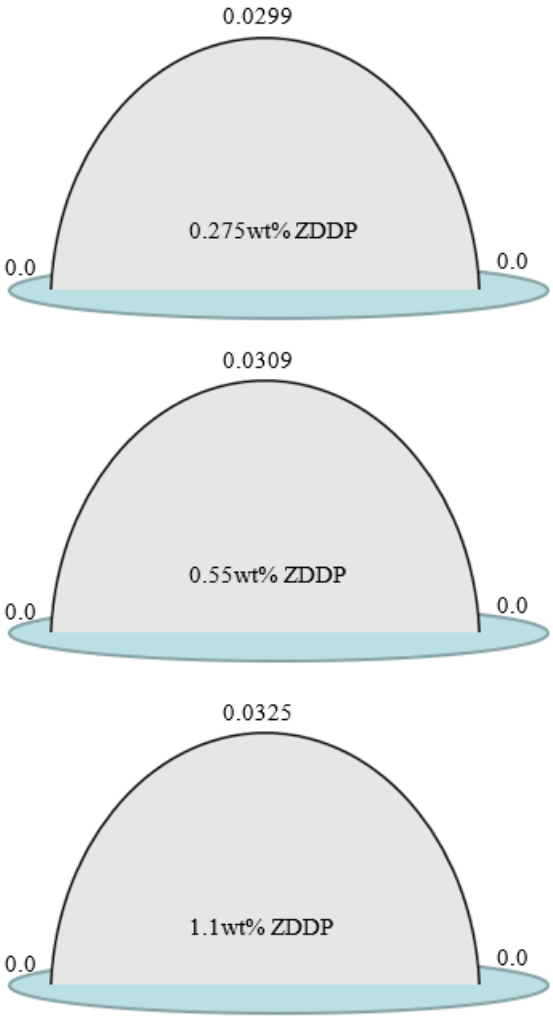

Figure 6-2: Schematic showing the lambda ratio profiles for each concentration

After the tests the samples were removed with tweezers, taking care to avoid the worn region and the upper surface as much as possible, and left to cool briefly on laboratory tissue. Once cool the samples were wiped with an n-heptane soaked piece of tissue [107] to remove excess oil and wrapped in clean tissue for storage.

6.2.2 Atomic Force Microscopy – Topography

For the initial topography scans, to determine the surface roughness after polishing, the samples were wiped with an acetone-soaked tissue and mounted onto a magnetic block. For all subsequent scans (post-tribometer testing) the sample surface was wiped with an n-heptane soaked tissue, to reduce any likelihood of chemical degradation of the tribofilm (as this is known to remove excess oil without damaging the polyphosphate layer [75]).

Post-test topography scans were taken at specific locations across the wear scar, as shown in Figure 6-3, such that the influence of reciprocating position could be considered. Scans were taken towards either end ("A" and "D"), in the regions with the lowest sliding velocity and two scans were taken in regions close together in the middle of the wear scar ("B" and "C"), in the region with the highest velocity.

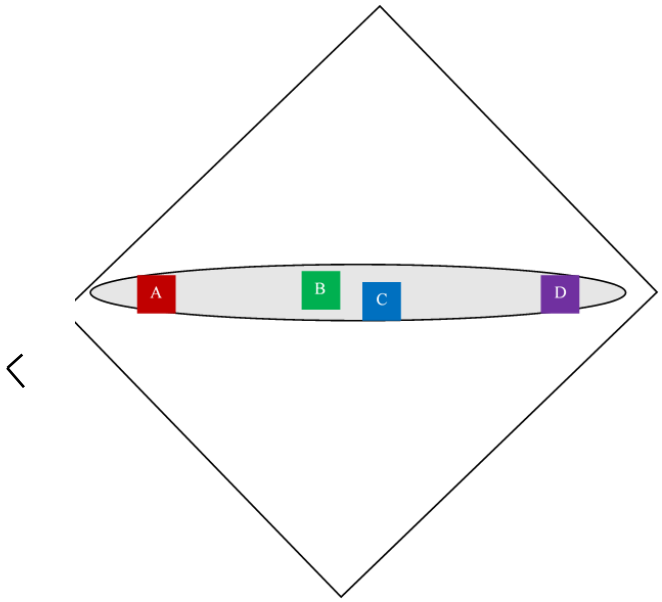

Figure 6-3: A schematic to show the regions selected for topographic analysis (not to scale).

All topography scans were taken across a 30µm by 30µm area at a fixed scan rate of 0.751Hz, using a Bruker Dimension Icon AFM with Scan Asyst enabled (to reduce the influence of feedback oscillations and to auto-adjust the gain). The scans were taken perpendicular to the stroke direction, at a fixed scan angle of 0°, with 512 "taps" per line and 512 lines per scan. The resultant scans were then analysed using the Bruker AFM companion

software, Nanoscope Analysis, such that comparative roughness analyses could be conducted. The most common roughness parameter considered in tribology is the R_a (arithmetic mean roughness) and so this was used here. R_a is calculated from a single line profile and so eight individual line cross-sections were taken across each topography scan, as shown in Figure 6-4a. After tribofilm removal further topography scans were taken of the wear scar and the R_a calculation was repeated. The post tribofilm removal R_a values were then compared to more traditionally obtained values determined using a Taylor Hobson Talysurf taken across the locations shown in Figure 6-4b.

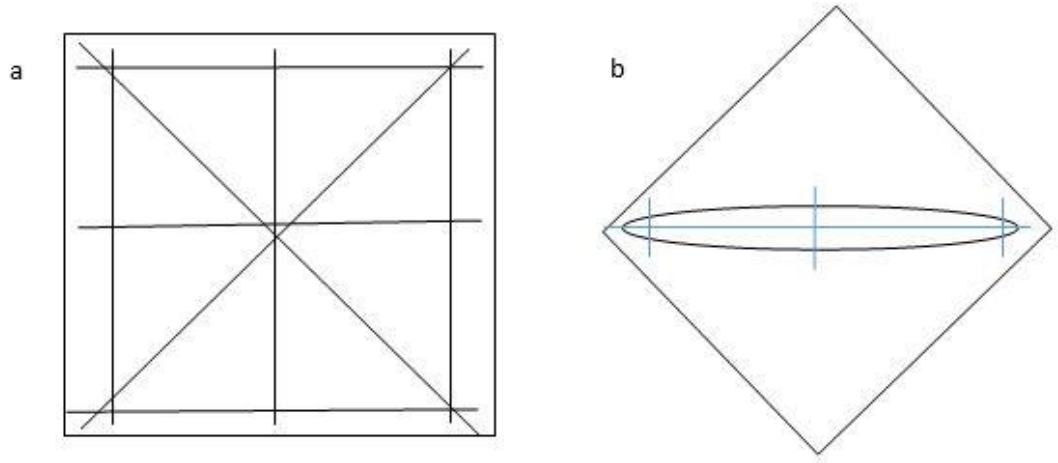

Figure 6-4: A schematic to show the locations used to determine surface roughness for (a) the AFM topography scans and (b) the full wear scar as analysed in the Talysurf.

6.2.3 Tribofilm Removal

To remove the tribofilm, to allow an analysis of the underlying wear scar, the samples were placed into individual containers and covered with 10ml of EDTA for one minute [102]. These were carefully dried, by wrapping each sample within a standard laboratory tissue, before being immersed in 10ml of acetone for a further one minute (to ensure that the dissolved ZDDP was removed from the surface). The samples were then dried with a standard laboratory tissue before being wiped clean with a lint free tissue and wrapped in a different lint free tissue for storage.

6.2.4 Statistical Analysis

The difference in R_a was calculated as a means of comparing apparent differences in topography between concentrations and across positions. For these analyses it was assumed that all regions denoted as “end” could be grouped together and so could all regions denoted as “middle”.

Differences between positions were compared using a two-tailed student t-test, assuming equal variance, at the 5% significance level. These tests were conducted using the compatibility enabled “T-Test” function within Microsoft Excel.

Differences between concentrations were compared using Single Factor Analysis of Variance (ANOVA) tests, at the 5% significance level. These tests were performed using the “Data Analysis” function within Microsoft Excel.

6.3 Results

The below results include findings relating to the morphology of tribofilm pads formed using different concentrations of ZDDP and the topography of the wear scar beneath each tribofilm. The complete topographic data set is included as “Appendix 1 – Comprehensive results for the Characterisation of ZDDP Tribofilms”.

6.3.1 Atomic Force Microscopy – Tribofilm Topography

6.3.1.1 Surface Parameters

Figure 6-5 shows the average arithmetic mean surface roughness (R_a) values taken from tribofilm topography scans, on the AFM, at different regions of the tribofilm. This enables a quantitative comparison to be made across the wear scar for each concentration.

The lowest concentration, 0.275wt%, shows a considerably lower R_a for the “A” region; however, this is not so for the “D” region, indicating these scans may not have been taken symetrically (with the same distance between the scan and the end of the wear scar). There is no major difference with position in the roughness of the middle regions (“B” and “C”), indicating that either these were taken with the position being more accurate or that the variation towards the middle of the scan is less pronounced. However, both measurements have a large standard deviation, possibly as a result of several prominent surface features skewing the data.

The middle concentration (0.55wt%, which is specifically considered below) also has a noticably lower R_a in the “A” region. However, again the “D” region is not notably different to the two middle regions. All of the roughnesses for the middle concentration appear to be lower than their equivalent regions in the lower concentration; however, these values have a very large variance.

The highest concentration has no distinction with position, with all of the measurements being very similar in magnitude. For this concentration (unlike the two lower concentrations) the middle regions do not both have higher roughnesses than the end regions, with "A" having a larger R_a than the "C" region.

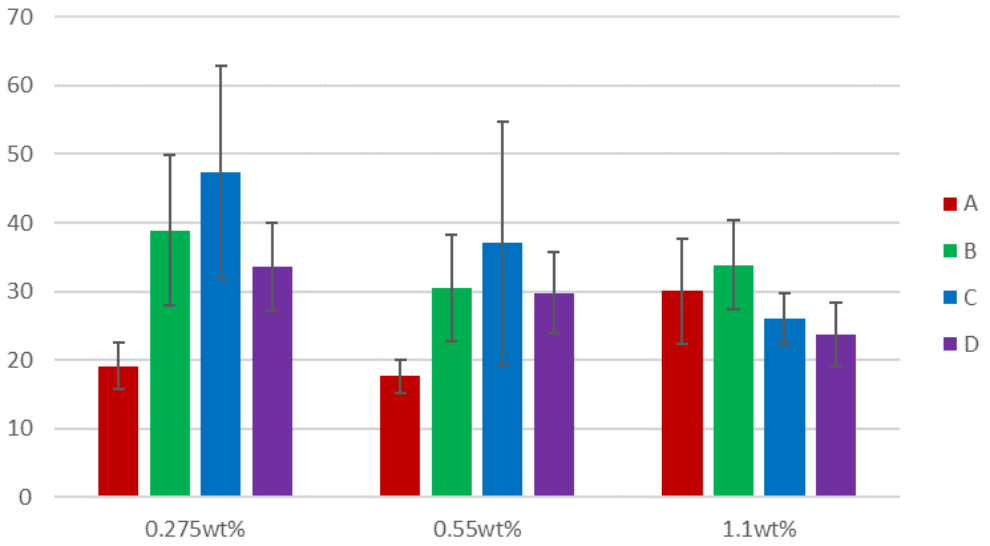

Figure 6-5: The tribofilm roughness (R_a) across different concentrations and positions, with the standard deviation.

The t-tests performed to determine if there was a difference between the tribofilm R_a values for the end and middle region, for the 0.275wt% concentration, determined that there was no significant difference (mean end = 28.75, mean middle = 43.15, SE = 8.098, t = 1.779, df = 5, p=0.135, effect size = 1.359). There were also no significant differences between positions for the 0.55wt% concentration (mean end = 25.71, mean middle = 33.75, SE = 5.563, t = 1.446, df = 5, p=0.208, effect size = 1.104) and the 1.1wt% concentration (mean end = 25.80, mean middle = 29.96, SE = 4.931, t = 0.842, df = 5, p=0.438, effect size = 0.643).

ANOVA tests performed to determine if there was a difference between the tribofilm R_a values between or within concentrations determined that there was no significant different at the end position (0.275wt% mean = 28.75, 0.55wt% mean = 25.71, 1.1wt% mean = 25.80, f = 0.161, df_b = 2, df_w = 9, p = 0.855, effect size (explained variance) = 0.051) nor the

middle position (0.275wt% mean = 43.15, 0.55wt% mean = 33.75, 1.1wt% mean = 29.96, f = 2.369, $df_b = 2$, $df_w = 9$, p = 0.149, effect size (explained variance) = 0.345).

Figure 6-6 shows that the pattern in the linear roughness profile (R_a) is not replicated in the surface profile (S_a). The S_a indicates a possible trend with concentration for the middle region, with an increasing concentration resulting in a decreasing S_a; however, this is not meaningful, due to the large variability, particularly for the 0.55wt% concentration. The end regions do not show a trend with concentration, with large overlapping error bars. The end region S_a values are lower than the middle region, both within concentrations and across them; however, this is again not meaningful due to the large variation between samples.

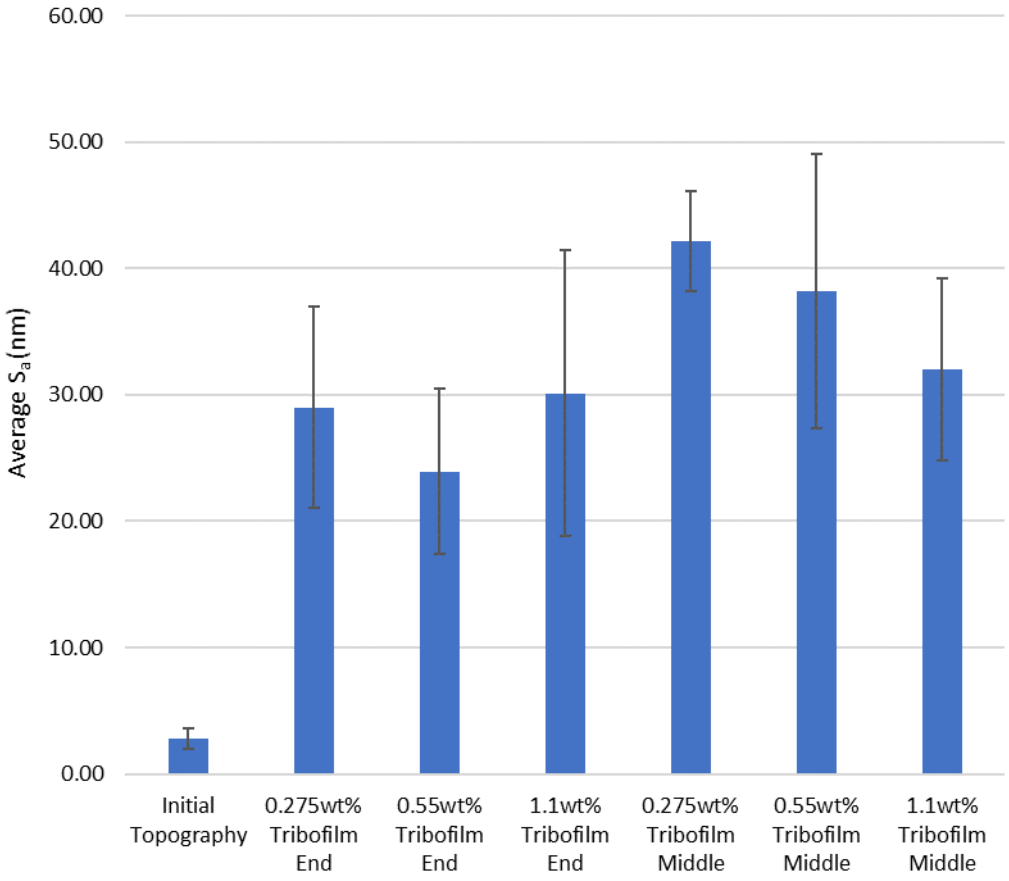

Figure 6-6: Tribofilm S_a values, for each concentration at both the end and middle positions, the errors bars indicate the standard deviations from the mean.

Figure 6-7 shows the surface skewness values for the tribofilms and for the initial topography scans. It can be seen that there is very large variability in the skewness between samples, even within the same tribofilm and location. Once again there is no obvious trend with concentration within the scans taken in the end regions; however, a trend may be present for the middle region scans. These indicate a possible increase in skewness with concentration, with more material above the mean line than below it; however, this is not meaningful. The range on the 0.55wt% and 1.1wt% middle region values is substantial, with the error seemingly also increasing with concentration. The end region scans all give negative skewness averages, indicating that for most scans the majority of the tribofilm lies below the mean line of the surface.

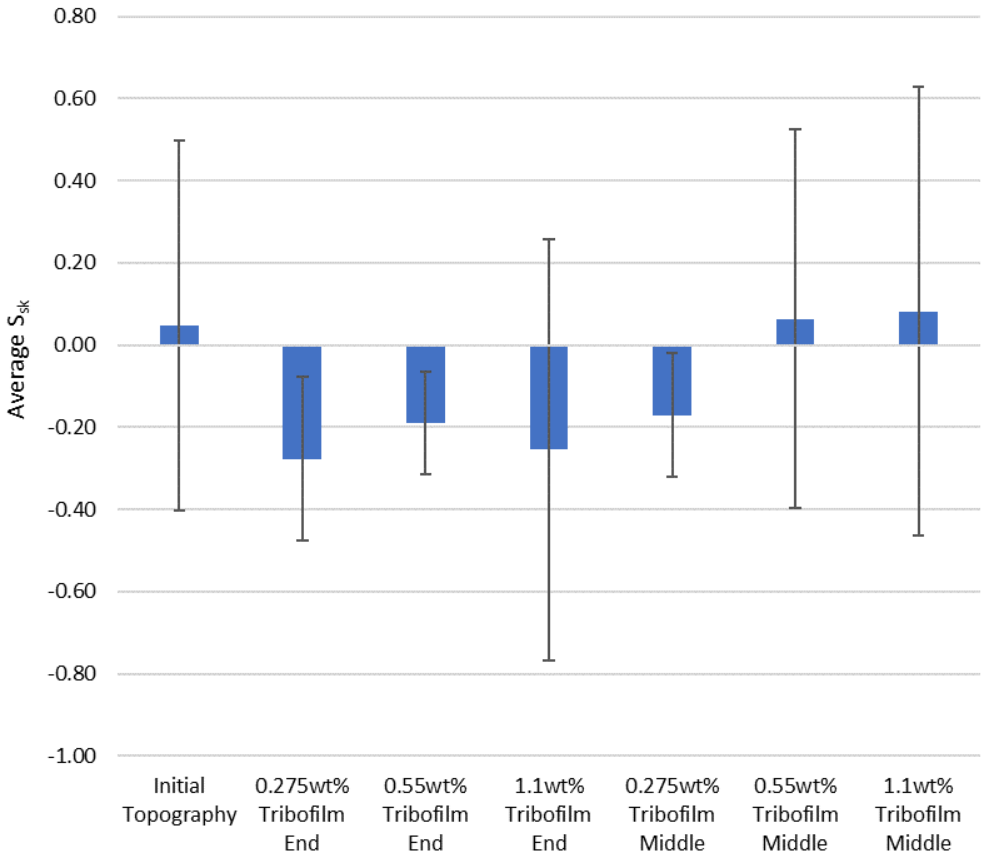

Figure 6-7: Tribofilm S_{sk} values, for each concentration at both the end and middle positions, the errors bars indicate the standard deviations from the mean.

Figure 6-8 shows that all of the samples experienced a decrease in surface kurtosis with testing, which is to be expected as asperities become covered by tribofilm pads. It can also be noted that the initial topography had the highest error in the kurtosis. There is no clear trend with either concentration or position on the tribofilm kurtosis, with all regions and concentrations having similar averages (between 2.8 and 3.2). There is a slight trend indicated for the middle regions, with a slight increase in the kurtosis with concentration; however, this is sufficiently small as to be within the noise of the data.

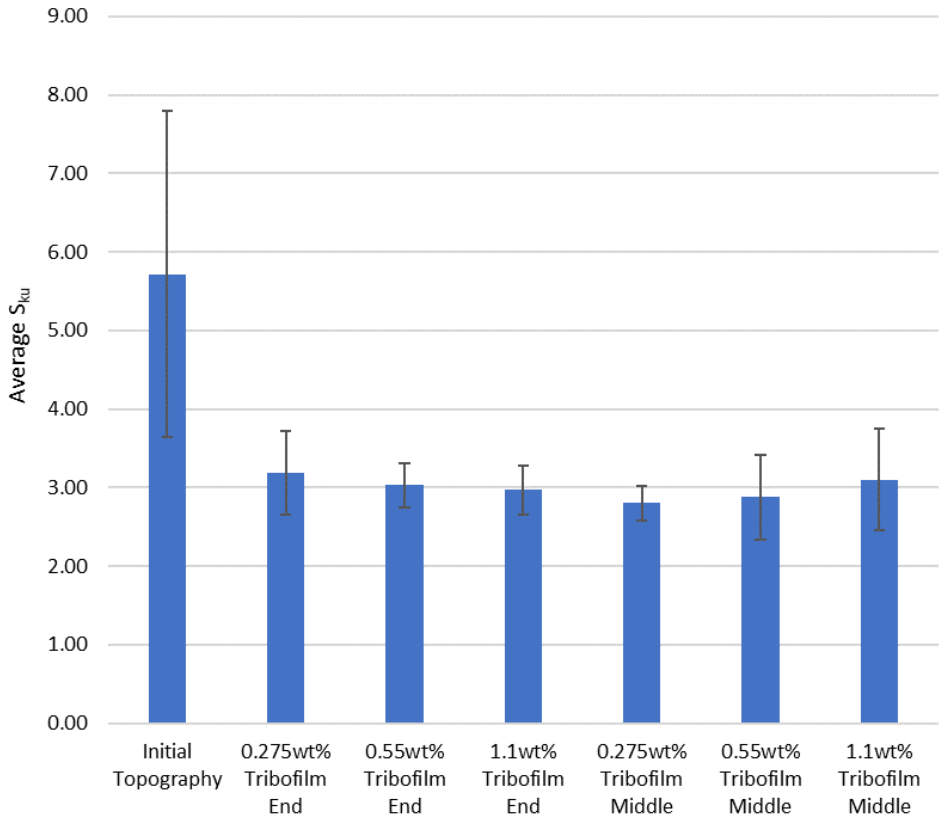

Figure 6-8: Tribofilm S_{ku} values, for each concentration at both the end and middle positions, the errors bars indicate the standard deviations from the mean.

A selection of specific topography scans will be presented and explained in sections 6.3.1.2 and 6.3.1.3. However, Table 6-1 shows representative topography scans for all four positions for each of the three concentrations. These have been included to aid in a visual comparison between the positions for each of the concentrations. The scans have been corrected such that they all have the same scale, from 0nm (darkest) to 392nm (lightest).

Table 6-1: A summary of tribofilm topography scans, indicating concentration and position.

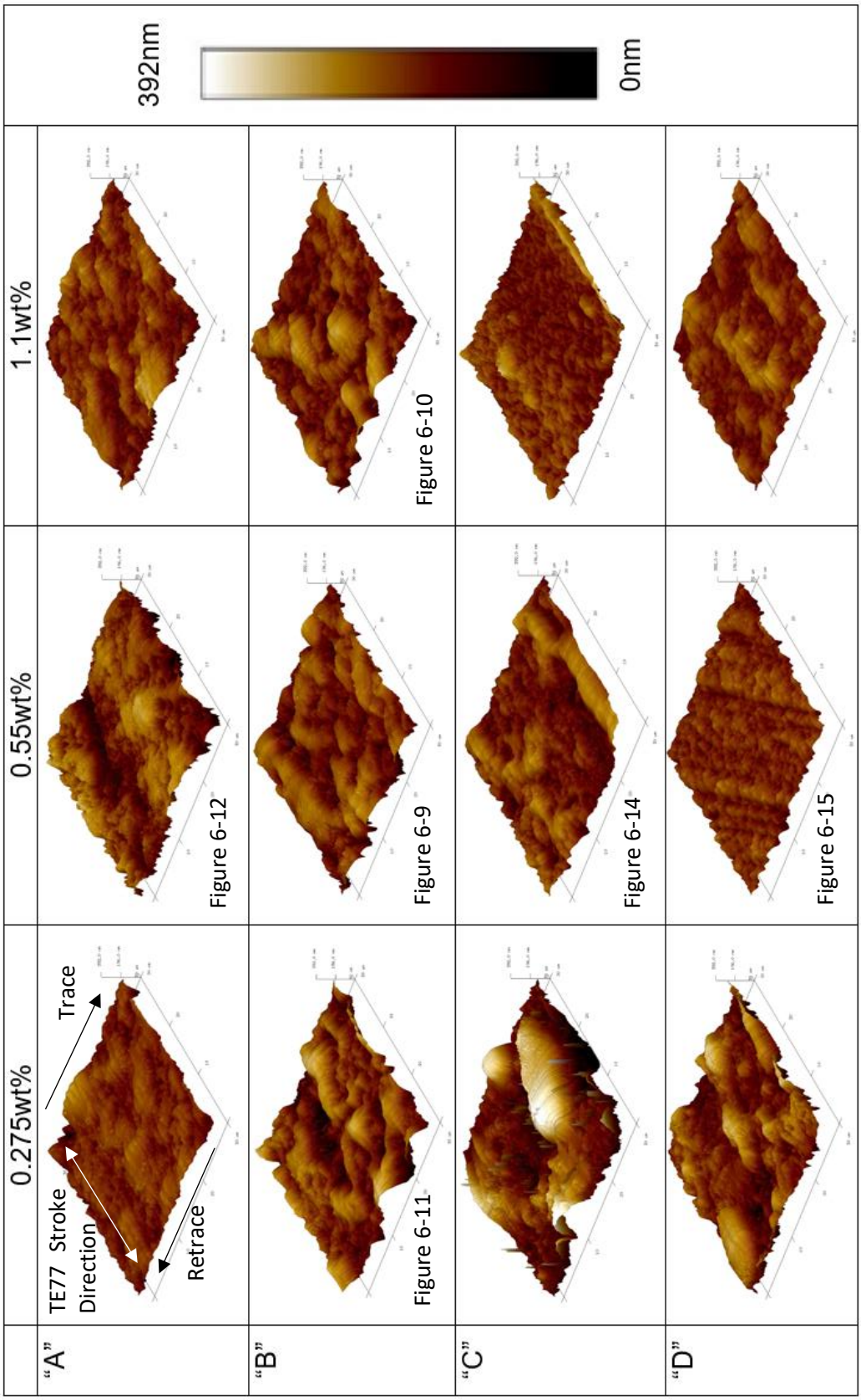

6.3.1.2 Tribofilm topography variations with concentration

It can be seen in Figure 6-9 that the middle concentration (0.55wt%) produces a tribofilm (in the middle region) formed of a mix of larger and smaller pads. The long pad to the top left of the scan (indicated using a red arrow) measures greater than 20µm in length, whereas the smaller pads (which appear recessed, marked with blue arrows) are about 5µm in diameter. The long pad is orientated such that it is elongated in the stroke direction. It is possible that a secondary elongated pad is either just forming or is continued past the edge of the scan (indicated with a green arrow). The visible portion of this pad is approximately 15µm in length (although this appears to extend beyond the edge of the scan, indicating a potentially longer pad than can be quantified), the width of the visible region is approximately 8µm. The height of all the larger pads appear to be greater than 300nm, whereas the smaller pads appear to have a height of less than 150nm. The true value of these heights may be different as the height is relative to the lowest portion of the scan, not the underlying steel.

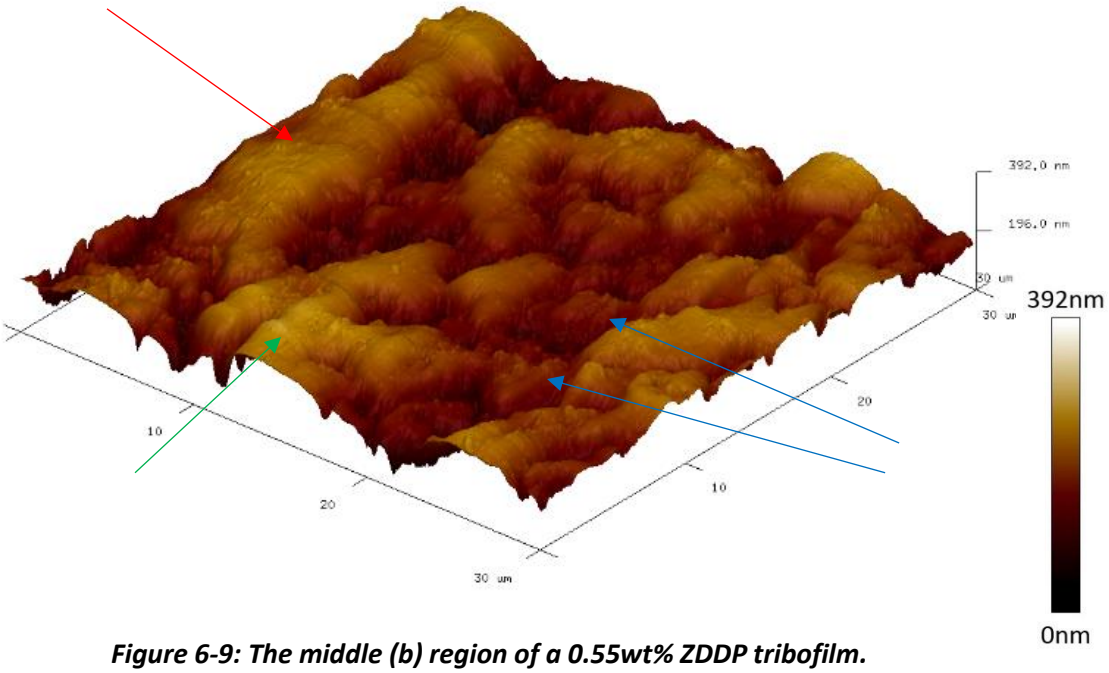

Figure 6-9: The middle (b) region of a 0.55wt% ZDDP tribofilm.

In Figure 6-10 it can be seen that the largest pads in the 1.1wt% tribofilm are smaller than in the middle concentration, at approximately 10µm in diameter (indicated with red arrows). The smallest pads appear to be approximately 2µm in diameter (indicated with blue arrows), and the height difference appears to be smaller (<100nm). This further indicates a more even coverage of the film, compared to the middle concentration. This scan also shows lines on the tribofilm pads (in the tribometer stroke direction) which are less obviously present in the lower concentrations. This may indicate a more rapid formation of the pads, or at least that the pads appear to have experienced more shear within the contact. These lines are more easily identified in the larger pads and are indicated on the edge pad towards the bottom of the scan (using green arrows).

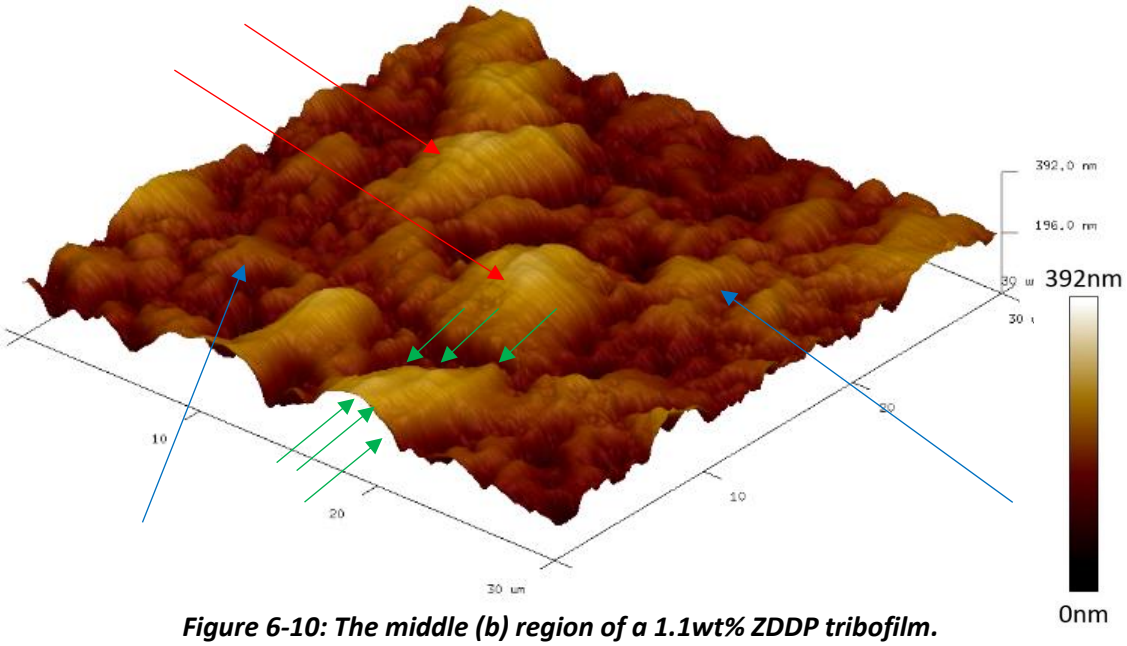

Figure 6-10: The middle (b) region of a 1.1wt% ZDDP tribofilm.

The 0.275wt% scan (Figure 6-11) shows more of the larger pads (as previously found in Figure 6-9) as well as some considerably smaller pads. The larger pads are greater than 10µm in length (indicated with the red arrows) whilst the smaller pads are approximately 3µm in length (blue arrows). The pads are also distinct in height, with the larger pads having a more prominent peak than the smaller pads. Another notable observation in this scan is what appears to be a scratch to the left of the scan (indicated with the green arrows) which indicates that the tribofilm pads are not sufficiently present as to mask the underlying surface features of the wear scar. Additionally, there is a large crevice in the scan (indicated with a purple arrow) which is likely to be another underlying surface feature. The depth of the crevice is further influencing the relative height scale such that the quantitative height of the pads is undeterminable; however, the qualitative heights appear to be a difference of approximately 200nm from the regions between pads and the maximum pad height.

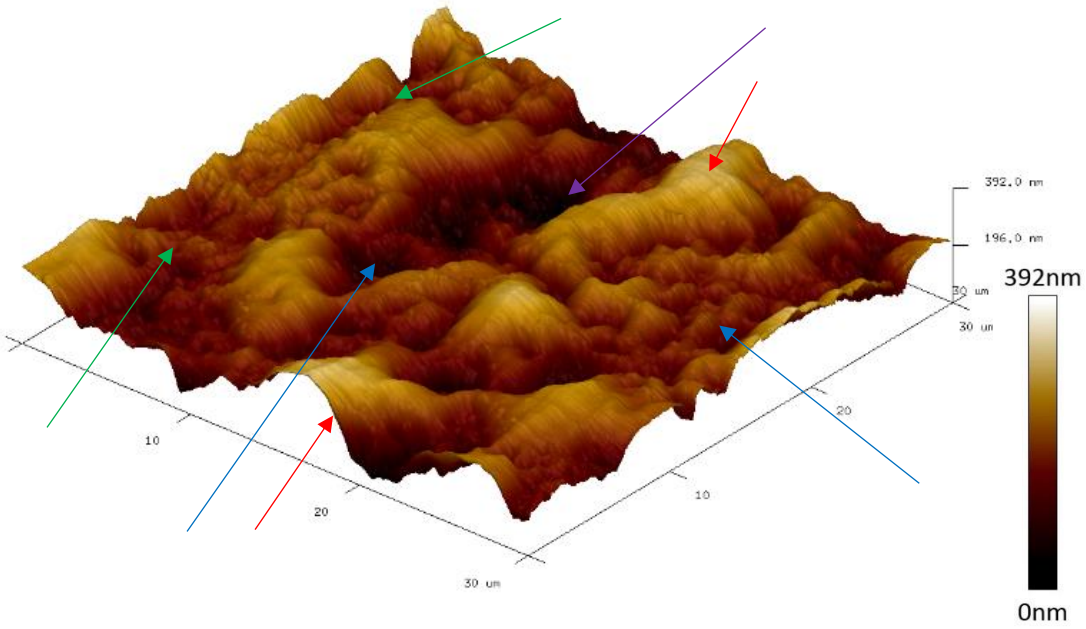

Figure 6-11: The middle (b) region of a 0.275wt% ZDDP tribofilm.

6.3.1.3 Tribofilm topography variations with position

It can be seen in Figure 6-12 that the end region of the tribofilm can display a more flattened topography, with the pads appearing to merge (as indicated with the red arrow). The smaller pads (indicated with blue arrows, approximately 3-5µm diameter), which are still present, have a very similar height to the larger pads. Additionally, the regions between pads appear to be smaller than in the previously seen middle scans, with several gaps being less than 1µm in width. Perhaps unexpectedly this region is also showing some evidence of an underlying surface feature (a crevice, indicated with the green arrows).

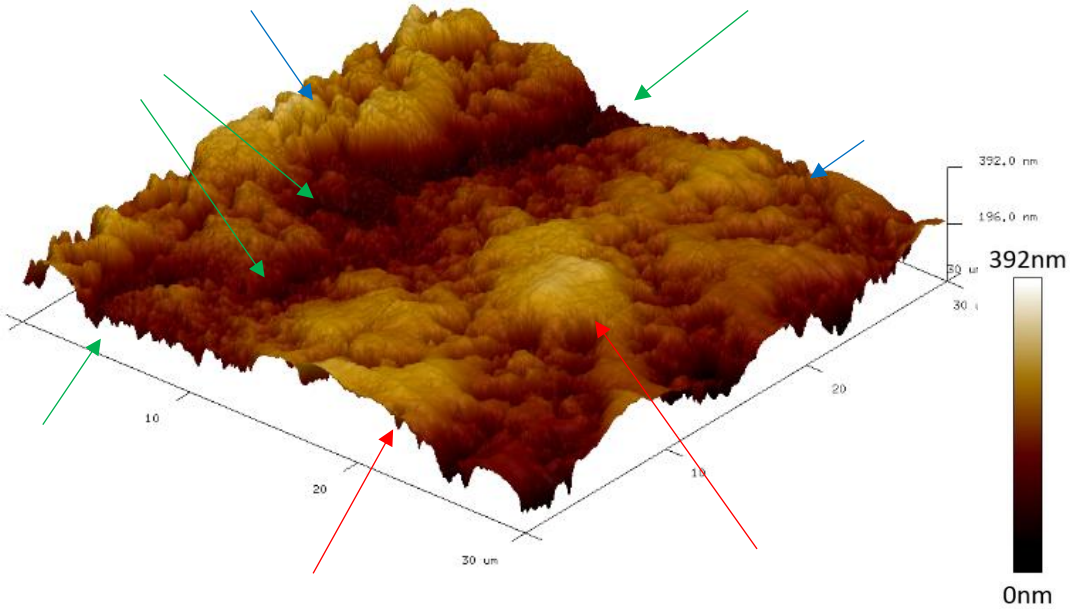

Figure 6-12: The "A" region of a 0.55wt% ZDDP tribofilm.

Figure 6-13 is a repeat of the scan shown as Figure 6-9. This is re-presented here to provide a more convenient contrast to the above end region scan and the below middle and end region scans. The important features are explained above; however, these are summarised again here:

- The larger pads are over 20µm in length whereas the smaller pads have a diameter of 5µm.
- There appear to be large pads which extend beyond the regions of the scan (with approximately 15µm of pad visible).
- The larger pads seem to have a greater height than the smaller (approximately 150nm difference).

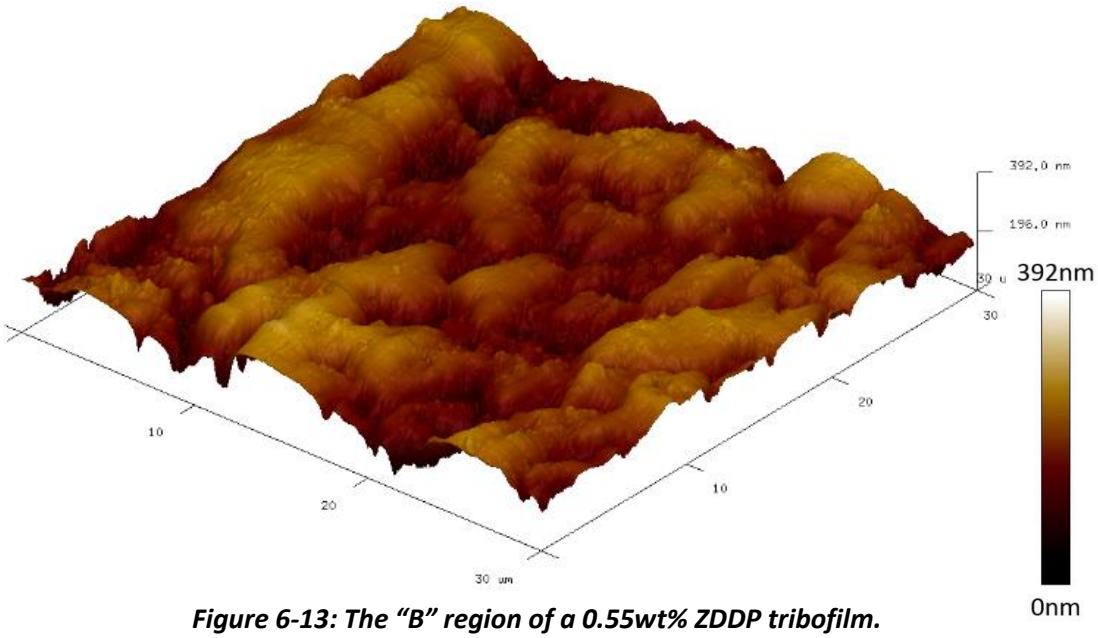

Figure 6-13: The "B" region of a 0.55wt% ZDDP tribofilm.

The below scan of the middle region (Figure 6-14) shows one very large pad (with a length in excess of the 30µm scan size, shown with a red arrow). Another potentially very long pad, which seems to be forming from two slightly smaller pads, each extending beyond the length of the scan (indicated with the blue arrows), and several much smaller pads (between 3 and 10µm in length, shown with the green arrows), seem to be oriented in the stroke direction. The potential large pad (blue arrows) also shows evidence of orientation in the stroke direction (indicated by purple arrows), whilst the clear large pad (red arrow) appears to be elongated in the stroke direction but does not display the same orientation marks. It is worth noting as well that there appears to be a small pitted region (indicated with a yellow arrow) which could be affecting the scan resolution. It is not thought that this pit is important in any other manner; however, its effect on the graduated colour of the scale bar is.

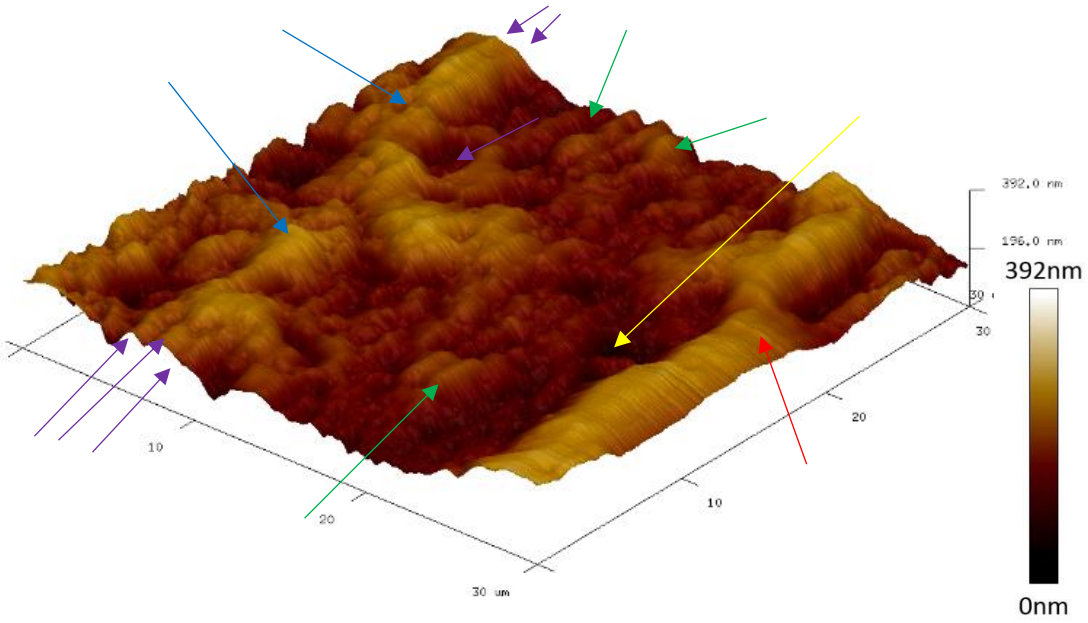

Figure 6-14: The "C" region of a 0.55wt% ZDDP tribofilm.

Figure 6-15 shows that the end region can have lots of very small pads in close proximity to each other. There is some evidence of these pads agglomerating to form slightly larger pads, or potentially to be become smaller distinct pads from previous larger pads. These small pads (indicated with the blue arrows) are typically between 2µm and 3µm in diameter, whereas the larger pads (indicated with the red arrows) are typically between 3µm and 8µm in length. It appears that there is a slight orientation to the clustered pads (indicated using green arrows), although this does not align with the stroke direction and so is likely a result of an underlying surface feature (such as residual machining marks).

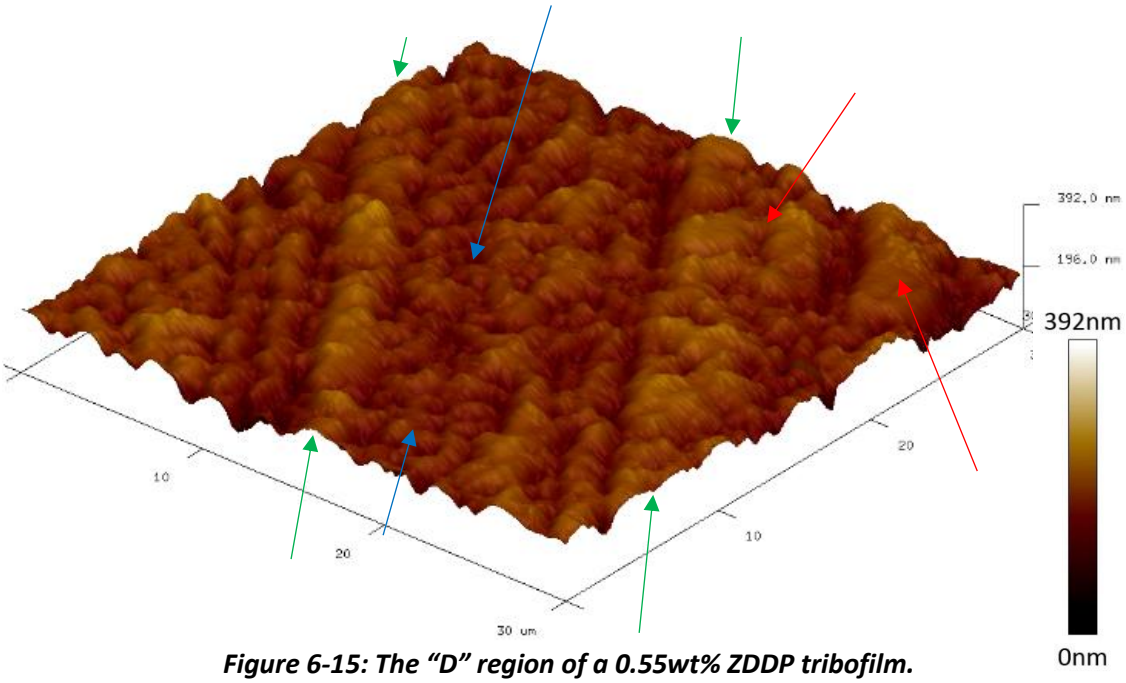

Figure 6-15: The "D" region of a 0.55wt% ZDDP tribofilm.

6.3.2 Atomic Force Microscopy – Wear Topography

After removal of the tribofilm the samples were returned to the AFM and further scans were taken to investigate the surface topography. However, it is worth noting that the location of these repeated scans is not the same as the previous tribofilm scans as an exact relocation is not achievable within the AFM. The scans were instead taken in the same approximate regions as specified within the method section. Nanoindentation was considered as a means of relocating the same position; however, it was determined that even with the indents it would not be possible to ensure the exact same scan area was considered as well as the likely risk of damaging the tribofilm and so it was decided that indentation would not be used.

As previously, a comparison is provided between the different concentrations as well as the reciprocating position. Any differences have been validated by comparison to initial topography scans taken at various positions across the surface. Figure 6-1 is re-presented below as Figure 6-16, this has been included to provide a direct comparison between an example of the initial topography and the post-test wear scar topography.

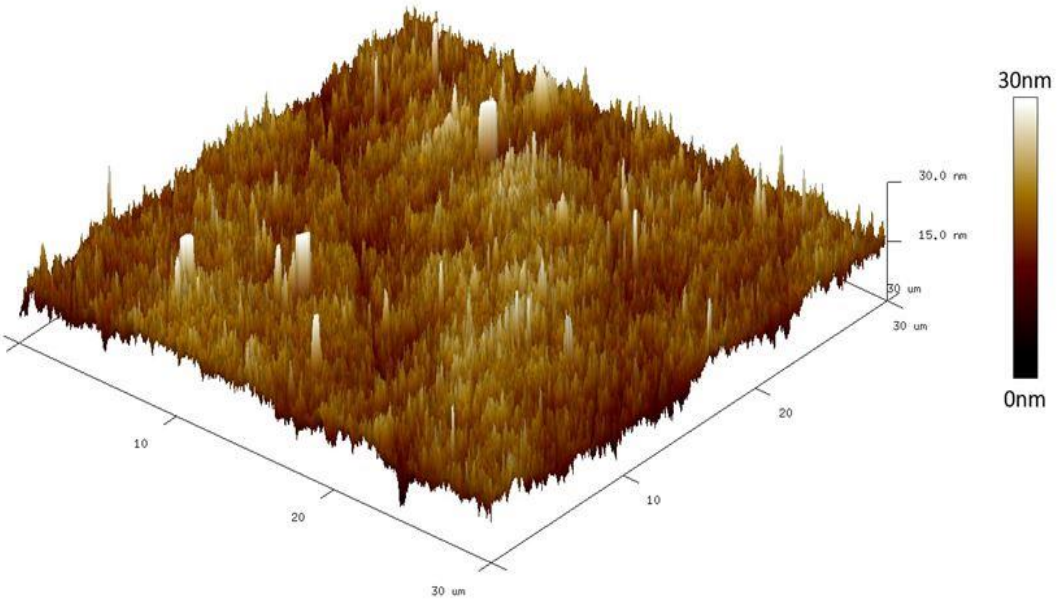

Figure 6-16: A representative scan of the surface topography for the initial TE77 samples.

6.3.2.1 Surface Parameters

The graph shown in Figure 6-17 compares the average surface roughness (R_a) for each of the regions considered, for each of the concentrations, as measured by the AFM.

For the 0.275wt% concentration it can be seen that there is a definite difference in the R_a with position. This is particularly apparent in the "D" result, which can also be seen to have the lowest standard deviation within these samples. The lower R_a for "A" is less apparent; however, there still appears to be clear distinction between the "A" and "C" measurements of surface roughness.

The 0.55wt% concentration has a lesser effect with position, particularly for "C" and "D", which have a very similar result. However, the results for "A" and "B" are distinctly different from each other, with "A" having a noticeably lower R_a than any of the other regions.

For 1.1wt% there is no obvious distinction in R_a with position; however, all of the R_a values for this higher concentration are lower than those found in the middle regions of both lower concentrations. This may indicate a more even coverage by the tribofilm pads for this concentration.

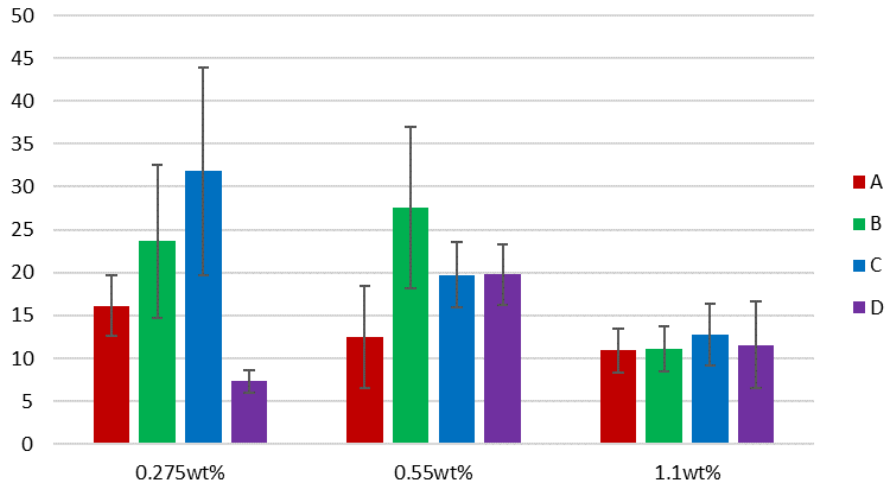

Figure 6-17: A graph to compare the wear scar roughness (R_a) across concentrations and positions, as measured by the AFM, with the standard deviations.

The t-tests performed to determine if there was a difference between the wear scar R_a values for the end and middle region, for the 0.275wt% concentration, determined that there was no significant difference (mean end = 11.73, mean middle = 27.74, SE = 10.293, t = 1.555, df = 6, p=0.171, effect size = 1.100). There were also no significant differences between positions for the 0.55wt% concentration (mean end = 16.10, mean middle = 23.65, SE = 7.053, t = 1.070, df = 6, p=0.326, effect size = 0.757) and the 1.1wt% concentration (mean end = 11.24, mean middle = 11.91, SE = 1.472, t = 0.475, df = 6, p=0.664, effect size = 0.323).

ANOVA tests performed to determine if there was a difference between the wear scar R_a values between or within concentrations determined that there was no significant different at the end position (0.275wt% mean = 11.73, 0.55wt% mean = 16.10, 1.1wt% mean = 11.24, f = 0.733, df_b = 2, df_w = 9, p = 0.507, effect size (explained variance) = 0.140) nor the middle position (0.275wt% mean = 27.74, 0.55wt% mean = 23.65, 1.1wt% mean = 11.91, f = 1.575, df_b = 2, df_w = 9, p = 0.259, effect size (explained variance).

Figure 6-18 shows the R_a values, as measured using the more conventional Talysurf. Due to the small areas used in the AFM scans it was not possible to ensure use of the exact same location for Talysurf measurements; however, due to the much larger area covered using this method it is understood that the area used in AFM has been recaptured. In addition to the known positions, R_a was measured along the length of the wear scar ("End to End"), to determine whether the specific locations had a different R_a to the "average" for the scar. From the graph it can be seen that the variation between areas is less defined than for AFM, with the maximum variation being 10nm between locations, including the R_a measured along the wear scar length. Talysurf measurements consist of a single line scan and due to the destructive nature of this measurement technique it is not possible to conduct repeats in the same location. Thus this is considered to be less reliable than the AFM.

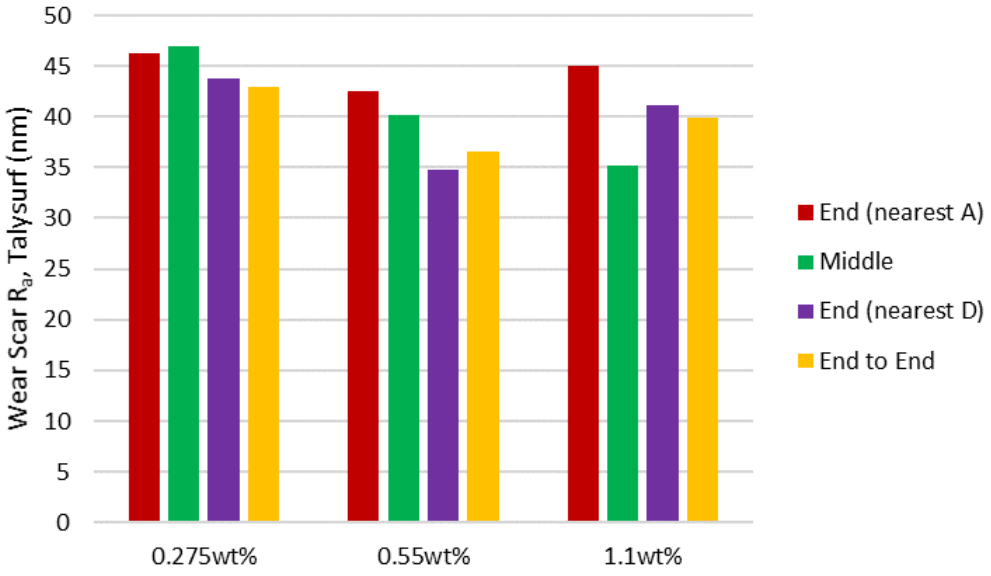

Figure 6-18: A graph to compare the wear scar roughness (R_a) across concentrations and positions, as measured by the Talysurf.

Figure 6-19 shows the S_a values for the cleaned wear scar. All of the surfaces have increased in roughness with values considerably higher than for the initial topography comparisons. There is a trend between the S_a and ZDDP concentration, with an increase in ZDDP concentration resulting in a decrease in underlying surface roughness. This is as would be expected for an anti-wear tribofilm; however, the variability means that these values are not meaningfully different, with particularly high variability for the lower concentrations. There is little difference between the end and middle regions for the 1.1wt% tribofilm, with similar averages and standard deviations for both. The lower concentrations, however, appear to have a difference in position, with this effect seemingly being more pronounced for the lowest concentration.

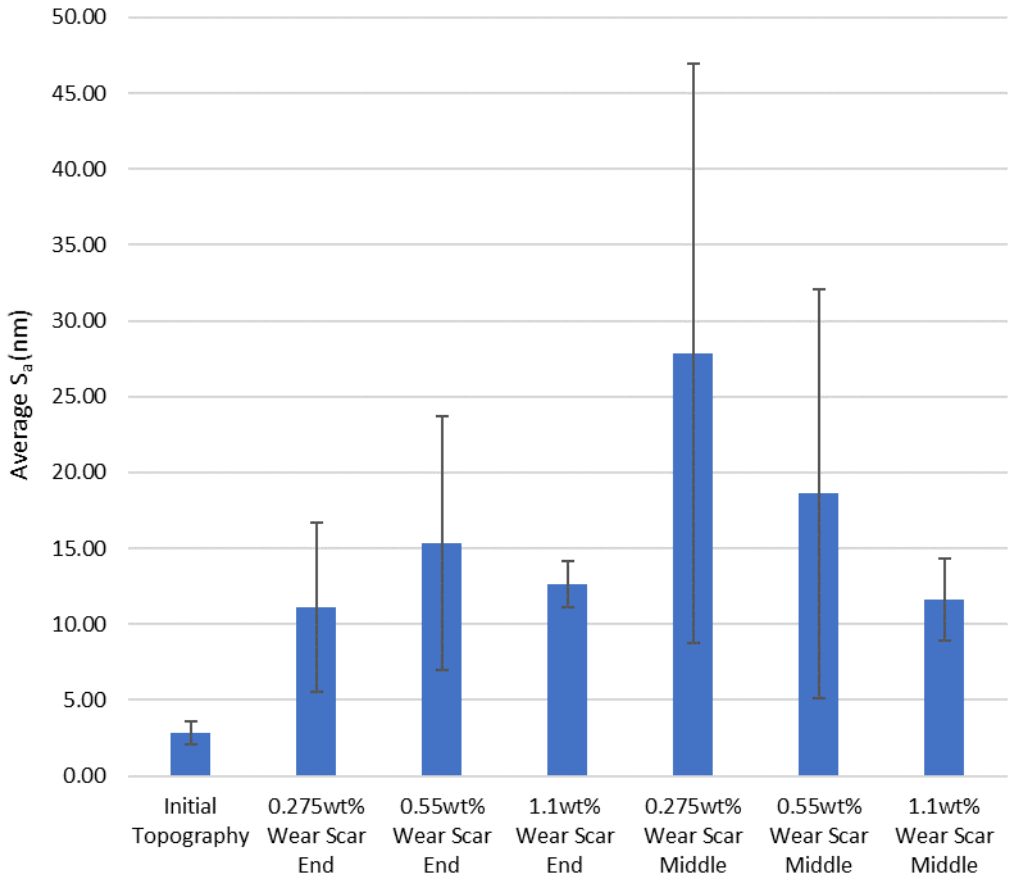

Figure 6-19: Wear Scar S_a values, for each concentration at both the end and middle positions, the errors bars indicate the standard deviations from the mean.

Figure 6-20 shows that for most concentrations, in most positions, the skewness becomes negative, the exception being the 0.275wt% end region scans, which had very large variability, with a scan showing positive skewness. There is no evidence that the skewness is affected by position along the wear scar and little evidence of an effect of differing concentration. There is an indication that for the middle region scans an increase in ZDDP concentration results in a decrease (negative increase) in the skewness; however, this is negligible compared to the variability of these results.

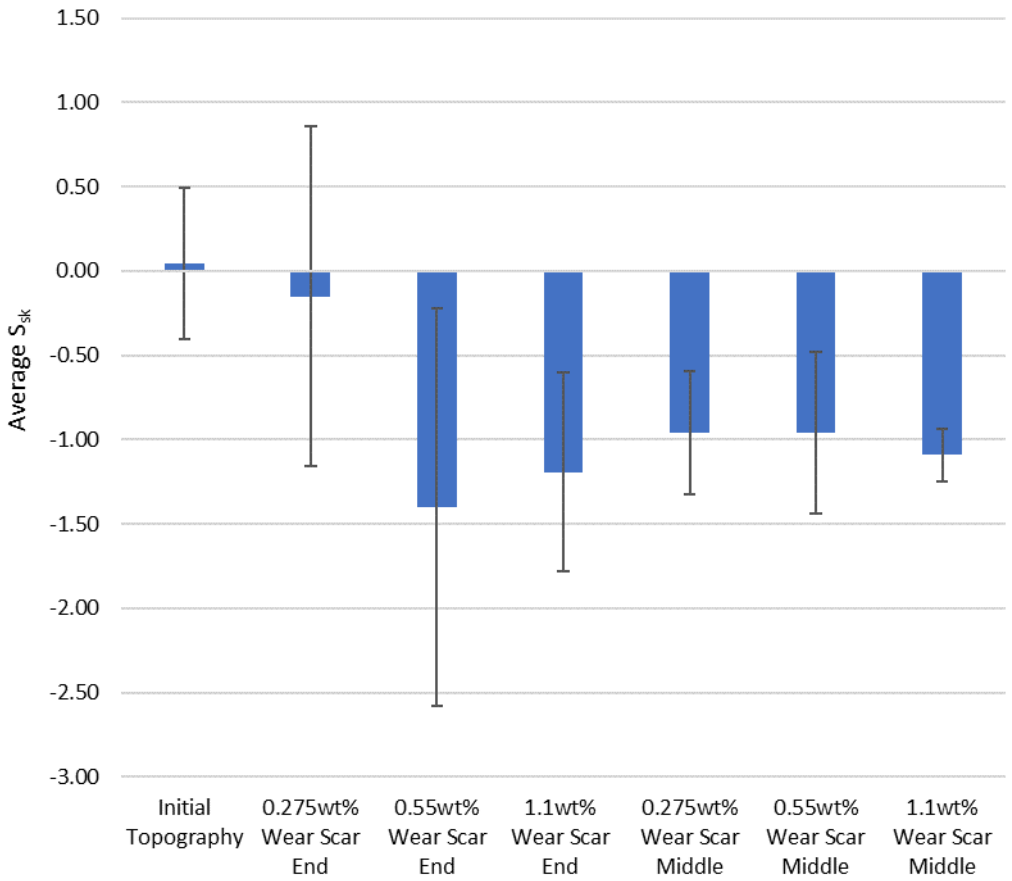

Figure 6-20: Wear Scar S_{sk} values, for each concentration at both the end and middle positions, the errors bars indicate the standard deviations from the mean.

Figure 6-21 shows the surface kurtosis of the worn region and the reference value for the initial topography scans. This shows that the kurtosis has not been meaningfully affected by the testing, with the asperity "sharpness" remaining the same. There is no evidence of an effect of concentration on the resultant asperity geometry; however, there is some evidence to indicate an effect of position. The scans taken in the middle regions of the wear scar appear to have lower kurtosis than the scans (of the same concentration) taken in the end regions of the wear scar.

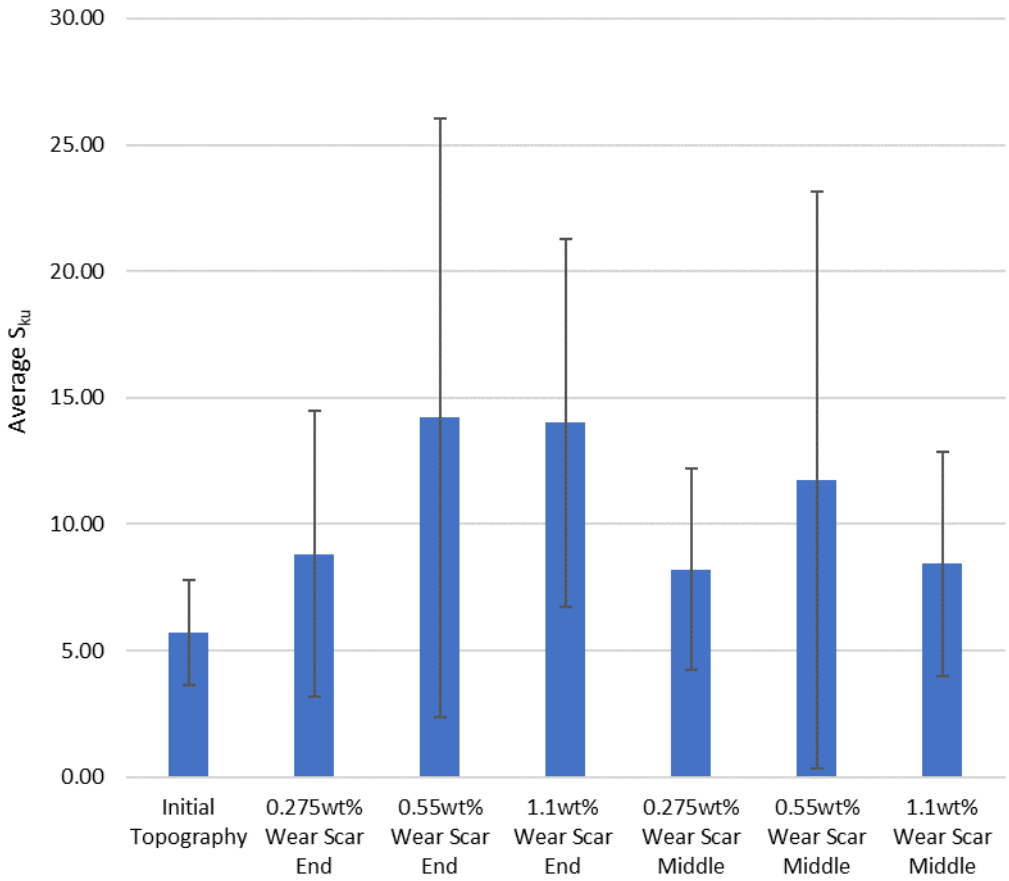

Figure 6-21: Wear Scar S_{ku} values, for each concentration at both the end and middle positions, the errors bars indicate the standard deviations from the mean.

6.3.2.2 Wear scar topography variations with concentration

To permit a visual comparison a table of the wear scar topographies is presented, Table 6-2. The scale for all scans considered ranges between 0nm (dark) and 250nm (light).

Table 6-2: A summary of underlying wear scar topography scans, indicating concentration and position.

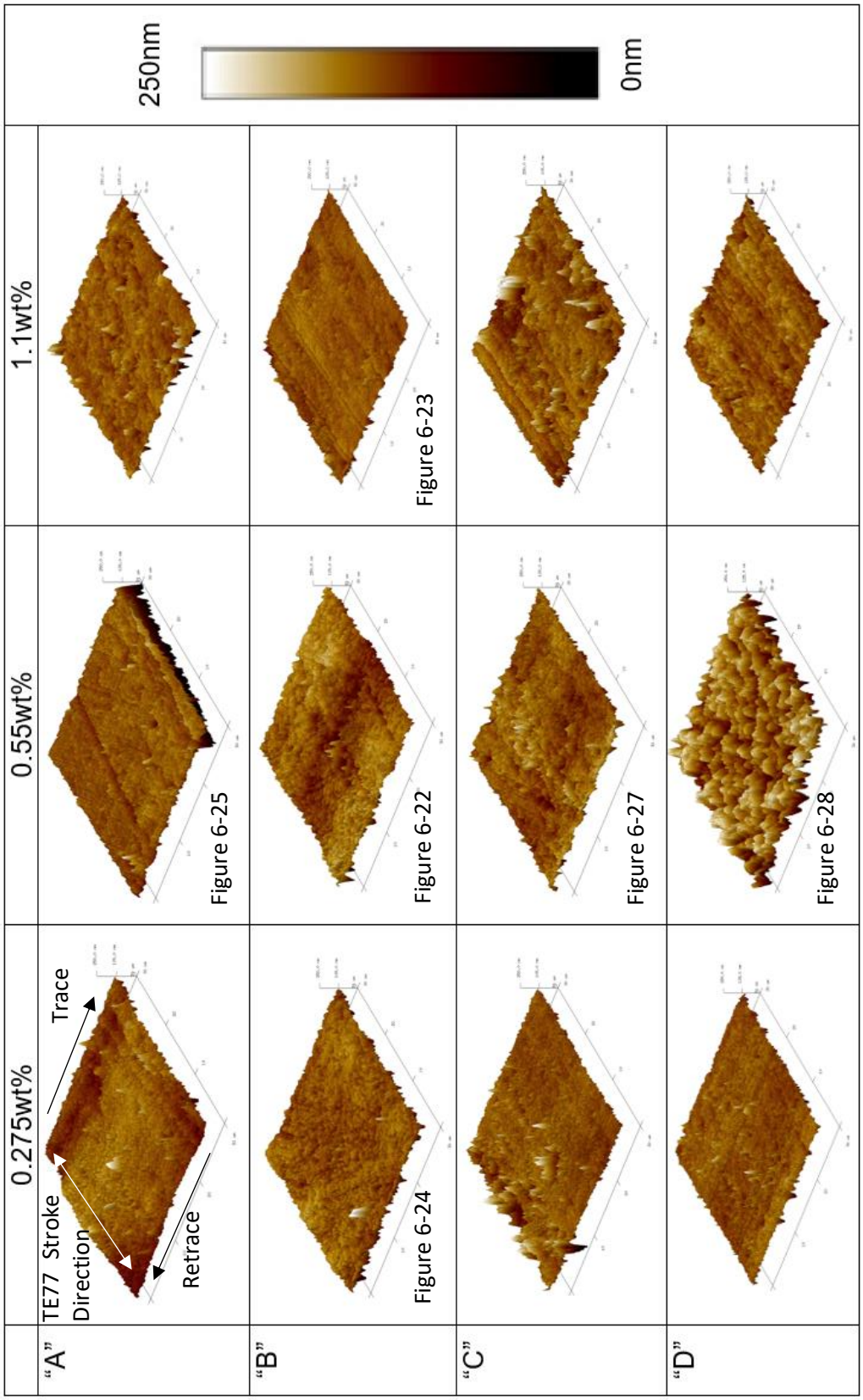

Whilst having a few apparent artefacts (an unavoidable consequence of the accuracy of the AFM used), which are indicated with a red arrow, it can be seen that the surface topography has definitely been altered between the sample before testing and Figure 6-22. This is to be expected but is still an important observation. The specific alterations are that the sharp asperities are no longer evident and instead the sample has much larger rounded regions, not dissimilar in general morphology to the very small pads observed in tribofilm scans previously (these pads are typically less than 1µm in diameter). There is a depression across the centre of the scan (shown with a blue arrow), perpendicular to the stroke direction. However, its proximity to the above-mentioned artefact may indicate it is another artefact, particularly as it is present in the same orientation as the scanning direction.

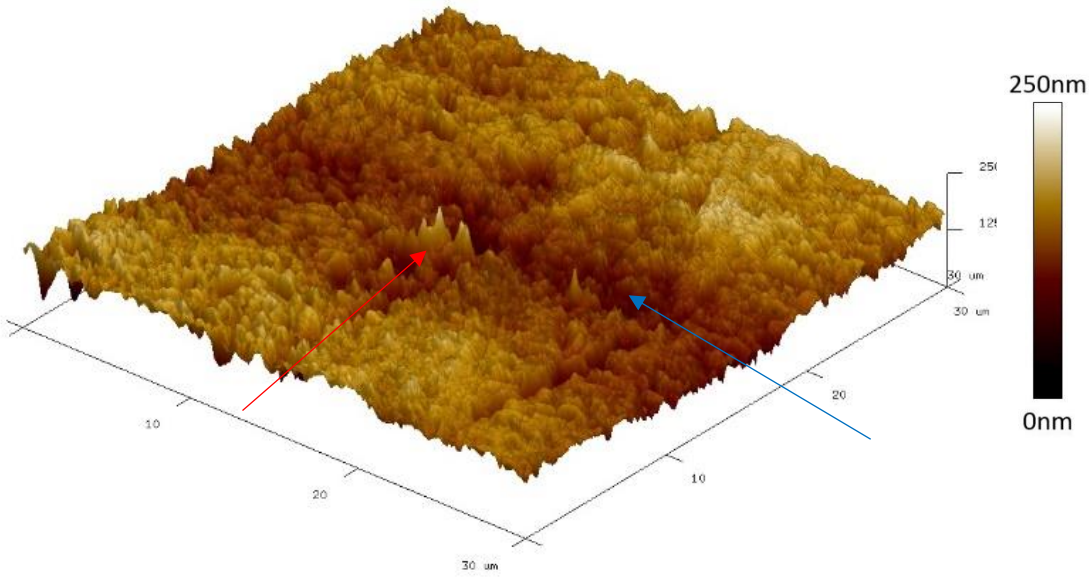

Figure 6-22: A topography scan of the middle region of the wear scar after removal of a 0.55wt% ZDDP tribofilm.

The lowest concentration wear scar (shown in Figure 6-23) has a much smoother topography, with little evidence of the rounded pad like structures shown in Figure 6-22. It also shows fewer areas with artefacts, although as mentioned above these cannot be entirely avoided in any scan. There are three apparent scratches on the surface, and as they are oriented in the stroke direction (and not the scanning direction) it is likely these are true scratches and are present on the surface, red arrows. It is also worth noting that whilst this scan is presented with a height scale between 0nm and 250nm (as all of the wear scar topography scans are) the true height variation is only over a range of approximately 100nm. This scale has been imposed to facilitate a visual comparison, particularly as the scale is only at most a semi-quantitative measure (as a result of the influence of surface artefacts on the maximum and minimum values).

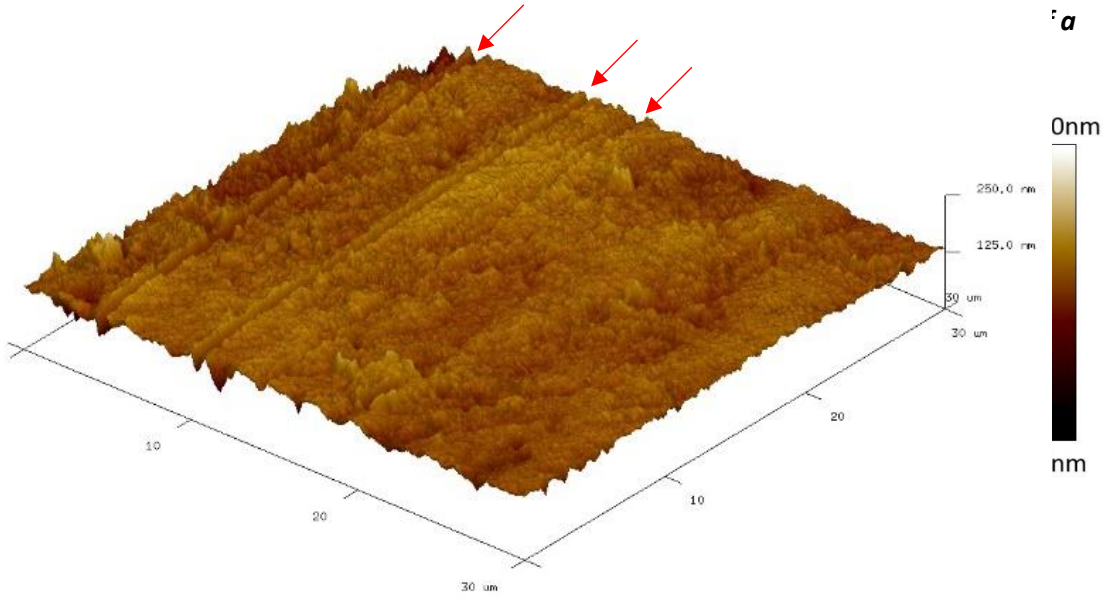

Figure 6-24 displays two obvious artefacts (indicated by red arrows) but otherwise displays more rounded pads (as observed in Figure 6-22). These rounded pads appear smaller than for the 0.55wt% scan (typically in the order of 0.5µm) with more distinct regions between them, particularly towards the centre of the scan. As for the 0.11wt% scan (Figure 6-23) the height scale is misleading with the true height range again only spanning approximately 100nm. The artefacts on this scan appear truncated as the scale has once again been imposed upon the scan to facilitate a visual comparison.

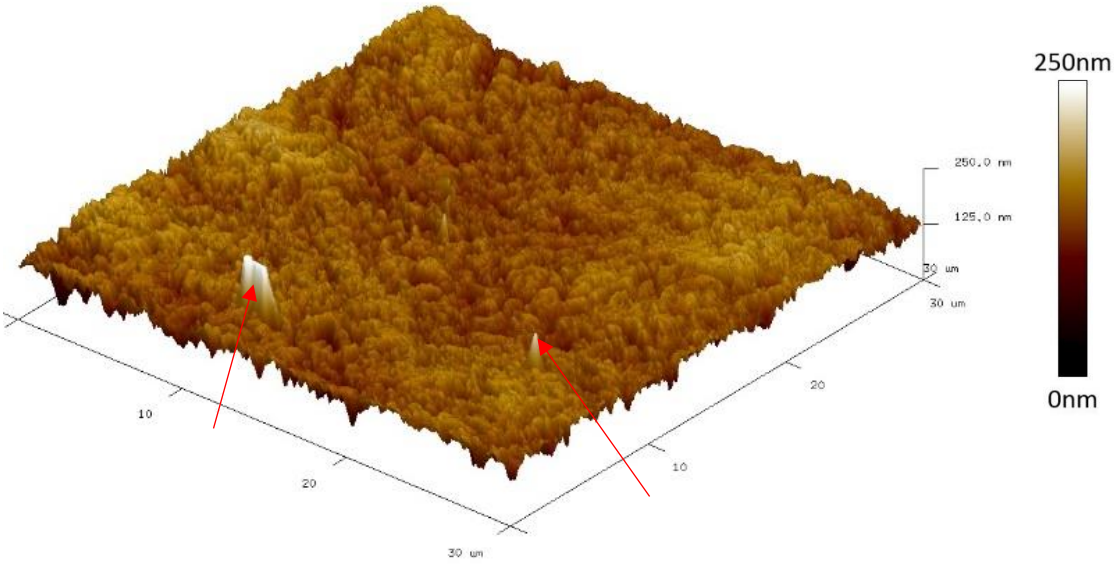

Figure 6-24: A topography scan of the middle region of the wear scar after removal of a 0.275wt% ZDDP tribofilm.

6.3.2.3 Wear scar topography variations with position

The end region (shown in Figure 6-25) has two scratches (indicated by red arrows) but otherwise has a smooth surface. There are several small peaks (indicated by blue arrows) which could be residual asperities but could also be artefacts. The variation in the position of these peaks across the scan indicate that these are real phenomena. There are also two small pits (indicated by green arrows), which could potentially be connected to nearby peaks although this could not be confirmed, and these do not appear to be artefacts either. The

edge of the scan, toward the right, appears peculiar; however, this is due to the edge of the scan happening to be at the apex of a raised region which is adjacent to one of the aforementioned scratches.

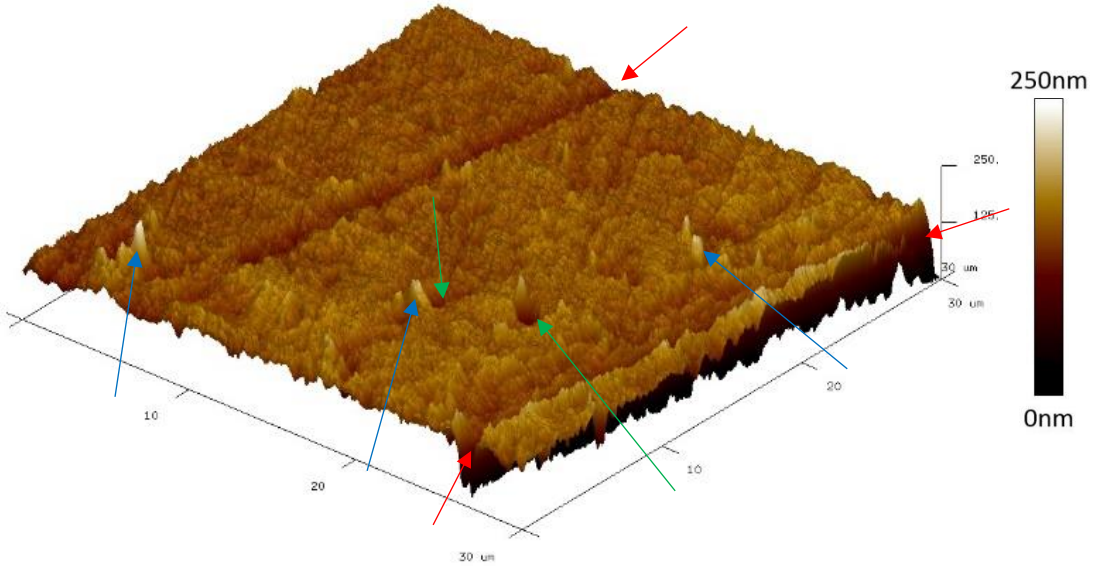

Figure 6-25: A topography scan of the "A" region of the wear scar after removal of a 0.55wt% ZDDP tribofilm.

Figure 6-26 is a re-presentation of the middle region shown in Figure 6-22. It has been re-presented here to aid in a comparison with the other regions.

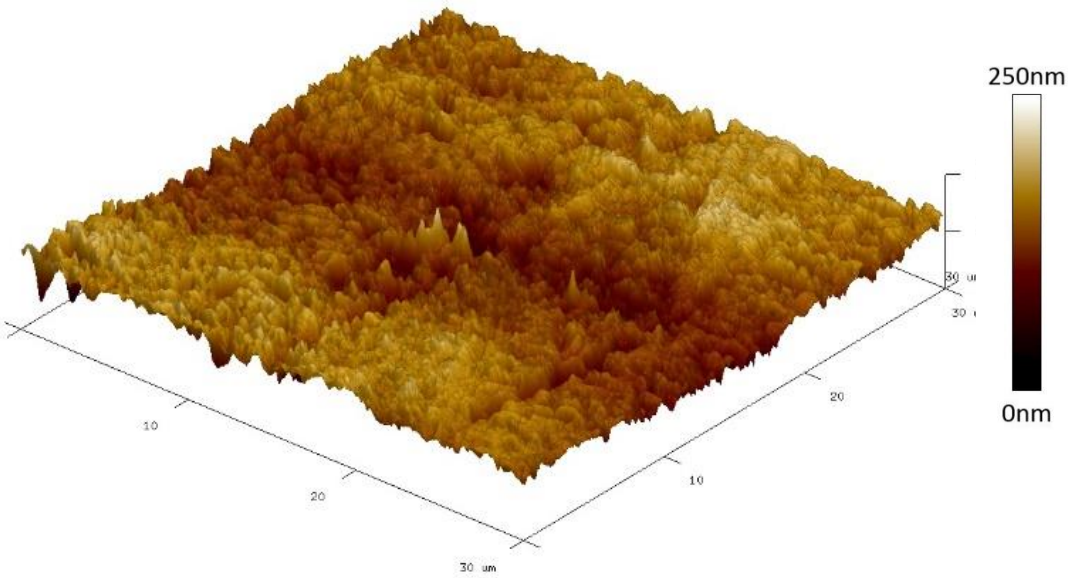

Figure 6-26: A topography scan of the "B" region of the wear scar after removal of a 0.55wt% ZDDP tribofilm.

The rounded mounds on the surface (indicated with red arrows) in Figure 6-27 are similar to those in Figure 6-26; however, these are interspersed with other sharper features (as indicated with blue arrows). Additionally, there are noticeably raised regions, some of which appear to be the result of the sharper features, perhaps indicating these are residual asperities. However, there is another raised region (indicated with the green arrow) which is linear in shape, as opposed to being random asperities. This is aligned in the stroke direction, not the scanning direction, indicating it is not an artefact. There appears to be a small trench next to it (in the foreground) which indicates that this feature is the result of displaced material caused by ploughing.

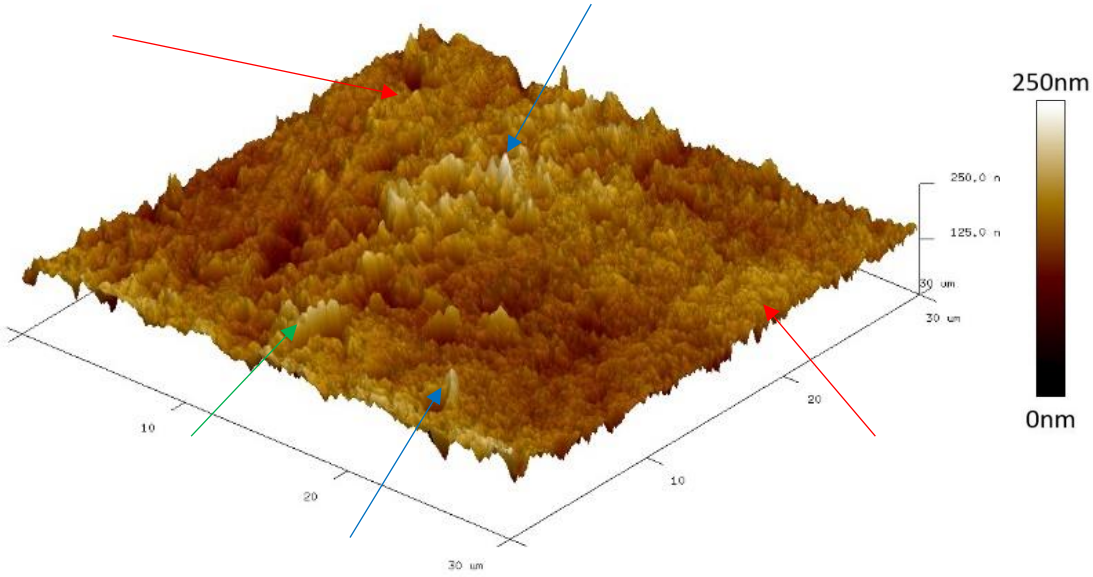

Figure 6-27: A topography scan of the "C" region of the wear scar after removal of a 0.55wt% ZDDP tribofilm.

The “D” region shown in Figure 6-28 has large rounded peaks (typically between 2 and 3 µm in diameter), which are very different to the sharp asperities observed for the initial topography scan. The scan shows no evidence of directional wear, with no features specifically in the stroke direction. There are also no obvious imaging artefacts. The height difference in this scan is the most severe out of any of those considered (although the same height scale has been used in each scan to facilitate comparisons). The unusual topography displayed within this scan could be as a result of its location across the width of the wear scar. Care was taken to limit the importance of width as a variable within this study; however, if the scan was taken towards the outer edge of the wear scar (perpendicular to the stroke direction) this may account for the large peaks.

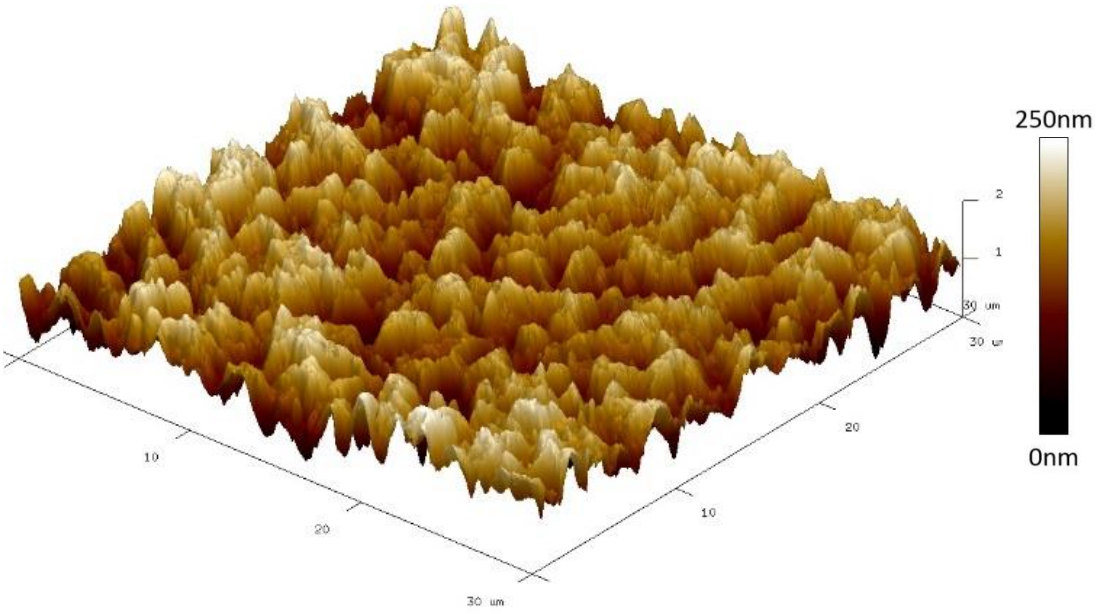

Figure 6-28: A topography scan of the “D” region of the wear scar after removal of a 0.55wt% ZDDP tribofilm.

6.5 Discussion

This study employed a small range of maximum lambda ratios. These were varied only by the influence of concentration on the pressure-viscosity coefficient. The maximum lambda ratios were 0.0299, 0.0309 and 0.0305, which are all considerably lower than the commonly quoted threshold for boundary lubrication ($\lambda = 1$). The small variation between these lambda ratios was as a result of maintaining constant test parameters between tests, with the only dependent variable being the concentration. These maximum lambda ratios could be increased by using a higher frequency, a lower force or a different material for the test samples. The conditions used in this study were selected to be both representative of the industrial contact and for comparison to previously published work.

6.5.1 Wear and Roughness

The results show that wear has occurred for all concentrations regardless of position. It is proposed that this wear occurs alongside tribofilm formation and evolution, instead of occurring purely before formation.

It has been seen that the position affects the tribofilm roughness (R_a) more in regions which have been exposed to a lower concentration of ZDDP; this may be due to the tribofilm forming less rapidly and with a less effective coverage. The topography scans appear to indicate that the lower concentration tribofilms, or pads forming in regions of higher lambda ratio, are less even, which is partially supported by the R_a measurements. From this it could be extrapolated that, given the sacrificial nature of ZDDP tribofilms, continued rubbing within an additive containing oil will result in a continual evolution of the tribofilm morphology until an even coverage is achieved. This would appear similar to the low lambda ratio region of the highest concentration tribofilm. This implies that the concentration and lambda ratio may only affect the initial tribofilm morphology, with continued testing resulting in a less distinctive difference. This would also support the concept that the 1.1wt% ZDDP tribofilm

topography is dominated by an even coverage of small pads that are on top of a uniform film, with these pads having a higher thickness. An attempt was made to quantify the thickness of the tribofilm, using the EDTA method presented in section 5.3.2; however, this was not successful enough to confirm this hypothesis.

Whilst the R_a values, for both the tribofilm and the cleaned wear region, show some evidence of differences as a result of the position and concentration these are not apparent in the more advanced surface parameters. There is a large variance in the other surface parameters between seemingly similar scans. The 3-dimensional aspect of these calculations results in a more complete understanding of the variable nature of ZDDP tribofilms and further indicates that the assumption of morphological uniformity across a tribofilm is wrong.

6.5.2 Topographic Comparison to Literature

As noted in the literature review no studies have previously conducted such a robust characterisation of the tribofilm topography; however, a number of topographic results have been presented as a secondary analysis. These papers do not state the specific locations of the scans within the wider wear scar, but a qualitative comparison is possible.

The larger pads, observed for the lower concentrations and the middle position, are not dissimilar to those presented by Narita et al [76], which are stated to be from the central region of a TE77 wear scar (although no definition of central is provided, meaning it could either be central along the stroke length of the wear scar width). The larger pads here are typically 10-20µm in length, as are the ones in the current study; however, these are elongated in the stroke direction. The current study shows some evidence of pad directionality; however, this is not as apparent as in Figure 6-29. This could be as a result of differing test durations or differing lambda ratios (these are not stated within the literature).

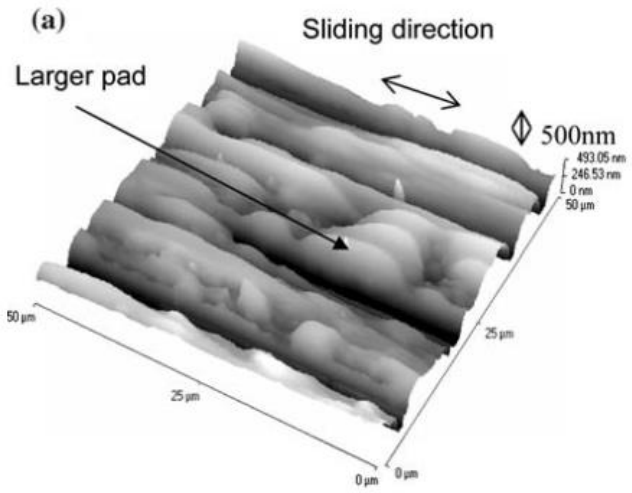

Figure 6-29: A topography scan of a ZDDP tribofilm, originally published by Narita et al [76]**.**

The smaller pads are reminiscent of the small pads observed in part of the alkyl ZDDP tribofilm shown in the Graham et al work [8], which also uses a reciprocating tribometer. The pads presented in the previous work, however, are somewhat smaller than those observed in the current work (the smallest of which were approximately 3µm), with a typical pad size of <2µm. The test conditions to generate the previous tribofilm were very similar to those used within the current study, with the primary difference being that the previous study used a lower initial peak Hertzian contact stress, indicating that the evolution of the tribofilm should have progressed to the same location. The presence of both large and small pads within Figure 6-30 supports the results presented in the current work; however, the current results did not replicate the apparent regional effect of these, with the distribution of both large and small pads being more even. The indication of the sliding direction indicates that the scan has been taken with the upper and lower portion being in different positions across the width of the wear scar, which will also have a distinction in lambda ratio, suggesting that further investigations may be required to also characterise the effect of lambda ratio, driven by conformity of the wear scar, on tribofilm morphology.

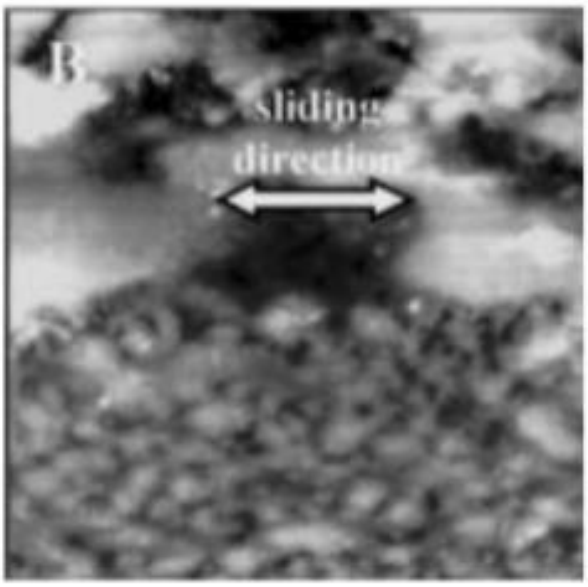

Figure 6-30: 25µm x 25µm topography scan of an alkyl ZDDP tribofilm [8]***.***

6.5.3 Tribofilm Formation Mechanism

The results show that for a high concentration in an area of low lambda ratio (end region) the tribofilm produces small pads (between 2 and 5µm). For a low concentration in an area of high lambda ratio (middle region) the tribofilm produces large pads (approximately 20µm in length); and for either a high concentration with a high lambda ratio or a low concentration with a low lambda ratio the tribofilm pads are of a variable size, with both large and small pads present.

A mechanism is proposed for how these are formed. The mechanism has three steps. The ZDDP in the lubricating oil is represented in our first stage, with step one (the process between the stages) being the thermal decomposition of the ZDDP chains into phosphate and polyphosphate chains (shown in stage two). The second step in the mechanism is the adsorption of these chains onto the surface (resulting in stage three). Once these chains are adsorbed onto the surface, and the sample is removed from the oil, the chains appear as pads on a macro scale (when viewed from above using an AFM). This is represented schematically in Figure 6-31.

This mechanism explains the effects of concentration and lambda ratio and how these can result in different shaped phosphate pads in the tribofilm. The concentration is shown in stage one, with a schematic representation of ZDDP chains in the oil. The lambda ratio (position) is shown by different magnifications of asperities in the contact. In a lower lambda ratio, there would be more asperity-asperity contact and thus more tribo-decomposition.

Whist it might be expected that for a high concentration of ZDDP in a region of high lambda ratio (“high-high”) one would see the intermediate size pads (likely between 5 and 15µm), as one does for the low concentration in a region of low lambda ratio (“low-low”), one would expect these to be more prevalent than for the “low-low” example. A potential reason for this not being the case in the presented results would be that there is an equilibrium state where increasing the concentration is ineffective because there are insufficient asperity-asperity contacts to result in the thermal decomposition, as Naveira-Suarez et al [68] found the contact was required to start the decomposition.

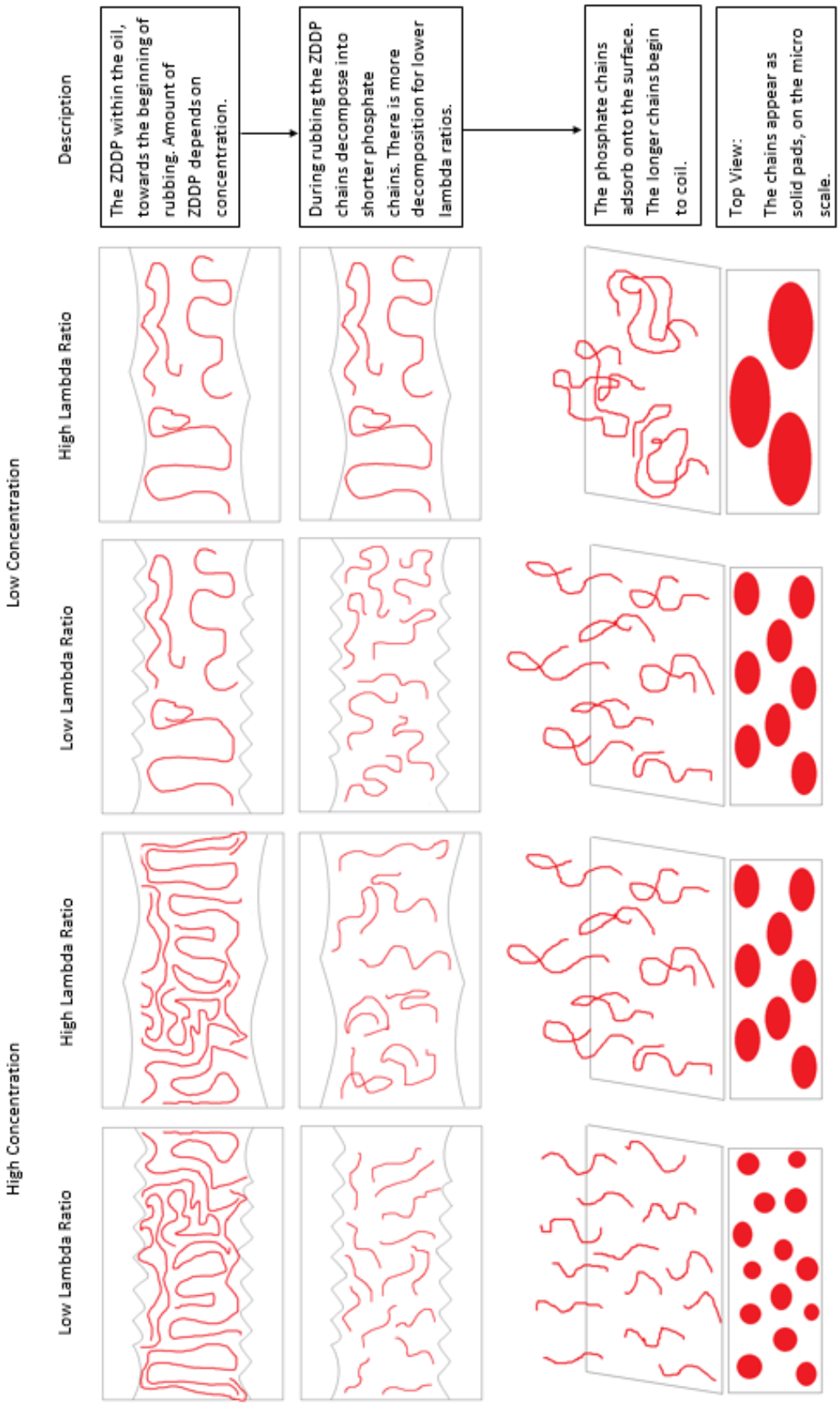

Figure 6-31: A schematic to represent the proposed hypothesis.

6.5.4 Applying Mechanism to Literature

The mechanism presented in Figure 6-31 presents steps previously suggested by both Naveira-Suarez et al [68] and Piras et al [67]. These consist of a two phase tribofilm decomposition method, consisting of both a rubbing and then adsorption stage. We expand the mechanism to take into consideration the effect of concentration as well as the effect of a varying lambda ratio in a reciprocating system.

Naveira-Suarez et al [68] presented their mechanism after observing images captured using a spacer layer interferometry system. However, this was attached to a unidirectional tribometer. The results presented for the SLIM aspect of their research show small pads (without a scale), but the additional AFM images included showed a range of topographies from smaller pads to a complete coverage. They theorise that the formation mechanism (ignoring the effect of position) starts with small pads, on the asperities themselves, and then these grow to form larger pads until a full coverage is present. If the assumption that the higher concentration can be assumed to represent a later stage of the tribofilm formation process is correct it would be expected, based on their research, to see a series of large pads. However, the results presented in this document show that for the large concentration there are a series of small pads. It is possible that the small pads seen in the 1.1wt% tribofilms are only the upper layer of a more complete tribofilm. This is supported by the tribofilm roughness (R_a) measurements, which indicate that whilst the topography appears to be rough, it is actually a smoother surface than those found in the majority of the lower concentration scans.

Gosvami et al [3] presented very small pads, over twenty in a 1µm x 1µm area. These would fit well with the proposed mechanism as these pads were generated in-situ in an AFM and the counter-surface was an AFM tip. The AFM tip can be assumed to act as a single asperity counter surface, resulting in a very low lambda ratio. This would mean that

independent of the ZDDP concentration there would be very short chains present and thus small pads. The quantity of pads observed in this research would indicate a high concentration of ZDDP was used; however, Gosvami et al [3] do not release the exact concentration in their paper. They state that the nucleation sites (adsorption sites) appeared to form randomly, as opposed to on asperities (as thought by Naveira Suarez et al [68]). This could also be explained by the current mechanism as for a single asperity contact the decomposed phosphate chains, prior to adsorption, would be only stimulated by the AFM tip, whereas in a traditional contact the adsorption would be stimulated by other asperities. This supports the presented theory that the chains are decomposed by asperities but are not necessarily immediately adsorbed to the surface.

Gosvami et al [3] also showed that the position of the reciprocating system had an effect on the tribofilm growth, with thicker (higher) pads being formed at the ends of the stroke length (shown by red arrows on Figure 6-32). This supports the theory that the lower lambda ratio end points are experiencing a more rapid formation of the pads, and that these pads are at a later stage of the tribofilm evolution. They also show that for a longer test (a higher number of sliding cycles) the pads begin to form an under layer with the small pads present on top, as shown by black arrows in Figure 6-32. This supports the theory that the 1.1wt% topography scans are only showing the top layer of a multi-layered tribofilm. Future work could investigate a potential method to determine the tribofilm thickness, to confirm whether the 1.1wt% tribofilm is thicker.

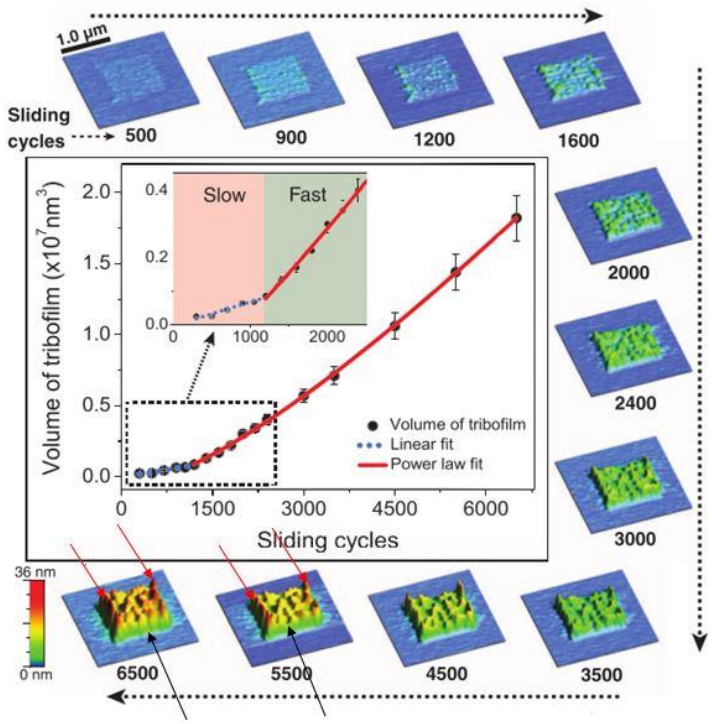

Figure 6-32: Morphology and volumetric growth of a ZDDP tribofilm, adapted from Gosvami et al [3]***. The green areas, marked with arrows, in 5500 and 6500 sliding cycles show a complete coverage with smaller pads on top.***

6.6 Summary

This section presented the method and results for the characterisation of ZDDP tribofilms. It was found that there is a difference in the pad morphology of tribofilms relating to the amount of ZDDP additive present in the oil used to form the tribofilm. When more additive is present the pads tend to be smaller (approximately 5µm) and there is a more even coverage of ZDDP across the surface. When there is less additive present the pads are often larger (approximately 20µm), with clear regions between them.

In addition, it was observed that the position along the reciprocating stroke length also affected the pad morphology, corresponding to the lambda ratio ($\lambda \leq 0.029$, 0.275wt%; $\lambda \leq 0.0309$, 0.55wt%; $\lambda \leq 0.0325$, 1.1wt%). In regions which experienced a higher velocity (and thus a higher lambda ratio) the pads were often larger (in the order of 10µm to 20µm), whereas the regions which experienced a lower velocity (and lower lambda ratio) were typically smaller (between 3µm and 5µm) and more evenly distributed.

A hypothesis has been presented to explain these differences in morphology, as a result of a marginally different formation mechanisms. It is proposed that the sections of tribofilm formed in regions of increased shear (lower lambda ratio) or in the presence of more ZDDP are formed from more, but shorter, polyphosphate chains adhering to the surface. This results in a smaller surface pad but with less distance between them, and generally more being present within the same area. The tribofilms generated in regions with less shear, or less ZDDP, are formed from fewer, but potentially longer, polyphosphate chains which adhere to the surface and result in larger, but more discrete, pads.

Chapter 7: Durability of ZDDP Tribofilms – Phase 2

This chapter summarises the second phase of this research project. It details the testing and analysis conducted to determine the tribofilm durability.

There were two sections to this aspect of the research, with a preliminary study and then the main activity. The preliminary study demonstrates that the technique being proposed can manipulate a ZDDP tribofilm. The main study investigates both the effect of concentration, if any, on the resultant tribofilm durability and whether the load applied by the AFM has a demonstrable effect on the rate of tribofilm manipulation.

This chapter proposes a methodology for tribofilm manipulation, and an analysis method to quantify the extent of tribofilm material displacement. It summarises results and presents explanations for important observations.

7.1 Introduction

Work by Gosvami et al [3] and Dorgham [112] showed that the AFM is more versatile than had previously been used in tribology. By generating tribofilms in-situ they showed tribologists that there were other possible uses for this long-standing analysis tool.

Having demonstrated that the AFM could be used to generate tribofilms, Gosvami et al effectively showed that the AFM can be used as a nano-tribometer. The fact that the AFM can be used as a nano-tribometer led to the question of what else it could be used to do.

This section of the research aimed to determine whether the AFM could be used to get a quantitative measure of the tribofilm and whether this could be done repeatably. An attempt was made to answer the following questions in this stage:

- Is it possible to change an existing tribofilm using a commercially- available AFM?
- Does the concentration of the oil used to generate the tribofilm, and the resultant difference in pad morphology, affect the extent to which the AFM can alter the tribofilm?
- Can a repeatable method be created to use the AFM as a nano-scratch tester, to deform or remove the tribofilm?
- Is it possible to create a standard analysis tool to quantify the extent to which the tribofilm is changed?
- Can the volume of material displaced be compared with the theoretical wear volume from Archard's wear law?

This phase of the research consisted of both a preliminary study and a main study. The results of each are presented separately, due to differing methodologies.

7.2 Tribofilm Generation

To allow for comparisons between the two phases of research a similar method was used to generate the ZDDP tribofilms in phase 2, as had previously been used in phase 1. The most important difference for phase 2 was that the initial topography was less controlled, with the samples not being subjected to an additional polish immediately prior to testing. This alteration was considered necessary due to the adverse effects on the TE77 of the initial testing campaign, specifically caused by the very small gradient created across the surface. Having opted to not polish the samples further, this phase of the research is more representative of the tribological testing typically done utilising a TE77 test rig.

The specific conditions used to generate the tribofilms are detailed in the following table, including the nominal surface roughness for a traditional TE77 test sample. As in phase 1 the oil used was a pre-blended ZDDP and PAO, gifted to the study by Afton Chemical.

Table 7-1: The parameters used to generate the tribofilm samples for the phase 2 analysis.

Parameter	Value
Test sample geometry	A 7mm x 7mm plate
Test sample material	EN31 steel
Test sample R_a	10nm (Standard deviation - 3nm)
Counter surface geometry	Cylinder, with end radius 10mm
Counter surface material	EN31 steel
Stroke length	7mm
Temperature	100°C
Frequency (representative speed)	25Hz (0.35m/s)
Load (max Hertzian contact stress)	65N (1.14GPa)
ZDDP concentrations	0.275wt% and 0.55wt%
Duration	60 minutes

After TE77 testing the samples were cleaned using n-heptane and a lint-free cloth, in accordance with the procedure established in phase 1.

7.3 Preliminary Study – AFM methodology

The TE77 samples were mounted onto a magnetic holder to ensure stability after insertion into the AFM. The wear track was orientated such that the original wear direction was perpendicular to the scanning direction of the AFM tip.

The AFM tip used for all aspects of the preliminary study was a Bruker Tap525 (which was a commercially available variant, subsequently withdrawn), which consists of an antimony doped silicon cantilever with a nominal spring constant of 375N/m. The initial tip radius (as specified by the manufacturer) was 10nm.

The sample was entirely exposed to air throughout the process, and to ensure the absence of particulate contaminants the surface was wiped with a dry lint-free cloth immediately prior to insertion into the AFM. Two different scan types were utilised in this part of the study; one to determine the changing topography of the sample and one to scratch the surface of the tribofilm to determine if it could be altered.

The topography of the surface was analysed using a scan area of 15µm x 15µm (corresponding to 512 “taps” per line and 512 lines), with a scan rate of 0.751Hz (the same scanning rate as had been utilised in phase 1, which determines the raster speed of the tip against the surface). The scanning mode chosen for this was the Peak Force Tapping Mode, with Scan Asyst, as this is the preferred option for use in determining topography. The load applied during each tapping motion was not permitted to exceed 10µN; however, the specific load in each contact was computationally controlled.

A “wear scan” was conducted as a series of contacting line profiles (scratches) across a 5µm x 5µm area (corresponding to a 258 measurements per line and 258 lines per scan), in the centre of the topography area (as indicated Figure 7-1). The scan rate was 0.528Hz, which was selected as a compromise to reduce the torsional strain on the cantilever whilst

ensuring the testing completed within a reasonable time frame. The load applied was specified as a fixed voltage, 5V.

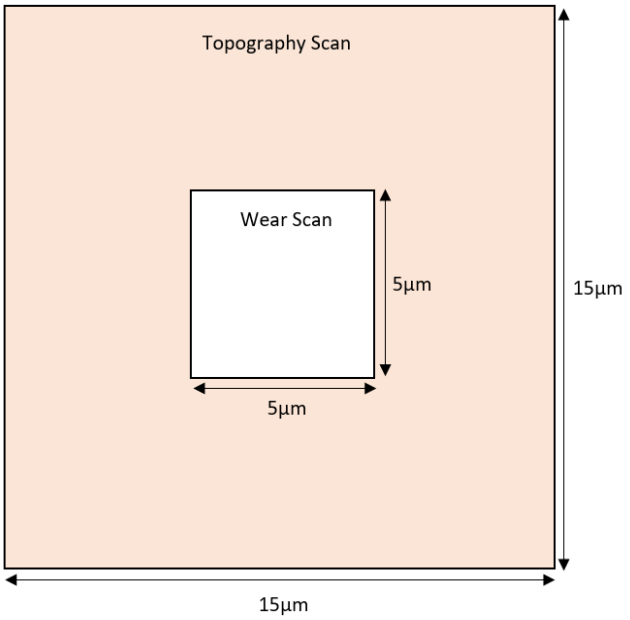

Figure 7-1: A schematic to show the relative positions of the scans used in the durability study.

The preliminary study consisted of two locations, each located in the middle (maximum speed) region of the wear scar. For simplicity these locations are simply referred to as “location 1” and “location 2”.

The scans were conducted in the following sequence, to enable continuous monitoring of the overall topography.

1. 15µm x 15µm topography scan
2. 5µm x 5µm wear scan x 5 times
3. 15µm x 15µm topography scan
4. Repeat steps 2 and 3 until 20 wear scans have been completed

7.4 Preliminary Study – Results

Figure 7-2 shows the progression of the topography with ongoing wear scans. After 5 scans there is evidence of some tribofilm displacement, with small raised regions when compared to the initial scan. After a further 5 scans (10 scans) there are two clear raised regions and the worn region can be clearly seen. Subsequent scans show larger raised regions and a very clear worn square. The left raised region (corresponding to displacement caused by the retrace motion) is larger than the right region (caused by the trace motion). The left region is unexpectedly longer than the worn region, with the displaced material covering an area approximately 7.5µm x 5µm.

The second location, Figure 7-3, shows tribofilm displacement occurring more immediately than observed in Figure 7-2. There is evidence of a worn region after 5 scans, as well as clear raised regions to either side. The raised region to the left (the retrace direction) has an unusual morphology, with the appearance of seemingly angled shapes, indicated by the red lines. The subsequent scans also show large raised regions, increasing in volume, which also consist of the strange angular shapes. The two-dimensional volume of the raised regions between the topography scans after 15 and 20 wear scans does not appear to increase; however, the height of the displaced material increases. This indicates that the worn region has not yet achieved an equilibrium.

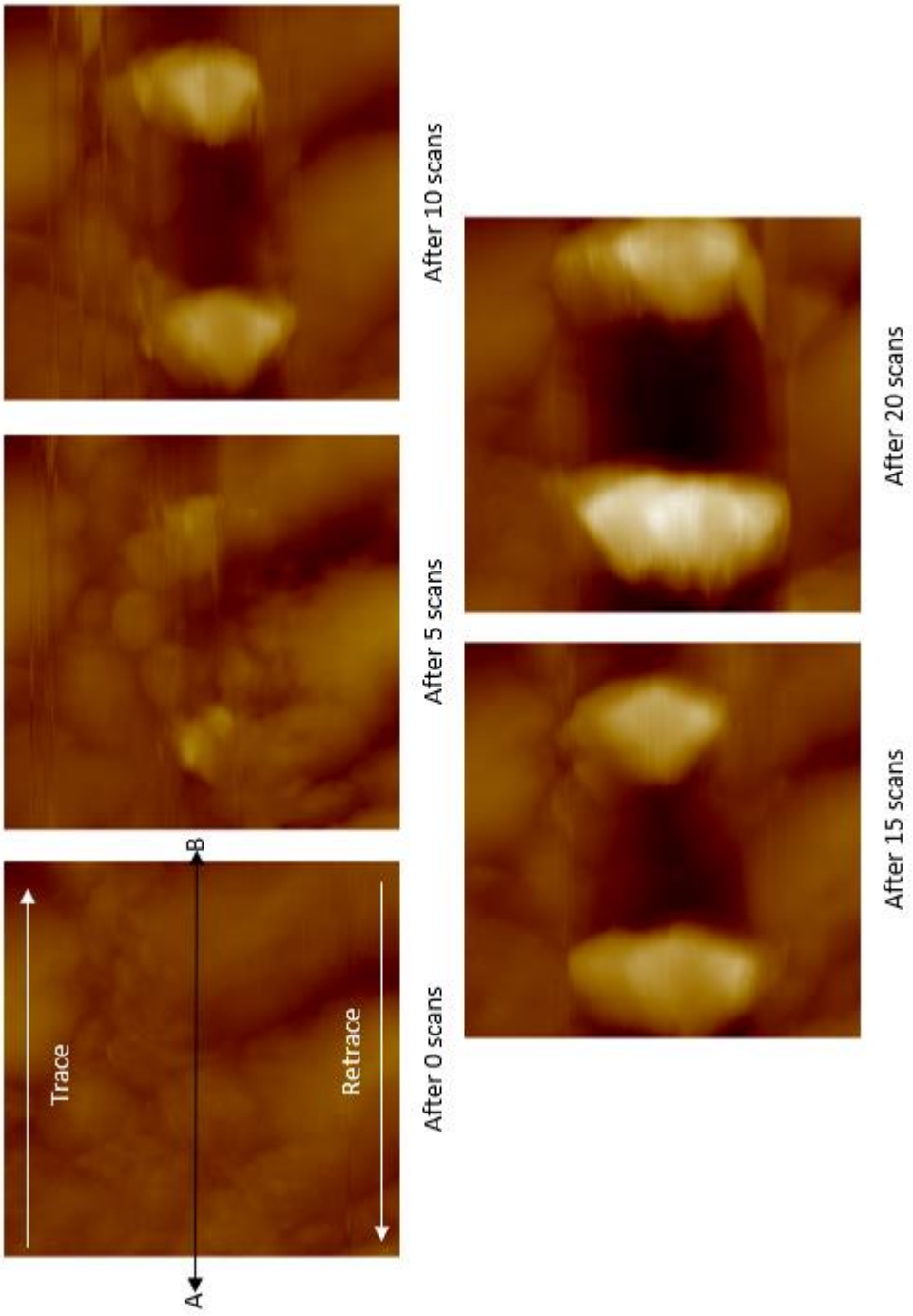

Figure 7-2: The topography progression in a 0.55wt% tribofilm – preliminary study test 1. A to B shows a representative location for the cross section used in Figure 7-4 and Figure 7-6

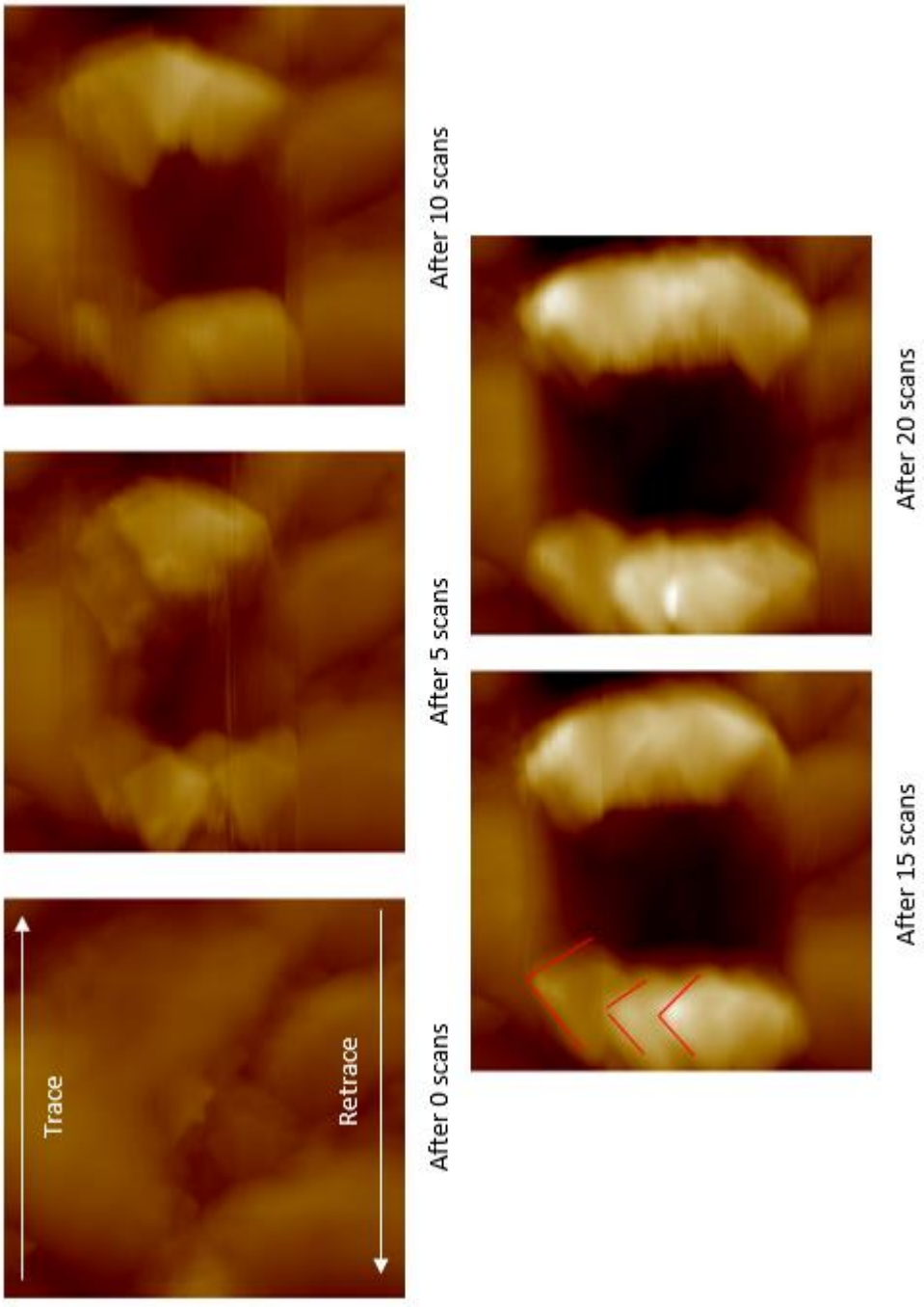

Figure 7-3: The topography progression in a 0.55wt% tribofilm – preliminary study test 2.

Figure 7-4 shows the specific areas used to quantify the decrease in relative height of the worn region, Figure 7-5. This shows that after 5 scans the scan "location 2" had been worn considerably less than the "location 1" scan. From 10 wear scans onwards the relationship between the number of wear scans and the relative depth of the wear region appears to have the same gradient for both locations.

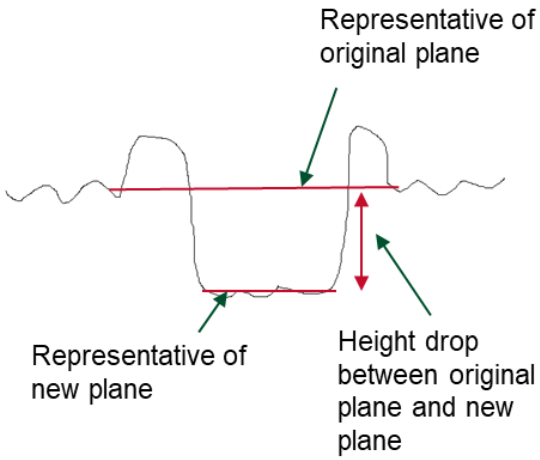

Figure 7-4: Representative cross-section of a topography scan, corresponding to the line A-B in Figure 7-2, indicating the worn region.

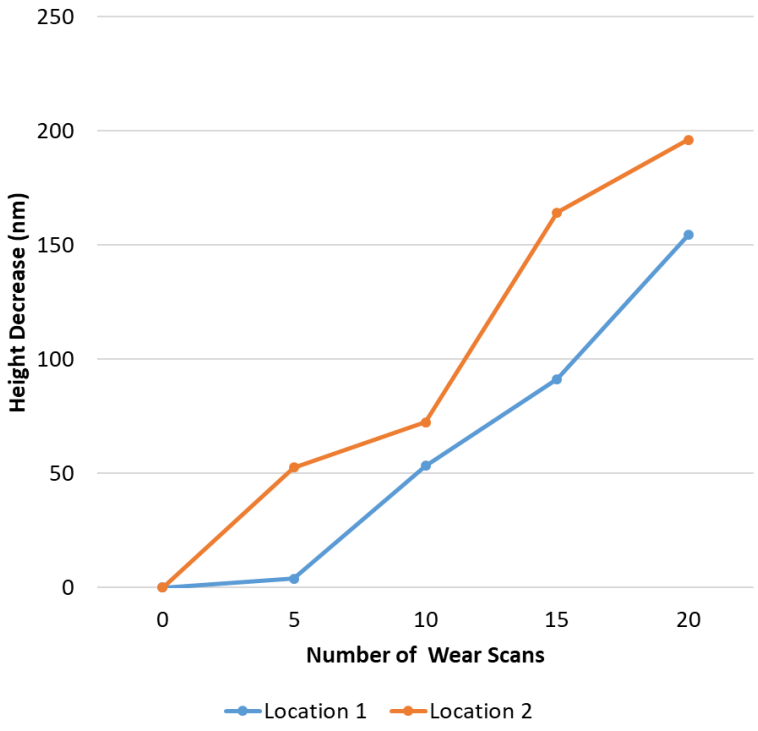

Figure 7-5: The relative change in height in the worn region.

Figure 7-6 shows the specific areas used to quantify the increase in the regions either side of the worn region, Figure 7-7. The trace values are taken from the raised region located to the right (as seen in the cross-section) and the retrace are taken from the raised region located to the left. There is no meaningful difference in the height of the raised regions caused by the trace and retrace motions.

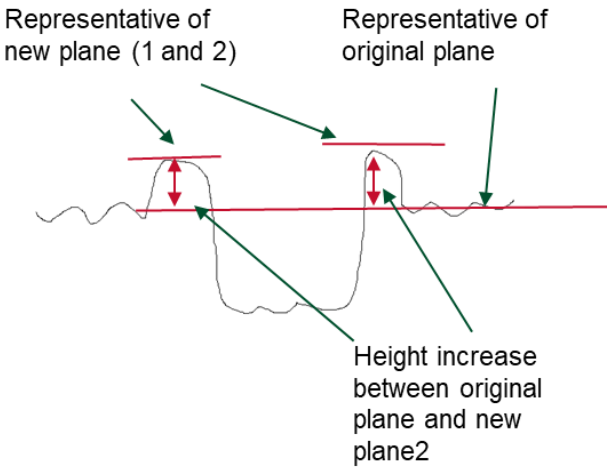

Figure 7-6: Representative cross-section of a topography scan, corresponding to the line A-B in Figure 7-3, indicating the raised region.

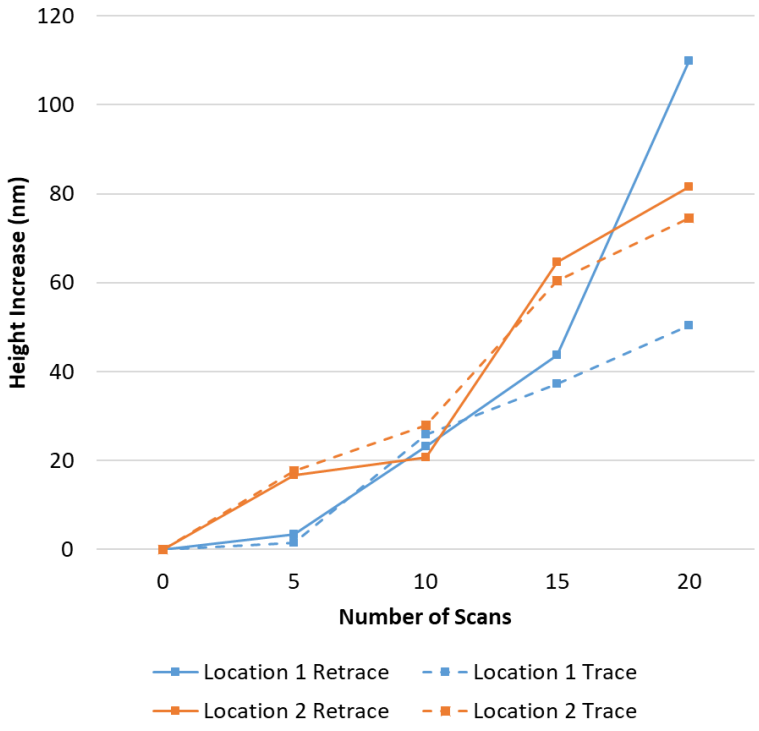

Figure 7-7: The relative change in height around the worn region.

7.5 Preliminary Study – Lessons Learned

The preliminary study showed that the methodology used, whilst effective, was not repeatable as the normal load applied to the tip was not constant between scan locations. The load applied was dependent on the spring constant of the cantilever. However, for financial and efficiency reasons the decision was made to use a different cantilever for the main study. This different cantilever resulted in a lower maximum possible load for the subsequent tests. Whilst likely reducing the extent to which the tribofilm could be manipulated a lower load capability enabled this researcher to determine the exact load applied and to ensure repeatability within the main study.

The preliminary study also showed that there was little difference in the height increase, caused by displaced material, between the trace and retrace directions, as well as some repeatability in the gradient for the material removal within the worn region. These findings supported the premise for the research, that it is possible to learn about ZDDP tribofilms using an AFM. The main study would build on these findings to determine the extent to which the AFM can be used, as well as to determine whether there is a difference in the durability of ZDDP tribofilms depending on the concentration of ZDDP in the oil used to generate them.

7.6 Atomic Force Microscopy – Scratch Test Methodology

To ensure an accurate comparison of the applied load between tests it was necessary to confirm the means by which the load measurement is applied in contact mode. This is achieved using the calibration of the AFM, which determines the spring constant and the deflection sensitivity for each tip.

Table 7-2: The calibration values for the AFM – to enable the calculation of applied load.

Test Name	Deflection Sensitivity	Spring Constant
0.275wt% 0.005mN 1	124.4nm/V	15N/m
0.275wt% 0.005mN 2	129.5nm/V	15.88N/m
0.275wt% 0.005mN 3	131.6nm/V	25.37N/m
0.55wt% 0.005mN 1	129.5nm/V	13.60N/m
0.55wt% 0.005mN 2	134.8nm/V	19.49N/m
0.55wt% 0.005mN 3	111.6nm/V	17.99N/m
0.55wt% 0.01mN 1	72.24nm/V	26.47N/m
0.55wt% 0.01mN 2	80.34nm/V	32.26N/m
0.55wt% 0.014mN 1	82.29nm/V	33.2N/m
0.55wt% 0.014mN 2	94.34nm/V	22.08N/m

7.6.1 Topography Method

The topography scans for the main study were gathered in almost the same way as the equivalent scans in the preliminary study. The only difference in test parameters for the main study was the substitution of a more economical cantilever (the Tap 525 was replaced by the RTespa 300). This alteration was programmatically driven to enable a fresh tip to be employed for each of the tests.

The parameters are summarised in Table 7-3 for completeness.

Table 7-3: A summary of the parameters used in the topography scans.

Parameter	Value
Tip material	Antimony doped silicon
Nominal tip radius	8nm
Tip classification	RTespa 300
AFM mode used	Peak Force Tapping with Scan Asyst
Scan area	15µm x 15µm
Scan rate	0.751Hz
Scan environment	Air

7.6.2 Contact Mode Method

The wear scans were conducted using a built-in analysis mode for the AFM, called contact mode in air. This enabled control over the applied force, as well as the scan rate and scan area.

As with the preliminary study the wear scan area was 5µm x 5µm, and the scan rate was 0.528Hz. The study was, again, conducted with a dry sample and the wear scanning was conducted in the centre of the larger topography scans, as in Figure 7-1. The load used in the concentration comparison study was 0.005mN, with 0.01mN and 0.014mN used to determine the effect of load.

The Scan Asyst function was not enabled for the wear scans, therefore, the AFM feedback was controlled using fixed values for both the integral gain (5) and the proportional gain (10). These values for the feedback were determined iteratively, over several initial contact scans. To control the load a conversion was necessary to convert the required force to an applicable voltage. The conversion is specific to each calibration, with a conversion constant being calculated from the calibration values (as per Equation 29). The required voltage is then calculated from the specific conversion using Equation 30.

$$\boldsymbol{Conversion = Spring\ constant \times \left(Deflection\ sensitivity \times 10^{-9}\right)}$$

(Equation 29)

$$Voltage = Force\ required \div Conversion \qquad \textit{(Equation 30)}$$

Table 7-4: A summary of the conversions and applied loads.

Test name	Conversion	Applied Voltage
0.275wt% 0.005mN 1	0.000001863N/V	2.684V
0.275wt% 0.005mN 2	0.0000020565N/V	2.431V
0.275wt% 0.005mN 3	0.000003338N/V	1.498V
0.55wt% 0.005mN 1	0.0000017612N/V	2.839V
0.55wt% 0.005mN 2	0.0000026373N/V	1.903V
0.55wt% 0.005mN 3	0.0000020077N/V	2.490V
0.55wt% 0.01mN 1	0.0000019122N/V	5.230V
0.55wt% 0.01mN 2	0.0000025918N/V	3.858V
0.55wt% 0.014mN 1	0.000002732N/V	5.230V
0.55wt% 0.014mN 2	0.000002083N/V	6.721V

Assuming that the conditions remain the same throughout the test, with the nominal tip radius, 8nm, being maintained, the maximum Hertzian contact stresses expected are summarised in Table 7-5.

It was assumed that the mechanical properties of the tribofilm dominated, with the film being sufficiently thick as to mask the mechanical properties of the underlying steel. The mechanical properties of the tribofilm have been shown to vary dependent on the position and thickness of the film. Bec et al [75] found that the Young's modulus varies between 15GPa and 40GPa. No value for Poisson's ratio could be determined and thus a value of 0.5 was assumed, because the film can be considered to be highly viscous and thus incompressible. The elastic modulus of the silicon nitride tip is assumed to be 112.4GPa (the maximum modulus for generic silicon) and the Poisson's ratio used is 0.28.

In order to determine whether the applied pressure is enough to indent any point in the tribofilm the maximum Hertzian contact pressure was calculated for both the lowest

possible Young's modulus value and the highest. It is acknowledged that these values are merely indicative, and do not provide a true calculation of the maximum Hertzian contact pressure. However, they do indicate that the contact conditions are sufficient to indent a generic ZDDP tribofilm, which has a hardness between 1 and 2 GPa [75].

Table 7-5: The maximum Hertzian contact stresses applied.

Test name	Load Required	Maximum Hertzian Contact Stress – (for Tribofilm Young's Modulus 15GPa)	Maximum Hertzian Contact Stress – (for Tribofilm Young's Modulus 40GPa)
0.275wt% 0.005mN 1	0.005mN	26.1GPa	43.7GPa
0.275wt% 0.005mN 2	0.005mN	26.1GPa	43.7GPa
0.275wt% 0.005mN 3	0.005mN	26.1GPa	43.7GPa
0.55wt% 0.005mN 1	0.005mN	26.1GPa	43.7GPa
0.55wt% 0.005mN 2	0.005mN	26.1GPa	43.7GPa
0.55wt% 0.005mN 3	0.005mN	26.1GPa	43.7GPa
0.55wt% 0.01mN 1	0.010mN	32.9GPa	55.0GPa
0.55wt% 0.01mN 2	0.010mN	32.9GPa	55.0GPa
0.55wt% 0.014mN 1	0.014mN	36.8GPa	61.5GPa
0.55wt% 0.014mN 2	0.014mN	36.8GPa	61.5GPa

The Hertzian contact stress was calculated using the Equation presented in section 2.4. The below Equations (31 to 42) show an example calculation. The example below is for a 0.005mN load test assuming a 40GPa Young's modulus for the tribofilm.

$$\psi = 1.5277 + 0.6023\, ln\left(\frac{8nm}{8nm}\right) \quad \textit{(Equation 31)}$$

$$\psi = 1.5277 \quad \textit{(Equation 32)}$$

$$\xi = 1.0003 + \frac{0.5968}{\frac{8nm}{8nm}} \quad \textit{(Equation 33)}$$

$$\xi = 1.5971 \quad \textit{(Equation 34)}$$

$$\frac{1}{E'} = \frac{1}{2}\left(\frac{1-0.28^2}{112.4\times10^9} + \frac{1-0.5^2}{40\times10^9}\right) \quad \textit{(Equation 35)}$$

$$E' = 74.213 \times 10^{9} \quad \textit{(Equation 36)}$$

$$a = \left(\frac{6 \times 1.0339^{2} \times 1.5971 \times 0.000005 \times 4 \times 10^{-9}}{\pi \times 74.213 \times 10^{9}}\right)^{\frac{1}{3}} \quad \textit{(Equation 37)}$$

$$a = 9.578 \times 10^{-9} \quad \textit{(Equation 38)}$$

$$b = \left(\frac{6 \times 1.5971 \times 0.000005 \times 4 \times 10^{9}}{\pi \times 1.0339 \times 74.213 \times 10^{9}}\right)^{\frac{1}{3}} \quad \textit{(Equation 39)}$$

$$b = 9.264 \times 10^{-9} \quad \textit{(Equation 40)}$$

$$Pmax = \frac{3 \times 0.000005}{2\pi \times 9.578 \times 10^{-9} \times 9.264 \times 10^{-9}} \quad \textit{(Equation 41)}$$

$$Pmax = 43.7GPa \quad \textit{(Equation 42)}$$

Due to the lower loads applied in the main study the number of wear scans required is predicted to increase. Each test will have 250 wear scans, with topography scans taken at least every 5 wear scans for the first 50 and then at least every 10 wear scans for the remainder of the test. The number of wear scans will be reduced if there is evidence of extreme tip wear, with the resolution of the topography images becoming noticeably affected.

7.7 Analysis Methodology

A computer program was developed to quantify differences between topography scans. This is summarised in this section and the complete code is included as "Appendix 2 – Durability Study Analysis Program".

The program was designed to accurately overlay different topography scans and to correct for small offsets. The amount of material displaced from within the contact region was quantified, as well as the increase in material in the adjacent areas.

Prior to using the analysis program, the results were subjected to a first order "flatten" which centred the data, removed tilt and corrected for minor surface artefacts, as shown in Figure 7-8.

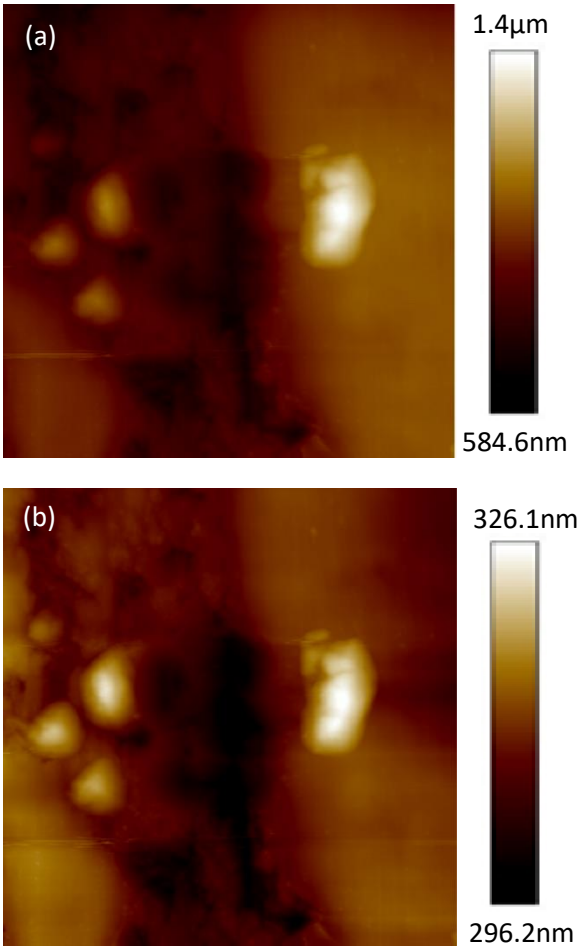

Figure 7-8: Example scan (a) pre-flatten, (b) post-flatten.

The first topography scan was subjected to a least squares plane fit, to create a known corrected scan. This fitted scan was then used as a baseline to which all subsequent scans were corrected, such that a direct quantitative comparison could be conducted

Subsequent scans were corrected by determining the “best offsets” between each scan and its corrected predecessor. The scans were corrected by determining the offsets within a given plane, to correct for thermal drift, but also in the z-axis, to allow for alterations in the zero point between scans, and to correct for plane fit errors. Regions which were included within the first scan but were not included in subsequent scans, due to thermal drift, were set to the original height value, whilst regions that were included in latter scans but were not included in the original scan were excluded from the analyses. An example of this is presented as Figure 7-9.

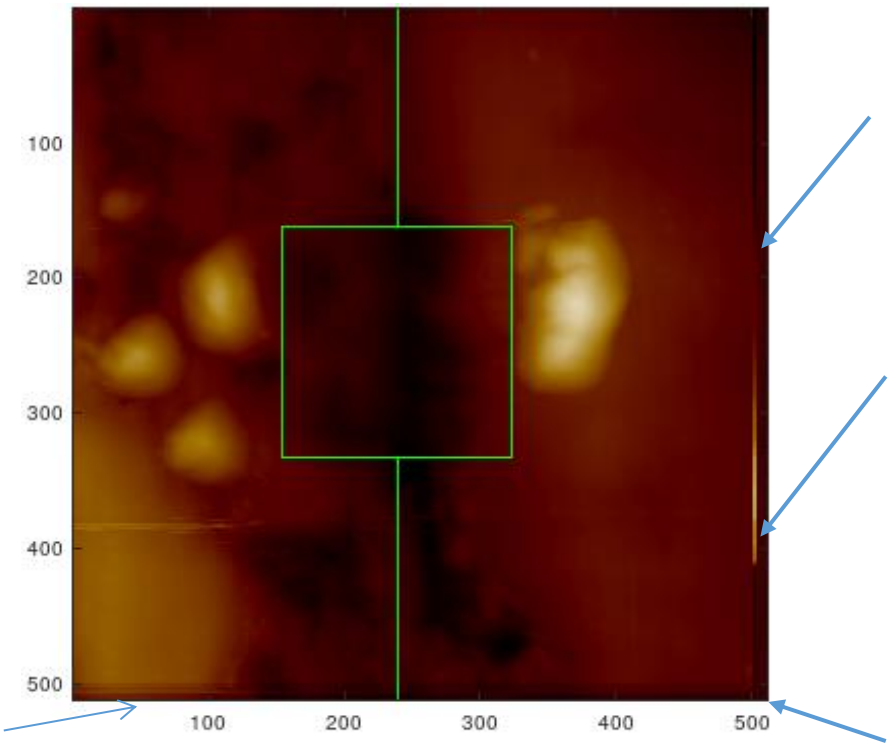

Figure 7-9: A corrected image (using three dimensional offsets) as output by MATLAB. Blue arrows indicate regions which have been auto filled with information from previous scans. The green box indicates the worn region and the green lines separate the remaining scan into left and right (corresponding to the retrace and trace directions, respectively).

The location of the original worn region is used as an input. The initial code (as used to analyse the scans in the preliminary study) determined the worn region as a given dimension (5µm x 5µm) around the location of the maximum height decrease; however, this method (used to analyse the scans in the main study) was revealed to be less than accurate, and an alternative method was developed. The new method assumes that the worn region is located at the centre of each corrected image, independent of the thermal drift. Whilst still moderately inaccurate this was found to be the most repeatable method for quantifying the height differences.

The height differences were ascertained by subtracting the z-values of each corrected initial topography scan from the z-values of the subsequent scan, Figure 7-10. The height difference within the prescribed worn region was considered to be due to the material removal, whilst the height difference outside of the worn region was assumed to be as a result of material displacement. The material lost from the worn region was calculated as a volume (relative to the neutral plane) as was the material gain to either side of the worn region.

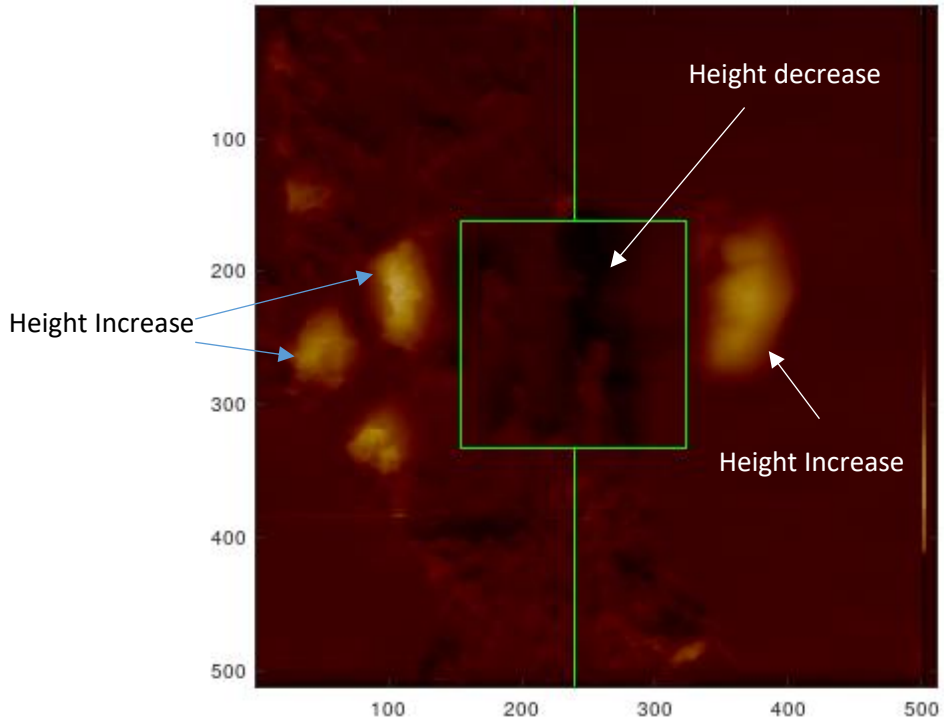

Figure 7-10: A "difference" image, as output by MATLAB, showing the final topography scan minus the initial topography scan for use in determining the volume change.

In addition to quantifying the displaced material the code was developed to create an animation with the topography scans displayed with appropriate delays to account for the wear scans. The animations have been used successfully in presentations to engage other researchers and industrialists with the research.

7.8 Durability Results

The results have been separated to allow for ease of reading. The effect of concentration of the original oil on the durability of the tribofilm will be presented first. This will be followed by a comparison between different normal loads applied to the AFM tip and any resultant change in the durability of tribofilms from 0.55wt% ZDDP.

7.8.1 Comparison between tribofilms formed from different concentrations

7.8.1.1 Topography

A selection of the topography scans is presented here, the full data set can be seen in "Appendix 3 – Durability Study Topography Scans". To aid in reader understanding a system of coloured arrows has been used to explain the scan differences. Typically arrows are only shown in the final topography scan, although noted features may be present in the previous scans as well, with the exception of an important phenomenon in Figure 7-13 which necessitated additional arrows. Any evidence of displaced, or increased, material is indicated by an orange arrow and any evidence of removed, or decreased, material is indicated by a blue arrow.

Figure 7-11 shows the topography progression when the load is applied in a region between tribofilm pads, in a tribofilm generated within a 0.275wt% ZDDP oil. It can be seen that there is little displaced material, even after 250 scans. There is some evidence of a raised region in the trace direction, indicated by the orange arrows in the final scan; however, there is no evidence of any corresponding displacement in the retrace direction. The worn region is likewise negligible with only a slight edge caused by the contact mode scans (indicated by the blue arrow). Peculiarly, there appears to be a very small mound of displaced material forming in the retrace direction, but outside of the apparent wear region. This is not apparent until the final topography scan and so it may be an artefact of the scan.

Figure 7-12 shows the topography progression when the load is applied directly to the edge of a pad, in a tribofilm generated within a 0.275wt% ZDDP oil. It can be seen that there is again little displacement of the material with a small raised line of material in the trace direction and a small mound of material to the bottom of the worn region in the retrace direction. There is a more important outline of the worn region, with a clear edge to the top, indicated by the blue arrow. In addition to the expected displaced material, and material decrease in the worn region, there is also some evidence of topographic changes within the worn region, indicated by the green oval in the first and second presented scan. There appear to be small pads being revealed, these will be considered further by studying the contact mode scans of the worn region (Figure 7-21).

Figure 7-13 shows an unusual topography progression when the tip is loaded against a small pad, in a tribofilm generated within a 0.275wt% ZDDP oil. The orange arrows in the second and third presented scans (after 35 and 40 contact scans) show there was a rapid build-up of displaced material in both the trace and retrace directions; however, when the sample was left unworn for a period of time (overnight) the displaced material relaxed and reformed a similar pad to the initial tribofilm. The third scan presented shows that there remained some small increased regions; however, these did not align with the end of the trace or retrace motion. Subsequent scans showed that the reformed tribofilm pad was more resistant to the motion, with small pads being formed in the trace and retrace directions, but not achieving the same geometric size as the original pads. This test was stopped prematurely due to increased levels of tip degradation, resulting in a decrease in the scan resolution.

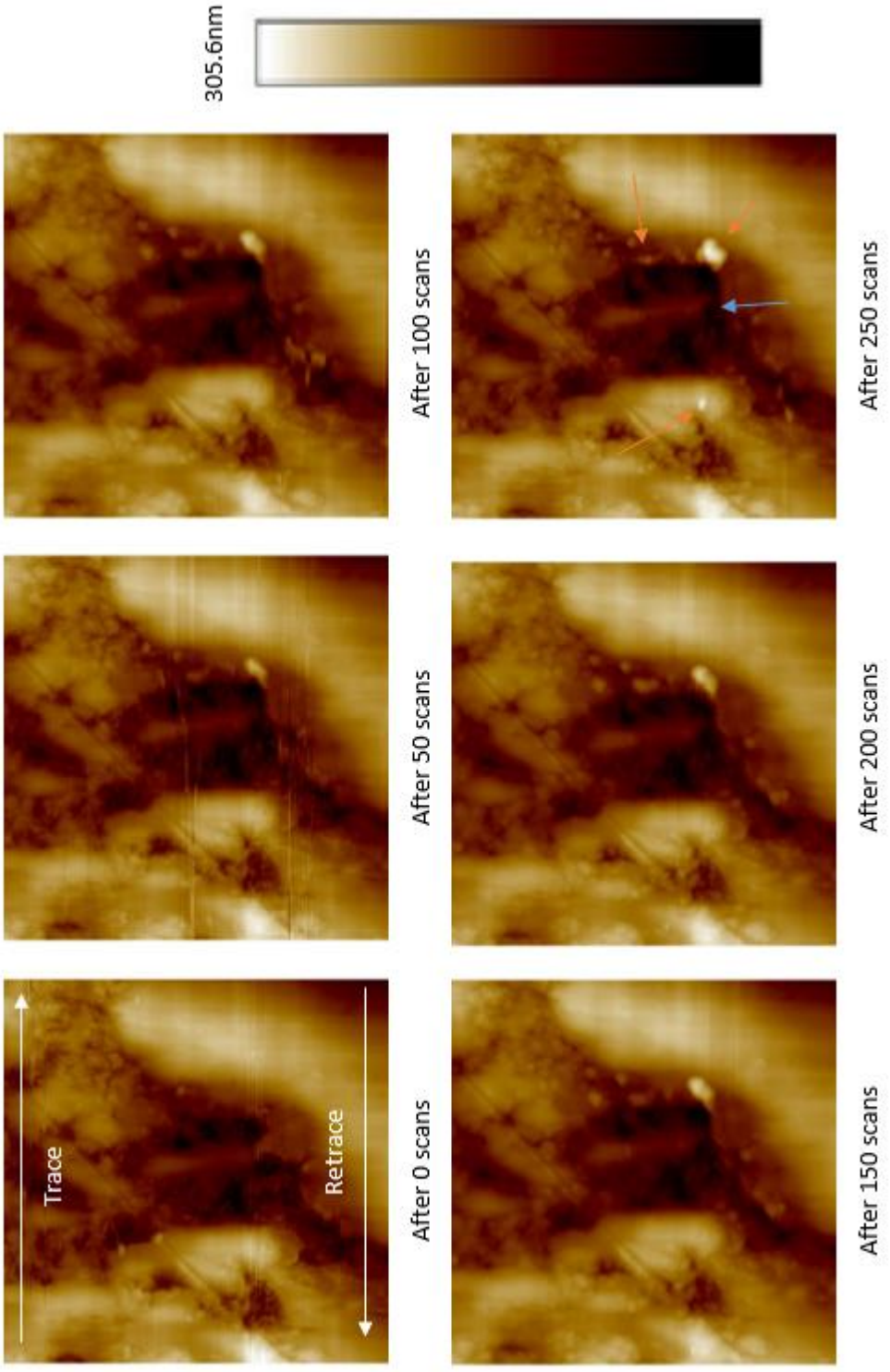

Figure 7-11: The topography progression between pads in a 0.275wt% tribofilm.

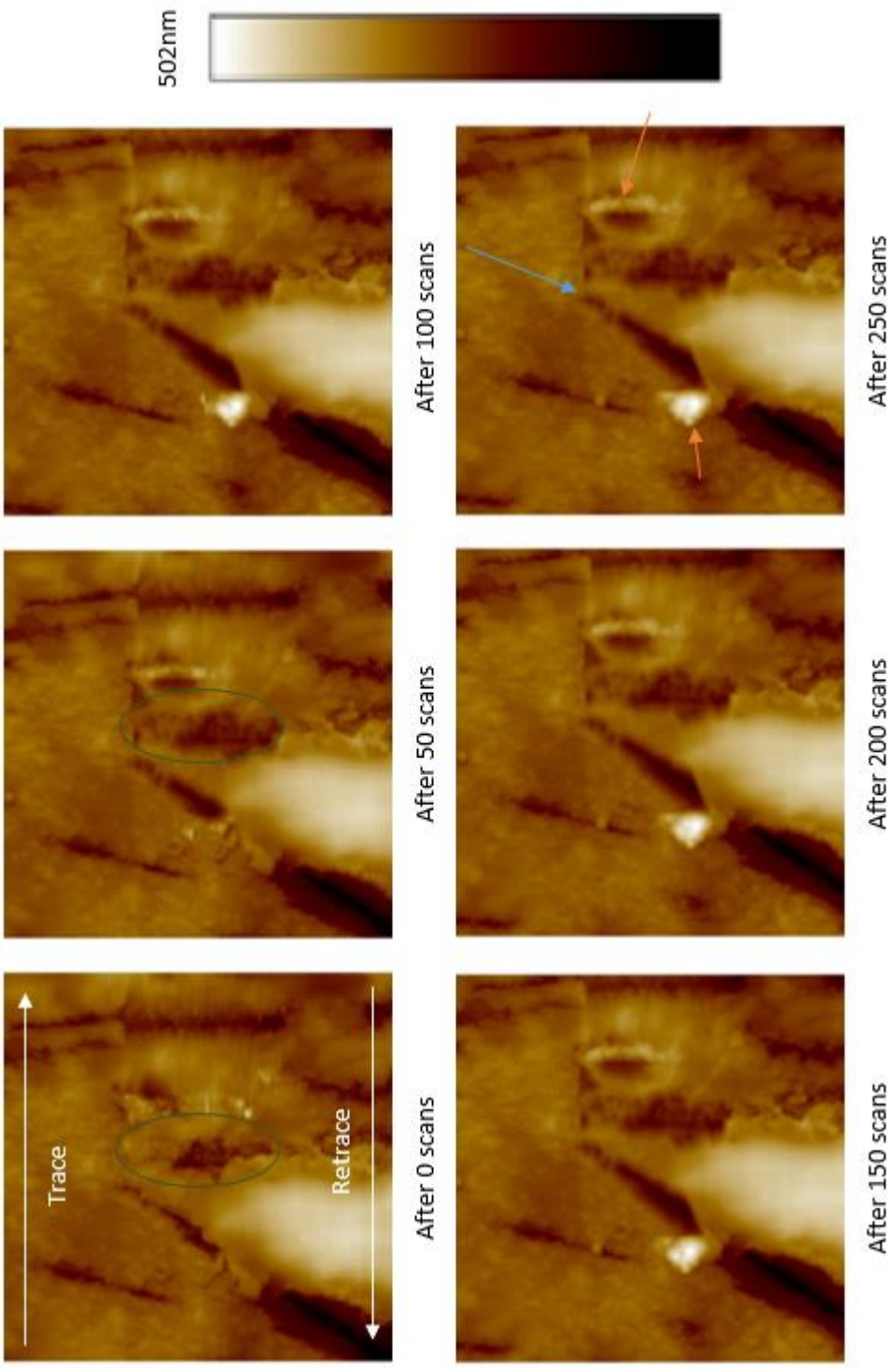

Figure 7-12: The topography progression on the edge of a pad in a 0.275wt% tribofilm.

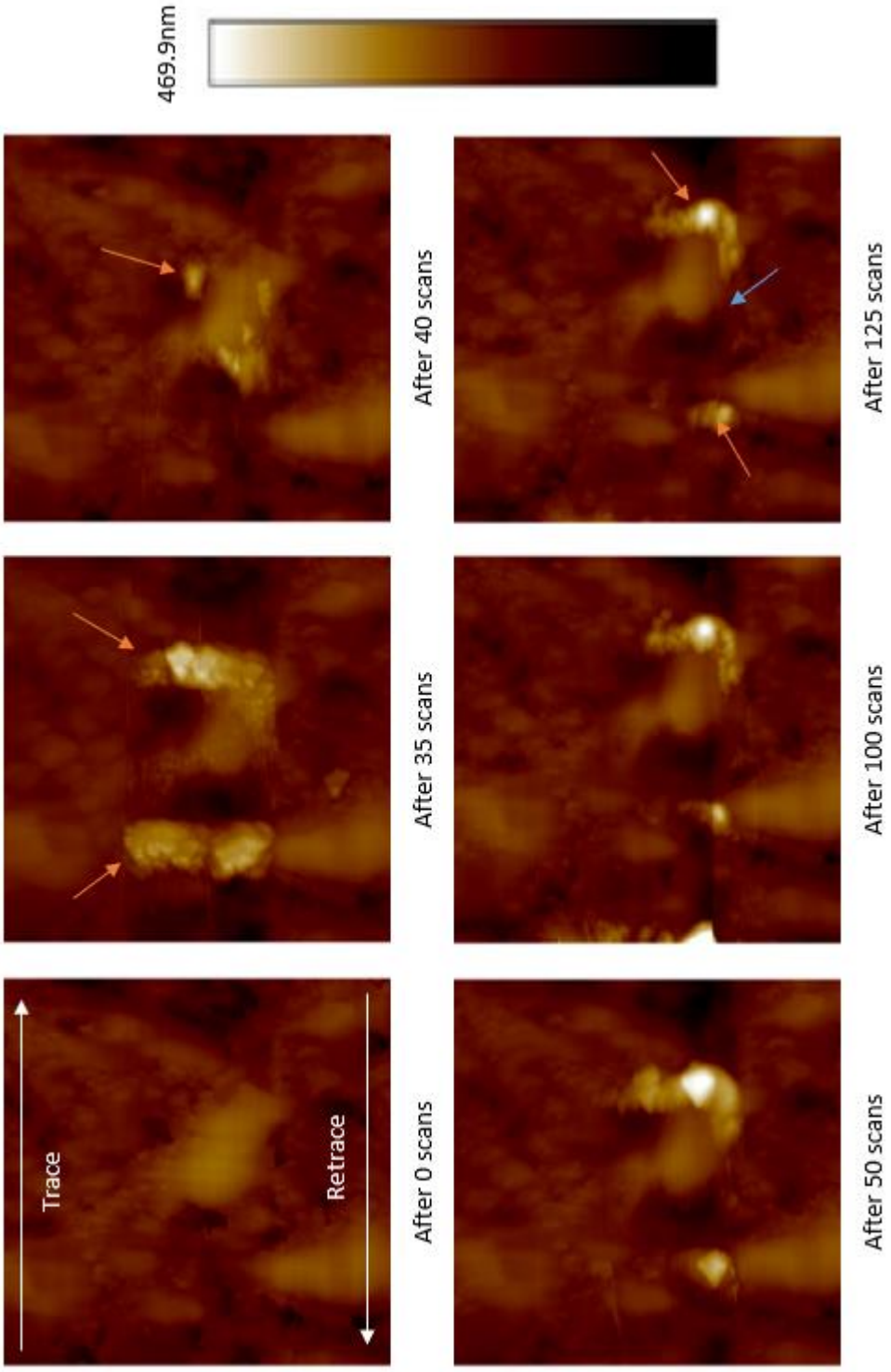

Figure 7-13: An unexpected topography progression of a small pad in a 0.275wt% tribofilm

The same system of coloured arrows was used to explain the scans conducted in a tribofilm generated in a 0.55wt% ZDDP oil. The orange arrows indicate areas of increased material and the blue arrows indicate the edges of the worn region.

Figure 7-14 shows the topography progression when the tip is loaded against a large roughened pad (which encompasses the entire topography scan). The edge of the worn region can be seen, even after only 50 contact scans. The scans appear to have experienced some thermal and relocation drift, with the prominent scratch (running through the entire scan, from top to bottom) moves towards the right of the scan with time. This process is progressive, indicating it is not a result of a localised motion and is instead an inherent property of the AFM, resulting in a rectangular worn region, with some parts not being worn to the same extent as others. This, also, results in the strange dual displacement, which is evident in the trace direction, as well as the unusual shape of the displaced material in the retrace direction. This appears to consist of four discrete mounds of displaced material all located near each other; however, in earlier topography scans it can be seen that this was a more agglomerated single mass.

Figure 7-15 shows the topography progression when the tip is loaded on the edge of a large pad. The worn region is again visible, even from the second presented scan, with the edge closest to the tribofilm pad the most defined (to the left of the displaced material, in the trace direction). The displaced material mound in the trace direction is clearly larger than the equivalent in the retrace direction, after 50 contact scans; however, the geometric volume of this appears to decrease in subsequent scans. Additionally, even after only 50 contact scans, there appear to be three distinct piles of displaced material in the retrace direction, this phenomenon becomes more apparent in the later scans. The leftmost of these discrete sites is not at the edge of the worn region, indicating that the location of the displaced material is not specifically caused by ploughing.

Figure 7-16 shows the topography progression when the tip is loaded between pads. The worn region is very clearly visible, with a clean cut to indicate the bottom of the scan. This clean cut is apparent even after only 50 contact scans, with a corresponding mass of displaced material in the retrace direction. The top of the scan is also visible; however, it is not so clearly cut. Both directions show a marked decrease in material displacement after the initial contact scans, with no discernible height differences detectable by eye.

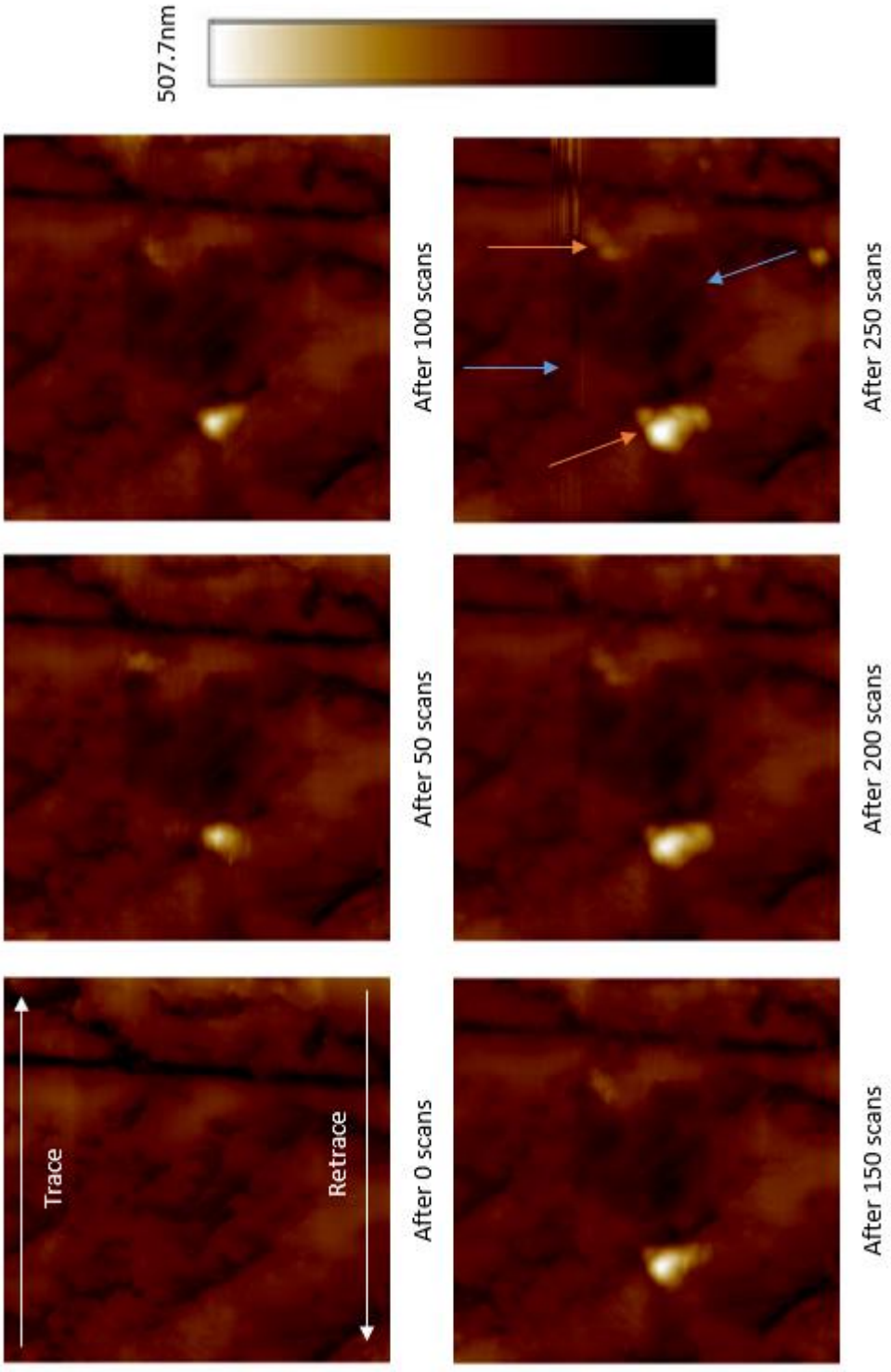

Figure 7-14: The topography progression of a large roughened pad in a 0.55wt% tribofilm.

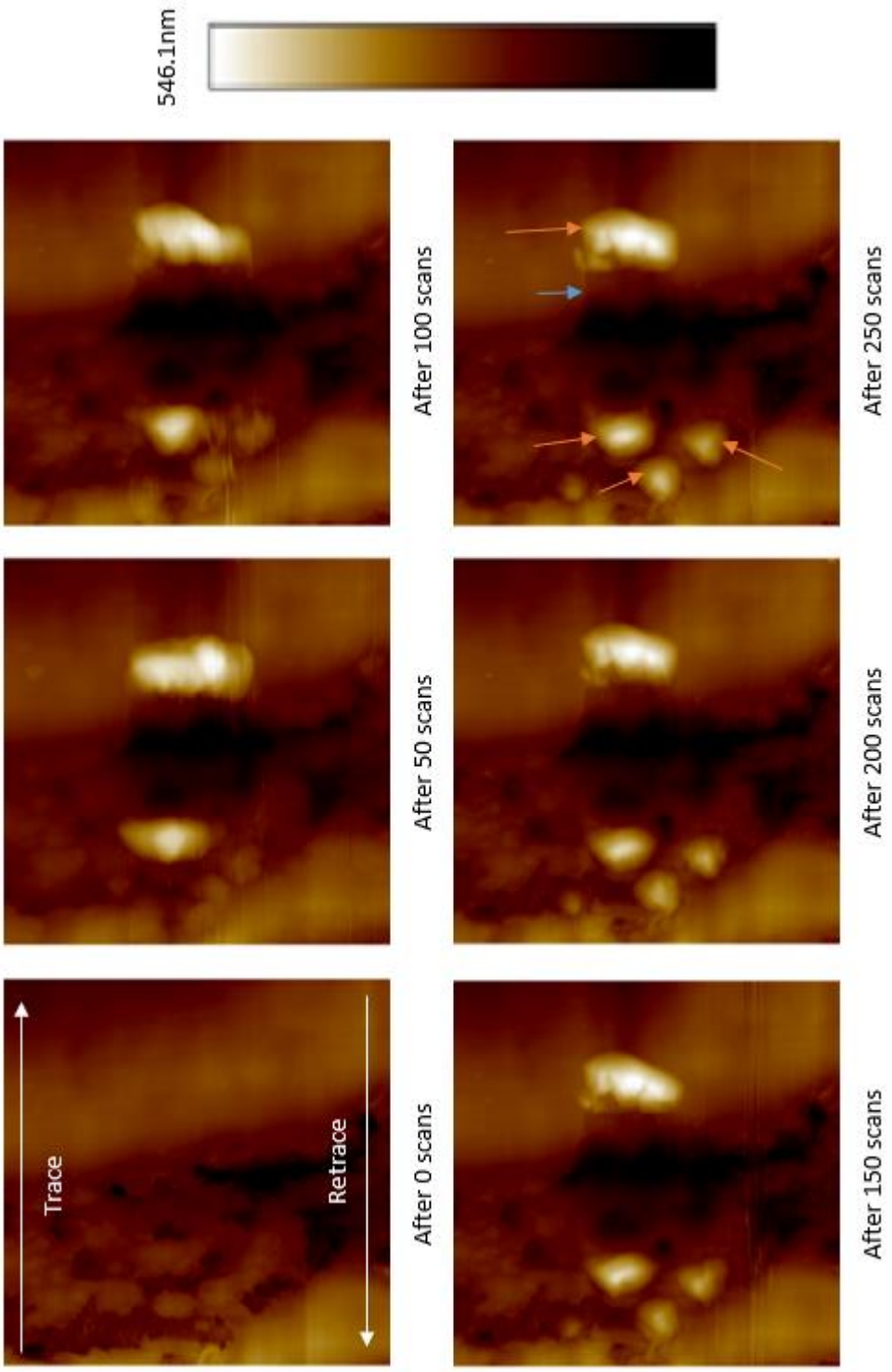

Figure 7-15: The topography progression on the edge of a pad in a 0.55wt% tribofilm.

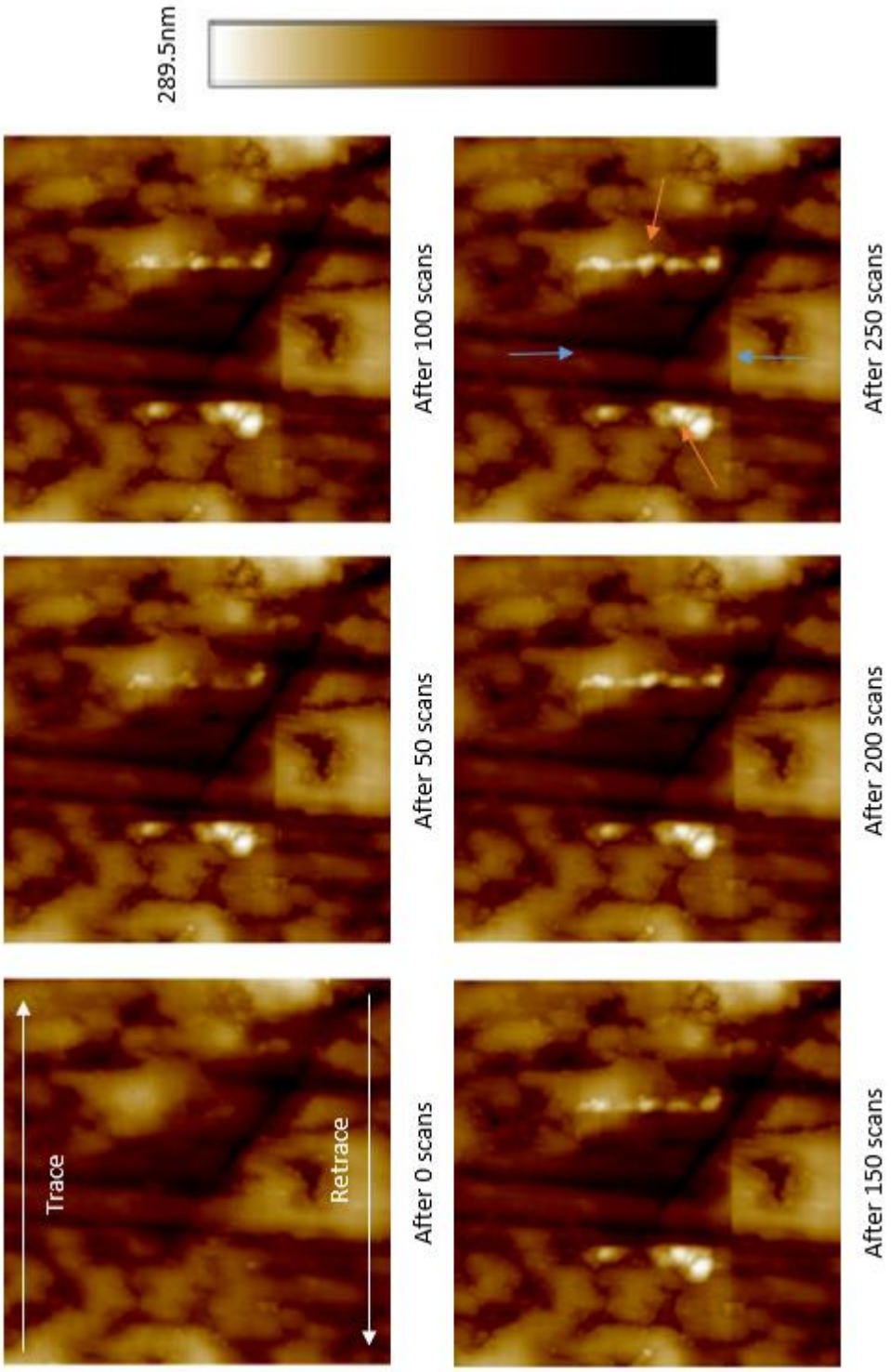

Figure 7-16; The topography progression between pads in a 0.55wt% tribofilm.

7.8.1.2 Quantification of Material Displacement

A number of graphs produced using the novel analysis program, outlined in section 7.7, are presented here. Examples have been chosen to reflect the usefulness of the technique as well as to provide a comparison between concentrations. Each point on the graph is the calculated volume for the topography scan conducted after the attested number of wear scans.

Figure 7-17 shows the analysis results for the test conducted on a pad, in a 0.275wt% tribofilm (Figure 7-13). This shows that the height increase, observed to the sides of the worn region in the pictorial representation of the scan, can be clearly quantified; however, the slight change in height in the worn region was less clearly captured. Unusually there is evidence of an initial decrease in the height either side of the worn region after the first 5 wear scans, indicating that the correction for z-axis offsets is not entirely accurate. The height of the worn region shows a slight increasing trend after approximately 55 wear scans, which may correspond to the revelation, or formation, of small pads within the contact region. This is explored in more detail in section 7.8.1.3.

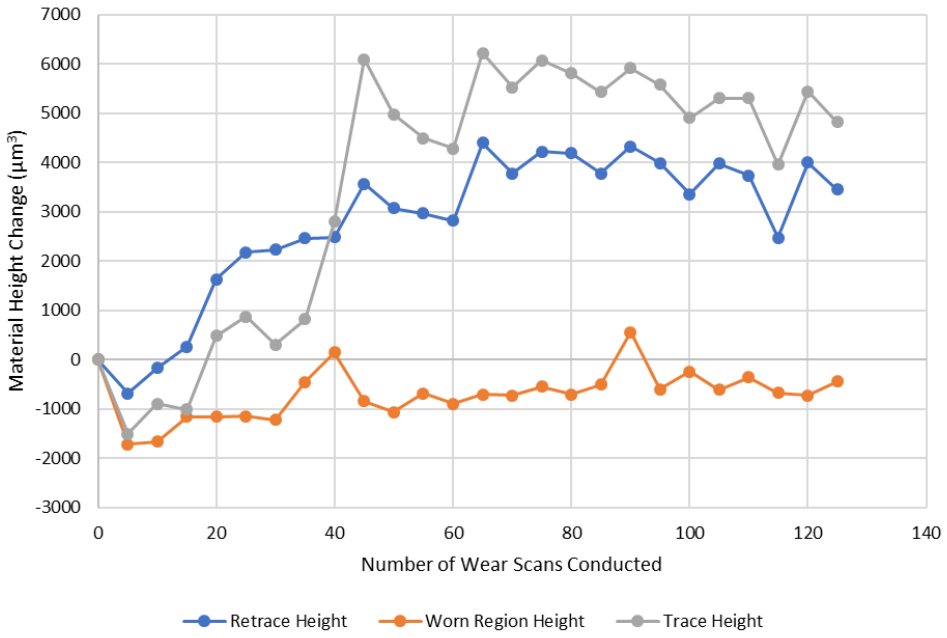

Figure 7-17: A good example trace for the material displacement for a 0.275wt% tribofilm.

Figure 7-18 shows the example trace for the test conducted on the edge of a pad, in a 0.275wt% ZDDP tribofilm (Figure 7-12). This shows that the analysis software identified a progressive decrease in height across the entirety of the scan. This is contrary to the observed height increase to either side of the worn region. This is potentially due to an incorrect correction for thermal drift, with subsequent scans being conducted with a lower measured zero point. This is difficult to correct for, particularly given the flatten function had already been applied to remove excess noise from the data set. A further indication that this test behaved abnormally, within the analysis program, is that at numerous points (particularly between 30 and 80 wear scans) the regions to either side of the worn area display a greater height decrease than the worn region itself.

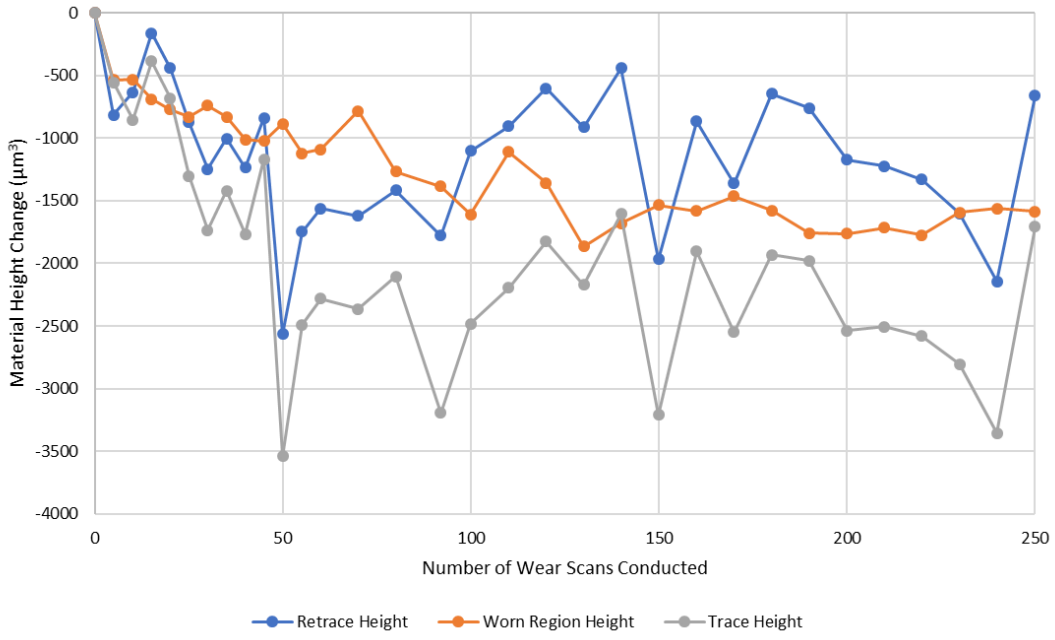

Figure 7-18: An example trace for the material displacement for a 0.275wt% tribofilm.

Figure 7-19 shows the material transfer for the edge of a pad in the 0.55wt% tribofilm (Figure 7-15). Once again this shows a clear increase in height in both the trace and retrace directions, with both trends being very similar in form. The graph also shows the worn region height as remaining very similar throughout the duration of the test, with the exception of a rapid increase after 5 wear scans. The images produced for the topography scans show no clear reason for this unusual increase; however, the gradient is present in all three of the measured parameters, indicating it is a feature of the entire scan and not a true reflection of a short-lived height increase.

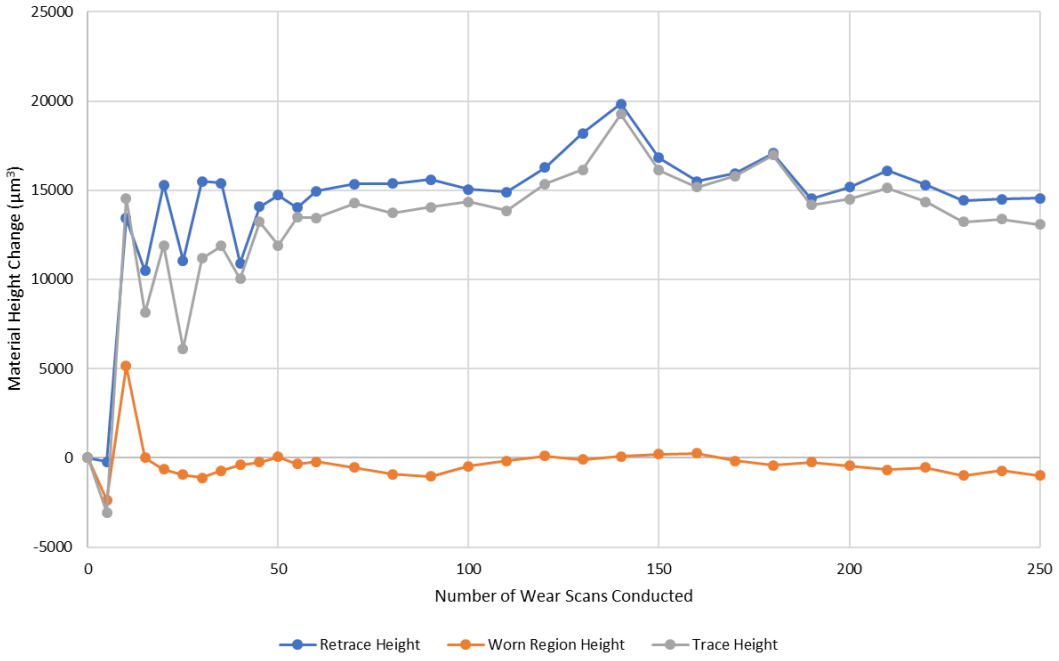

Figure 7-19: A good example trace for the material displacement for a 0.55wt% tribofilm.

Figure 7-20 shows an example trace for the scans conducted between pads on a 0.55wt% ZDDP tribofilm (Figure 7-16). This shows extreme fluctuations in the height change outside of the worn region, with both the trace and retrace heights varying across a range of 2500µm^3. This trend is not reflected in the height change for the worn region which becomes progressively lower in height for the majority of the test. An exception is in the topography scans conducted after 15 wear scans, where the height appeared to increase across the entire scan. This may be caused by the same thermal drift anomaly that affected the test conducted on the edge of a pad in a 0.275wt% tribofilm. The height decrease in the worn region appears to have achieved a plateau after approximately 110 wear scans, which relates directly to the behaviour that could be observed optically in the scans; however, this behaviour was observed to have occurred more rapidly, and coincided with a cessation in the height changes to either side of the worn region that is not demonstrated in the below graph.

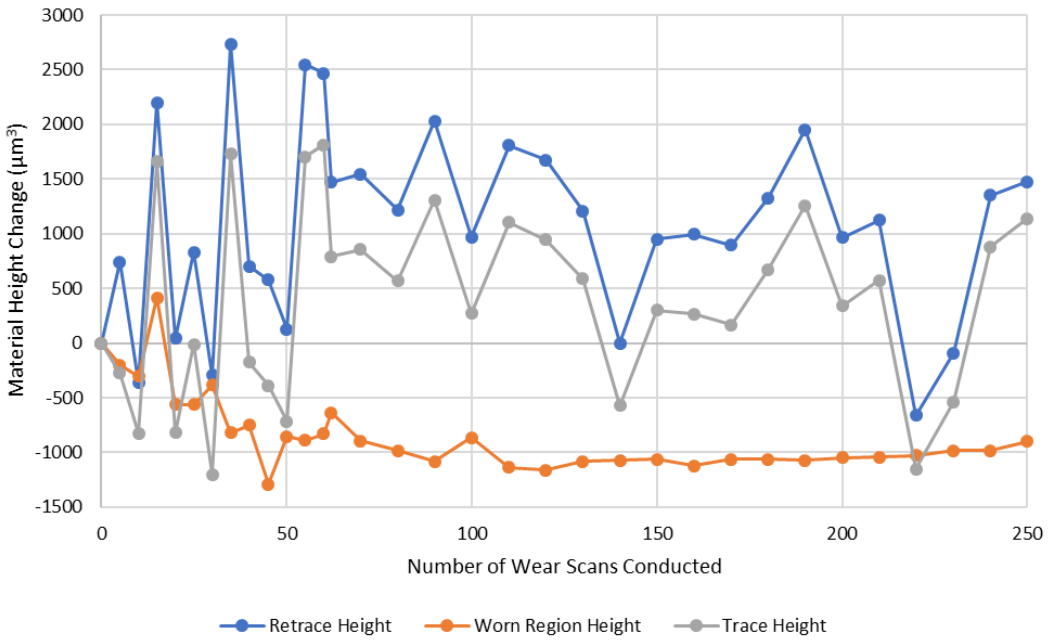

Figure 7-20: An example trace for the material displacement for a 0.55wt% tribofilm.

7.8.1.3 The worn region

Figure 7-21 shows a selection of wear scan images, which correspond to the wear region in Figure 7-12. There is a noticeable difference between the first and mid-scan, with the edge of the pad moving from the left of the scan towards the centre. There is no similar difference between the mid and last scans, with the relative position of the topographic features remaining the same, indicating that the motion was not caused by thermal drift. This motion may account for the unexpected small pad in Figure 7-12, which appeared to be outside of the worn region. When comparing the first and last scan smaller differences can also be seen, with small pads seeming to appear by the last scan (indicated by the green arrows). It is unclear whether these have been revealed by the removal of loosely adhered material, or if these have been formed as a result of the rubbing motion on the film.

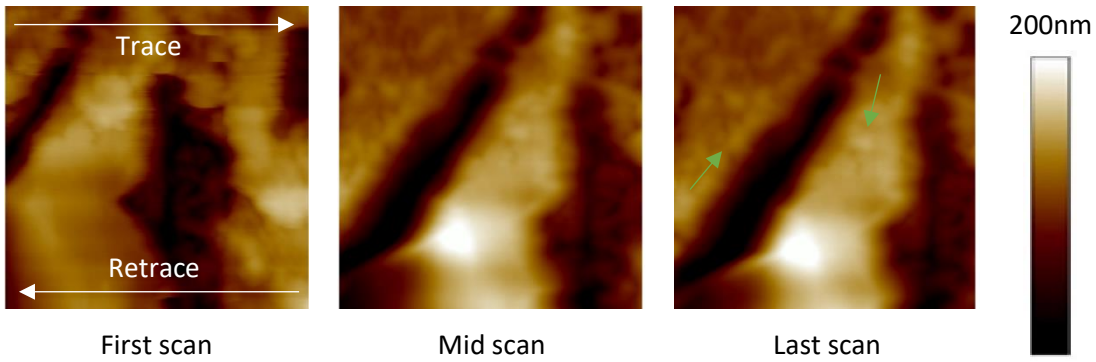

Figure 7-21: Wear scan images for a 0.275wt% - edge of pads.

Figure 7-22 shows a selection of wear scan images, which correspond to the wear region in Figure 7-11. There is no clear evidence of the wear scan moving, with all of the important topographic features maintaining the same relative position within the scan area. There is, again, some evidence of small pads appearing between the first and last scan. These small pads are most apparent in the darker region, between the two small elongated pads (indicated by the green arrows). Other small pads are visible to the bottom right of the scan (indicated by the grey arrow), these are partially visible in the first scan, and become clearer as the test progresses.

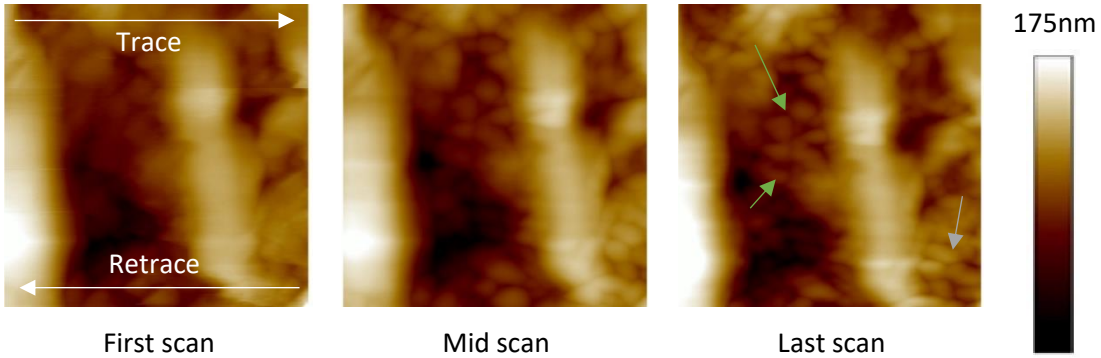

Figure 7-22: Wear scan images for a 0.275wt% - between pads.

Figure 7-23 shows a selection of wear scan images which correspond to the wear region in Figure 7-13. There is evidence of tip drift in these scans which appears to be progressive, likely as a result of thermal drift. The first scan shows vertical lines (perpendicular to the scanning direction) in the tribofilm pad; however, these are less visible in the mid scan. The same location in the last scan shows more evidence of small pads appearing; however, neither vertical lines nor small pads seem to appear in the mid scan.

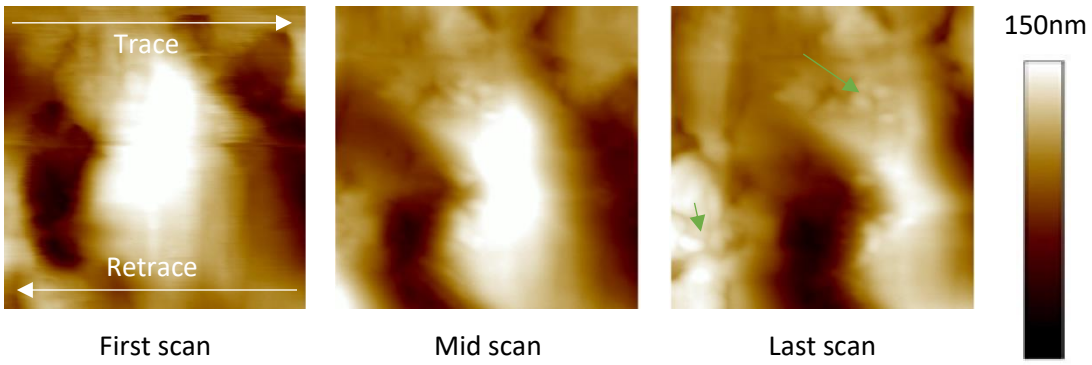

Figure 7-23: Wear scan images for a 0.275wt% - on a pad.

Figure 7-24 shows a selection of wear scan images which correspond to the wear region in Figure 7-14. The scans show a progressive movement, with the topographical features moving towards the right throughout the test. The black arrows show the locations of unusual features, which may be indicative of the large roughened tribofilm topography, that are not visible in the subsequent contact mode scans.

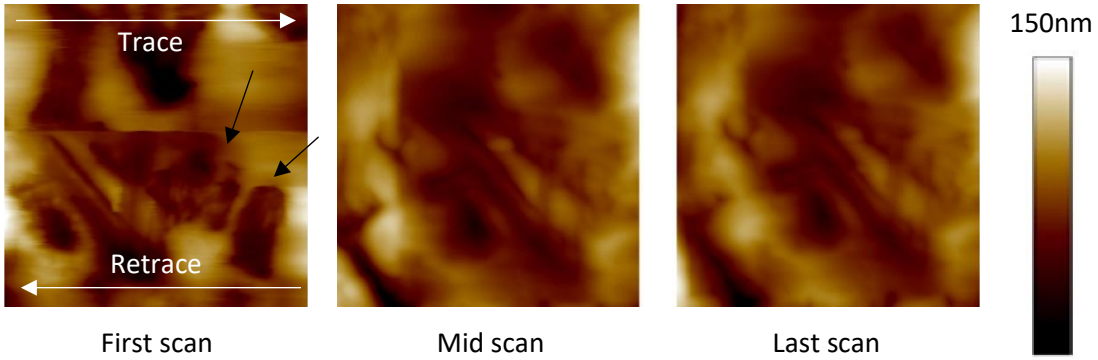

Figure 7-24: Wear scan images for a 0.55wt% tribofilm – on a large pad.

Figure 7-25 shows a selection of wear scan images which correspond to the wear region in Figure 7-15. The edges of the pads become less defined as the test progresses with the valley between the pads becoming distorted and apparently less deep. In addition, there appear to be small pads in the first scan (in the left large pad) which become more clearly defined, although potentially smaller in subsequent scans (indicated by the grey arrows). There are also some small pads forming in the right large pad, these are clearest in the last scan and are indicated by the green arrows.

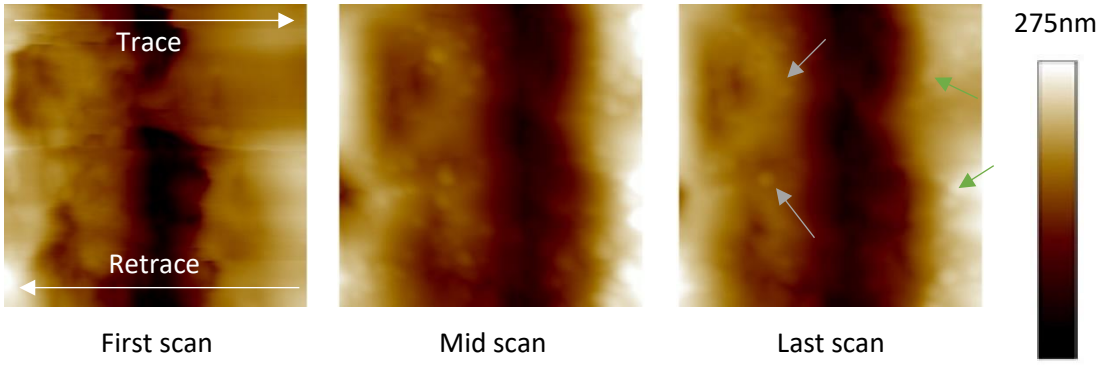

Figure 7-25: Wear scan images for a 0.55wt% tribofilm – on the edge of pads.

Figure 7-26 shows a selection of wear scan images which correspond to the wear region in Figure 7-16. There is no evidence of any horizontal tip drift for this test; however, between the first and mid scans the scratch (45°, starting at the bottom right of the first scan) appears to drift downwards, indicating a small amount of vertical drift. There is no similar distinction between the mid and last scan, which suggests that this drift was due to an external cause and is not due to an inherent issue of the AFM (such as thermal drift). There are no apparent changes in the tribofilm topography itself with the test progression.

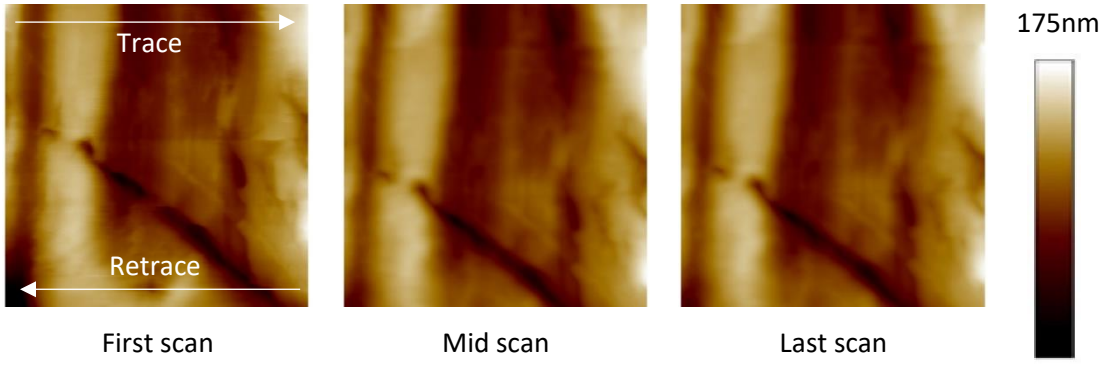

Figure 7-26: Wear scan images for a 0.55wt% tribofilm – between pads.

7.8.1.4 Effect on surface parameters in the worn region

Figure 7-27 shows that the arithmetic mean surface roughness, S_a, of the worn region did not meaningfully change over the course of any of the tests. The test with the largest S_a value was the test conducted on the edge of a pad formed in a 0.55wt% ZDDP oil, with a minimum value of 39.3nm. This is to be expected due to the large crevice running vertically through the entire scan. The test with the lowest S_a value was the test conducted on the large roughened pad formed in a 0.55wt% ZDDP oil, which had the more uniform topography by eye. None of the tests (with the exception of the aforementioned edge of pad, 0.55wt% ZDDP tribofilm test) were markedly out of family, with similar progressions for each test. There had been an expectation that the roughness would be lowered over the course of the test. However, the only tests with a negative gradient are the tests conducted on a tribofilm pad (for both concentrations) and the between pads scan on a tribofilm formed from a 0.275wt%ZDDP oil. There also appears to be an effect of dwell time on the tribofilm surface parameters, with some tests showing an increase in S_a with dwell (the tests conducted on the edge of or between pads of a tribofilm formed from a 0.275wt% ZDDP oil) and others an increase (the tests conducted on a large pad or on the edge of a pad of a tribofilm formed from a 0.275wt% ZDDP oil.).

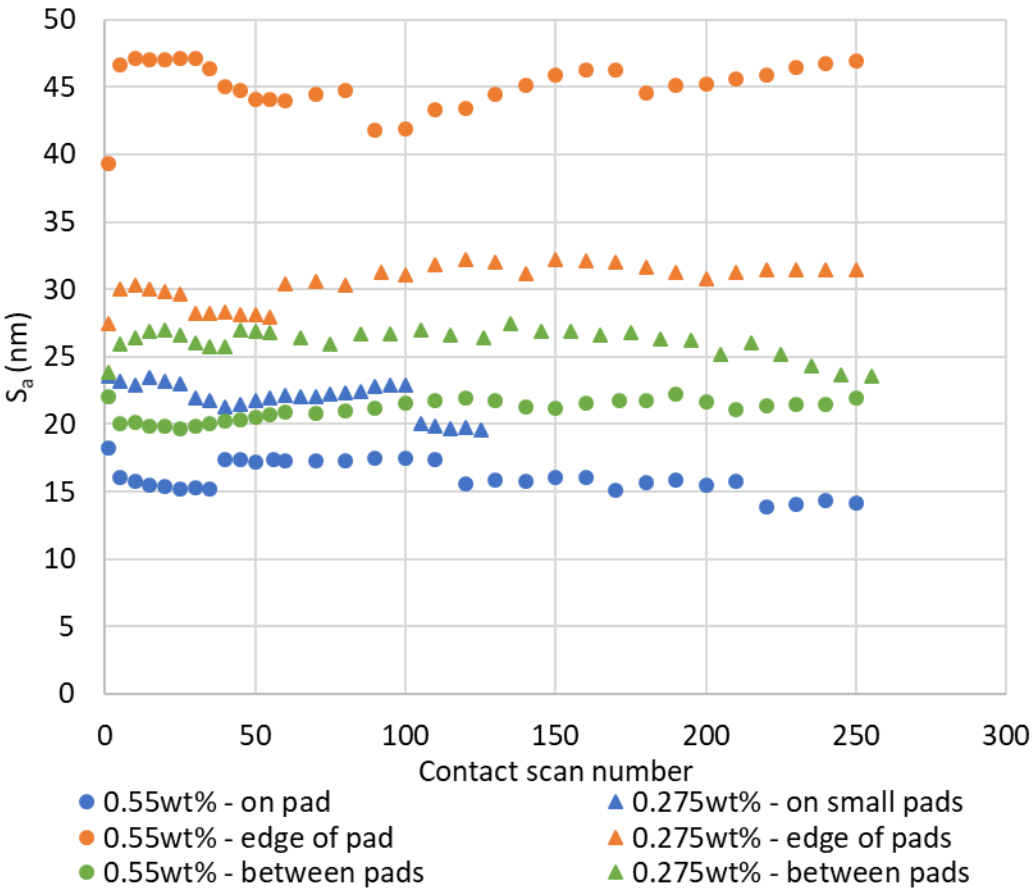

Figure 7-27: The progression in S_a.

Figure 7-28 shows that the surface kurtosis did not meaningfully change throughout the duration of the test. It was expected that the initial kurtosis would be low, due to the smooth nature of ZDDP tribofilm pads; however, the ploughing motion during the contact scans was predicted to alter this. Instead, the values for each of the scans remains fairly constant throughout the testing, with the exception of the scan conducted on a small pad in a tribofilm formed in a 0.275wt% ZDDP oil which was terminated early due to extreme tip degradation. The extreme tip degradation presented as visible noise in the topography scans; however, the kurtosis indicates that the noise was also present during the wear scans.

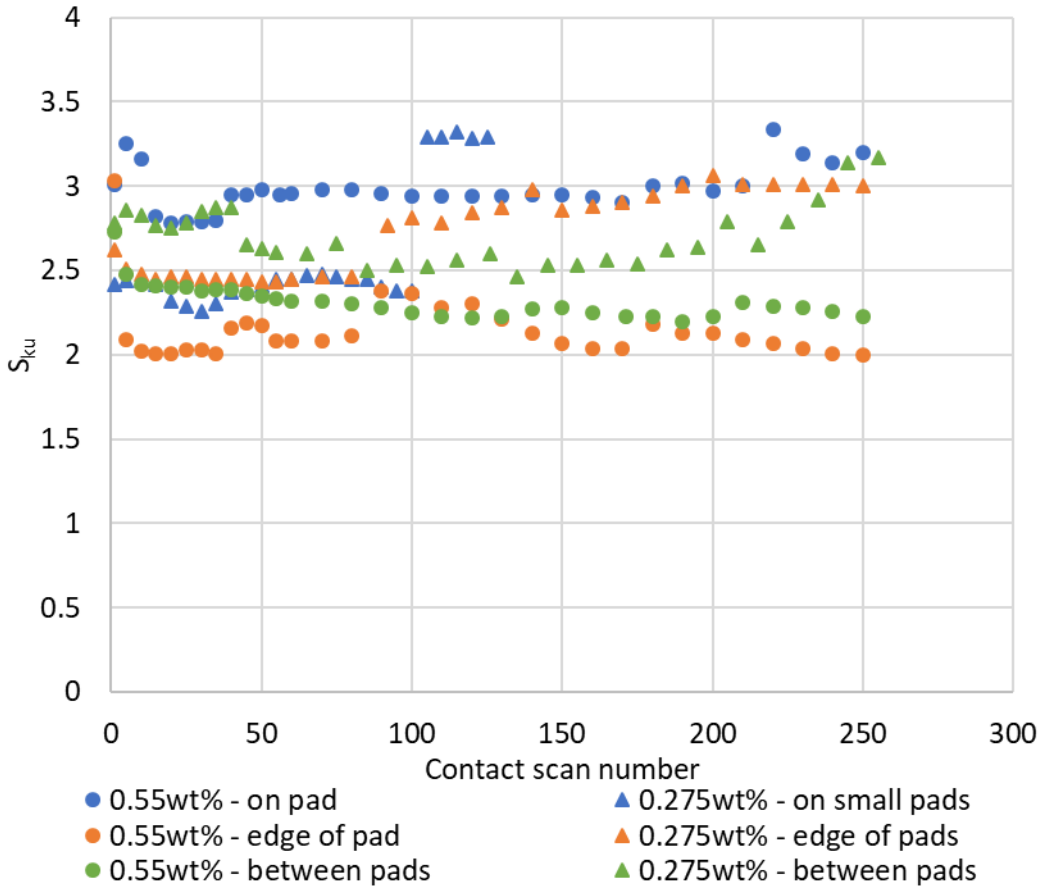

Figure 7-28: The progression in S_{ku}.

Figure 7-29 shows that the surface skewness of the contact scans varied considerably across the duration of the tests. The only test which did not display such variability was the test conducted between the pads of a tribofilm formed of a 0.55wt% ZDDP oil. The fact that

this test did not show any notable alterations in topography throughout the test has previously been noted so the skewness remaining stable is not a surprise. The step change in the skewness of the scan on the edge of a pad in a tribofilm formed in a 0.275wt% ZDDP oil can be explained by the aforementioned change in the scan location, which was speculated to occur as a single jump, rather than thermal drift. However, a similar jump in position was postulated as an explanation for the scan conducted on the edge of a pad formed in a 0.55wt% tribofilm, which was understood to have experienced a single jump in scanning location and yet presents a very variable skewness behaviour throughout the test. There also appears to be an effect of dwell on the skewness, with values (typically) increasing after a period of dormancy, possibly due to the tip being re-initialised during the re-start process. This would alter the "zero point" for the topography in the first subsequent scan.

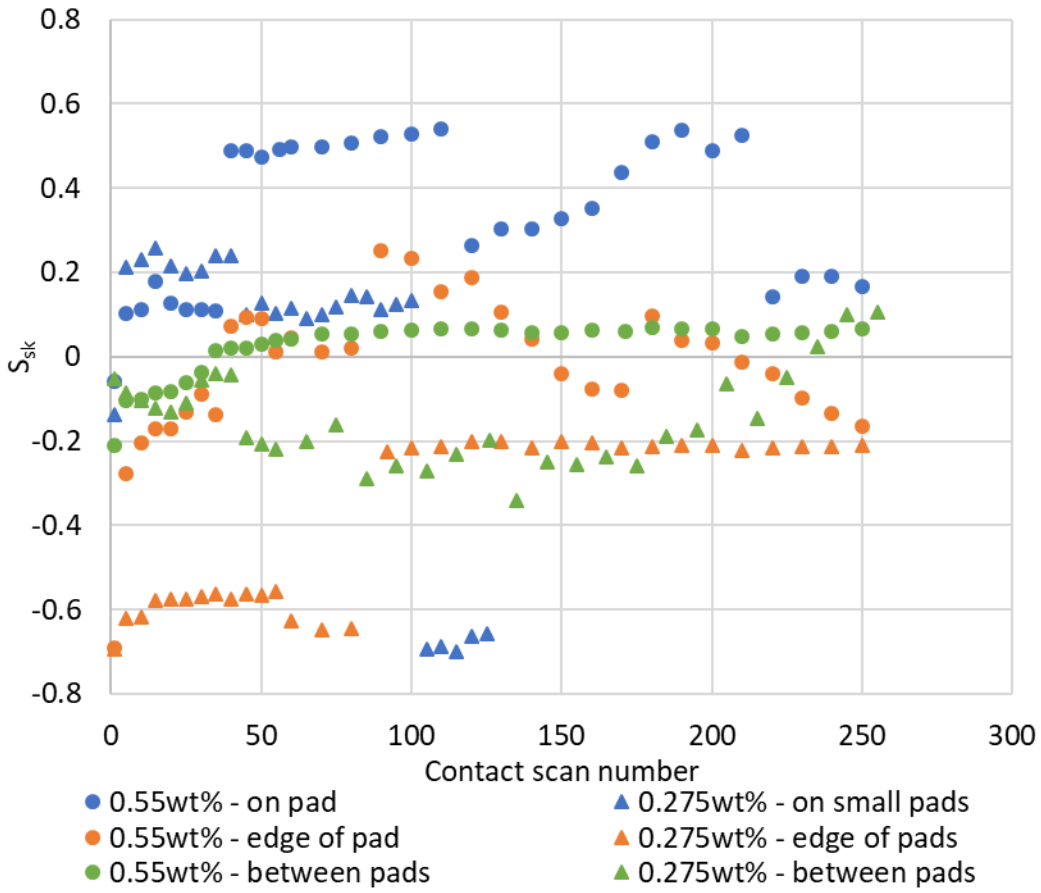

Figure 7-29: The progression in S_{sk}.

Figure 7-30 shows that the isotropy of the surface varies throughout the test; however, once again there does not appear to be an important pattern to the progression. There is a noticeable influence of dwell on the isotropy, with each section of testing having a clear distinction, but there is no pattern to this either. The scans conducted on a tribofilm pad, formed from a 0.55wt% ZDDP oil, had a very unusual end of test performance, with the surface suddenly becoming approximately 30% more isotropic for the final 40 contact mode scans. The scans conducted on a small pad and on the edge of pads in a tribofilm formed from 0.275wt% ZDDP oil each displayed unusual isotropy with the edge of pads test showing high isotropy for the second day of testing, before returning to a much lower value, and the on a pad test showing a similarly high isotropy for the final 5 scans. It must be noted that the final 5 scans for the on a pad test, in the 0.275wt% tribofilm, has been previously noted as anomalous, due to the extreme tip degradation present.

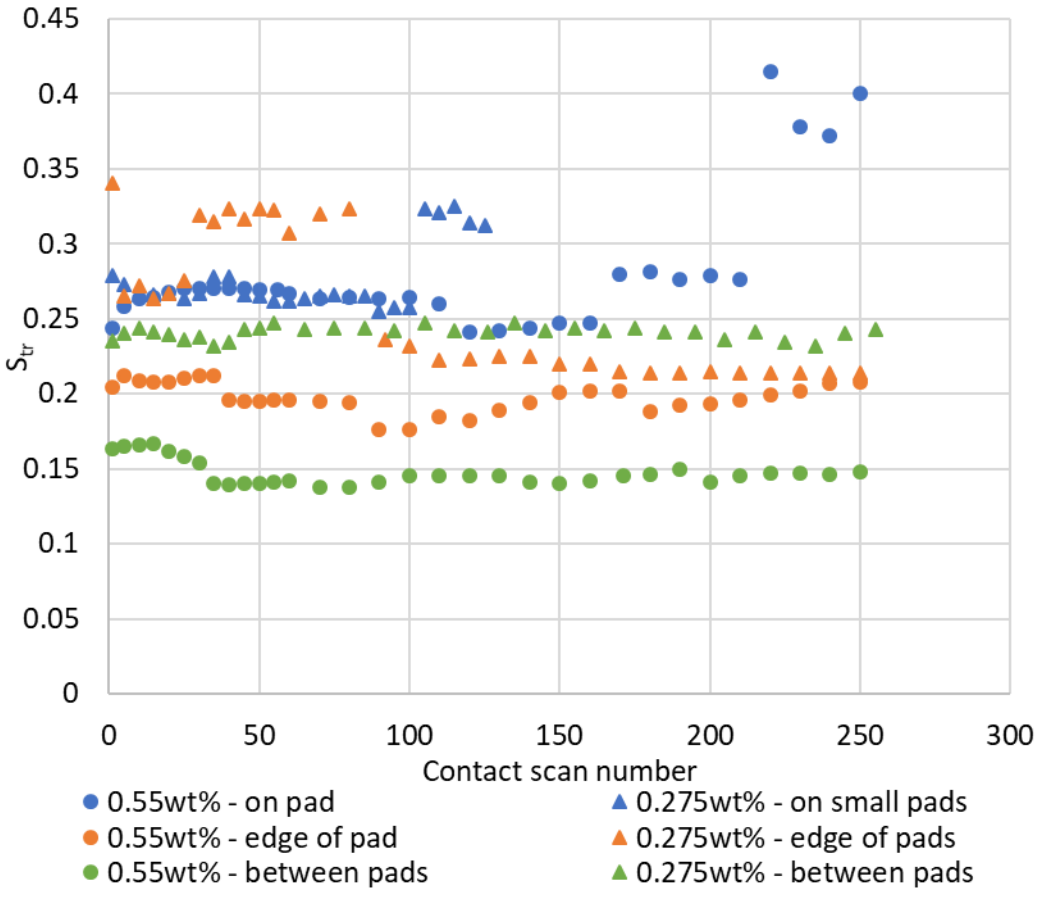

Figure 7-30: The progression in S_{tr}.

7.8.2 Effect of increased load

7.8.2.1 Topography

Figure 7-31 shows the topography progression when the tip is loaded with 0.010mN on a pad in a tribofilm formed in a 0.55wt% ZDDP oil. It can be seen that the majority of the material displacement occurs prior to the topography scan after 50 wear scans. The displaced material in the trace direction appears to be larger than the displaced material in the retrace direction. However, there is an unusual small area of displaced material to the bottom of the worn region (to the left) as indicated by an orange arrow. There is no obvious change in this small displaced material region in subsequent scans.

Figure 7-32 shows the topography progression when the tip is loaded with 0.010mN on a tribofilm formed in a 0.55wt% ZDDP oil. It can be seen that the behaviour in this test was not as expected. The region exposed to the contact scans increased in height, with unusual pads forming in later scans. After 50 scans the worn region can be clearly seen, as well as large pads in both the trace and retrace directions (with more material in the retrace direction); however, by 100 scans the displaced material in the trace direction begins to encroach into the worn region. The displaced material in the retrace direction is showing small pads on the surface of the larger mount, by 50 scans; however, the resolution deteriorates too far to see whether these are present in the subsequent scans. From 150 scans the worn region can no longer be discerned, with large pads forming within it. The volume of these large pads is increasing throughout the remainder of the test.

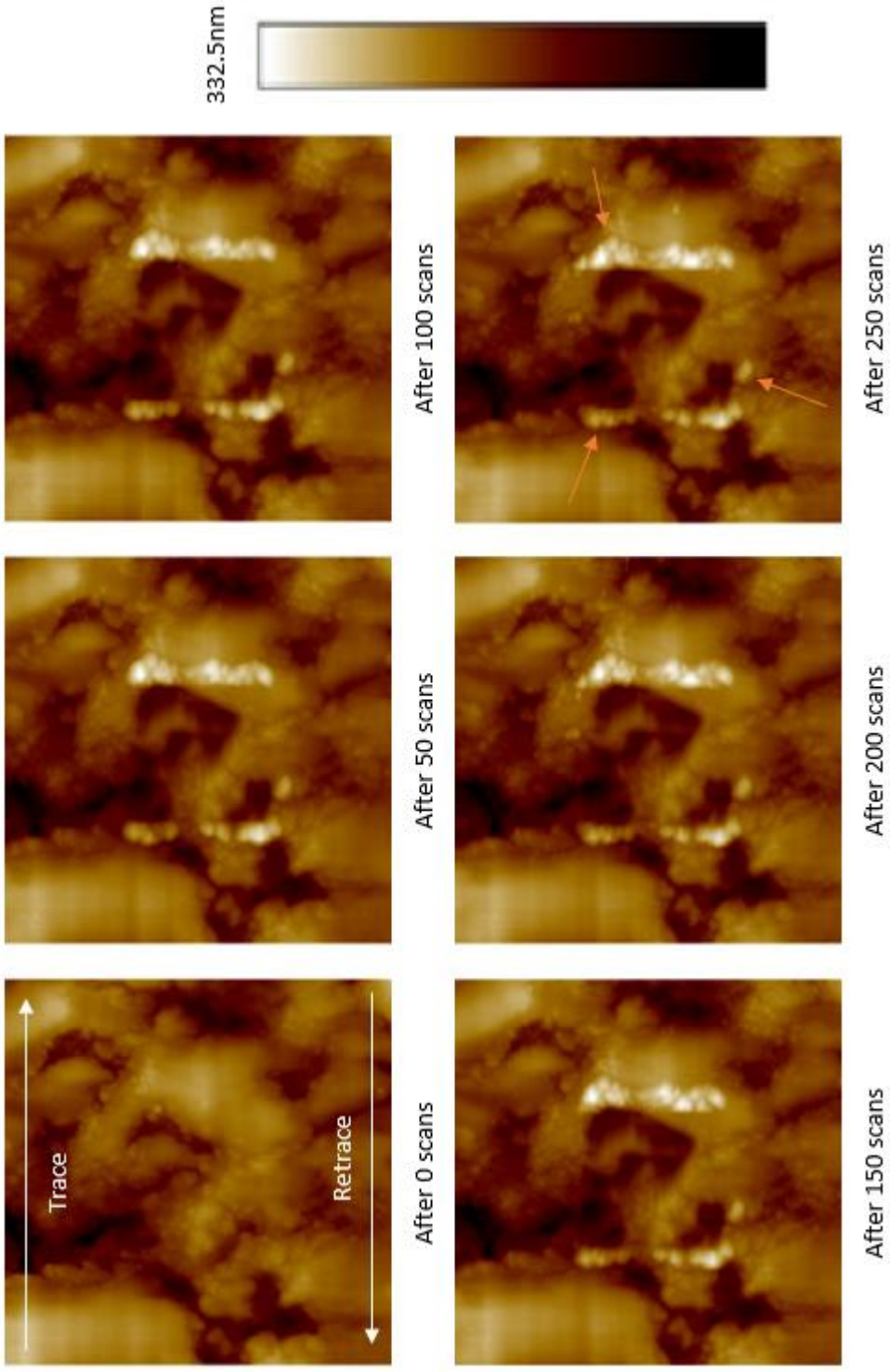

Figure 7-31: The topography progression on a pad in a 0.55wt% tribofilm, with 0.01mN applied load.

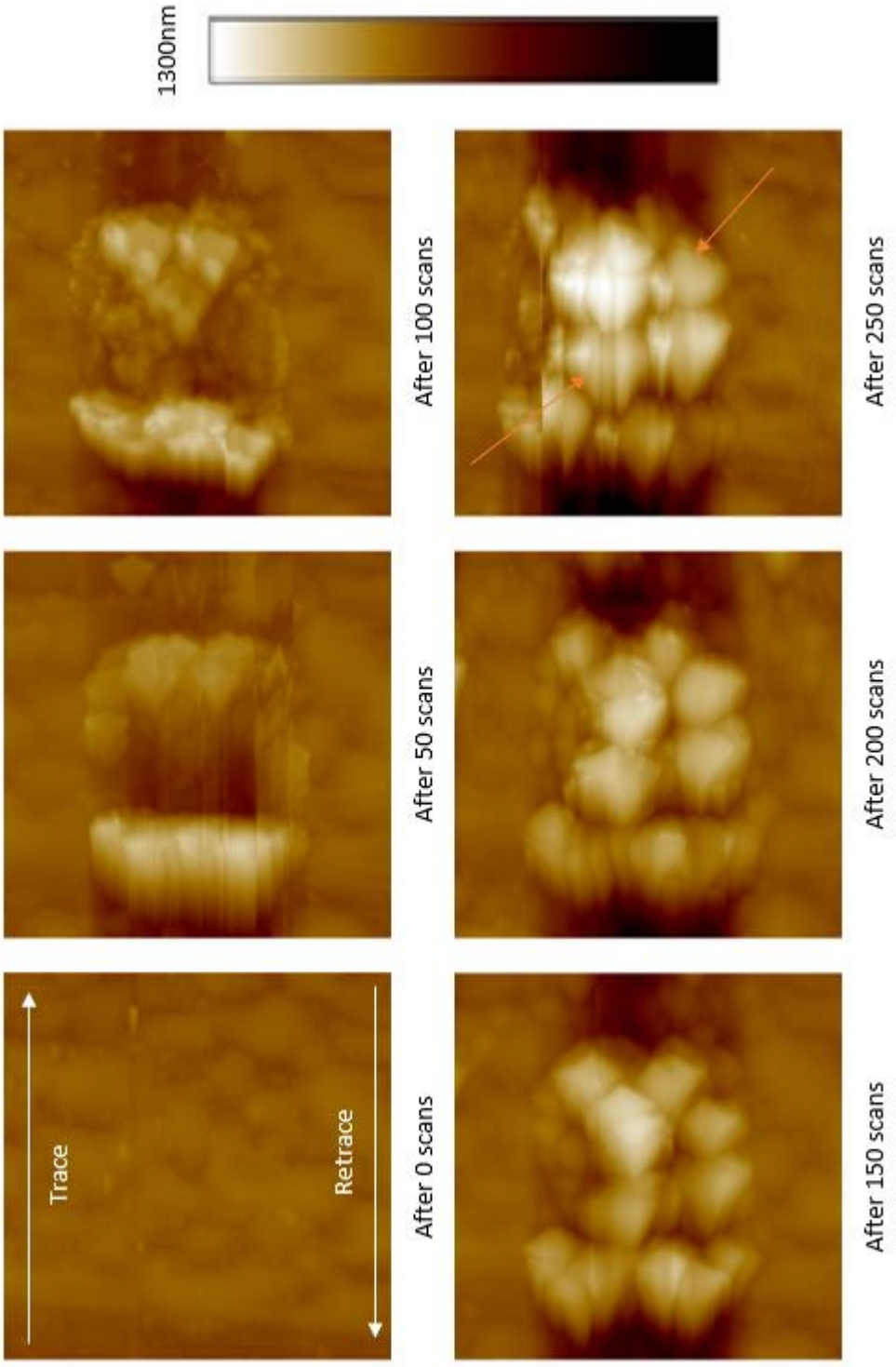

Figure 7-32: The topography progression of a pad film in a 0.55wt% tribofilm, with 0.01mN applied load.

Figure 7-33 shows the topography progression when the tip is loaded with 0.014mN on a pad in a tribofilm formed in a 0.55wt% ZDDP oil. The material displaced is progressive throughout the duration of the tests, with regions indicated by the orange arrows increasing in size with each subsequent scan. In addition, it can be seen that the tribofilm pad has a roughened surface, with lines in the direction of the original tribometer stroke (indicated by the blue arrows). The contact scans were conducted perpendicular to the stroke direction, resulting in a clear worn region. Also, the worn region becomes progressively deeper, between the displaced material mounds, further indicating the tribofilm is still being worn at the end of the test.

Figure 7-34 shows the topography progression when the tip is loaded with 0.014mN on a tribofilm formed in a 0.55wt% ZDDP oil. It can be seen that, again, the material displacement appears to occur primarily prior to the topography scan after 50 wear scans and experiences little more displacement after this. Unusually the material displacement appears to be fairly uniform around the entire worn region, not just at the ends of the wear stroke. Additionally, there is some displaced material extending beyond the bottom of the topography scan, over 10µm from the edge of the worn region. Due to this material extending beyond the topography scan area it is not possible to determine the size of this material mound. The worn region is not altered noticeably after the second presented topography scan, further indicating that the tribofilm is no longer being worn.

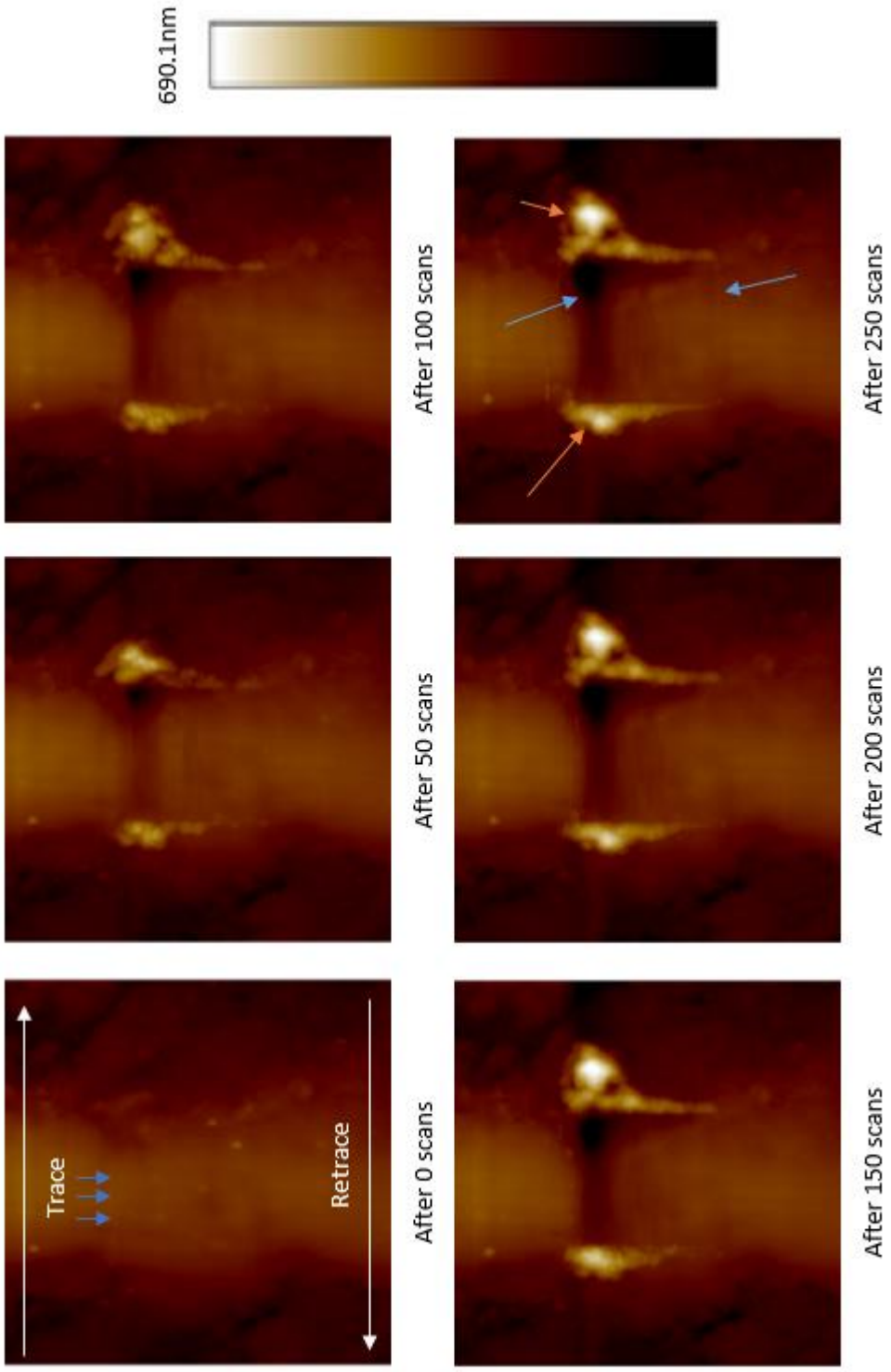

Figure 7-33: The topography progression on a tribofilm pad in a 0.55wt% tribofilm, with 0.014mN applied load.

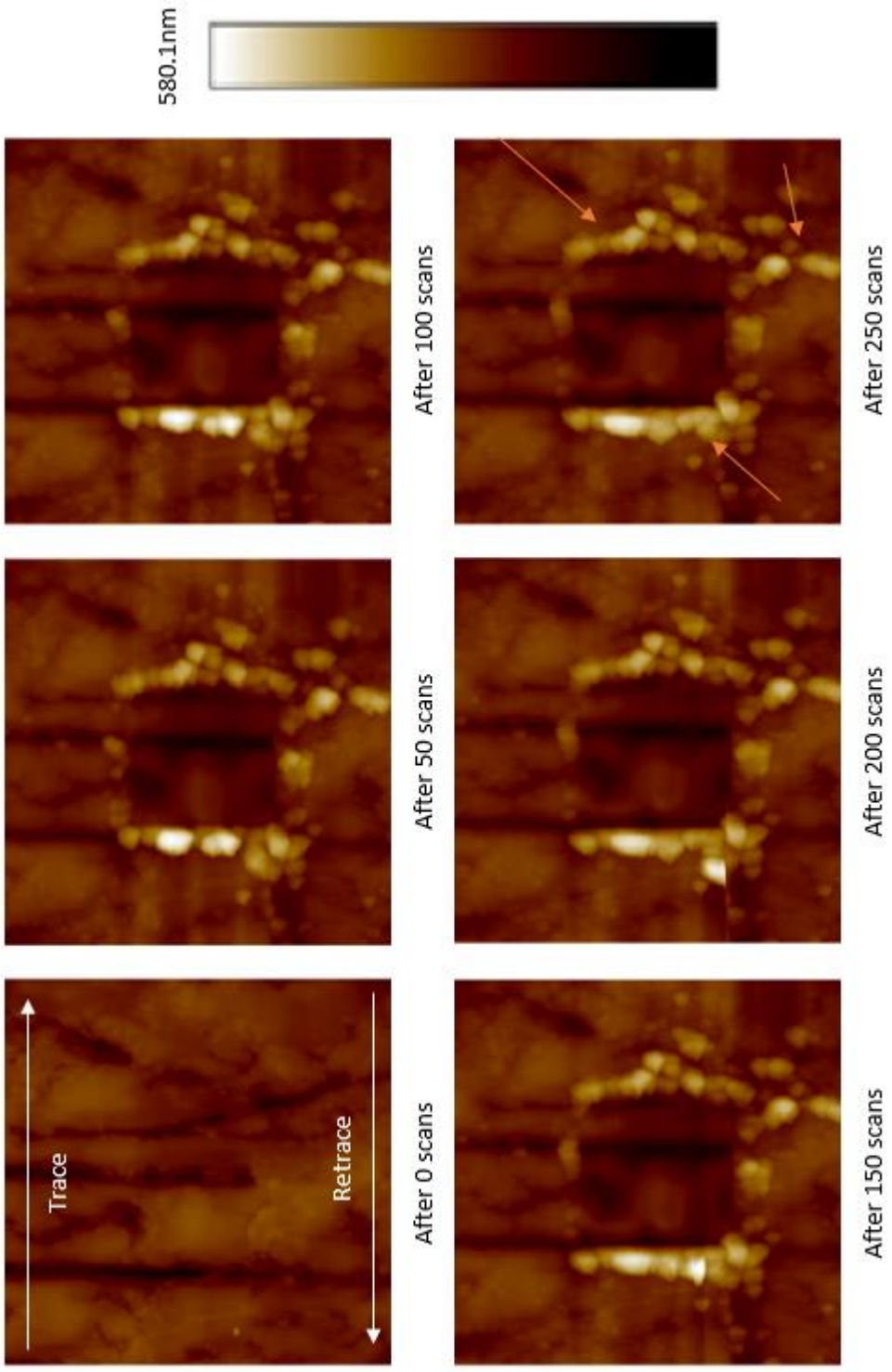

Figure 7-34: The topography progression of a pad film in a 0.55wt% tribofilm, with 0.014mN applied load.

7.8.2.2 Quantification of Material Displacement

Having observed the variability between different graphs produced using the analysis program fewer examples have been included in this section. This is to allow a slight comparison to be made between applied loads whilst acknowledging the limits of this technique.

Figure 7-35 shows an example trace for the scans conducted on a pad in a 0.55wt% ZDDP tribofilm, with a 0.01mN applied tip load. This shows a rapid decrease in height within the worn region, reaching a plateau after 5 wear scans, and a corresponding increase in height in the regions beside the worn area. The exception to this increase occurred in the topography scan taken after 160 wear scans which shows a substantial decrease in height in both the trace and retrace directions. This notable decrease is not reflected in the worn region height, indicating that it is not a property of the entire scan area.

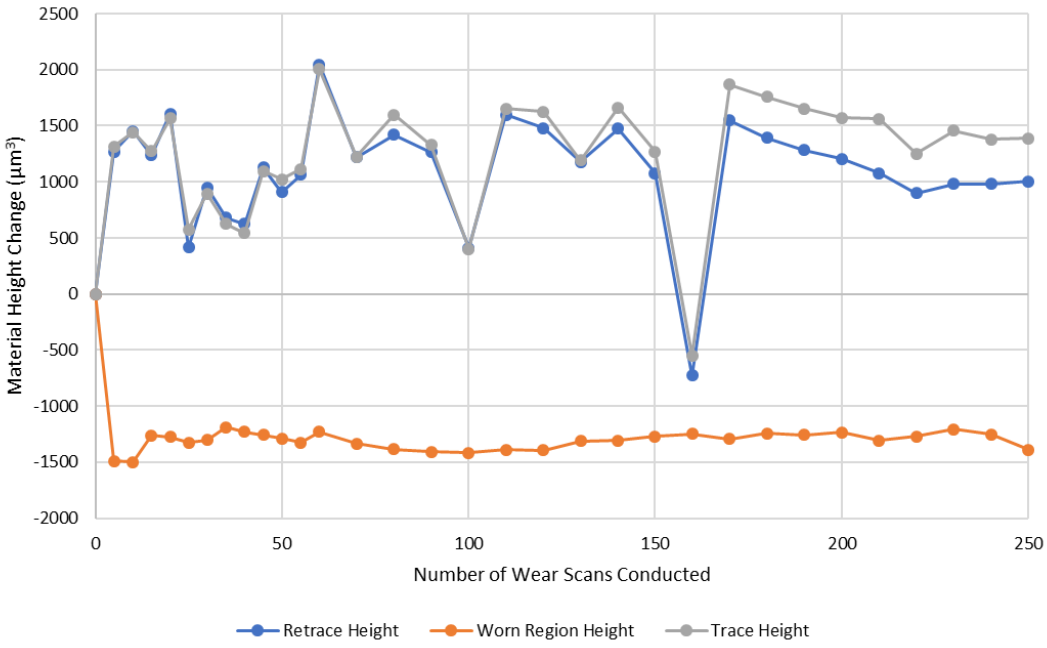

Figure 7-35: An example trace for a 0.55wt% ZDDP tribofilm worn with a 0.01mN load.

Figure 7-36 shows an example trace for a pad film, which has been worn by a 0.014mN load. This shows a very clear, and rapid, decrease in the worn region height and an equivalent increase in the height to either side of the worn region. This is the only trace that showed such a clear distinction, with no unusual height increases or decreases in a single anomalous scan. This graph shows that whilst there must be some material displacement, due to the height decrease within the worn region, there is an additional behaviour that results in a much greater volume gain than the volume loss. This is understood to be due to the change in geometry of the phosphate chains in the relocated material, resulting in an apparent increase in size.

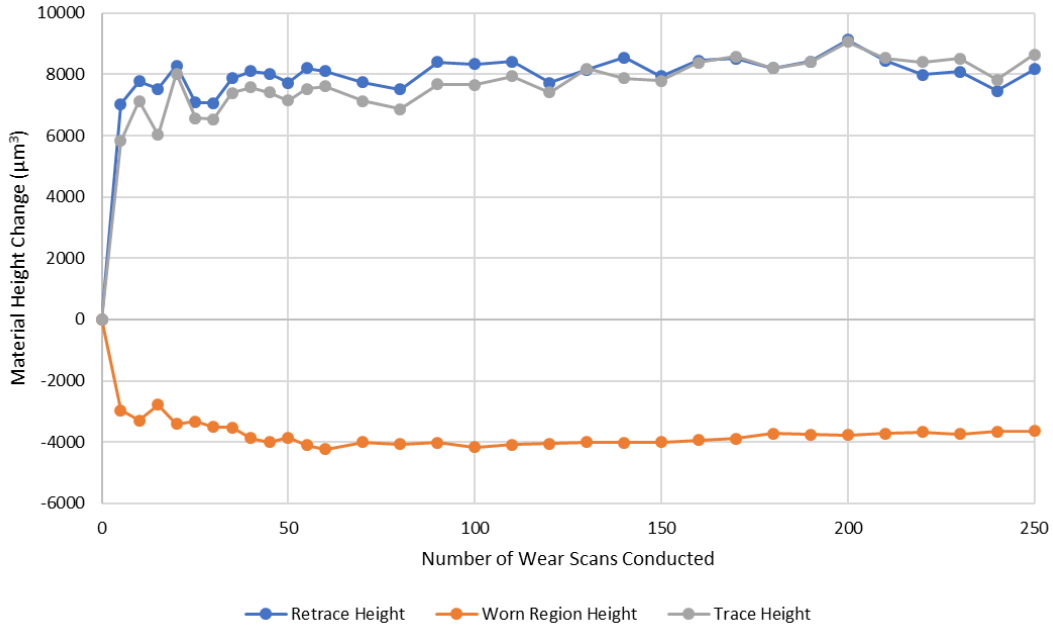

Figure 7-36: An example trace for a 0.55wt% ZDDP tribofilm worn with a 0.014mN load.

7.8.2.3 The worn region

Figure 7-37 shows a selection of wear scan images which correspond to the wear region in Figure 7-31. This shows that the AFM experienced some drift, which progressed throughout the test, with the scan region moving towards the top and left of the topography scan. The tip does not seem to have experienced unusual degradation, with the resolution of the last scan being similar to the resolution of the first scan. There is some evidence of small pads during the test, these are indicated by the green arrows; however, these appear to have been present from the initial contact scan and do not seem to be developing throughout the test. The small pads present in the lower region appear to be less defined in the last scan, indicating that these are being worn, not uncovered by the contact mode scans.

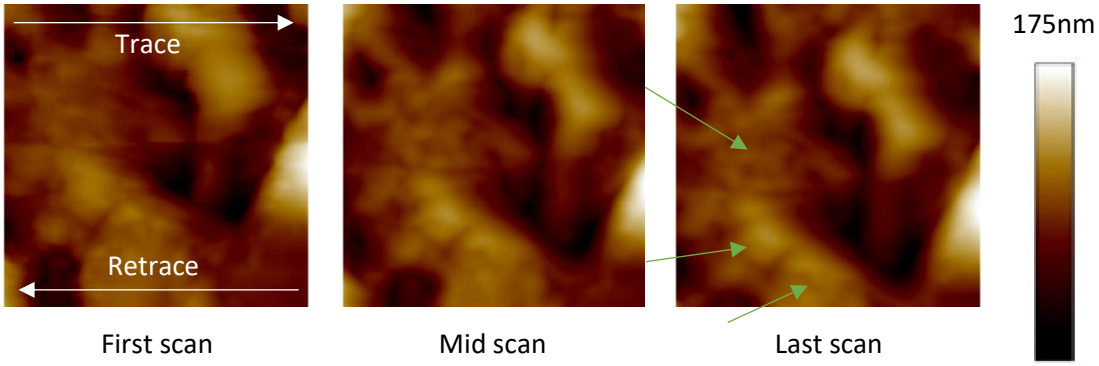

Figure 7-37: Wear scan images for a 0.55wt% tribofilm, with 0.01mN applied load - across pads.

Figure 7-38 shows a selection of wear scan images which correspond to the wear region in Figure 7-32. As was apparent in Figure 7-32 the worn region in this test did not behave as was expected, with the region height increasing throughout the test. It can be seen from the mid scan that the increased height is forming in a triangular shape, with at least four distinct pads present (to the right of the scan). The directionality of these indicate that they are being formed as a result of material displacement in the trace direction; however, there are few signs of material removal to account for this. In the last scan these distinct shapes have become less apparent, with the triangular shapes seemingly

agglomerating. In addition, a single long pad is formed to the left of the scan, with a clear crevice between this and the pads to the right of the scan.

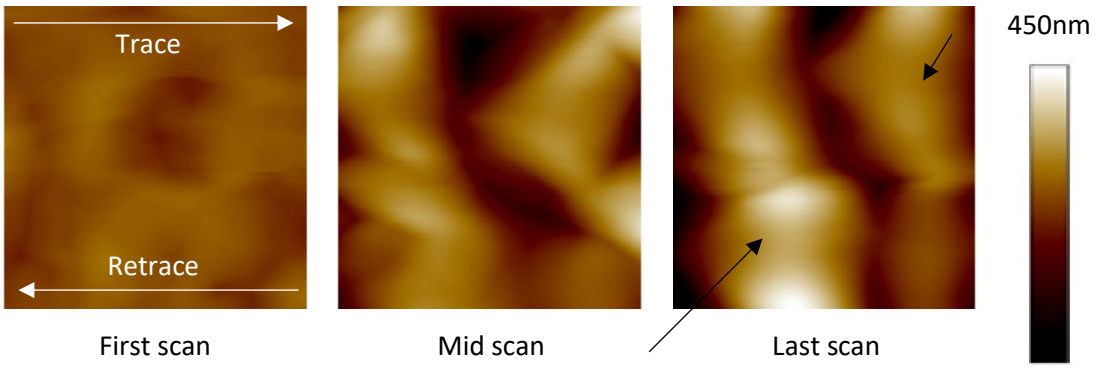

Figure 7-38: Wear scan images for a 0.55wt% tribofilm, with a 0.01mN applied load – on a pad film.

Figure 7-39 shows a selection of wear scan images which correspond to the wear region in Figure 7-33. It can be seen that the directionality on the tribofilm pad, previously indicated in Figure 7-33 is also apparent in the contact mode scans, this is indicated by the black arrows in the first scan. As the test progresses the topography of the initial elongated pad becomes distorted, with the directionality being completely obfuscated by the last scan. By the mid scan there is some evidence of material being displaced, with the edges of the pad becoming less defined and some material removed from the edges of the scan. By the last scan the directionality of the contact can be seen (indicated by the black arrow); however, this is focused towards the upper half of the scan, which supports the location of the displaced material in Figure 7-33.

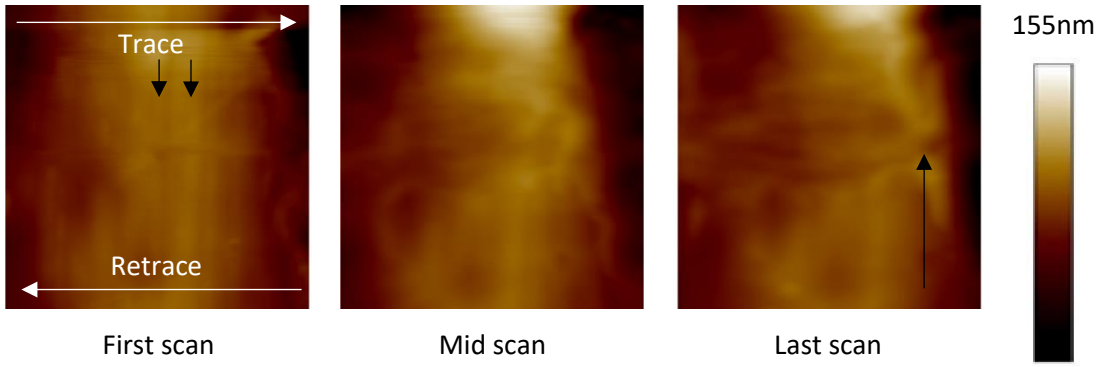

Figure 7-39: Wear scan images for a 0.55wt% tribofilm, with a 0.014mN applied load – on a pad.

Figure 7-40 shows a selection of wear scan images which correspond to the wear region in Figure 7-34. These show that this test experienced some drift; however, the primary movement appears to have occurred between the first and mid scan, indicating this is not merely caused by thermal drift but is instead caused by an external source. There is some evidence of small pads being revealed within this test; however, these are clearest in the mid scan not the last scan. There is still some evidence of these in the last scan, as indicated by the green arrows; however, they appear to be larger and less defined. In addition, there appears to be an increase in height within this scan, specifically the height of the rounded portion of the tribofilm (to the left of the scan, indicated by a green arrow).

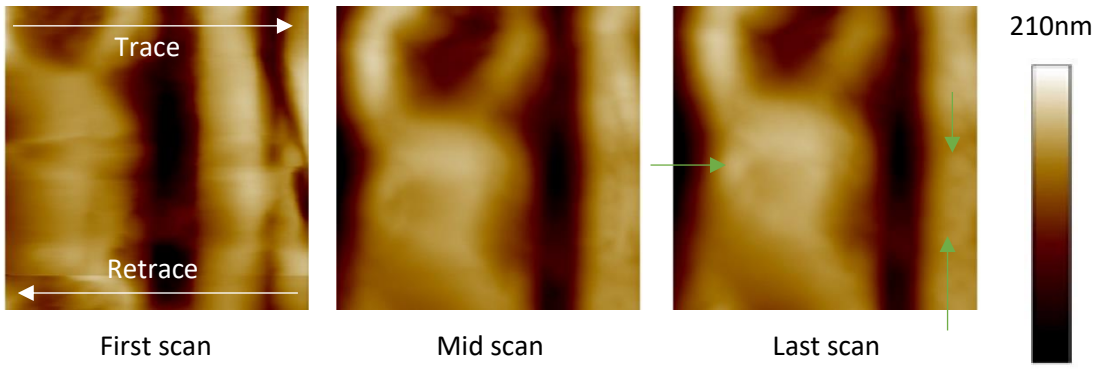

Figure 7-40: Wear scan images for a 0.55wt% tribofilm, with a 0.014mN applied load – on a pad film.

7.8.2.4 Effect on surface parameters in the worn region

The progression of the arithmetic mean roughness across the surface of the worn region is shown in Figure 7-41. This shows that there is more of an influence of the position within the tribofilm on the durability of the tribofilm, than the applied load. It can be seen that there is no apparent correlation between the applied load and the surface roughness, with the middle load value resulting in a higher surface roughness for all possible tribofilm positions. As with Figure 7-27 it can be seen that there is an effect of dwell on the S_a values, but otherwise there is no substantial change in S_a as the test progresses. The exception to this is the test conducted on a pad film with a 0.01mN load, which was the test that was previously noted as having experienced an unusual height increase during the test. This

experienced a progressive increase in S_a, which likely corresponded to the formation of the unusual triangular pads. This is beginning to plateau towards the end of the test, likely corresponding to the agglomeration of these pads. The other seemingly anomalous result is the test conducted on the edge of a pad, with a tip load of 0.005mN. This has previously been commented on and is believed to correspond to the large crevice running vertically through the scan area.

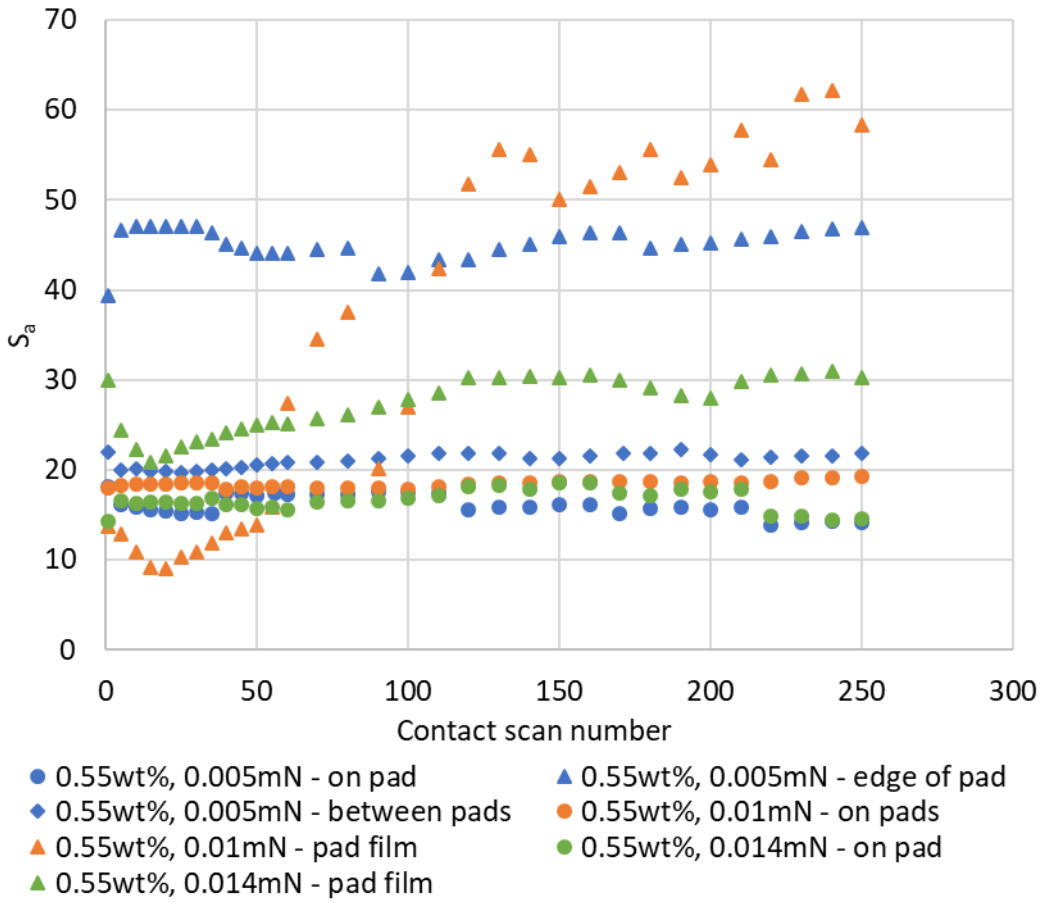

Figure 7-41: The progression of S_a, across different loads.

The progression of the surface skewness is presented in Figure 7-42. It can be seen that, again, there is no clear correlation between the load applied to the tip and a resultant change in the surface skewness. The S_{sk} values for the tests conducted with a 0.014mN load appear to be notably out of family, with initial values 1.0 lower than the other tests. This is due to the very deep regions within these scans; due to the elongated pad in Figure 7-39 there are deep regions to either side but a smoothened (with the exception of the

directionality markings) upper surface and in Figure 7-40 there is a deep crevice running through the worn region.

The progression of the skewness for the scans shown in Figure 7-40 remains stable from the 50th contact scan, with the variation prior to this likely a result of the slight relocation of the scan area in the initial testing. However, the S_{sk} progression for the scans shown in Figure 7-39 display an unusual behaviour, with an increase between the 50th scan and the 130th scan and a subsequent decrease from the 130th scan to the 220th scan and then a plateau until the end of the test. This unusual increase and subsequent decrease in S_{sk} may be due to the material displacement filling the crevices on either side of the elongated pad with material, which is then subsequently moved farther from the middle and out of the scan region. This is supported by the continued increase in material mass, in the displaced material mounds on either side of the worn region, throughout the test shown in Figure 7-32.

The only other particularly notable S_{sk} progression is for the test conducted at 0.01mN tip load on a pad film, the test noted for the unusual increase in height within the worn region. This test experienced an initial increase in S_{sk} from the beginning of the test until the 45th scan and then experienced a progressive decrease in S_{sk} until the 120th scan after which the S_{sk} appears to plateau. The initial increase in S_{sk} is likely due to the formation of the unusual triangular pads and the subsequent decrease is likely due to the removal of surrounding material and the formation of the large crevice between the final two elongated pads.

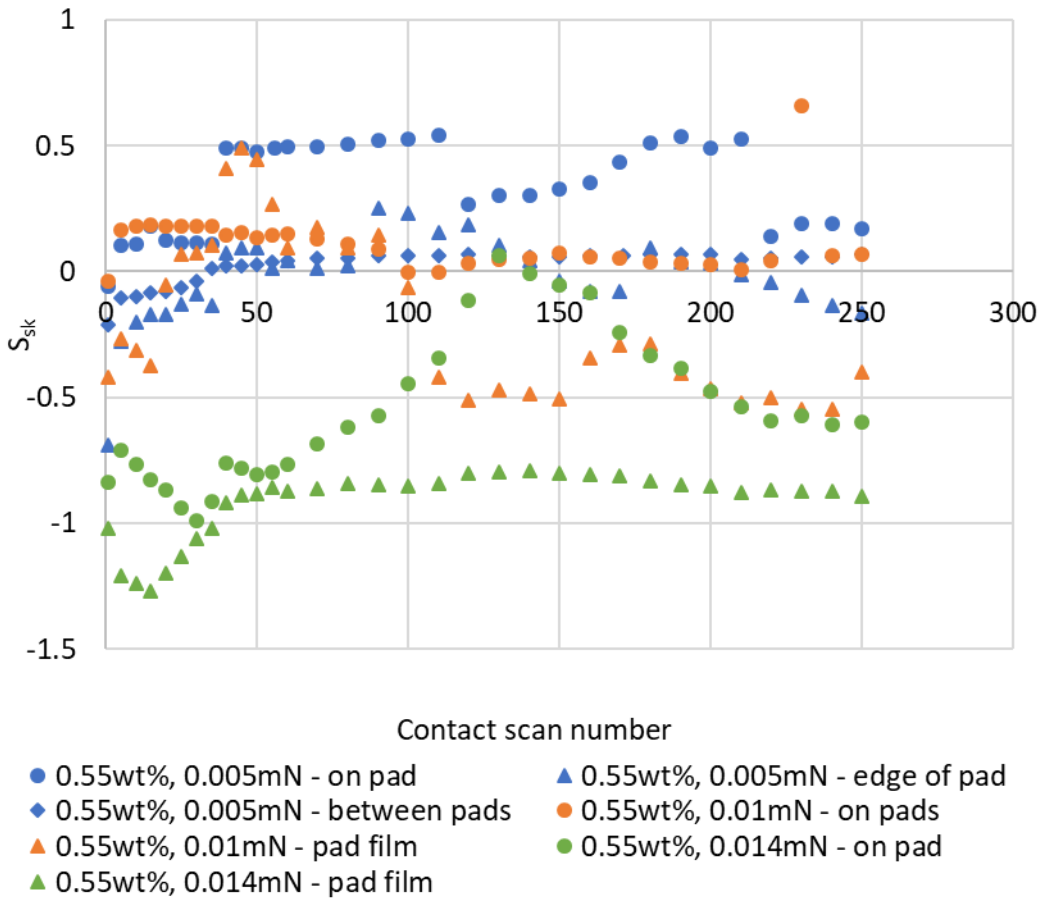

Figure 7-42: The progression of S_{sk}, across different loads.

The progression of the surface kurtosis is presented in Figure 7-43; which shows that there is no major effect of tip load on the surface kurtosis. It can be seen, once again, that the behaviour of the two scans conducted at 0.014mN appears to be out of family, with both tests displaying an increase, and subsequent decrease, in the kurtosis within the first 50 scans. Some of this behaviour could be due to AFM errors in gathering the data, resulting in small artefacts on the scans; however, if this were the case it would be expected that the increased S_{ku} would persist throughout the test, which is does not. This indicates that these are real phenomena.

The increased initial kurtosis in the test on a pad film (whose wear scans are summarised in Figure 7-40) is likely due to the rapid displacement of material, occurring in the initial contact mode scans, and then the subsequent smoothening of the surface once the material displacement appears to have ceased. This is supported by the overall

topography images presented in Figure 7-34 which indicate that there is no further material displacement after 50 scans.

The initial unusual behaviour in the test on a pad can be explained by the immediate creation of ploughed channels due to the contact mode scans (these can be seen toward the top of the first scan in Figure 7-39). The reduction in S_{ku} can then be explained by the increased tip geometry, resulting in less defined channels, with overlapping edges (it can be seen from the mid scan in Figure 7-39 that the scratch marks have been obfuscated). The increase in S_{ku} from the 160th scan to the end of the test (with a reduction between the 210th scan and the 220th scan, caused by dwell) is due to the odd valleys form within the pad, these are indicated in the last scan in Figure 7-39, which are less defined than the initial scratches (resulting in the S_{ku} only increasing to approximately 5 instead of 6.5).

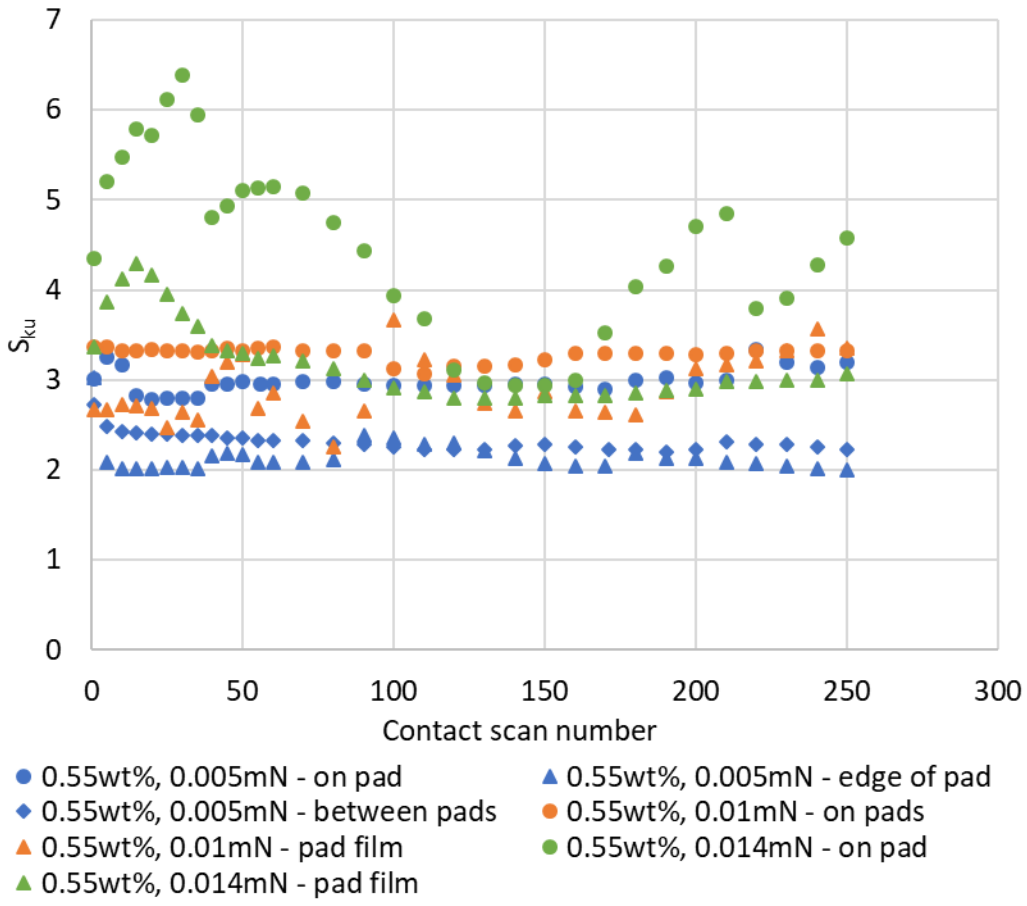

Figure 7-43: The progression of S_{ku}, across different loads.

Figure 7-44 shows the progression in the surface isotropy throughout the test. It can be seen that despite the contact scans inducing linearity the majority of scans maintain a constant level of anisotropy throughout the test and there is no clear connection between the applied load and the resultant surface directionality. In addition to the obviously anomalous behaviour of the test conducted at 0.01mN on a pad film it is worth noting the lack of an effect of pad directionality on the isotropy of the test conducted at 0.014mN on a pad. This test has been noted as displaying specific topography on the surface of the elongated pad, which was predicted to result in an increased isotropy for this test; due to the contact scans being conducted perpendicular to the original wear. The fact that this test does not display a different level of directionality indicates that the S_{tr} is not biased towards initial topography and instead is only affected by the contact scans.

The test conducted at 0.01mN on a pad film displays initially high levels of isotropy (0.5) which decreases to 0.2 (moderate anisotropy) from the 15th contact scan to the 35th scan. This then rapidly increases to 0.65 between the 45th and 50th scan, remaining high until the 150th scan, after which it returns to a moderate anisotropy (0.2). This fluctuation between highly isotropic and moderately anisotropic is unusual and can be related to the odd topography behaviour present in this test. The initial isotropy is likely due to the completeness of the tribofilm, with a full pad film present. This then becomes much more anisotropic once the surface has been exposed to contact mode scans, with ploughing channels being formed rapidly. Then, as the unusual triangular pads begin to form the surface becomes more isotropic, with the overall topography (pads and small valleys) becoming the dominant surface features. Once the pads have become fully formed the surface becomes more anisotropic again with the surface of the pads being worn (as can be seen in the last scan in Figure 7-38.

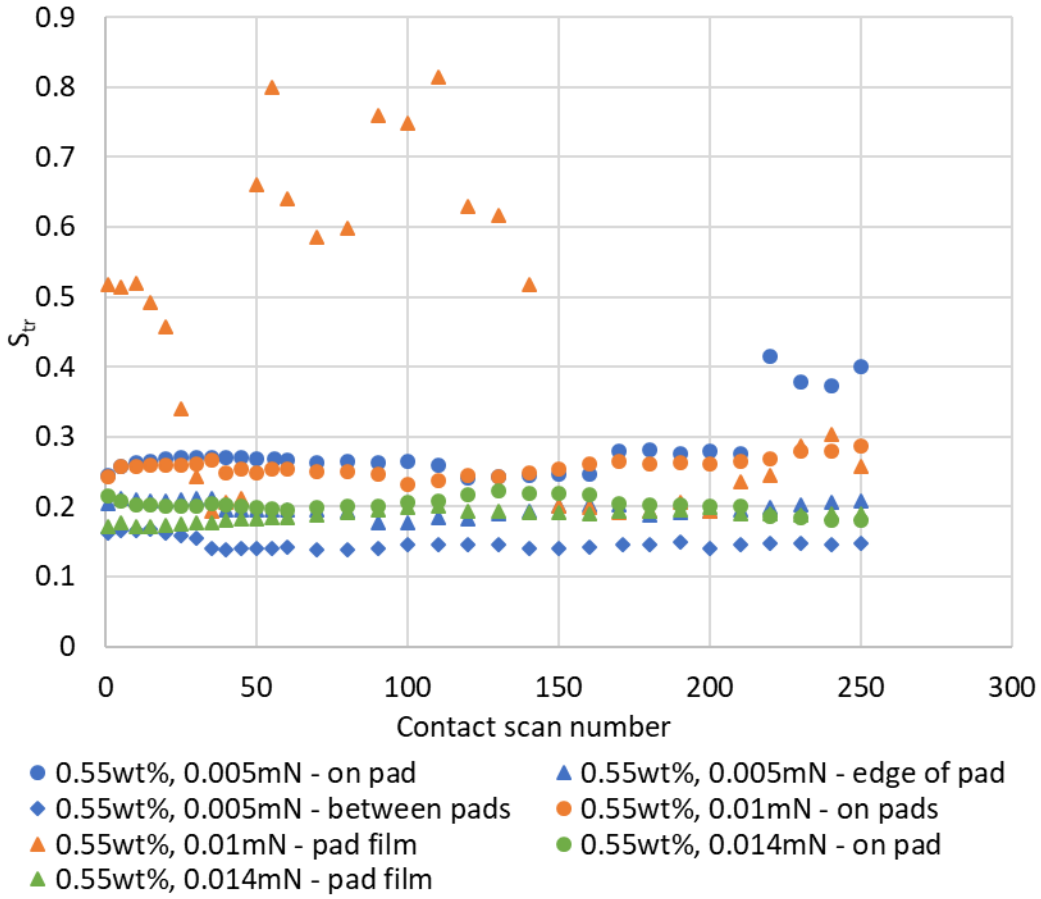

Figure 7-44: The progression of S_{tr}, across different loads.

7.9 Durability Discussion

To aid in readability and comparisons some results will be illustrated again here. These results have previously been explained in section 7.8 accompanied by a two-dimensional image.

7.9.1 Preliminary Testing

The preliminary tests indicated that the AFM would be able to wear a tribofilm, with the material being easily displaced and the tip degradation appearing to be minimal. However, due to cost constraints it was decided that the expensive TAP525 AFM probe, with a nominal spring constant of 375N/m, would be replaced with the more available RTespa 300, which has a nominal spring constant of 40N/m. This difference results in the forces applied by the tip being several orders of magnitude lower in the latter tests.

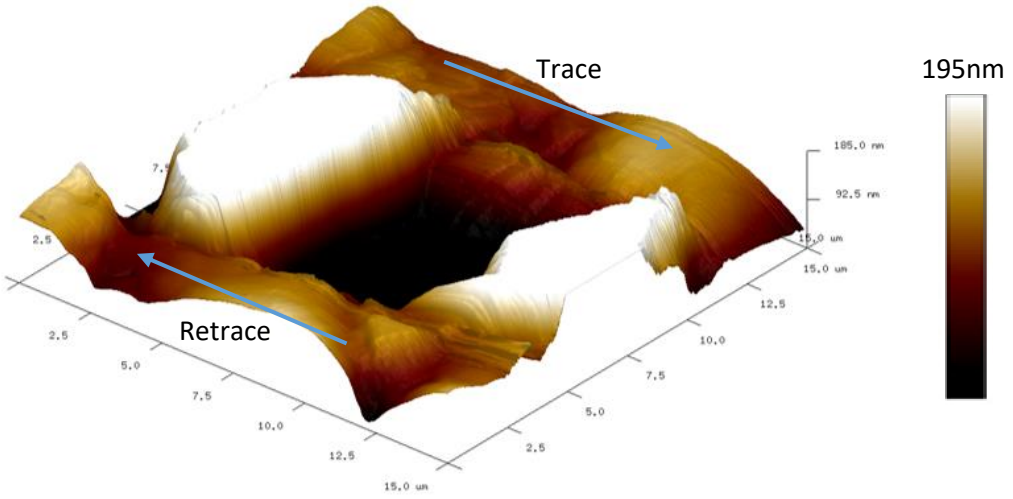

Figure 7-45: Topography after 25 scans in preliminary study.

There was no evidence of the tribofilm being displaced preferentially in the trace or retrace direction. This is consistent with the AFM applying an equal lateral force in both directions, as well as maintaining a constant applied normal load. Therefore, the two sides can be treated as equivalent when analysing the durability of the tribofilm with an AFM.

The analysis program was initially developed to quantify the amounts of displaced material in the preliminary tests, with the heights of the displaced material mounds being

measured, alongside the depth of the worn region. Unexpectedly the volume of material displaced (into the mounds) exceeded the volume of material lost from the worn region. This might be explained by the tribofilm being fluidic [112]. Under this hypothesis the displaced material has been “melted” back into a more fluid state than the traditional ex-situ glassy film and then moved to the outer regions. When the material is permitted to “cool” and re-crystallise into a new glassy film the orientation of the long chain polyphosphates may be different, resulting in an apparent change in volume.

Another theory to explain the volume difference is that the AFM is unable to accurately determine the depth of the worn region, due to feedback problems in the peak force tapping mode, caused by the increased height in the displaced material mounds. This theory is believed to be less likely due to the absence of artefacts in these scans, indicating that the AFM was performing correctly [59].

7.9.2 Effect of Concentration on Tribofilm Durability

The results presented as Figure 7-11 to Figure 7-30 show that there may be a change in the tribofilm durability with concentration of ZDDP. The amount of material displaced (with the exception of the unusual initial durability in Figure 7-13) appears, visually, to be greater for the higher concentration. However, the results from the analysis program were too noisy to quantify this effect.

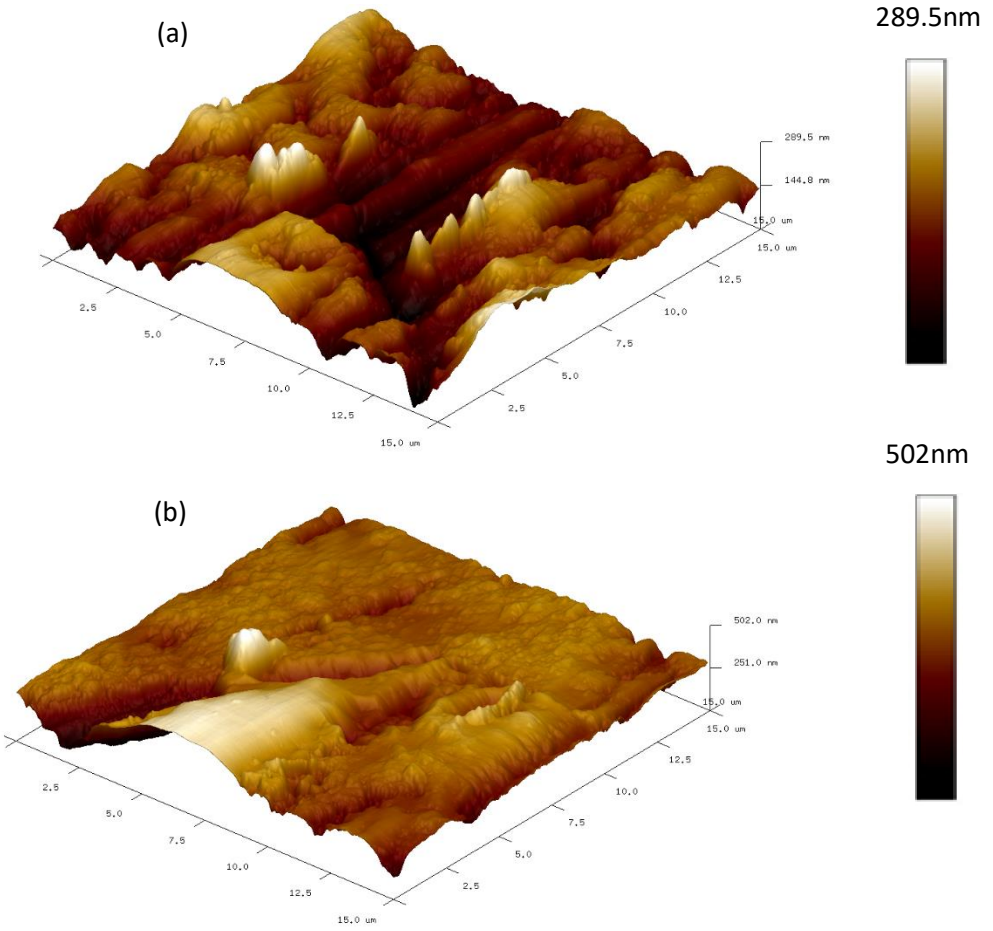

Figure 7-46: Topography comparison after 250 scans for 0.55wt% ZDDP (a) and 0.275wt% ZDDP (b).

This apparent increase in displaced material with concentration, Figure 7-46, indicates that there is a difference in the durability of the polyphosphate layer of the tribofilm when it is formed in a more ZDDP rich oil. However, this researcher believes that the increased quantity of alkyl phosphates present in the higher concentration oil results in an increased adherence of these phosphates to the hardened polyphosphate layer and that the material displaced is primarily made up of these molecules instead. It has been stated [75] that the thick layer of alkyl phosphates present over the surface is easily removed by n-heptane, such that the hardened glassy polyphosphate layer is all that remains, Figure 7-47. However, the ease with which the limited amount of material was removed indicates that the upper surface of these ZDDP tribofilms is poorly adhered, as is understood to be the case for the alkyl phosphate layers. The removed material was displaced rapidly, often with little further

displacement of material, further indicating that only the top layer is being affected. This researcher is inclined to believe that the displaced material is an adhered alkyl phosphate layer, as opposed to a hardened polyphosphate layer, because the underlying topography is not affected by the displacement. This indicates that the displaced material is not a part of the underlying tribofilm pads and is instead a thin layer on top of these, which does not contribute to the overall topography.

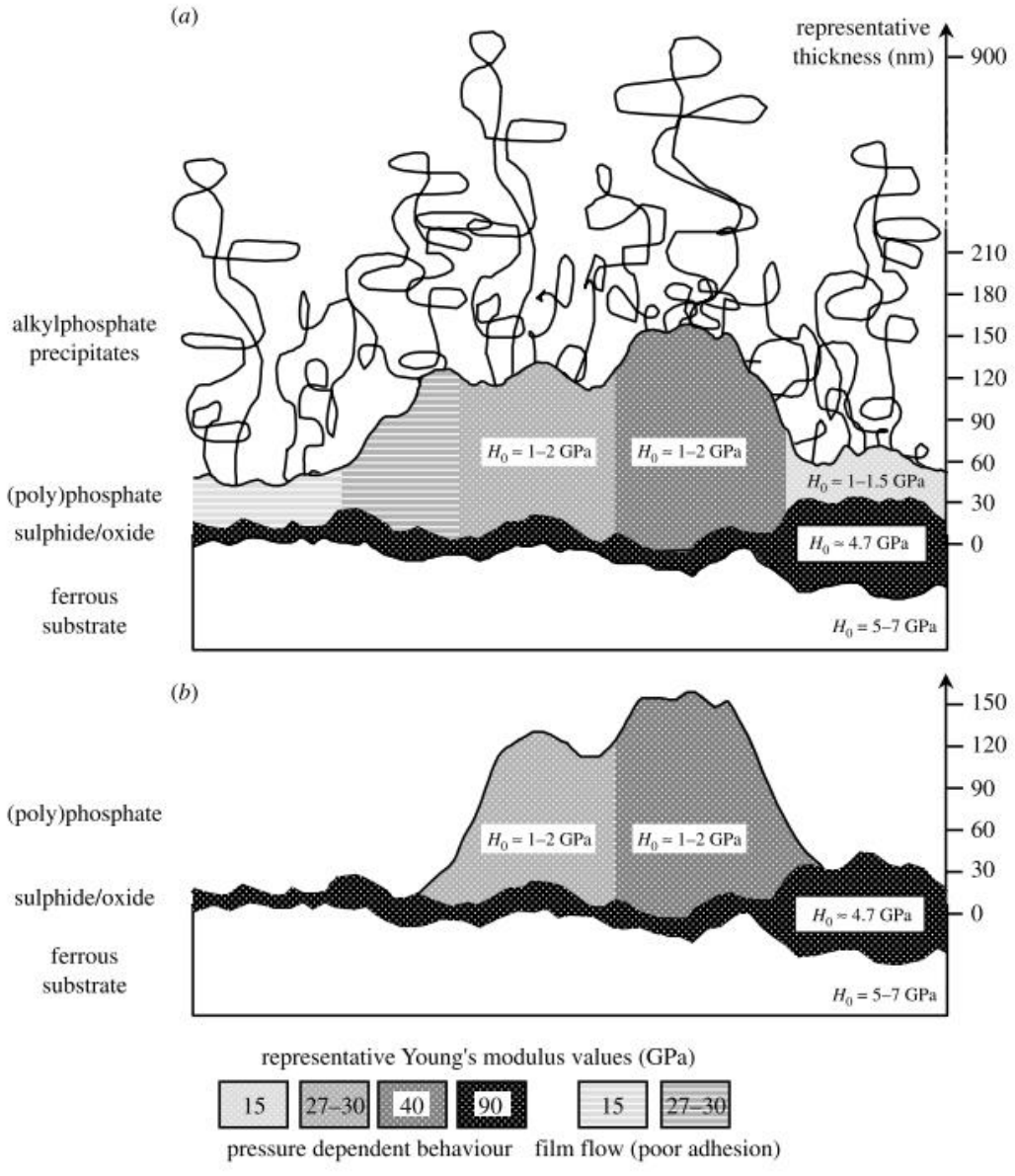

Figure 7-47: Schematic representation of the structure and mechanical properties of a ZDDP tribofilm, according to Bec et al [75]***, (a) prior to solvent washing (b) after solvent washing.***

Additionally, the increased quantity of apparently displaced material for the tribofilms produced with higher concentrations of ZDDP is unexpected. The original hypothesis was that the smaller pads (and more even coverage) produced when shearing higher concentrations of ZDDP would have a higher durability and a lower pliability. This is because a more even coverage means more adherence sites (such as has been suggested is the case for higher concentrations, in phase 1. Work conducted by Bec et al [75] suggests that the compression process (carrying the load) results in an increased Young's modulus for the tribofilm, when the pads are unable to slip, Figure 7-47. This suggests that the Young's modulus of tribofilms formed in higher concentrations of ZDDP would be greater than the equivalent tribofilms formed in lower concentrations. However, the results presented in this document do not agree, with more material being displaced for the higher concentration. This further indicates that the displaced material is not a component of the hardened polyphosphate layer and is instead a remnant of the loosely adhered alkyl phosphate layer. It is proposed that the increased material displacement for the higher concentration is due to the presence of more long polyphosphate chains which results in an increased number of sites for the alkyl phosphate to become loosely adhered.

The unusual phenomenon observed when the tip is sheared against a pad in the 0.275wt% tribofilm supports the hypothesis that the lower concentration tribofilm has a lower Young's modulus than the equivalent higher concentration tribofilm. The large material displacements observed during the scans conducted on the first day of scanning appear to return to approximately their original positions when the scanning is stopped for approximately fourteen hours. This phenomenon was not observed in any other scans and so this researcher can only hypothesise that this is a result of the initial adherence sites (the points at which the polyphosphate chains are adhered to the underlying oxide and sulphide layers) not being displaced, with the long chains being moved fluidically and then "relaxing"

back into their original positions. The preliminary tests were scanned within a single day and then removed from the AFM, precluding the possibility of observing this phenomenon.

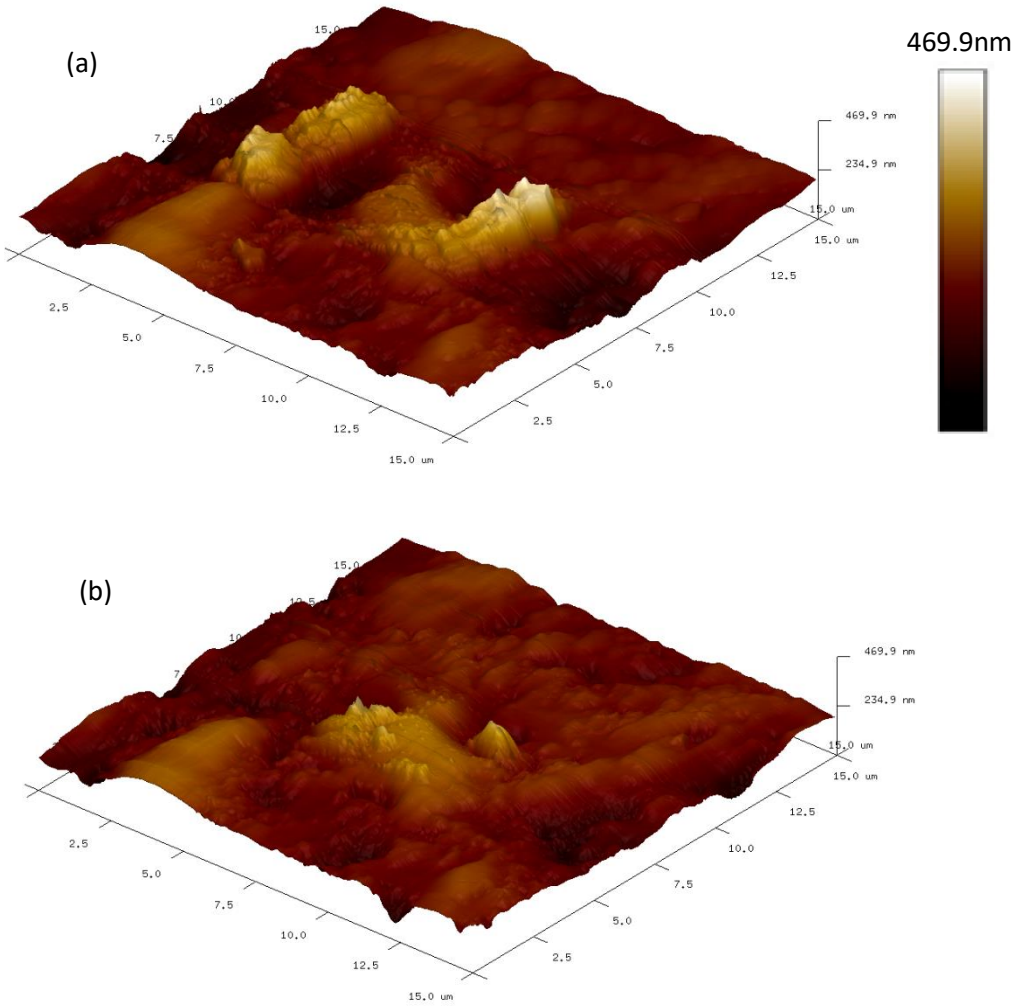

Figure 7-48: Topography progression for the unusual phenomena in 0.275wt% (a) after 35 scans (b) after 40 scans.

7.9.3 Effect of Load on Tribofilm Durability

There is clearly an effect on the durability caused by the difference between the preliminary study and the main study, Figure 7-49. This is likely a result of the vastly different Hertzian contact pressures used. The contact pressures applied for the preliminary study were between 98.4GPa and 164.4GPa (for an assumed Young's modulus between 15GPa and 40GPa [75]) whereas the contact pressures for the highest load used in the main study were between 36.8GPa to 61.5GPa. The reason for the discrepancy between these pressures (despite using approximately the same applied voltage) is the considerable decrease in the

cantilever spring constant for the main study. The nominal spring constant for the RTespa 300 cantilever is 40N/m (with a stated range between 20N/m and 80N/m) whereas the nominal spring constant for the TAP525 is 200N/m (with a stated range between 100N/m and 400N/m).

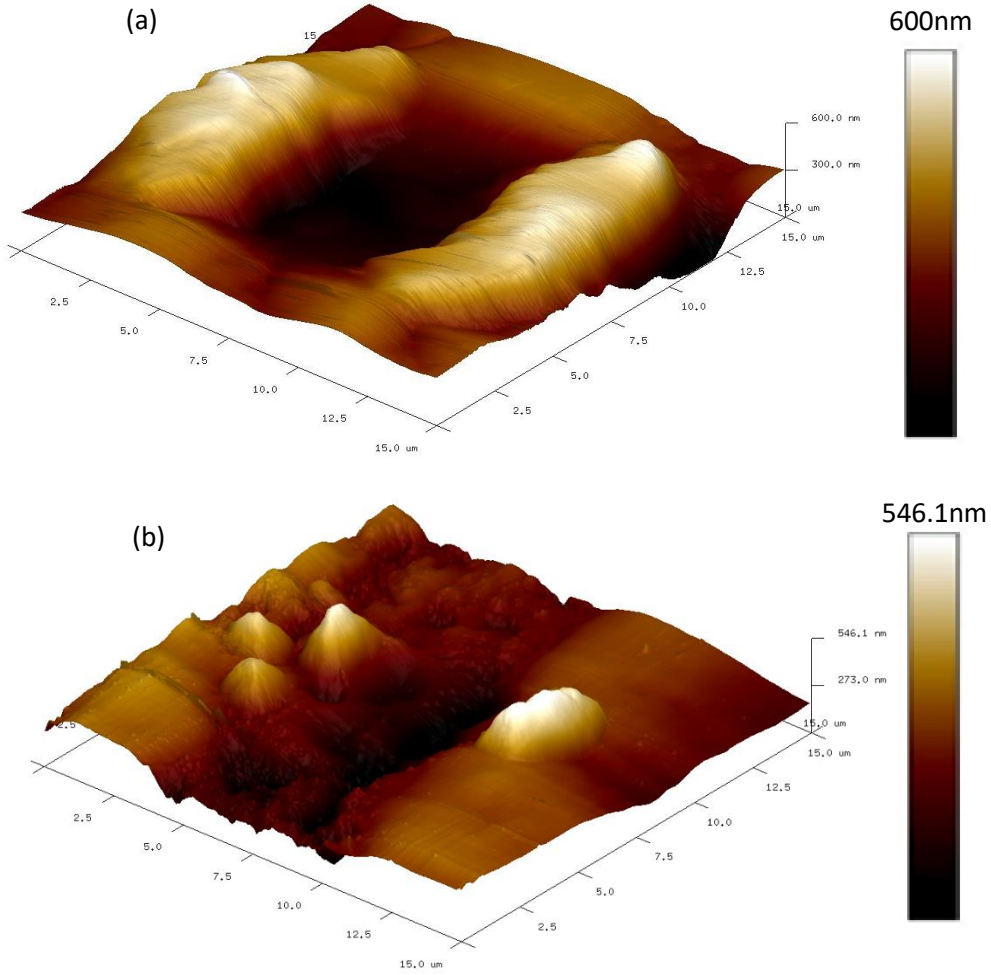

Figure 7-49: Final topography image (a) preliminary study, after 20 scans (b) main study, after 250 scans.

Having determined that decreasing the load from 0.267mN to 0.014mN does result in a difference in the durability of the tribofilm it is now necessary to discuss the range of loads between 0.005mN and 0.014mN, Figure 7-50. The results show that there is no repeatable effect of increasing the load, with similar amounts of material displacement observed for all three applied loads (including 0.01mN). This suggests that the applied pressures are insufficient to indent the tribofilm pads, which supports the theory that the only material displaced is the loosely adhered remnant alkyl layer. The initial Hertzian contact calculations

indicated that the load applied would result in a pressure that was sufficient to indent the tribofilm; however, the variable nature of tribofilms and the limited mechanical data available may have resulted in an inaccurate calculation. It was originally intended that a component of this study would be to determine the mechanical properties of the specific tribofilms being analysed, but on consultation with the resident expert in nanoindentation it was decided that the tribofilm was too thin to accurately measure these. The fact that the tribofilm is sufficiently thin that nanoindentation is unable to separate the tribofilm and substrate properties suggests that the tribofilm mechanical properties are not the only ones needed to determine the Hertzian contact pressure.

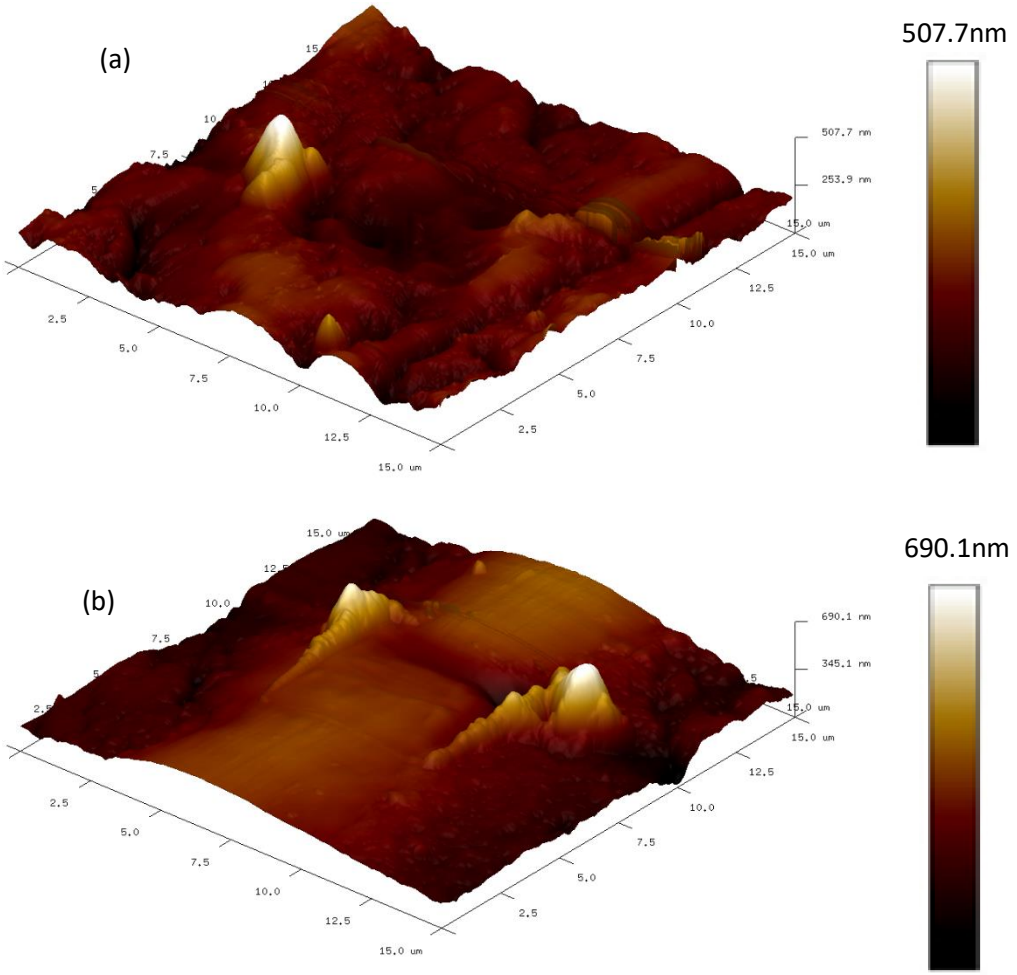

Figure 7-50: Topography comparison between loads (a) 0.005mN (b) 0.014mN.

Unusual behaviour was observed in the test on a pad film, with a 0.01mN load, Figure 7-51, which showed film growth within the worn region. This unusual behaviour is believed

to be as a result of an excess of remnant alkyl phosphates, likely due to an inadequate cleaning with n-heptane. When this layer is exposed to the load and sheared the alkyl phosphates are broken down into shorter chains and these are then chemically bonded to the ends of the pre-existing polyphosphate chains. The unusual geometry of the increasing pads is likely as a result of the shearing motion, with the hardening chains being moved in linear directions. This is supported by the appearance of the “new” pads directly on top of the “original” pads, although it can be difficult to see these in the initial topography scans, further indicating the presence of a secondary film. This is different from the supposed pad film tested with the 0.14mN load, which had a very clear initial topography. This indicates that these were perhaps not directly comparable, as had originally been intended.

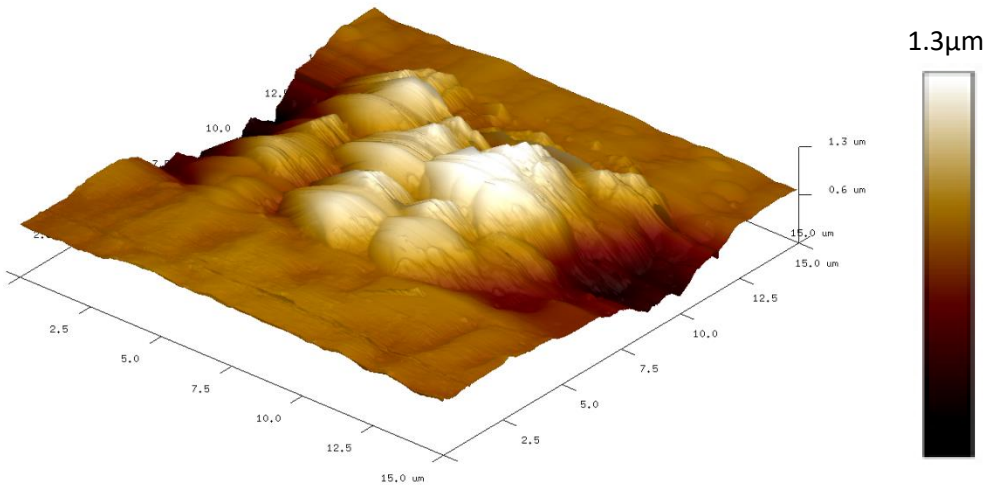

Figure 7-51: The unusual phenomena for 0.01mN.

7.9.4 Explanation for material displacement

Two hypotheses to explain the material displacement are presented; both are formed on the understanding that the remnant alkyl phosphates are loosely adhered to the polyphosphate chains. This can be represented schematically as shown in Figure 7-52, which is an amended version of the final stage of the formation hypothesis presented in section 6.5.2.

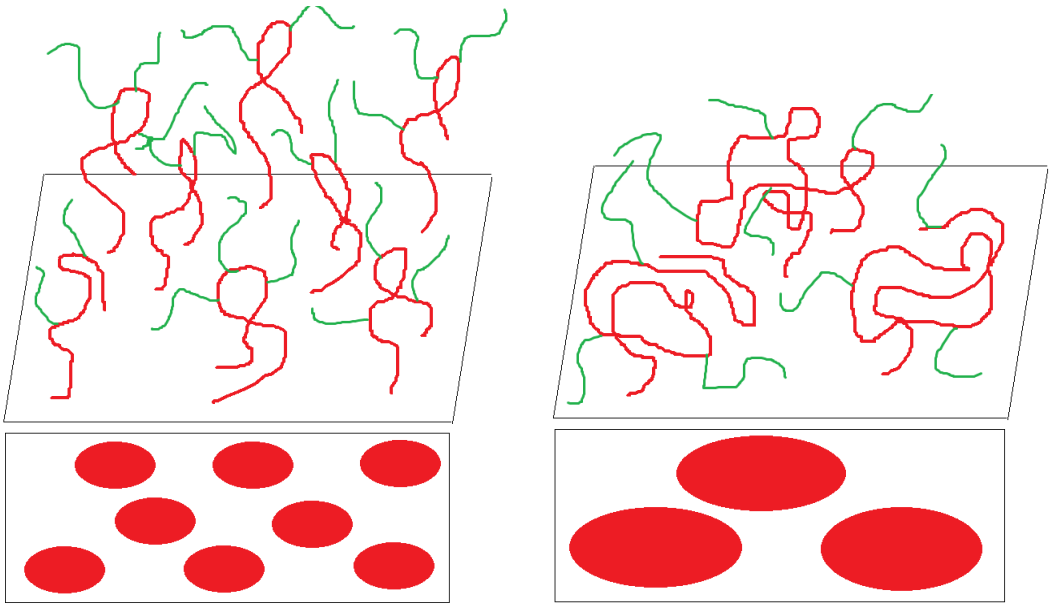

Figure 7-52: Amended ZDDP formation schematic to include alkyl phosphates.

The difference between the two presented hypotheses relates to whether the loosely adhered alkyl phosphates are entirely moved when sheared, or whether the adhered portion of the chain remains in its original location with the rest of the chain being straightened. Both of these suggest a fluidic nature to the alkyl phosphates, which is supported by the work of Bec et al [75] and Dorgham [112]. These hypotheses are displayed schematically in Figure 7-53, which shows how the chains might be entirely moved, and Figure 7-54, which shows how the chains might be straightened.

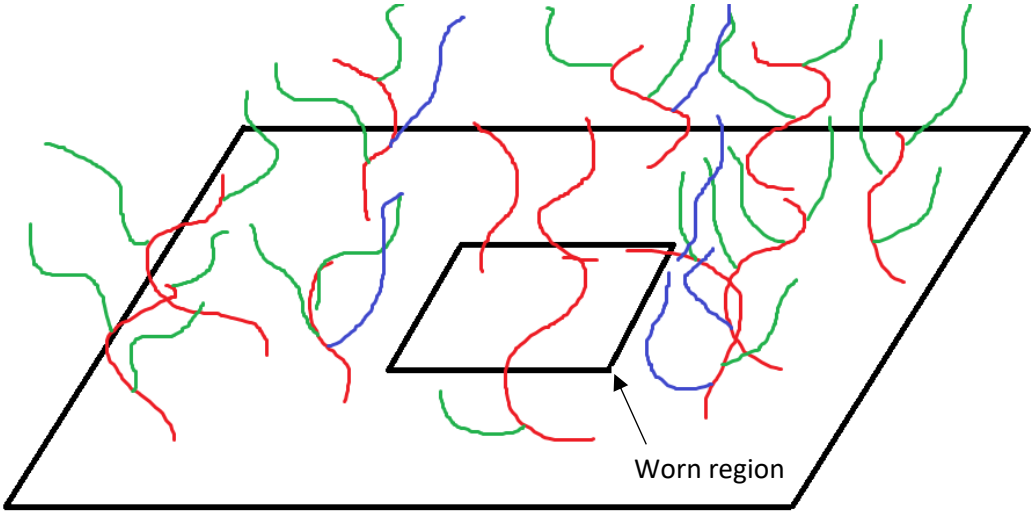

Figure 7-53: Alkyl phosphate chains with new attachment sites. Red lines represent the ends of the polyphosphate chains, green lines represent unworn alkyl phosphate chains and blue lines represent moved alkyl phosphate chains.

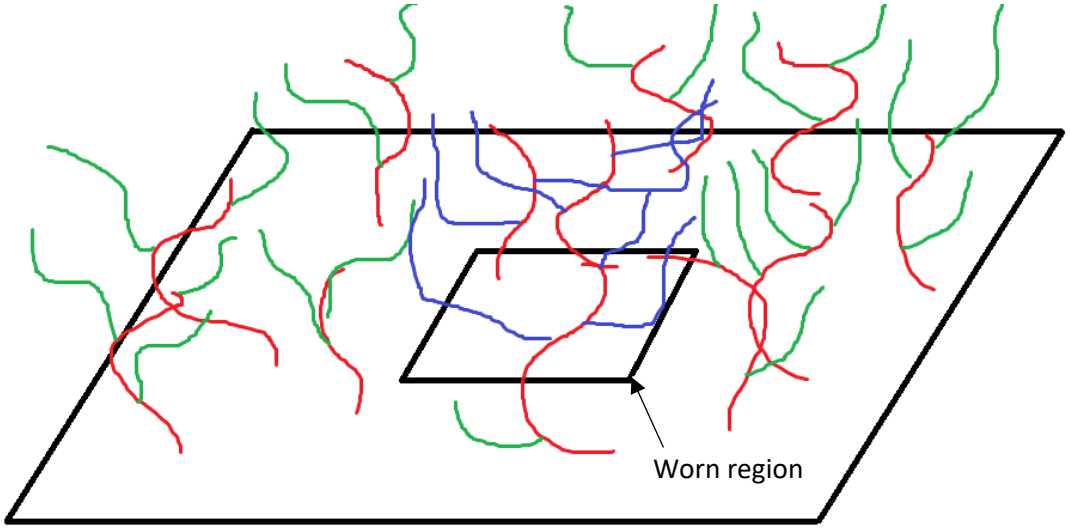

Figure 7-54: Alkyl phosphate chains which have been straightened. Red lines represent the ends of the polyphosphate chains, green lines represent unworn alkyl phosphate chains and blue lines represent worn alkyl phosphate chains.

This research was unable to conclusively determine which of these hypotheses is correct. However, this researcher is inclined towards the first, that the chains are entirely detached. This is because work conducted previously indicates that the alkyl phosphates are very loosely bonded to the polyphosphate chains and can be easily removed by n-heptane [75]. Whilst solvent cleaning does not appear to have been sufficient to remove all of the alkyl phosphate chains in this research, due to the ease with which some material could apparently be moved, this theory indicates that the chains are likely to become detached when sheared. This is supported by the understanding that the alkyl phosphates support the bulk of the load and are sheared sacrificially within the boundary contact. Some of the removed alkyl phosphates may be transferred to the AFM tip. However, the displaced material mounds on either side of the worn region indicate that the bulk of the material is deposited onto the surface outside of this region.

7.9.5 Explanation for change in worn region topography

The proposed explanation for the apparent appearance of small pads within the worn region is that these small pads are present throughout the test and are revealed when the alkyl phosphates are displaced. This further supports that the alkyl phosphates are removed

from the worn region, instead of being straightened. The small pads might be formed during the initial tribofilm generation from the ends of the long polyphosphate chains, which are likely to have been less work hardened that the bulk pad, made from newer short chain polyphosphates being chemically bonded to the pre-existing polyphosphate chains. This supports the theory that ZDDP tribofilms can self-replenish, with short chain polyphosphates adsorbing onto the ends of the remnant longer chain polyphosphates.

It is likely that the large pad structures are dominant, as suggested in the characterisation of tribofilms section, with the bulk form being apparent through the alkyl phosphate layer, whilst the small pad structures are sufficiently small (relative to the large pads) as to be obscured by the alkyl phosphate layer. This would explain why these forms are not observed in traditional tribofilm topography yet appear when the loosely adhered alkyl phosphate layer is removed by an AFM.

An alternate theory would be that the polyphosphates are being further broken down during the contact process and that the newly shortened chains are forming small pads on top of the pre-existing pads. This theory is considered less likely as it is understood that the formation process requires ZDDP molecules, and this testing was conducted in the absence of fresh ZDDP. In future work it is recommended that this process be conducted again in the presence of fresh ZDDP to confirm whether these pads are revealed more rapidly, indicating a formation process as opposed a revealing process.

7.9.6 Efficacy of Analysis Program

This research intended to compare the quantified results to Archard's wear law. However, as has been shown, the analysis program was unable to quantify the effect of wear for all of the results. This problem resulted in the development of several iterations of the software, with the results presented within this document being the outcome of the method which worked well for the largest number of tests.

It is worth noting that the analysis program was able to quantify all of the results for the preliminary study, potentially due to the more progressive and extreme material displacement. This indicates that if this investigation were to be repeated with a higher applied load (and a stiffer cantilever) the analysis program should be able to quantify the effect of load and confirm the observed differences in durability for different ZDDP concentrations.

7.10 Limitations of the Study

The main limitation of this study was that there is no existing literature that can be employed to validate the current results. Work, conducted in 2019, by Ueda et al [9] has considered the durability of a tribofilm; however, that work was so fundamentally dissimilar to the work conducted as part of this study as to render any comparisons impossible. Therefore, the only way to truly validate the results presented within this section is conduct like for like repeats of these experiments.

The tip geometry is not accurately measured throughout the test, and the final tip radii are unknown. It can be inferred that the final tip radii are less than the resolution of a single scan pixel (30nm); however, the true tip degradation is difficult to determine due to the peak force errors caused by the displaced material mounds. Given the contact pressure is governed by the tip radius, for a Hertzian contact, determining the true tip radius would enable the researcher to quantify the change in pressure throughout the test. Several possible methods were considered to measure the change in tip radius; however, these could not be implemented due to time constraints. The simplest method to determine the final tip radius was to scan and measure the tip radius using an SEM, Figure 7-55. This could be coupled with EDS chemical analysis to determine whether any of the tribofilm has been adhered to the tip. The same method could be applied to various tips, each used to contact the surface for a different number of contact mode scans This would give an understanding of whether the tip geometry change is linear or whether the majority of the degradation occurs in the first scans.

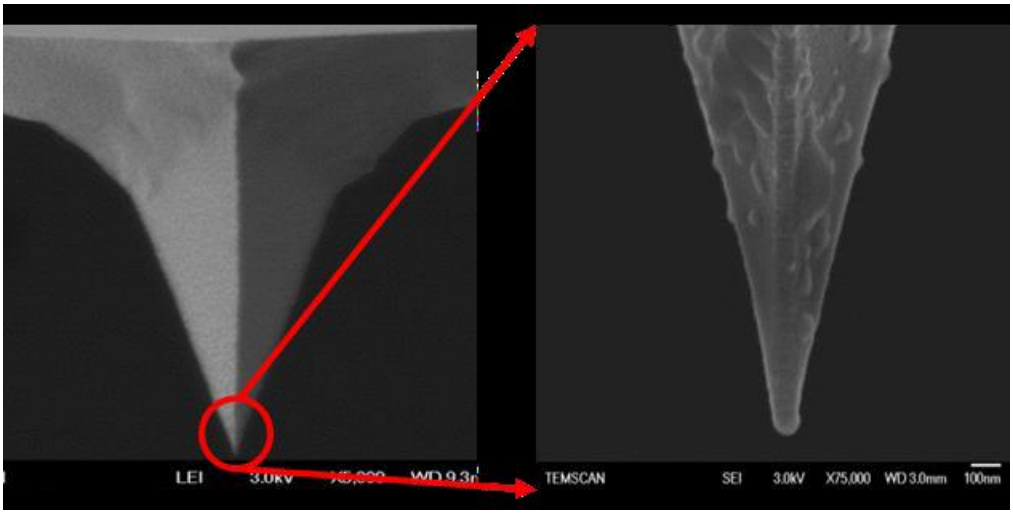

Figure 7-55: SEM of an AFM tip [116]***.***

Another concern is that it was not possible to use a second probe to measure the topography of the surface. Using a consistently sharp tip, in tapping mode, would enable the scan to more accurately detect small changes in the surface. This would be particularly useful to investigate the small pads which are revealed (or perhaps created) within the worn region as the test progresses. It was determined to be impossible due to the inherent difficulty in accurately returning the tip to same location within the tribofilm post change. In addition, the AFM requires calibration during each tip change, which precludes the use of multiple tips within a single test. However, since the testing for this research activity was concluded, research has been published by Gosvami et al [7] within which tests were conducted utilising multiple AFM cantilevers. This demonstrates that it is possible to use multiple probes within a single test; however, no details are provided to explain the calibration method. One method would be to use two separate AFM heads and control systems; however, commercially available AFMs are not equipped with the facility to use multiple control systems and so this was not the solution they used.

A less important concern relates to the surface being exposed to air over long periods of time (averaging five days) and the resultant settling of dust onto the tribofilm surface. This was mitigated by enclosing the AFM within a soundproof unit, which was left closed throughout the test duration. To further mitigate this risk the surface was carefully wiped

with a lint-free tissue immediately prior to insertion in the AFM. The AFM enclosure is kept closed between tests, with the door being opened for as short a duration as possible. However, the unit was not originally designed to mitigate against dust and thus several ingress routes are still possible. There is no clear evidence of contamination, such as visible debris, within any of the current scans but this is a potential risk for any future testing.

The aforementioned soundproof box was originally intended to mitigate against audible noise induced vibrations. The AFM is particularly sensitive to such vibrations, with some of the artefacts observed in the ZDDP characterisation scan likely being induced by this. Figure 7-56 gives an example of the effect of noise on a topography scan. The AFM used in this research is unfortunately located directly beneath a main hallway and thus is exposed to periods of extreme vibration. The soundproof box was designed to mitigate against this; however, this researcher also ensured that whenever possible the most sensitive scans (the topography scans) were scheduled to occur outside of these particularly extreme vibration periods. In addition, care was taken to reduce the vibration within the immediate vicinity of the AFM; this was done by restricting access to the AFM laboratory and clearly indicating the presence of a noise sensitive test. The risk posed by noise is present for all AFM tests and thus many of the mitigations used for this part of the study had also previously been employed for the ZDDP characterisation research. As well as audible noise the AFM is particularly susceptible to electrical noise and thus care was taken to ensure all aspects of the equipment were adequately grounded and sources of this noise were minimised, where possible.

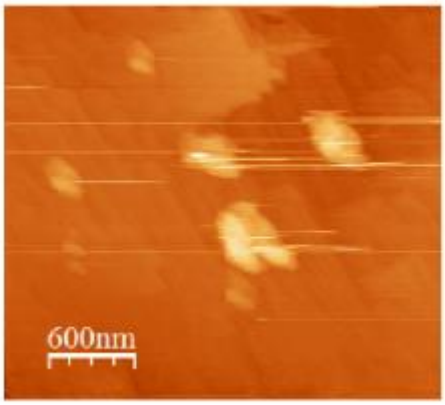

Figure 7-56: Noise induced AFM artefacts [117]**.**

The preliminary study was conducted at 0.267mN load; however, work by Gosvami et al [7] suggests that the maximum load that can be applied by an AFM without damaging the cantilever mount is only 20μN (0.02mN). The applied load is determined by the cantilever calibration, with the voltage required to attain a specific load being dependent on the specific cantilever. The maximum possible applied voltage, for the Dimension Icon, is 9V, which for the nominal spring constant used in the main study results in approximately a 0.02mN load. To ensure repeatability between different calibrations the final maximum load was set to be 0.014mN, with a potential increased load of 0.019mN held in reserve. The higher spring constant cantilever used in the preliminary study, whilst less cost effective, has been shown to provide a much higher load and thus merits consideration in any future tests using this method.

An additional concern is that the contact mode scans needed to be stopped after 250 scans, to ensure the tip was not too severely degraded. A more severely degraded tip could alter the deflection sensitivity of the cantilever, particularly as relates to the lateral stiffness, and thus change the calibration and alter the applied load. In particular, the presence of small pads, within the contact region, would be ideal for extended study. However, this would require a solution to the limitation on the number of scans. A solution for the limitation on the number of scans would be to change the tip material. In addition to altering the cantilever, to provide a larger spring constant, it is possible to mount different tip materials

to provide a harder tip surface, which would not be as easily damaged. One possible alternative tip material is diamond, with high spring constant cantilever options available. Changing the tip material would alter the Hertzian contact stress, ensuring that even when applying a lower load (if this was still necessary, due to the cantilever) the stress would be sufficient to indent and plough the tribofilm.

The limited number of tests conducted is a further limitation of this research. Due to the extended test durations and the high demand to use the AFM it was necessary to reduce the scale of the test campaign to consider three loads and two concentrations. The original test plan included all three previously tested concentrations (including the 1.1wt% ZDDP) at a minimum of five loads. The test duration could not be reduced by increasing the scan rate without also changing the cantilever or tip material as the increased rate would result in an increase in tip wear, with a resultant reduction in the scan resolution. If the cantilever material was changed, to enable an increased scan rate, the loading applied would likely increase as well, due to the different material properties which would further reduce the duration of the test campaign.

The conducted tests displayed limited repeatability, with the behaviour being very different between different locations. This is partially due to the worn region being located on different parts of tribofilm pads (the middle and the edge) and on regions of the tribofilm where there appears to be no pads. However, it is also caused by the inherent variability within a ZDDP tribofilm. The characterisation work displayed that whilst the topography is related to both position and concentration it is not uniform between similar tribofilms, and even displays differences within the same region of a single tribofilm. The variability caused by wearing the tribofilm on different parts of a pad could be offset by conducting the research across the entirety of a pad, either by using the more even tribofilm produced in a higher concentration (such as in the 1.1wt% tribofilms) or by using a tribofilm which has small pads, such as the tribofilms produced by Gosvami et al [3]. To ensure that a tribofilm had

sufficiently small pads it would be necessary to generate these within a single asperity contact, using an AFM tip as the counter surface, which would enable a comparison to be made regarding the effect of other parameters, such as temperature or the presence of pure base oil, on the durability of the tribofilm.

7.11 Durability Summary

In this section the method and results of the preliminary and main durability studies were presented. It was shown that there appears to be an increase in the amount of displaced material when the concentration of oil used to generate the initial tribofilm is increased. In addition, there appears to be a substantial difference in the amount of material displaced between the high load applied in the preliminary study and the much lower load used in the main study; however, there is no evidence of smaller variations in load causing such an effect.

A calculation had been conducted to ensure that the loads applied in the main study would be sufficient to indent the tribofilm; however, this was proven to be inaccurate as the bulk pad geometry was not noticeably affected. There was evidence of some material being deposited to either side of the worn region but this did not appear to be as a result of material being removed from the tribofilm pads. A hypothesis has been proposed to explain this. It is understood that a thick layer of alkyl phosphates is present above a ZDDP tribofilm, prior to cleaning with n-heptane, and that this is easily removed prior to post-test analysis. However, the results of this study indicate that a thin loosely adhered layer of material remains. Given the bulk morphology does not appear to be altered considerably it is believed that this loosely adhered layer consists of remnant alkyl phosphates.

Analysis of the contact mode scans showed the appearance of small pads within the worn region as the test progressed. A hypothesis was made to explain these small pads, namely that these are present within the tribofilm from the beginning of the test and that the removal of loosely adhered alkyl phosphate layers enable these to be observed.

Chapter 8: Conclusions, Impact and Future Works

This chapter shall present the conclusions of the research, across both phases of the activity, as well as the impact of these. In addition, some recommendations for related future research are presented as well as some possible outcomes of these.

8.1 Conclusions

The first main research phase of this activity showed that **there are noticeable differences in the morphology of tribofilms formed in oils of different concentrations** (using 0.275wt%, 0.55wt% and 1.1wt% ZDDP). It was found that having more additive in the base oil during tribofilm formation appears to result in smaller polyphosphate pads (typically around 5µm in diameter), with less pronounced space between them. Tribofilms formed in a lower ZDDP concentration oil had pads which were larger in length (up to 20µm) with pronounced spaces between them. The apparent differences in height were quantified using the surface R_a values and were found to not be significant.

The first phase also determined that **for lower concentrations the position along a reciprocating stroke can affect the pad morphology**. Parts of the tribofilm which form in a region with a lower lambda ratio ($\lambda \rightarrow 0$, as a result of a lower velocity) typically have smaller pads (<10µm) than other parts of the tribofilm that have formed in a region with a higher lambda ratio (maximum $\lambda = 0.0309$). In addition, it was found that the tribofilm morphology for a lower concentration in an area of low lambda ratio is similar to the morphology of a tribofilm formed in a higher concentration oil at a higher lambda ratio.

A hypothesis was presented to explain the differing tribofilm morphologies that have been observed. It is believed that in regions of lower lambda ratio the ZDDP molecules experience more shear and are broken into smaller polyphosphate chains. These smaller chains then adsorb to the surface, with the resultant pads appearing smaller than the pads formed in higher lambda ratio regions which have experienced less shear. When the

molecules are broken into smaller chains there are more adsorption sites, as a result of more chains being present, which results in an apparent increase in the number of pads and a more even distribution across the surface. This same effect has been observed in higher concentration tribofilms, where the number of adsorption sites are higher as a result of an increased number of initial molecules being decomposed.

Phase 2 showed that **when correctly utilised the AFM is capable of manipulating and displacing material from a ZDDP tribofilm**. It has also been shown that the current understanding of the mechanical properties of ZDDP tribofilms may be incorrect as the cantilever chosen for the main study was unable to penetrate the tribofilm surface, despite the calculations indicating this should have occurred.

Hypotheses have been presented to explain the material relocation shown in this activity. It is believed that for the main study the primary material displacement observed was the relocation of loosely adhered alkyl phosphates, as opposed to the more solidified polyphosphate layer. This is primarily due to the rate at which the displacement occurred and the displacement plateau that was observed. The first hypothesis consists of the detachment of the loosely adhered chain from within the worn region and the subsequent reattachment to a polyphosphate chain located outside of the worn region. The second hypothesis regards the directional flattening of the loosely adhered chains, with the attachment sites being maintained, and the unattached ends of the alkyl chain being moved to the edges of the worn region.

There is also some evidence that the worn region morphology is changing as a result of the contact, with small pads being exposed within the region. It is proposed that these are likely to have been present throughout the test but were obscured by the overlayer of alkyl phosphates which follow the bulk geometry of the polyphosphate pads. However, an

alternate hypothesis is that these are formed as a result of weaker polyphosphate chains being sheared and forming pads (as in the bulk pad formation presented in phase 1).

There is some evidence that the concentration of the oil used to generate a ZDDP tribofilm corresponds to the amount of material that can be displaced. This research activity was unable to confirm this effect; however, it has been shown that for a higher concentration the amount of loosely adhered alkyl phosphate, remnant on the surface after n-heptane cleaning, appears to be greater and that this can be easily manipulated within an AFM.

Whilst the main study could not quantitively determine whether the load applied by the AFM tip affects the tribofilm manipulation the difference between the loads applied in the main study and the preliminary study show that a determination of the effect of load across a wider load range is feasible. In addition, a repeatable method for quantifying the amount of material that has been displaced was developed. This was utilised to determine the amount of material relocated from the worn region in the preliminary study and has been found to be robust.

8.1.1 Novelty of the Work

This work builds on the existing work relating to the general understanding of ZDDP tribofilm topography but also on work, dating from 2015 onwards, that expand the uses of AFM as it relates to ZDDP tribofilms.

Specifically, this work investigates the fundamental relationship between lambda ratio (governed by both speed and concentration) and tribofilm morphology. Previous work has utilised topography analyses as a secondary consideration, with most articles including a single image to represent the entire tribofilm, with no consideration given to its position. This study has novelty by robustly characterising the tribofilm at the regions of highest and lowest lambda ratio, across a range of concentrations, determining that there is indeed a difference in topography.

This work also considers that if the AFM can be used to create tribofilms, as well as the more common topographic analyses, it may be possible to also use it to further characterise the tribofilms, specifically as it relates to their durability. This is novel as the initial work demonstrating the increased versatility of the AFM was only published in 2015, with emerging research avenues building on this, such as the durability analysis within this study.

8.1.2 Contributions to Knowledge

The primary outcomes of this research are:

- The topography of a ZDDP tribofilm varies along the position of a reciprocating stroke, and with concentration, meaning it is not sufficient to include a single “representative” topography image when using the AFM as a secondary analysis method.
- The pad morphology of ZDDP tribofilms can be directly related to the lambda ratio, as this relates to reciprocating speed, with regions of lower lambda ratio typically having smaller pads than regions of higher lambda ratio.
- The AFM cannot just be used to generate and image ZDDP tribofilms but can also manipulate and deform them, enabling an assessment of tribofilm durability.

8.2 Impact to Industry

This research benefits the automotive industry by challenging a fundamental concept in the research of ZDDP additives. Until now it has been believed that reciprocating tribometer testing is representative of component level contacts between a piston ring and the cylinder lining. However, whilst the motion profile is the same it has been shown that the lambda ratio profile affects the morphology of the tribofilm which is formed, with lower lambda ratios producing a more even coverage of ZDDP pads. This is important as the velocities tested at tribometer level may not be representative of the true velocities at component level, resulting in different lambda ratios between the two. The automotive industry is particularly concerned about this as the attempts to identify a non-phosphorus-based additive to replace ZDDP will focus on tribological testing at the tribometer level. This research reinforces the need for multi-scale tribological testing, as well as highlighting the need for a more detailed and systematic investigation into the differences between tribometer level and component level ZDDP tribofilms.

The research also benefits the oil additive manufacturing industry by highlighting an underappreciated method of analysis. This research shows that the AFM can be used to compare the tribofilms formed with different concentrations of ZDDP and that the AFM can be used to understand the tribofilm on a more fundamental level. This is important for the oil additive manufacturing community as it enables novel analysis techniques to be used to investigate tribofilms on an asperity scale; as well as potentially enabling the in-situ analysis of tribofilms by both generating and then analysing tribofilms within an AFM. In this research the AFM has been shown to be capable of comparing the durability of tribofilms. However, this research also revealed that the AFM has previously been used to consider micro-rheology, in biological media. Future studies which employed this unusual technique would further increase the understanding of the potentially fluidic nature of tribofilms.

The research benefits the research community focussing on ZDDP tribofilms, which is extensive both within universities and automotive oil suppliers, by highlighting a potential flaw in the current understanding of these films. It has been assumed previously that the morphology of ZDDP tribofilms was solely governed by the chemical constituents of the oil; however, this research has shown that it is also governed by the tribological conditions (lambda ratio) within which the additive is degraded. As the morphology of the tribofilm directly relates to its load carrying ability the implications of assuming a uniform morphology may be considerable.

In addition, this research suggests that the assumption that ex-situ analysis is sufficient may be incorrect. Previous work by Bec et al [75] claimed that the alkyl phosphate layer within a contact was well established, but was easily removed using n-heptane and thus was not usually present in post-tribometer analyses. This research has indicated that the n-heptane is not entirely successful at removing the entire alkyl phosphate layer, with a small amount remaining. It is unknown at this time whether the limited quantity of alkyl phosphate considered in ex-situ analysis is truly representative of the bulk in-situ tribofilm. If ex-situ analysis is not representative of the true contact, as has been suggested at the University of Leeds, then the fundamental assumptions about ZDDP tribofilms that have been used for research to date may be incorrect. A more accurate understanding of the tribofilm is needed in order to determine a suitable replacement additive.

8.3 Future Works

8.3.1 Relating to Phase 1

The current work has been limited by the range of maximum lambda ratios that have been considered. This was required to include representative test conditions and concentrations. Future work would benefit from expanding the range of test conditions such that the maximum lambda ratios are more varied. This can be achieved by testing a single concentration but varying the load or frequency to impose a greater variation on lambda ratio. Having demonstrated that there is an effect of reciprocating position as it relates to lambda ratio, the current work could be validated by increasing the maximum lambda ratio so that the variation across the stroke length is more pronounced, with the intention that this will result in further variations in topography, validating the current activity.

It is advised that in the future further testing is undertaken to characterise tribofilm morphology in at least one additional location (such that there exists information for the end, middle and " ¾ " positions). This will provide a greater understanding of the extent to which the position along the reciprocating stroke affects the pad topography. The current research activity has shown that such an effect can be compared to the topography differences between concentrations, therefore, it is advised that additional scans be conducted across all three tested concentrations.

Having determined that the position across the reciprocating stroke length can affect the tribofilm concentration it can be assumed that other factors can affect this as well. One factor of interest is the position across the stroke width. Differing locations across the contact area of the pin will experience different contact pressures as well as different lubricant thicknesses. If there is a difference in morphology with the lambda ratio then it may be assumed that a similar relationship will be present across the width of the wear scar as

well. This research would further develop the understanding of ZDDP tribofilms and aid in the identification of a potential replacement additive.

8.3.2 Relating to Phase 2

The current work could be validated by conducting future experiments repeating the current comparisons on the effect of concentration and cantilever load using the more robust cantilever employed in the preliminary study (TAP 525). The current results were unable to quantify the apparent relationship between concentration and tribofilm durability, with the topography scans suggesting a relationship but this being so negligible as to be missed by the analysis program. The TAP 525 cantilever was able to manipulate the tribofilm such that the analysis program was able to clearly quantify the material removed from the worn region and the material displaced to the sides, this was done without penetrating through to the underlying substrate, meaning that a comparison between tribofilms would be possible.

The cantilever used in the preliminary durability study was able to displace more material than the main study, therefore, it has been shown that the cantilever can have an important effect on the tribofilm manipulation. Future work could consider a wider variation in the applied load, by using different spring constant cantilevers, with the same tip material and geometry, to apply loads of different magnitudes. The contact pressure could also be varied by using cantilevers with the same spring constant and different tip materials or radii. Larger variations in the contact pressure will provide a more complete understanding of the effect of shear stress on the tribofilm durability, with the ultimate aim of correlating this to the micro-rheology.

In addition, it is recommended that the activity be repeated with characterised AFM tips, such that the true tip radius is determined for each as well as the chemical composition at the beginning of the test. This will enable researchers to determine whether material is

transferred to the tip, and how the transfer of material may influence the Hertzian contact stress within the contact. A determination of a difference in transferred material could also be attained for the differing concentrations and locations considered in phase 1. It has been shown that there may be a small increase in the amount of remnant alkyl phosphate with an increase in ZDDP concentration, this may result in an increased transfer of material during the initial contact scans. Transferred material would alter the Hertzian contact stress as well as potentially lubricating the contact. If tribofilm transfer occurs this technique could be used to simulate a starved contact on an asperity level.

8.3.3 General

As previous work has shown that the AFM can be used to generate tribofilms in-situ [7,33], and that the topography of these can be different depending on the position along the stroke [3], it is suggested that the durability of these micro-scale tribofilms may be able to provide information about the macro-scale tribofilm. Specifically, a full characterisation and durability analysis of the full tribofilm would be possible in these tribofilms, whereas similar analyses of traditional tribofilms must be conducted in discrete sections. In addition, these tribofilms can be analysed in-situ, permitting a more complete assessment of the functional tribofilm durability. The in-situ technique can also be used to determine an effect of temperature, by returning the tribofilm to typical operational temperatures, allowing a more representative condition for further durability tests; this would further expand the general understanding of ZDDP tribofilms and could facilitate the identification of a replacement additive.

This work has observed differences in the morphology and durability of tribofilms formed in a reciprocating tribometer. Having observed the differences in morphology caused by the speed profile across a reciprocating stroke it can be extrapolated that there may exist similar differences across the width of a unidirectional stroke, as a result of small differences

in angular velocity. Future research should consider the morphology of tribofilms formed in the MTM SLIM as this can permit in-situ imaging of the pad morphology and be used to compare in-situ tribofilm topography with the ex-situ morphology and durability. An improved understanding of the morphology of ZDDP within a unidirectional contact will enable a replacement additive to be qualified for use in both a piston (reciprocating) and a cam-shaft (unidirectional).

Chapter 9: References

[1] Walsh MP. The future of Vehicle Emissions Regulation in the EU and Internationally. 2013. https://doi.org/10.1039/b711747g.

[2] Martin W, Ray M. A technical summary of Euro 6/VI vehicle emission standards. Int Counc Clean Transp 2016:1–17.

[3] Gosvami NN, Bares JA, Mangolini F, Konicek AR, Yablon DG, Carpick RW. Mechanisms of antiwear tribofilm growth revealed in situ by single-asperity sliding contacts. Science (80-) 2015;348:102–6.

[4] Neville A, Morina A. Wear and Chemistry of Lubricants. Wiley; 2005.

[5] Spikes H. The history and mechanisms of ZDDP. Tribol Lett 2004;17:469–89. https://doi.org/10.1023/B:TRIL.0000044495.26882.b5.

[6] Ghanbarzadeh A, Parsaeian P, Morina A, Wilson MCT, Van Eijk MCP, Nedelcu I, et al. A Semi-deterministic Wear Model Considering the Effect of Zinc Dialkyl Dithiophosphate Tribofilm. Tribol Lett 2016;61. https://doi.org/10.1007/s11249-015-0629-8.

[7] Gosvami NN, Ma J, Carpick RW. An In Situ Method for Simultaneous Friction Measurements and Imaging of Interfacial Tribochemical Film Growth in Lubricated Contacts. Tribol Lett 2018;66:1–10. https://doi.org/10.1007/s11249-018-1112-0.

[8] Graham JF, Mccague C, Norton PR. Topography and nanomechanical properties of tribochemical films derived from zinc dialkyl and diaryl dithiophosphates. Tribol Lett 1999;6:149–57. https://doi.org/10.1023/A:1019124026402.

[9] Ueda M, Kadiric A, Spikes H. On the Crystallinity and Durability of ZDDP Tribofilm. Tribol Lett 2019;67:1–13. https://doi.org/10.1007/s11249-019-1236-x.

[10] North Altlantic Treaty Organisation Scientific Affairs Division. Micro/Nanotribology

and Its Applications. Springer Science & Business Media; 1997.

[11] Jost P, Duncan D, Colleagues at the Department of Education. Lubrication (tribology) : education and research : a report on the present position and industry's needs / [by the Lubrication and Engineers (Education and research) Working Group, 1965, H.Peter Jost, Chairman]. London HMStationary Off 1966.

[12] UK Tribology: What is Tribology? UK Tribol 2015. http://www.uktribology.net/tribology-benefits (accessed January 22, 2016).

[13] Dašić P, Franek F, Assenova E, Radovanović M. International standardization and organizations in the field of tribology. Ind Lubr Tribol 2003;55:287–91. https://doi.org/10.1108/00368790310496437.

[14] Bruce RW. CRC Handbook of Lubrication: Theory and Practice of Tribology, Volume II: Theory and Design. CRC Press; 2010.

[15] Priest M. Introduction to Tribology. Work Unit 2. Friction and Wear of Surfaces. 2014.

[16] Introduction to Tribology. Soc Tribol Lubr Eng n.d. http://www.stle.org/files/What_is_tribology/Tribology_Friction.aspx (accessed January 25, 2016).

[17] Bowden FP, Moore AJW, Tabor D. The ploughing and adhesion of sliding metals. J Appl Phys 1943;14:80–91. https://doi.org/10.1063/1.1714954.

[18] Dowson D. History of Tribology. 2nd ed. UK: Wiley; 1998.

[19] European Space Tribology Laboratory. Space Tribology Handbook. ESR Technology; 2015.

[20] Hutchings IM. Tribology Friction and Wear of Engineering Materials. 5th ed. London: Arnold, Hodder Headline Group; 1999.

[21] Bhushan B. Tribology in practice series: Introduction to tribology (2). 2nd ed. Wiley;

2013.

[22] Kandeva M, Vencl A. Advanced Tribological Coatings for Heavy-Duty Applications : Case Studies. Prof. Marin Drinov Publishing House of Bulgarian Academy of Sciences; 2016.

[23] Gohar R, Rahnejat H. Fundamentals of Tribology. 2nd ed. London: Imperial College Press; 2012.

[24] Ghosh MK, Majumdar BC, Sarangi M. Theory of Lubrication. McGraw hill Education (India) Private limited; 2012.

[25] Hamrock BJ, Dowson D. Elastohydrodynamic Lubrication of Elliptical Contacts for Materials of Low Elastic Modulus I—Fully Flooded Conjunction. J Lubr Technol 1978;100:236. https://doi.org/10.1115/1.3453152.

[26] Hamrock BJ, Dowson D. Minimum Film Thickness in Elliptical Contacts for Different Regimes of Fluid-Film Lubrication. NASA Tech Pap 1342 1978.

[27] Priest M. Introduction to Tribology. Work Unit 3. Lubrication. 2014.

[28] Hoopen JGTEN. Piston Ring tribology: a Literature Survey. Julkaisija-Utgivare; 2002.

[29] Total. How do additives work? n.d. https://www.total.co.uk/how-do-oil-additives-work (accessed June 8, 2020).

[30] ELF. What are oil additives? n.d. https://www.elf.com/en/lubricants-faq/about-lubricants/what-are-oil-additives (accessed June 8, 2020).

[31] Osei-Agyemang E, Berkebile S, Martini A. Decomposition Mechanisms of Anti-wear Lubricant Additive Tricresyl Phosphate on Iron Surfaces using DFT and Atomistic Thermodynamic Studies. Tribol Lett 2018;66. https://doi.org/https://doi.org/10.1007/s11249-018-0998-x.

[32] Lu R, Kobayashi K, Nanao H, Mori S. Deactivation effect of Tricresyl Phosphate (TCP)

on tribochemical decomposition of hydrocarbon oil on a nascent steel surface. Tribol Lett 2009;33:1–8. https://doi.org/10.1007/s11249-008-9379-1.

[33] Dorgham A, Parsaeian P, Azam A, Wang C, Morina A, Neville A. Single-asperity study of the reaction kinetics of P-based triboreactive films. Tribol Int 2019;133:288–96. https://doi.org/10.1016/j.triboint.2018.11.029.

[34] Jones RB, Coy RC. The chemistry of the thermal degradation of zinc dialkyldithiophosphate additives. ASLO Trans 1981;24:91–7.

[35] Willermet PA, Dailey DP, Carter III DP, Schmitz PJ, Zhu W. Mechanism of formation of antiwear films from zinc dialkyldithiophosphates. Tribol Int 1995;28:177–87.

[36] Martin JM, Minfray C. Antiwear Chemistry in Presence of ZDDP. World Tribol. Congr. III, Vol. 1, ASME; 2005, p. 599–600. https://doi.org/10.1115/WTC2005-63960.

[37] Fujita H, Spikes HA. The formation of zinc dithiophosphate antiwear films. Proc Inst Mech Eng Part J J Eng Tribol 2004;218:265–78. https://doi.org/10.1243/1350650041762677.

[38] Morina A, Neville A. Tribofilms: aspects of formation, stability and removal. J Phys D Appl Phys 2007;40:5476–87. https://doi.org/10.1088/0022-3727/40/18/S08.

[39] Bec S, Tonck A, Georges J-M, Georges E, Loubet J-L. Improvements in the indentation method with a surface force apparatus. Philos Mag A 1996;74:1061–72. https://doi.org/10.1080/01418619608239707.

[40] Taylor L, Spikes H, Camenzind H. Film-Forming Properties of Zinc-Based and Ashless Antiwear Additives. 2000. https://doi.org/10.4271/2000-01-2030.

[41] Sheasby JS, Caughlin TA, Blahey AG, Laycock KF. A reciprocating wear test for evaluating boundary lubrication. Tribol Int 1990;23:301–7. https://doi.org/10.1016/0301-679X(90)90003-8.

[42] Cann P, Cameron A. Studies of thick boundary lubrication — influence of zddp and oxidized hexadecane. Tribol Int 1984;17:205–8. https://doi.org/10.1016/0301-679X(84)90024-0.

[43] Priest M. Introduction to Tribology. Work Unit 1. Introduction to Tribology. 2014.

[44] Plint C. Te77 High Frequency Friction Machine. n.d.

[45] Institute of Functional Surfaces - Pin-on-disk n.d. https://institutes.engineering.leeds.ac.uk/functional-surfaces/facilities/tribology/pin_on_disk.shtml (accessed June 30, 2016).

[46] Thorp JM. A novel tri-pin-on-disc tribometer designed to retain lubricants. Tribol Int 1981;14:121–5. https://doi.org/10.1016/0301-679X(81)90012-8.

[47] INSTRUMENTS PC. MTM 2 Mini-Traction Machine. 2013.

[48] Greaves M, Topolovec-Miklozic K. Film forming behavior of oil soluble polyalkylene glycols. Ind Lubr Tribol 2015;67:133–8. https://doi.org/10.1108/ILT-01-2013-0014.

[49] Sedlaček M, Podgornik B, Vižintin J. Correlation between standard roughness parameters skewness and kurtosis and tribological behaviour of contact surfaces. Tribol Int 2012;48:102–12. https://doi.org/10.1016/j.triboint.2011.11.008.

[50] INSTRUMENTS PC. HFRR (High Frequency Reciprocating Rig). 2013.

[51] Plint C. TE 99 UNIVERSAL WEAR MACHINE. 2000.

[52] Landauer AK, Barnhill WC, Qu J. Correlating mechanical properties and anti-wear performance of tribofilms formed by ionic liquids, ZDDP and their combinations. Wear 2016;354–355:78–82. https://doi.org/10.1016/j.wear.2016.03.003.

[53] Patel M, Aswath PB. Role of thermal, mechanical and oxidising treatment on structure and chemistry of carbon black and its impact on wear and friction: Part 2 – Boundary lubrication condition. Tribol - Mater Surfaces Interfaces 2015;9:19–32.

https://doi.org/10.1179/1751584X14Y.0000000087.

[54] Qu J, Barnhill WC, Luo H, Meyer HM, Leonard DN, Landauer AK, et al. Synergistic Effects between Phosphonium-Alkylphosphate Ionic Liquids and Zinc Dialkyldithiophosphate (ZDDP) as Lubricant Additives. Adv Mater 2015;27:4767–74. https://doi.org/10.1002/adma.201502037.

[55] Barnhill WC, Gao H, Kheireddin B, Papke BL, Luo H, West BH, et al. Tribological Bench and Engine Dynamometer Tests of a Low Viscosity SAE 0W-16 Engine Oil Using a Combination of Ionic Liquid and ZDDP as Anti-Wear Additives. Front Mech Eng 2015;1:1–8. https://doi.org/10.3389/fmech.2015.00012.

[56] Wright RAE, Wang K, Qu J, Zhao B. Oil-Soluble Polymer Brush-Grafted Nanoparticles as Effective Lubricant Additives for Friction and Wear Reduction. Angew Chemie Int Ed 2016:1–6. https://doi.org/10.1002/anie.201603663.

[57] Yang L, Neville A, Brown A, Ransom P, Morina A. Effect of lubricant additives on the WDLC coating structure when tested in boundary lubrication regime. Tribol Lett 2015;57:1–12. https://doi.org/10.1007/s11249-015-0464-y.

[58] ISO/TC 213. ISO 25178-2 Geometrical product specifications (GPS) - Surface Texture: Areal - Part 2: Terms, definitions and surface texture parameters 2012.

[59] Kaemmer SB. Application Note # 133 Introduction to Bruker's ScanAsyst and PeakForce Tapping AFM Technology 2011:1–12.

[60] Keyence Corporation. Area Roughness Parameters 2019. https://www.keyence.com/ss/products/microscope/roughness/surface/parameters.jsp (accessed November 26, 2019).

[61] Bingley R, Buttery M, Romera F. The Effect of Surface Production Techniques on the Tribological Behaviour of Fluid Lubricants. Proc 8th ESMATS 2019.

[62] Mcdonald MJ. Friction modifier for drilling fluids. EP20090793417, 2011.

[63] Mortier RM, Fox M, Orszulik ST. Chemistry and Technology of Lubricants (Google eBook) 2011:574.

[64] Rudnik LR. Zinc Dithiophosphates. Lubr. Addit. Chem. Appl., CRC Press; 2003, p. 29–45.

[65] Dawczyk J, Morgan N, Russo J, Spikes H. Film Thickness and Friction of ZDDP Tribofilms. Tribol Lett 2019;67:1–15. https://doi.org/10.1007/s11249-019-1148-9.

[66] Spedding H, Watkins RC. The antiwear mechanism of ZDDP's Part I. Tribol Int 1982;15:9–12.

[67] Piras FM, Rossi A, Spencer ND. Combined in situ (ATR FT-IR) and ex situ (XPS) study of the ZnDTP-iron surface interaction. Tribol Lett 2003;15:181–92. https://doi.org/10.1023/A:1024800900716.

[68] Naveira-Suarez A, Tomala A, Pasaribu R, Larsson R, Gebeshuber IC. Evolution of ZDDP-derived reaction layer morphology with rubbing time. Scanning 2010;32:294–303. https://doi.org/10.1002/sca.20207.

[69] Fujita H, Spikes HA. Study of Zinc Dialkyldithiophosphate Antiwear Film Formation and Removal Processes, Part II: Kinetic Model. Tribol Trans 2005;48:567–75. https://doi.org/10.1080/05698190500385187.

[70] Oblak E, Kalin M. Relationship between the Nanoscale Topographical and Mechanical Properties of Tribochemical Films on DLC Coatings and Their Macroscopic Friction Behavior. Tribol Lett 2015;59:1–16. https://doi.org/10.1007/s11249-015-0575-5.

[71] Ye J, Kano M, Yasuda Y. Evaluation of local mechanical properties in depth in MoDTC / ZDDP and ZDDP tribochemical reacted films using nanoindentation 2002;13:41–7.

[72] Nicholls MA, Do T, Norton PR, Kasrai M, Bancroft GM. Review of the lubrication of

metallic surfaces by zinc dialkyl-dithiophosphates. Tribol Int 2005;38:15–39. https://doi.org/10.1016/j.triboint.2004.05.009.

[73] Warren OL, Graham JF, Norton PR. Nanomechanical properties of films derived from zinc dialkyldithiophosphate. Tribol Lett 1998;4:189–98. https://doi.org/10.1023/A:1019194903262.

[74] Jelita Rydel J, Vegter RH, Rivera-Díaz-Del-Castillo PEJ. Tribochemistry of bearing steels: A new AFM method to study the material-tribofilm correlation. Tribol Int 2016;98:74–81. https://doi.org/10.1016/j.triboint.2016.01.055.

[75] Bec S, Tonck A, Georges JM, Coy RC, Bell JC, Roper GW. Relationship between mechanical properties and structures of zinc dithiophosphate anti-wear films. Proc R Soc A Math Phys Eng Sci 1999;455:4181–203. https://doi.org/10.1098/rspa.1999.0497.

[76] Narita K, Priest M. Friction characteristics and topography of tribofilms from anti-wear additives applied to metal V-Belt type CVT fluids. Tribol Lett 2009;35:45–56. https://doi.org/10.1007/s11249-009-9432-8.

[77] Technical Committee of Petroleum Additive Manufacturers in Europe. Lubricant Additives and the Environment. Atc 2007;49.

[78] Wiquist RC, Twiss SB, H. LE. Distribution of an EP film on wear surfaces. ASLE Trans 1960;3:40–7.

[79] Costa HL, Spikes HA. Impact of ethanol on the formation of antiwear tribofilms from engine lubricants. Tribol Int 2016;93:364–76. https://doi.org/10.1016/j.triboint.2015.09.021.

[80] Austin L, Liskiewicz T, Kolev I, Zhao H, Neville A. The influence of anti-wear additive ZDDP on doped and undoped diamond-like carbon coatings. Surf Interface Anal

2015;47:755–63. https://doi.org/10.1002/sia.5763.

[81] Sharma V, Erdemir A, Aswath PB. An analytical study of tribofilms generated by the interaction of ashless antiwear additives with ZDDP using XANES and nano-indentation. Tribol Int 2015;82:43–57. https://doi.org/10.1016/j.triboint.2014.09.019.

[82] Vengudusamy B, Green JH, Lamb GD, Spikes HA. Influence of hydrogen and tungsten concentration on the tribological properties of DLC/DLC contacts with ZDDP. Wear 2013;298–299:109–19. https://doi.org/10.1016/j.wear.2013.01.020.

[83] Zhang J, Yamaguchi E, Spikes H. The Antagonism between Succinimide Dispersants and a Secondary Zinc Dialkyl Dithiophosphate. Tribol Trans 2014;57:57–65. https://doi.org/10.1080/10402004.2013.845275.

[84] Ratoi M, Niste VB, Zekonyte J. WS2 nanoparticles – potential replacement for ZDDP and friction modifier additives. RSC Adv 2014;4:21238. https://doi.org/10.1039/c4ra01795a.

[85] Parsaeian P, Ghanbarzadeh A, Wilson M, Van Eijk MCP, Nedelcu I, Dowson D, et al. An experimental and analytical study of the effect of water and its tribochemistry on the tribocorrosive wear of boundary lubricated systems with ZDDP-containing oil. Wear 2016;358–359:23–31. https://doi.org/10.1016/j.wear.2016.03.017.

[86] Williamson WB, Gandhi HS, Heyde ME, Zawacki GA. Deactivation of Three-Way Catalysts by Fuel Contaminants - Lead, Phosphorus and Sulfur. 1979 SAE Int. Fall Fuels Lubr. Meet. Exhib., 1979. https://doi.org/10.4271/790942.

[87] Kärkkäinen M, Kolli T, Honkanen M, Heikkinen O, Huuhtanen M, Kallinen K, et al. The Effect of Phosphorus Exposure on Diesel Oxidation Catalysts—Part I: Activity Measurements, Elementary and Surface Analyses. Top Catal 2015:961–70.

https://doi.org/10.1007/s11244-015-0464-z.

[88] Rokosz MJ, Chen AE, Lowe-Ma CK, Kucherov A V., Benson D, Paputa Peck MC, et al. Characterization of phosphorus-poisoned automotive exhaust catalysts. Appl Catal B Environ 2001;33:205–15. https://doi.org/10.1016/S0926-3373(01)00165-5.

[89] Sanskriti K. Strategic Technologies of Complex Environmental Issues-A Sustainable Approach. 1st ed. New Dehli: Excellent Publishing House; 2014.

[90] AA. Euro Emissions Standards 2013. https://www.theaa.com/motoring_advice/fuels-and-environment/euro-emissions-standards.html (accessed June 23, 2016).

[91] Kalyani K, Jaiswal V, Rastogi RB, Kumar D. Tribological investigations on β-lactam cephalosporin antibiotics as efficient ashless antiwear additives with low SAPS and their theoretical studies. RSC Adv 2014;4:30500. https://doi.org/10.1039/C4RA03596H.

[92] Szlufarska I, Chandross M, Carpick RW. Recent advances in single-asperity nanotribology. J Phys D Appl Phys 2008;41:123001. https://doi.org/10.1088/0022-3727/41/12/123001.

[93] Binnig G, Quate CF. Atomic Force Microscope. Phys Rev Lett 1986;56:931.

[94] Matey JR, Blanc J. Scanning capacitance microscopy. J Appl Phys 1985;57:1437–44. https://doi.org/10.1063/1.334506.

[95] Giessibl FJ. Advances in atomic force microscopy. Rev Mod Phys 2003;75:949–83. https://doi.org/10.1103/RevModPhys.75.949.

[96] Ohnesorge F, Binnig G. True Atomic Resolution by Atomic Force Microscopy Through Repulsive and Attractive Forces Published by : American Association for the Advancement of Science True Atomic Resolution by Atomic Force Microscopy Through Repulsive and Attractive Forces. Science (80-) 1993;260:1451–6.

[97] Carpick RW, Salmeron M. Scratching the Surface: Fundamental Investigations of Tribology with Atomic Force Microscopy. Chem Rev 1997;97:1163–94. https://doi.org/10.1021/cr960068q.

[98] Kennedy E, Al-Majmaie R, Al-Rubeai M, Zerulla D, Rice JH. Quantifying nanoscale biochemical heterogeneity in human epithelial cancer cells using combined AFM and PTIR absorption nanoimaging. J Biophotonics 2015;8:133–41. https://doi.org/10.1002/jbio.201300138.

[99] Guz NV, Dokukin ME, Woodworth CD, Cardin A, Sokolov I. Towards early detection of cervical cancer: Fractal dimension of AFM images of human cervical epithelial cells at different stages of progression to cancer. Nanomedicine Nanotechnology, Biol Med 2015;11:1667–75. https://doi.org/10.1016/j.nano.2015.04.012.

[100] Guz NV, Dokukin ME, Woodworth CD, Cardin A, Sokolov I. Supplementary Information for Towards early detection of cervical cancer: Fractal dimension of AFM images of human cervical epithelial cells at different stages of progression to cancer. Nanomedicine Nanotechnology, Biol Med 2015;11:1667–75. https://doi.org/10.1016/j.nano.2015.04.012.

[101] Boitor R, Sinjab F, Strohbuecker S, Sottile V, Notingher I. Towards quantitative molecular mapping of cells by Raman microscopy: using AFM for decoupling molecular concentration and cell topography. Faraday Discuss 2016;187:199–212. https://doi.org/10.1039/C5FD00172B.

[102] Topolovec-Miklozic K, Forbus TR, Spikes HA. Film thickness and roughness of ZDDP antiwear films. Tribol Lett 2007;26:161–71. https://doi.org/10.1007/s11249-006-9189-2.

[103] Cannara RJ, Eglin M, Carpick RW. Lateral force calibration in atomic force microscopy : A new lateral force calibration method and general guidelines for optimization

calibration method and general guidelines for optimization 2007;77. https://doi.org/10.1063/1.2198768.

[104] Tran Khac BC, Chung KH. Quantitative assessment of contact and non-contact lateral force calibration methods for atomic force microscopy. Ultramicroscopy 2016;161:41–50. https://doi.org/10.1016/j.ultramic.2015.10.028.

[105] Li Q, Kim KS, Rydberg A. Lateral force calibration of an atomic force microscope with a diamagnetic levitation spring system. Rev Sci Instrum 2006;77. https://doi.org/10.1063/1.2209953.

[106] Varenberg M, Etsion I, Halperin G. An improved wedge calibration method for lateral force in atomic force microscopy. Rev Sci Instrum 2003;74:3362–7. https://doi.org/10.1063/1.1584082.

[107] Burkinshaw M, Neville A, Morina A, Sutton M. ZDDP and its interactions with an organic antiwear additive on both aluminium-silicon and model silicon surfaces. Tribol Int 2014;69:102–9. https://doi.org/10.1016/j.triboint.2013.09.001.

[108] Abdullah Tasdemir H, Tokoroyama T, Kousaka H, Umehara N, Mabuchi Y. Influence of zinc dialkyldithiophosphate tribofilm formation on the tribological performance of self-mated diamond-like carbon contacts under boundary lubrication. Thin Solid Films 2014;562:389–97. https://doi.org/10.1016/j.tsf.2014.05.004.

[109] Ozkan D, Kaleli H. Surface and Wear Analysis of Zinc Phosphate Coated Engine Oil Ring and Cylinder Liner Tested with Commercial Lubricant. Adv Mech Eng 2015;6:150968–150968. https://doi.org/10.1155/2014/150968.

[110] Burkinshaw M, Neville A, Morina A, Sutton M. Calcium sulphonate and its interactions with ZDDP on both aluminium-silicon and model silicon surfaces. Tribol Int 2012;46:41–51. https://doi.org/10.1016/j.triboint.2011.06.014.

[111] Topolovec-Miklozic K, Forbus TR, Spikes H. Film Forming and Friction Properties of Overbased Calcium Sulphonate Detergents. Tribol Lett 2008;29:33–44. https://doi.org/10.1007/s11249-007-9279-9.

[112] Dorgham A. Reaction kinetics and rheological characteristics of ultra-thin P-based triboreactive films. Unviersity of Leeds, 2017.

[113] Dorgham A, Wang C, Morina A, Neville A. 3D tribo-nanoprinting using triboreactive materials. Nanotechnology 2019;30. https://doi.org/10.1088/1361-6528/aaf70c.

[114] Hamrock BJ, Schmid SR, Jacobson BO. Fundamentals of Fluid Film Lubrication. 2nd ed. CRC Press; 2004.

[115] Hamrock BJ, Dowson D. Isothermal Elastohydrodynamic Lubrication of Point Contacts: Part III—Fully Flooded Results. J Lubr Technol 1977;99:264–75. https://doi.org/10.1115/1.3453074.

[116] Boularas A, Baudoin F, Teyssedre G, Clain S. 3D modelling of electrostatic force distance curve between the AFM probe and dielectric surface 2014:27–9.

[117] Jeuken LJC. AFM study on the electric-field effects on supported bilayer lipid membranes. Biophys J 2008;94:4711–7. https://doi.org/10.1529/biophysj.107.122887.

Appendix 1 – Comprehensive results for the Characterisation of ZDDP Tribofilms

Initial Topography

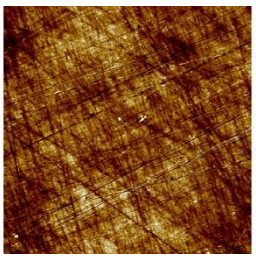

Initial Topography

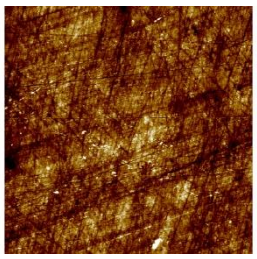

Initial Topography

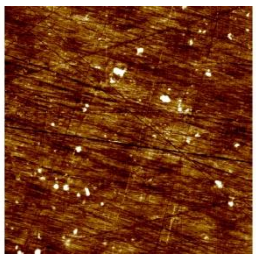

Initial Topography

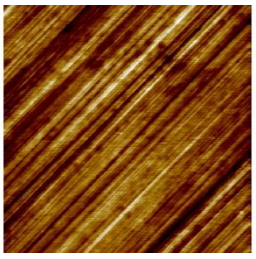

Initial Topography

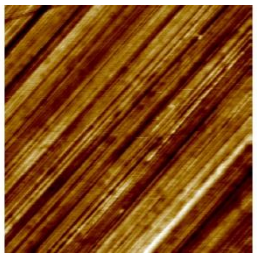

Initial Topography

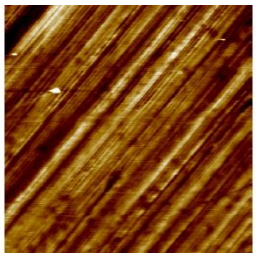

0.275wt% End – Tribofilm Topography

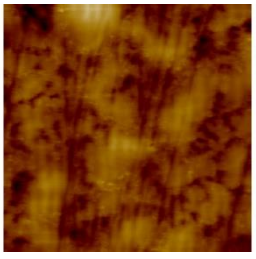

0.275wt% End – Tribofilm Topography

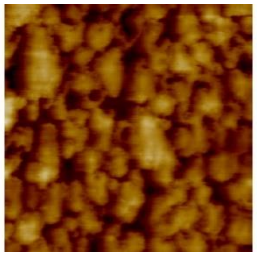

0.275wt% End - Tribofilm Topography

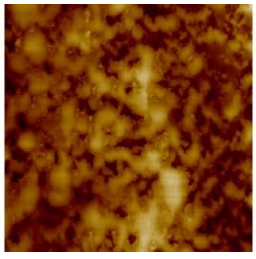

0.275wt% End – Tribofilm Topography

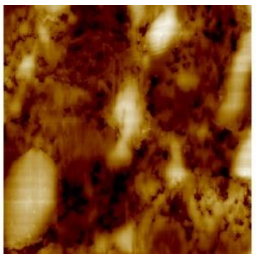

0.275wt% Middle – Tribofilm Topography

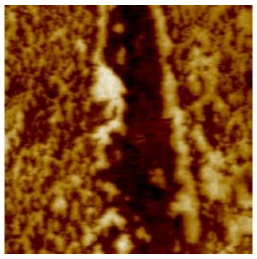

0.275wt% Middle – Tribofilm Topography

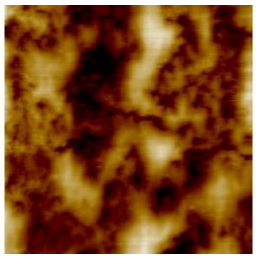

0.275wt% Middle – Tribofilm Topography

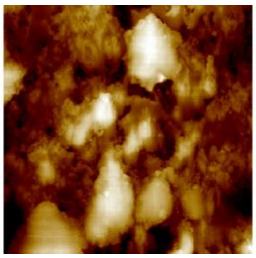

0.55wt% End – Tribofilm Topography

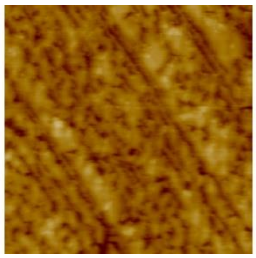

0.55wt% End – Tribofilm Topography

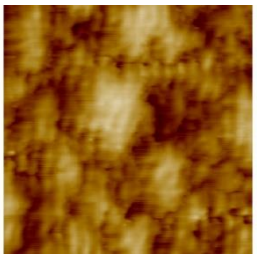

0.55wt% End – Tribofilm Topography

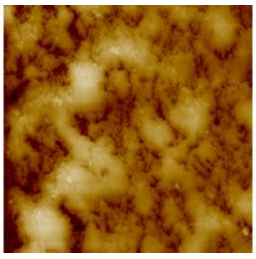

0.55wt% Middle – Tribofilm Topography

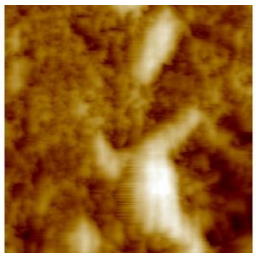

0.55wt% Middle – Tribofilm Topography

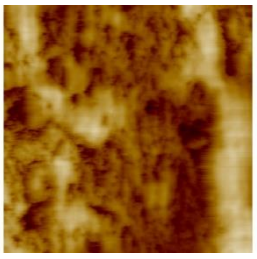

0.55wt% Middle – Tribofilm Topography

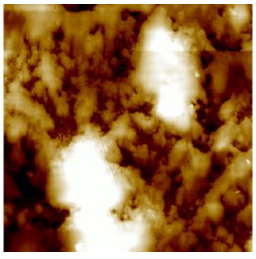

0.55wt% Middle – Tribofilm Topography

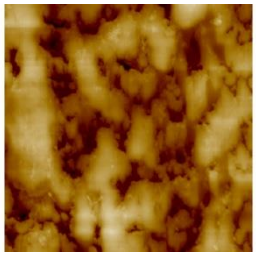

1.1wt% End – Tribofilm Topography

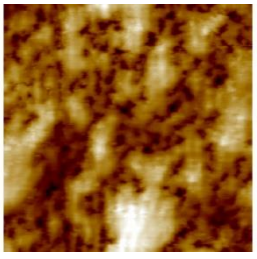

1.1wt% End – Tribofilm Topography

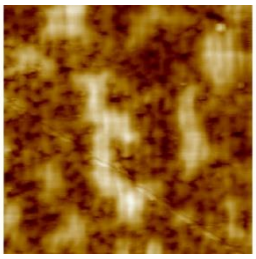

1.1wt% End – Tribofilm Topography

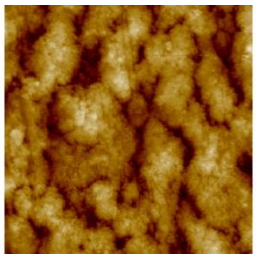

1.1wt% End – Tribofilm Topography

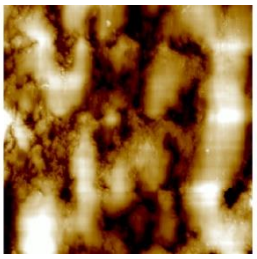

1.1wt% Middle – Tribofilm Topography

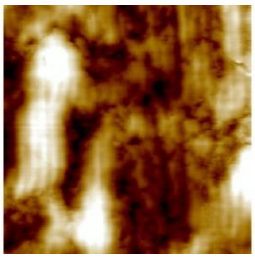

1.1wt% Middle – Tribofilm Topography

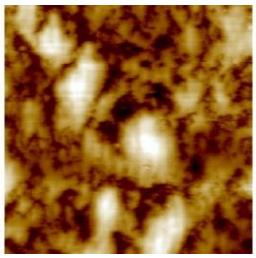

1.1wt% Middle – Tribofilm Topography

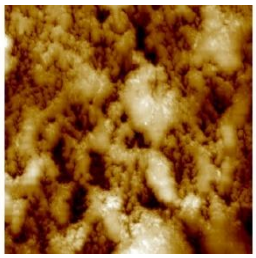

1.1wt% Middle – Tribofilm Topography

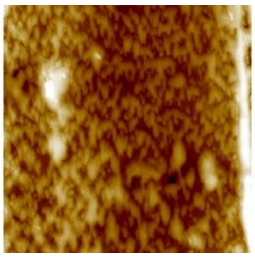

0.275wt% End – Wear Scar Topography

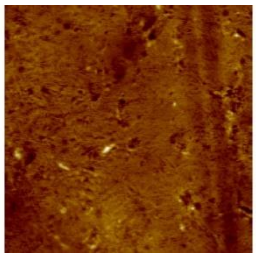

0.275wt% End – Wear Scar Topography

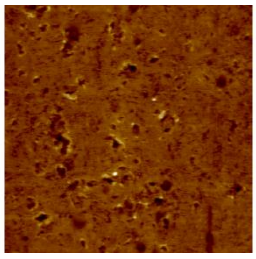

0.275wt% End – Wear Scar Topography

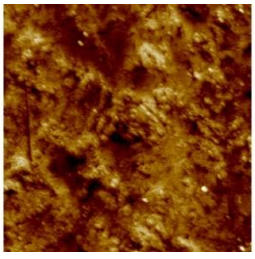

0.275wt% End – Wear Scar Topography

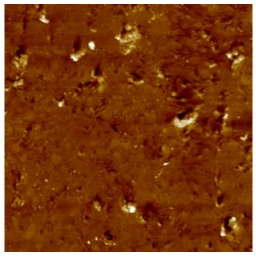

0.275wt% Middle – Wear Scar Topography

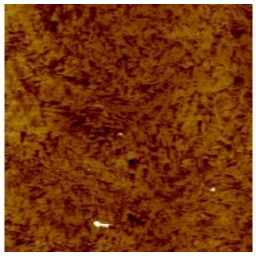

0.275wt% Middle – Wear Scar Topography

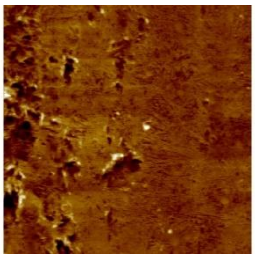

0.275wt% Middle – Wear Scar Topography

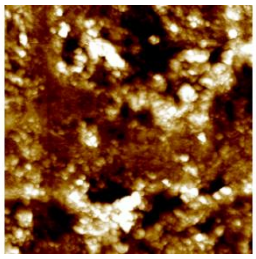

0.275wt% Middle – Wear Scar Topography

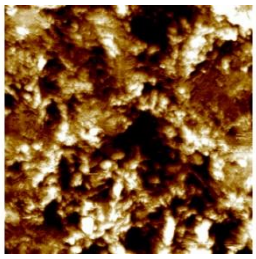

0.55wt% End – Wear Scar Topography

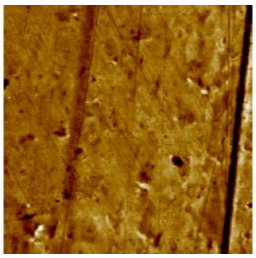

0.55wt% End – Wear Scar Topography

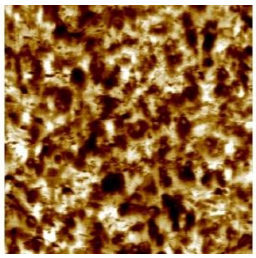

0.55wt% End – Wear Scar Topography

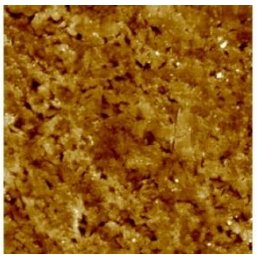

0.55wt% End – Wear Scar Topography

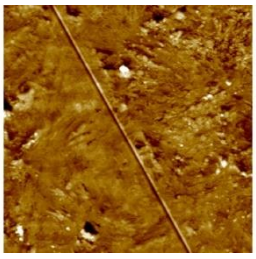

0.55wt% Middle – Wear Scar Topography

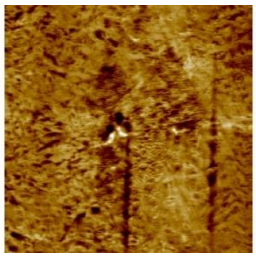

0.55wt% Middle – Wear Scar Topography

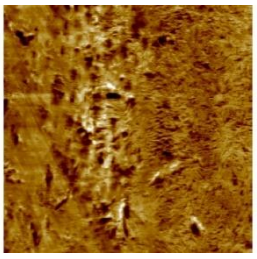

0.55wt% Middle – Wear Scar Topography

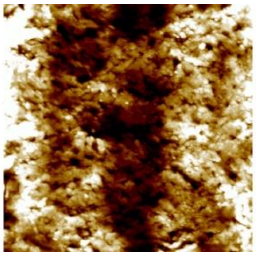

0.55wt% Middle – Wear Scar Topography

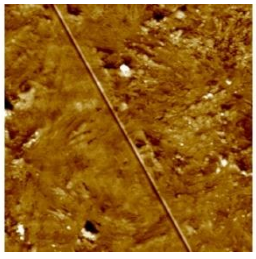

1.1wt% End – Wear Scar Topography

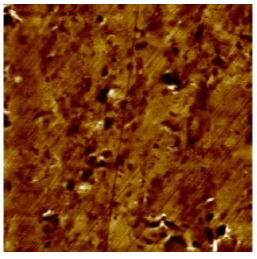

1.1wt% End – Wear Scar Topography

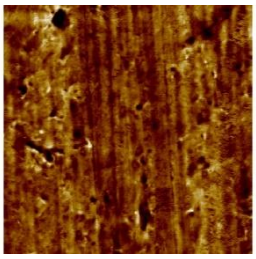

1.1wt% End – Wear Scar Topography

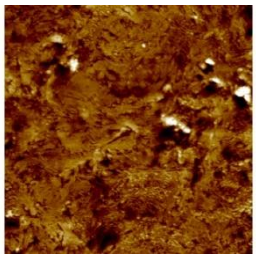

1.1wt% End – Wear Scar Topography

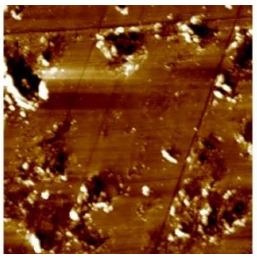

1.1wt% Middle – Wear Scar Topography

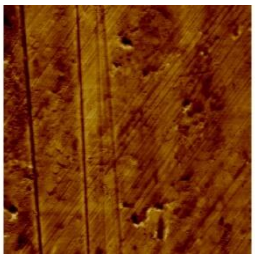

1.1wt% Middle – Wear Scar Topography

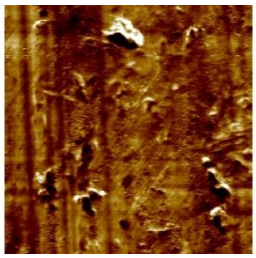

1.1wt% Middle – Wear Scar Topography

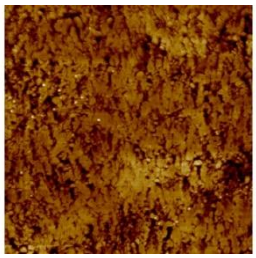

1.1wt% Middle – Wear Scar Topography

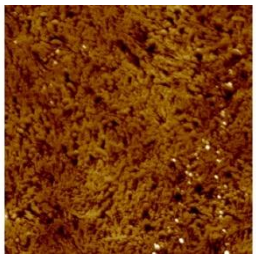

Appendix 2 – Durability Study Analysis Program

```
1; %Line with no output to prevent the first line from beginning
with "function"

%Reads in data from AFM text files
function [surfacePlots, numbersOfWearScans] =
loadSurfacePlots(folderName,height,width)

  fileList = dir(folderName); %Get list of files from named folder
  fileNameList = cell(1,0); %Creates an empty list to store
filenames
  numbersOfWearScans = []; %Creates empty array to store the number
of contact scans occuring before each topography scan

  %Find scan files and record the number of scans
  for i = 1:length(fileList)
      fileName = fileList(i).name; %Grabs name from file properties

      %If the file isn't a scan then skip it
      scanFilePrefix = 'Topography after ';
      scanFileSuffix = '.txt';
      prefixLength = length(scanFilePrefix);
      suffixLength = length(scanFileSuffix);
      if length(fileName) < prefixLength + suffixLength %Checks
length of filename is long enough
        continue
      end
      if not(strcmp(fileName(1:prefixLength),scanFilePrefix))
%Checks filename starts correctly
        continue
      end
      if not(strcmp(fileName(end-(suffixLength-
1):end),scanFileSuffix)) %Checks filename ends correctly
        continue
      end

      %Find number of contact scans
      firstDigit = prefixLength + 1;
      lastDigit = prefixLength + 1;
      while isdigit(fileName(lastDigit + 1)) %Increase lastDigit
until the end of the number is found
        lastDigit = lastDigit + 1;
      end

      numbersOfWearScans = [numbersOfWearScans,
str2num(fileName(firstDigit:lastDigit))];
      fileNameList = [fileNameList, fileName];
  end

  %Puts filenames in order of number of contact scans
  [numbersOfWearScans, I] = sort(numbersOfWearScans);
  fileNameList = fileNameList(I);

  numberOfSurfaces = length(fileNameList); %Number of topography
scans in dataset

  surfacePlots = zeros(height,width,numberOfSurfaces);

  %Reads text files into array
```

```
  for i = 1:numberOfSurfaces
     fprintf('Current plot: %d\n',i);

     fileName = [folderName, "/", fileNameList{i}];

     file = fopen(fileName,'r');

     columnHeading = fgetl(file); %First line isn't data, so ignore
it
     for y = 1:height
       for x = 1:width
         surfacePlots(y,x,i) = str2num(fgetl(file)); %Get next line
and put it in array
       end
     end

     fclose(file);

  end

  surfacePlots = flip(surfacePlots); %Corrects fact that plots are
upside down

end

%Displays surface plots as successive images to show topography
progression
function
animateSurfacePlots(surfacePlots,numbersOfWearScans,duration,varargi
n)

  %If there are extra arguments then they give the position and size
of the worn region
  if nargin > 3
    y = varargin{1};
    x = varargin{2};
    regionHeight = varargin{3};
    regionWidth  = varargin{4};
  end

  maxSurface = max(max(max(surfacePlots)));
  minSurface = min(min(min(surfacePlots)));
  height = size(surfacePlots,1);
  width = size(surfacePlots,2);
  numberOfSurfaces = size(surfacePlots,3);

  for k = 1:numberOfSurfaces
    imagesc(surfacePlots(:,:,k),[minSurface maxSurface]);
    hold on
    axis square
    %If the position and size of the worn region are defined then
mark the worn region and split the image
    if nargin > 3

rectangle('Position',[x,y,regionWidth,regionHeight],'EdgeColor','gre
en')
      line([x+regionWidth/2, x+regionWidth/2], [0, y], 'color',
'green')
      line([x+regionWidth/2, x+regionWidth/2], [y+regionHeight,
height], 'color', 'green')
    end
```

```
    if k < numberOfSurfaces
        pause((duration)*(numbersOfWearScans(k+1)-
numbersOfWearScans(k)));
    end
  end

  hold off

end

%Applies a first-order plane fit based on the top and bottom of each
image
function coefficients = planeFit(surfacePlot)

  height = size(surfacePlot,1);
  width = size(surfacePlot,2);
  numberOfDataPoints = height*width;

  coordinates = zeros(numberOfDataPoints,3);
  zValues = zeros(numberOfDataPoints,1);

  %This populates the matrices with data representing the top of the
scan
  dataPointNumber = 1;
  for i = 1:height
    for j = 1:width
      coordinates(dataPointNumber,:) = [i j 1];
      zValues(dataPointNumber)= surfacePlot(i,j);
      dataPointNumber = dataPointNumber + 1;
    end
  end

  %(z values column vector) = (Coordinatees matrix)*(Coefficients
column vector)
  coefficients = pinv(coordinates)*zValues;
end


function tiltedPlots = tiltedPlots(surfacePlots, coefficients)

  height = size(surfacePlots,1);
  width = size(surfacePlots,2);
  numberOfSurfaces = size(surfacePlots,3);

  % z = ay + bx + c
  a = coefficients(1);
  b = coefficients(2);
  c = coefficients(3);

  %Plane of best fit
  plane = zeros(height, width);
  for i = 1:height
    for j = 1:width
      plane(i,j) = a*i + b*j + c;
    end
  end

  %Corrects surface plots to match best fit plane
  tiltedPlots = zeros(size(surfacePlots));
  for k = 1:numberOfSurfaces
    tiltedPlots(:,:,k) = surfacePlots(:,:,k) - plane;
```

```
  end

end

%Determines offset at which given matrices best align
function [zOffset, yOffset xOffset] =
findBestOffset(matrix1,matrix2)

  [height width] = size(matrix1);

  maximumOffset = 50;

  bestDifference = Inf;

  %For any potential offset the average difference between the
surfaces is found for the region where they overlap
  for i = -maximumOffset:maximumOffset
    for j = -maximumOffset:maximumOffset
      matrix1Overlap =
matrix1(max(1,i+1):min(height,height+i),max(1,j+1):min(width,width+j
));
      matrix2Overlap = matrix2(max(1,-i+1):min(height,height-
i),max(1,-j+1):min(width,width-j));
      numberOfOverlapPixels = prod(size(matrix1Overlap));
      matrixDifference = matrix2Overlap-matrix1Overlap;
      averageDifference = median(matrixDifference(:));
      variance = sum(sum(abs(matrixDifference.-
averageDifference)))/numberOfOverlapPixels;
      %If the difference is the lowest so far then record the offset
      if variance < bestDifference
        bestDifference = variance;
        zOffset = averageDifference;
        yOffset = i;
        xOffset = j;
      end
    end
  end

end

%Adjust surface scans based on best offset between consecutive scans
function [offsetPlots, offsets] = offsetPlots(surfacePlots)

  height           = size(surfacePlots,1);
  width            = size(surfacePlots,2);
  numberOfSurfaces = size(surfacePlots,3);

  offsets = zeros([numberOfSurfaces 3]);
  offsetPlots = zeros(size(numberOfSurfaces));

  %Determine if there is an offset, and if so what it is
  for k = 1:numberOfSurfaces
    fprintf('Current plot: %d\n',k);
    if k == 1 %No offset for scan 1 since it is the reference
      zOffset = 0;
      yOffset = 0;
      xOffset = 0;
    else %Calculate offset relative to reference
      [zOffsetDiff, yOffsetDiff, xOffsetDiff] =
findBestOffset(surfacePlots(:,:,k-1), surfacePlots(:,:,k));
      zOffset = zOffset + zOffsetDiff;
```

```
      yOffset = yOffset + yOffsetDiff;
      xOffset = xOffset + xOffsetDiff;
    end
    offsets(k,1) = xOffset;
    offsets(k,2) = yOffset;
    offsets(k,3) = zOffset;
    overlapMatrix = surfacePlots(max(1,-
yOffset+1):min(height,height-yOffset),max(1,-
xOffset+1):min(width,width-xOffset),k)  .- zOffset; %Region of
current scan which overlaps first scan
    %Saves current scan to corrected location, and updates all later
scans so that any regions outside overlap will have the most recent
data available
    for l = k:numberOfSurfaces

offsetPlots(max(1,yOffset+1):min(height,height+yOffset),max(1,xOffse
t+1):min(width,width+xOffset),l) = overlapMatrix;
    end
  end

end

%Locates the wear scan region
function [y, x] = findWornRegion(offsets, numbersOfWearScans,
height, width, regionHeight, regionWidth)

  numberOfSurfaces = length(numbersOfWearScans);

  totalXOffset = 0;
  totalYOffset = 0;

  for k = 1:numberOfSurfaces-1
    xOffset = (offsets(k,1)+offsets(k+1,1))/2;
    yOffset = (offsets(k,2)+offsets(k+1,2))/2;
    numberOfWearScans = numbersOfWearScans(k+1)-
numbersOfWearScans(k);
    totalXOffset = totalXOffset + xOffset*numberOfWearScans;
    totalYOffset = totalYOffset + yOffset*numberOfWearScans;
  end

  totalNumberOfWearScans = numbersOfWearScans(numberOfSurfaces);
  averageYOffset = totalYOffset/totalNumberOfWearScans;
  averageXOffset = totalXOffset/totalNumberOfWearScans;

  y = round(averageYOffset+(height-regionHeight)/2);
  x = round(averageXOffset+(width-regionWidth)/2);

end

function volumeChanges =
volumeChanges(surfacePlots,y,x,regionHeight,regionWidth,scanHeight,s
canWidth)

  height = size(surfacePlots,1);
  width  = size(surfacePlots,2);
  numberOfSurfaces  = size(surfacePlots,3);

  volumeChanges = zeros(numberOfSurfaces,3);

  for k = 1:numberOfSurfaces
    differencePlot = surfacePlots(:,:,k) - surfacePlots(:,:,1);
```

```
    halfX = x + floor(regionWidth/2);

    leftSurfaceVolume = sum(sum(differencePlot(1:height,1:halfX)));
    rightSurfaceVolume =
sum(sum(differencePlot(1:height,(halfX+1):width)));
    leftWornRegionVolume = sum(sum(differencePlot(y:y+regionHeight-
1,x:halfX)));
    rightWornRegionVolume = sum(sum(differencePlot(y:y+regionHeight-
1,(halfX+1):x+regionWidth-1)));

    volumeChanges(k,1) = leftSurfaceVolume - leftWornRegionVolume;
    volumeChanges(k,2) = leftWornRegionVolume +
rightWornRegionVolume;
    volumeChanges(k,3) = rightSurfaceVolume - rightWornRegionVolume;
  end

  volumeChanges = volumeChanges * (scanHeight/height) *
(scanWidth/width);
end


colormapimage = double(imread('AFM SCALE.PNG'));
colormapimage = colormapimage(end:-1:1,:,:);
colormap(permute(colormapimage,[1 3 2])/255);

folderName = input('Which folder are the txt files in? ','s'); %txt
files should be in a folder in the same folder as this program
fprintf('\n');
outputFileName = [folderName, '/output']; %input('Which name should
be used for outputs? ','s');

height = 512; %input('How many lines per scan? ');
width = 512; %input('How many points per line? ');
scanHeight = 15000; %input("What is the height of the scan area? (In
nm) ");
scanWidth = 15000; %input("What is the width of the scan area? (In
nm) ");
wornHeight = 5000; %input("What is the height of the worn area? (In
nm) ");
wornWidth = 5000; %input("What is the width of the worn area? (In
nm) ");

%Size of worn region in pixels
regionHeight = floor(height * wornHeight/scanHeight);
regionWidth = floor(width * wornWidth/scanWidth);

fprintf('Loading Surface Plots\n');
[surfacePlots, numbersOfWearScans] =
loadSurfacePlots(folderName,height,width);
numberOfSurfaces = size(surfacePlots,3);
fprintf('Number of plots: %d\n\n',numberOfSurfaces);
duration = 0.2;

% if input('Do you wish to see the animation? (Y/n) ','s') == 'Y'
%   duration = input('Specify delay in animation: ');
%   animateSurfacePlots(surfacePlots,numbersOfWearScans,duration);
%   while input('Repeat animation? (Y/n) ','s') == 'Y'
%     duration = input('Specify delay in animation: ');
%     animateSurfacePlots(surfacePlots,numbersOfWearScans,duration);
%   end
% end
```

```
fprintf('Fitting Plane\n');
coefficients = planeFit(surfacePlots(:,:,1));
tiltedPlots = tiltedPlots(surfacePlots, coefficients);

fprintf('\n');
fprintf('Correcting for offset\n');
[offsetPlots, offsets] = offsetPlots(tiltedPlots);

 fprintf('\n');
% if input('Do you wish to see the corrected animation? (Y/n) ','s')
== 'Y'
%   duration = input('Specify delay in animation: ');
%   animateSurfacePlots(offsetPlots,numbersOfWearScans,duration);
%   while input('Repeat animation? (Y/n) ','s') == 'Y'
%     duration = input('Specify delay in animation: ');
%     animateSurfacePlots(offsetPlots,numbersOfWearScans,duration);
%   end
% end

colormapimage = double(imread('AFM SCALE.PNG'));
colormapimage = colormapimage(end:-1:1,:,:);
colormap(permute(colormapimage,[1 3 2])/255);
saveAnimation(offsetPlots,numbersOfWearScans,duration,folderName,'Of
fsetAnimationNew');

fprintf('\n');
% if input('Do you wish to measure worn region? (Y/n) ','s') == 'Y'
fprintf('\n');
fprintf('Finding worn region\n');
[y, x] = findWornRegion(offsets, numbersOfWearScans, height, width,
regionHeight, regionWidth);
volumeChanges =
volumeChanges(offsetPlots,y,x,regionHeight,regionWidth,scanHeight,sc
anWidth);
csvwrite([outputFileName
'RegionsChangeNew.csv'],cat(2,numbersOfWearScans(:),volumeChanges));
csvwrite([outputFileName 'OffsetsNew.csv'],offsets);
fprintf('Columns are: number of contact mode scans, left bump height
increase, worn region height increase and right bump height
increase')

fprintf('\n');
%if input('Do you wish to see the animation with worn region marked?
(Y/n) ','s') == 'Y'
% duration = input('Specify delay in animation: ');
% animateSurfacePlots(offsetPlots,numbersOfWearScans,duration,y,
x,regionHeight,regionWidth);
% while input('Repeat animation? (Y/n) ','s') == 'Y'
%   duration = input('Specify delay in animation: ');
%   animateSurfacePlots(offsetPlots,numbersOfWearScans,duration,y,
x,regionHeight,regionWidth);
% end
%end

colormapimage = double(imread('AFM SCALE.PNG'));
colormapimage = colormapimage(end:-1:1,:,:);
colormap(permute(colormapimage,[1 3 2])/255);
saveAnimation(offsetPlots,numbersOfWearScans,duration,folderName,'Ma
rkedAnimationNew',y, x,regionHeight,regionWidth);
```

```
differencePlots = zeros(size(offsetPlots));
for k = 1:numberOfSurfaces
  differencePlots(:,:,k) = offsetPlots(:,:,k) - offsetPlots(:,:,1);
end

fprintf('\n');
%if input('Do you wish to see the difference animation with worn
region marked? (Y/n) ','s') == 'Y'
% duration = input('Specify delay in animation: ');
% animateSurfacePlots(differencePlots,numbersOfWearScans,duration,y,
x,regionHeight,regionWidth);
% while input('Repeat animation? (Y/n) ','s') == 'Y'
%   duration = input('Specify delay in animation: ');
%
animateSurfacePlots(differencePlots,numbersOfWearScans,duration,y,
x,regionHeight,regionWidth);
% end
%end

colormapimage = double(imread('AFM SCALE.PNG'));
colormapimage = colormapimage(end:-1:1,:,:);
colormap(permute(colormapimage,[1 3 2])/255);
saveAnimation(differencePlots,numbersOfWearScans,duration,folderName
,'DifferenceAnimationNew',y, x,regionHeight,regionWidth);

fprintf('\n');
fprintf('End\n');
fprintf('\n');
```

Appendix 3 – Durability Study Topography Scans

0.275wt% ZDDP Tribofilm – 0.005mN – Between pads

After 0 Wear Scans

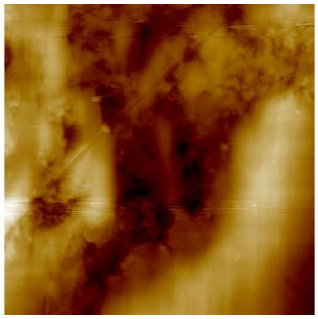

After 5 Wear Scans

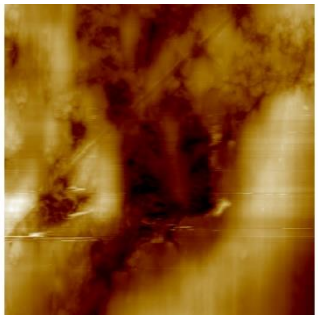

After 10 Wear Scans

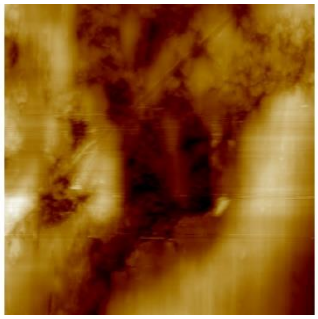

After 15 Wear Scans

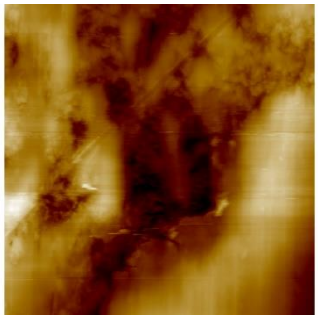

After 20 Wear Scans

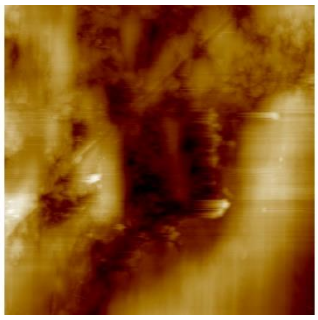

After 25 Wear Scans

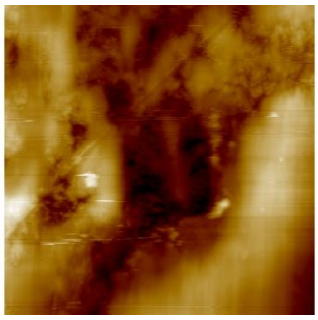

After 30 Wear Scans

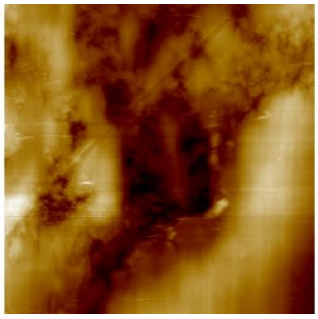

After 35 Wear Scans

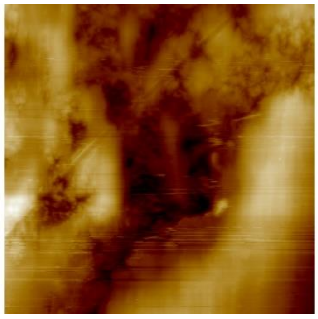

After 40 Wear Scans

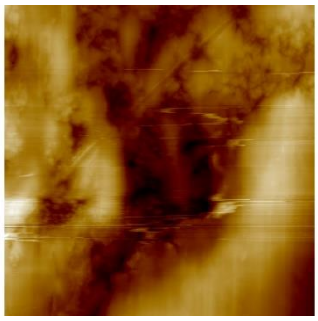

After 45 Wear Scans

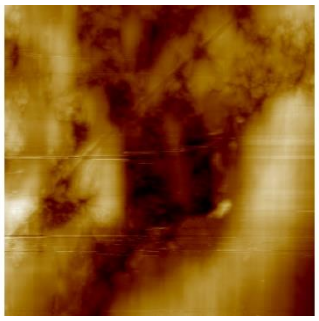

After 50 Wear Scans

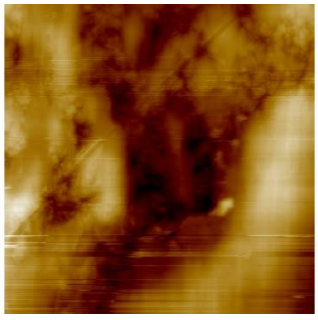

After 55 Wear Scans

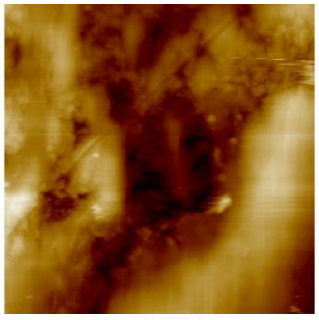

After 65 Wear Scans

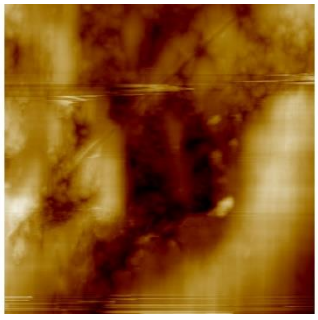

After 75 Wear Scans

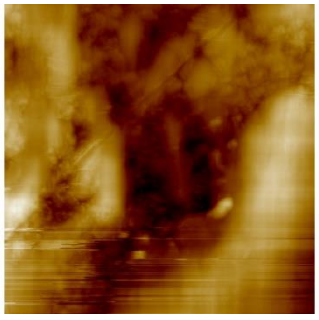

After 85 Wear Scans

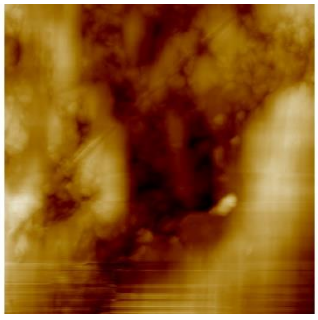

After 95 Wear Scans

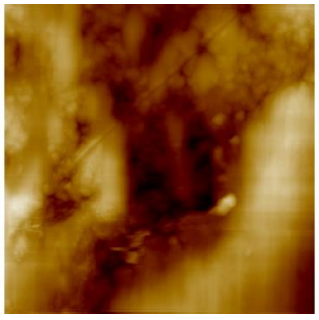

After 105 Wear Scans

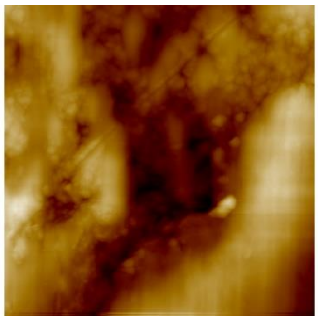

After 115 Wear Scans

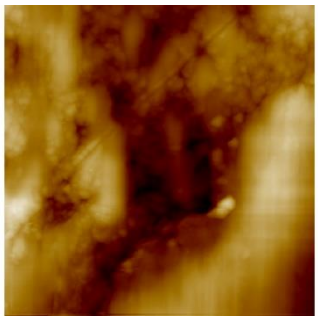

After 126 Wear Scans

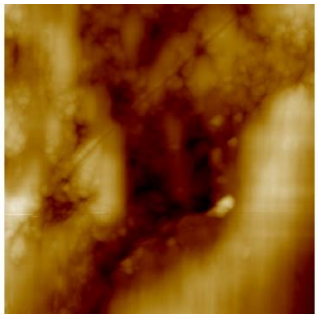

After 135 Wear Scans

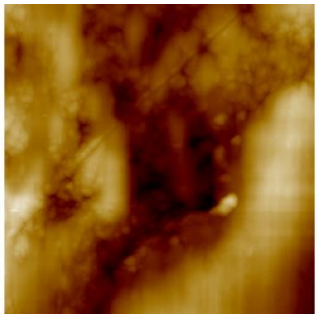

After 145 Wear Scans

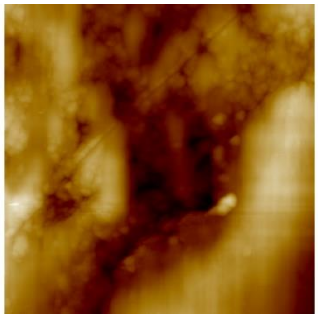

After 155 Wear Scans

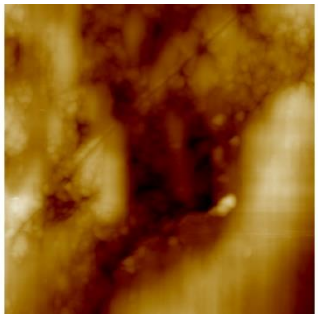

After 165 Wear Scans

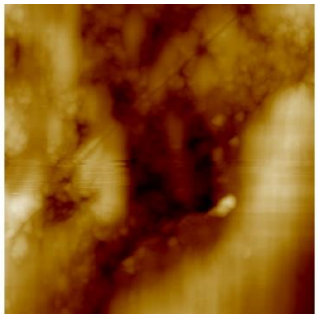

After 175 Wear Scans

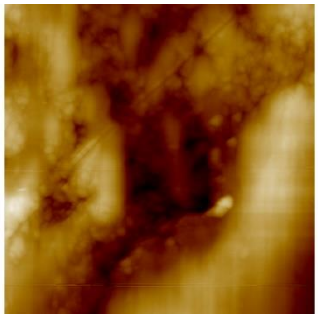

After 185 Wear Scans

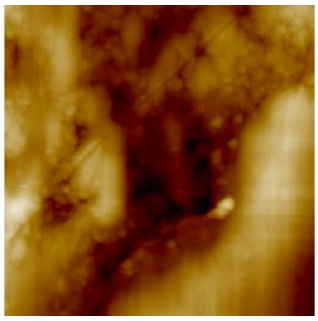

After 195 Wear Scans

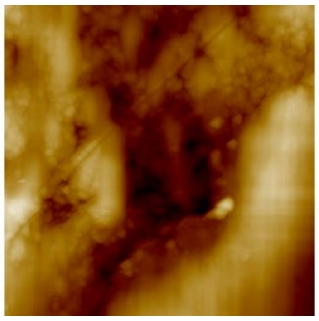

After 205 Wear Scans

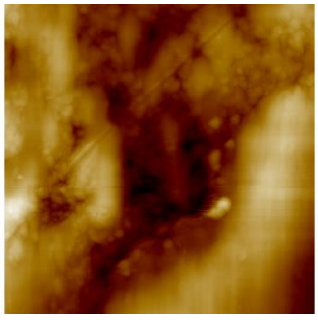

After 215 Wear Scans

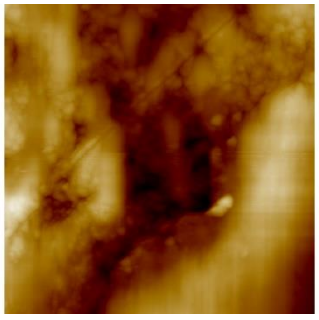

After 225 Wear Scans

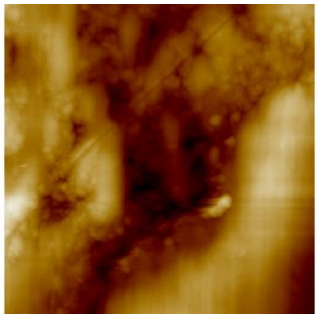

After 235 Wear Scans

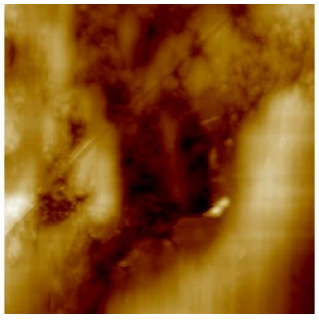

After 245 Wear Scans

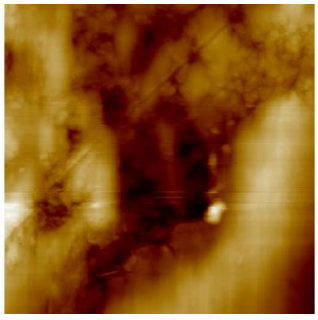

After 255 Wear Scans

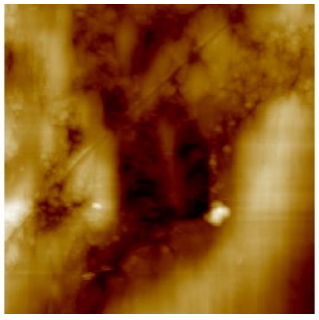

0.275wt% ZDDP Tribofilm – 0.005mN – On the edge of a pad

After 0 Wear Scans

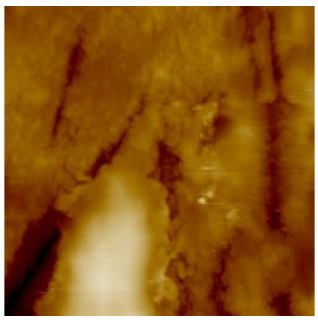

After 5 Wear Scans

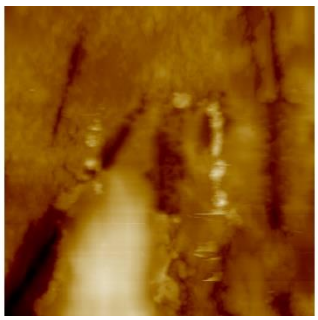

After 10 Wear Scans

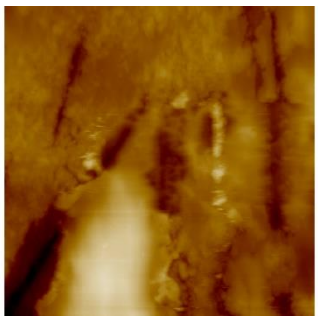

After 15 Wear Scans

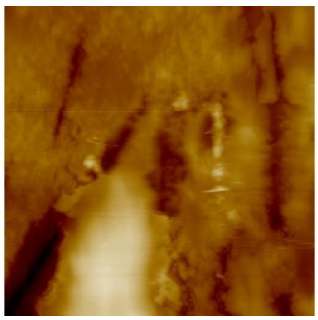

After 20 Wear Scans

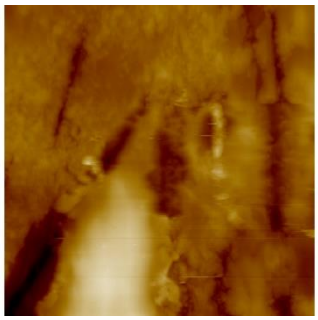

After 25 Wear Scans

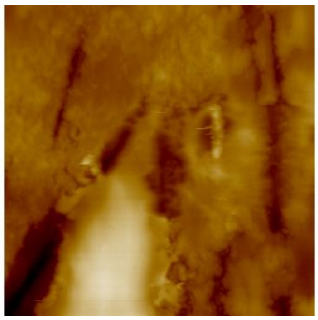

After 30 Wear Scans

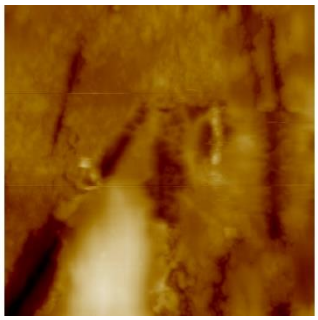

After 35 Wear Scans

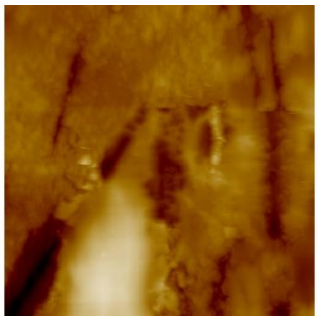

After 40 Wear Scans

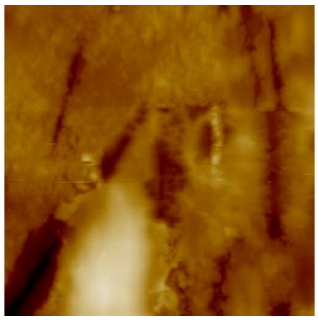

After 45 Wear Scans

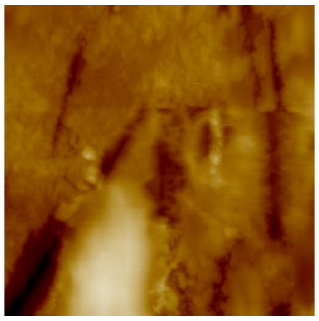

After 50 Wear Scans

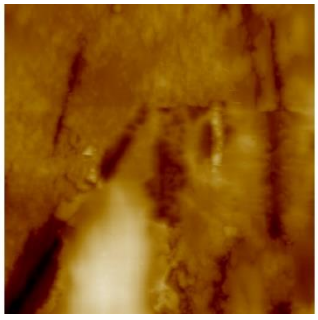

After 55 Wear Scans

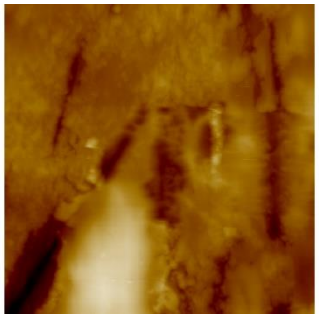

After 60 Wear Scans

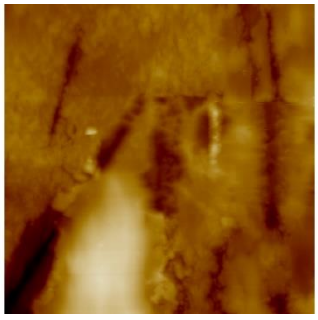

After 70 Wear Scans

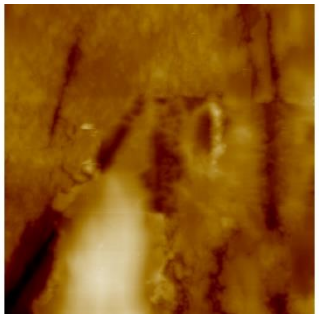

After 80 Wear Scans

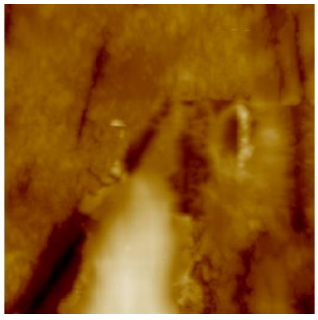

After 92 Wear Scans

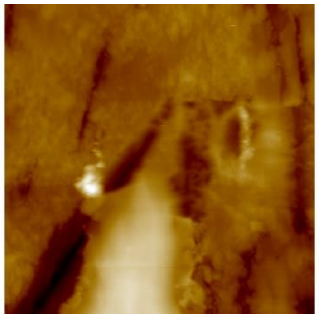

After 100 Wear Scans

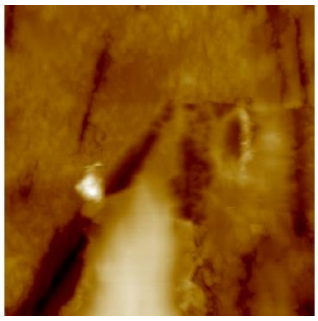

After 110 Wear Scans

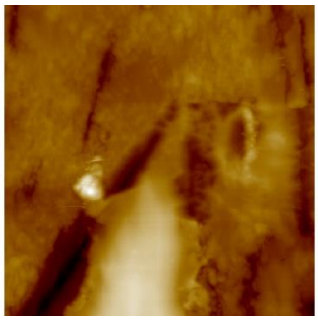

After 120 Wear Scans

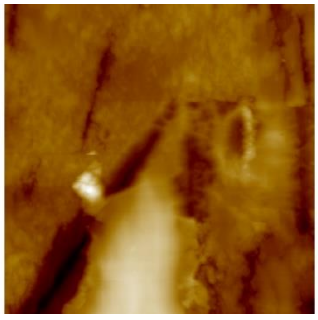

After 130 Wear Scans

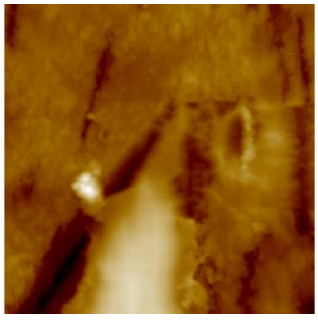

After 140 Wear Scans

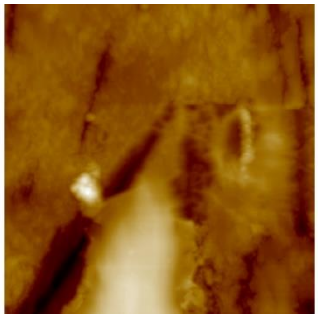

After 150 Wear Scans

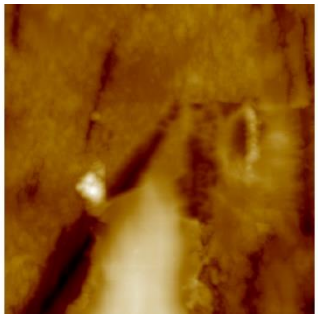

After 160 Wear Scans

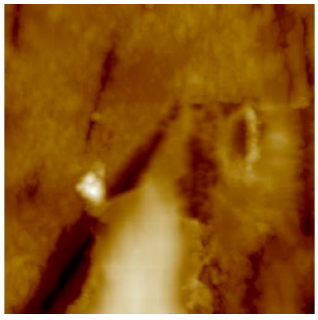

After 170 Wear Scans

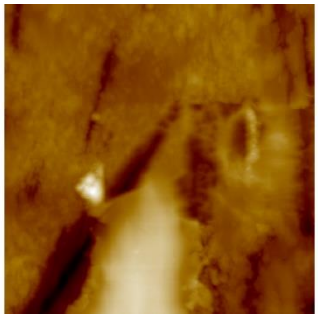

After 180 Wear Scans

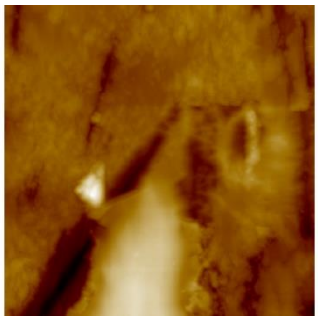

After 190 Wear Scans

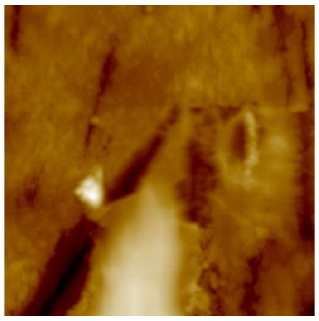

After 200 Wear Scans

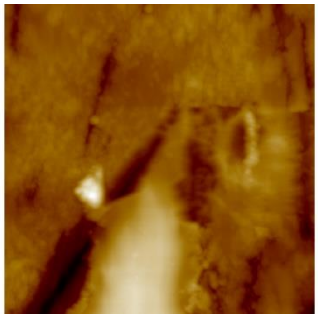

After 210 Wear Scans

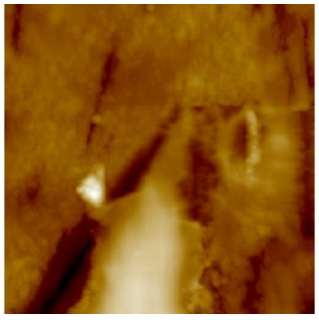

After 220 Wear Scans

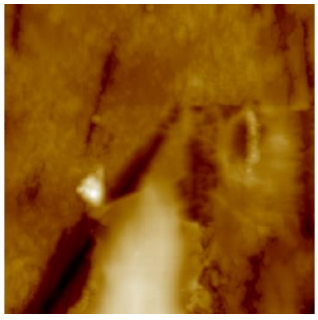

After 230 Wear Scans

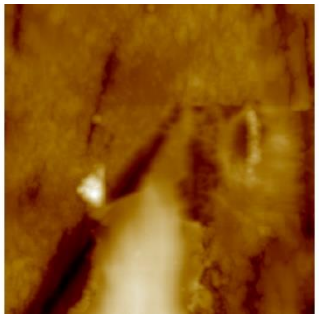

After 240 Wear Scans

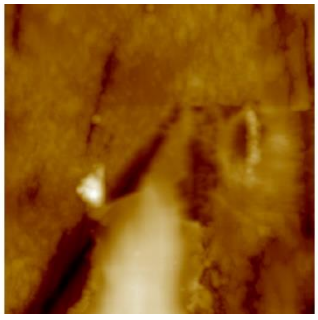

After 250 Wear Scans

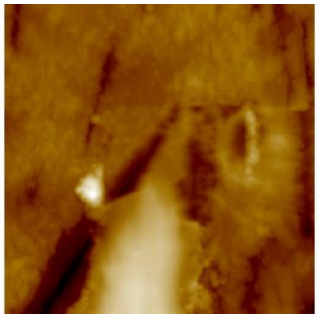

0.275wt% ZDDP Tribofilm – 0.005mN – On a pad

After 0 Wear Scans

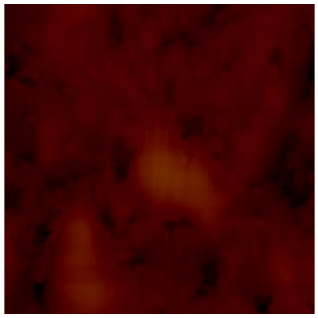

After 5 Wear Scans

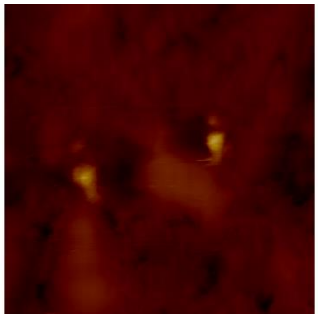

After 10 Wear Scans

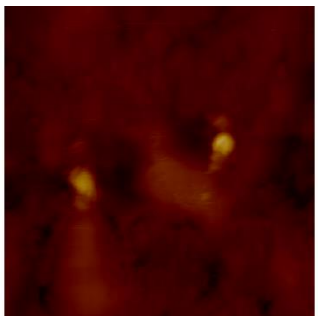

After 15 Wear Scans

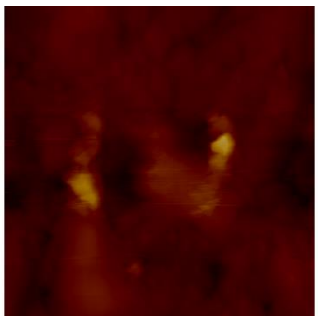

After 20 Wear Scans

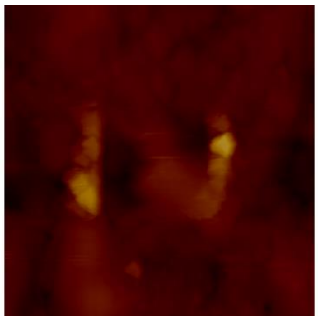

After 25 Wear Scans

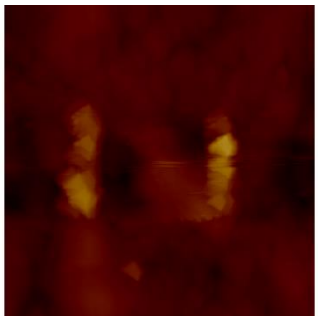

After 30 Wear Scans

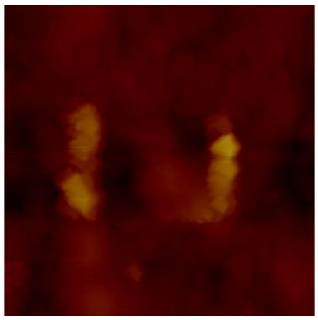

After 35 Wear Scans

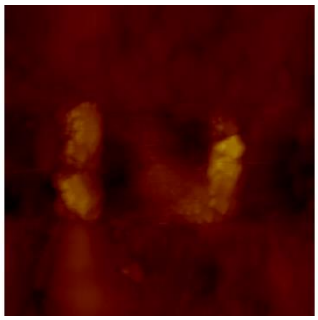

After 40 Wear Scans

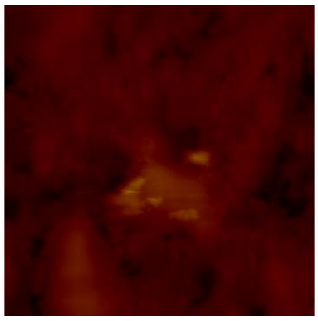

After 45 Wear Scans

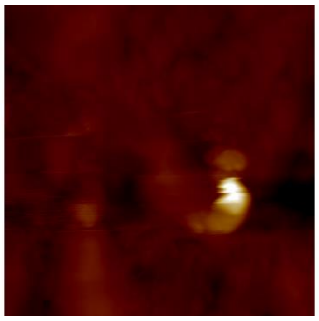

After 50 Wear Scans

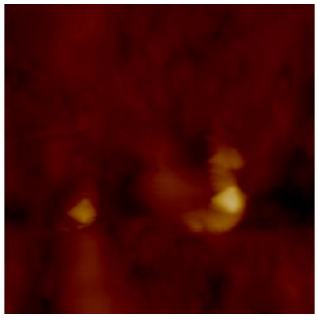

After 55 Wear Scans

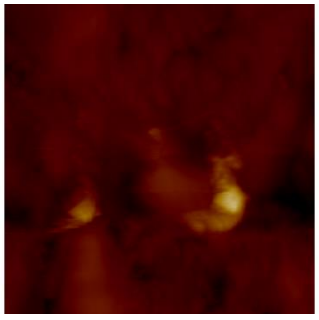

After 60 Wear Scans

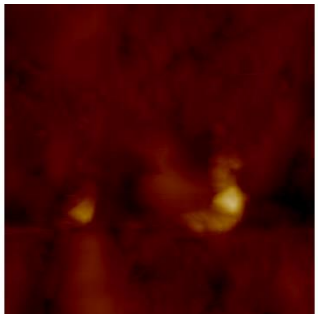

After 65 Wear Scans

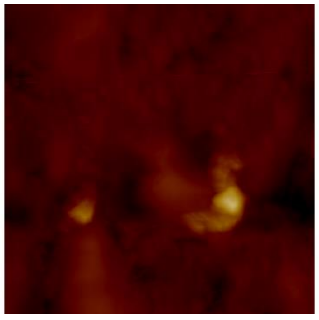

After 70 Wear Scans

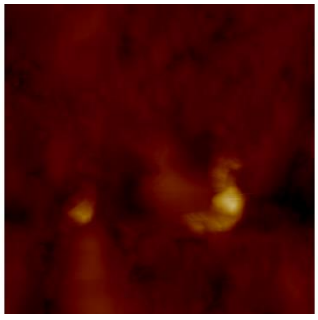

After 75 Wear Scans

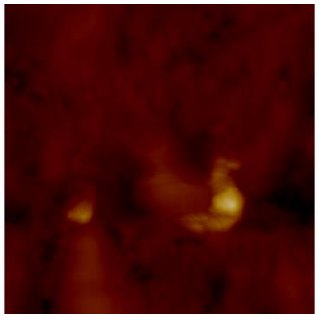

After 80 Wear Scans

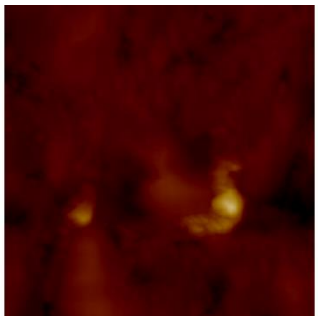

After 85 Wear Scans

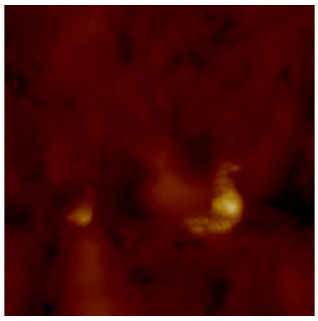

After 90 Wear Scans

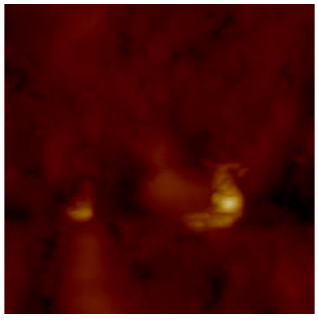

After 95 Wear Scans

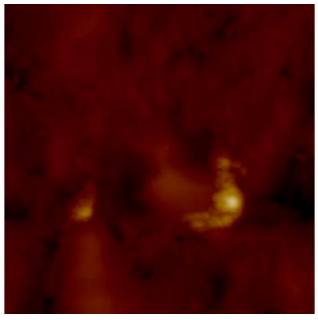

After 100 Wear Scans

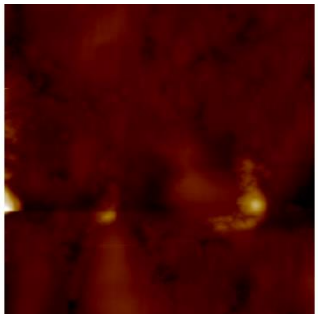

After 105 Wear Scans

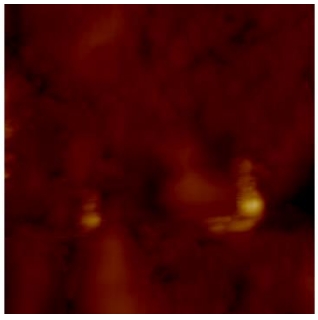

After 110 Wear Scans

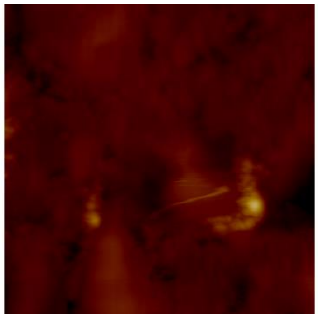

After 115 Wear Scans

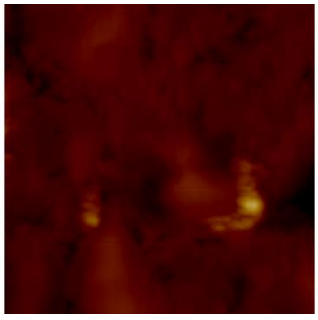

After 120 Wear Scans

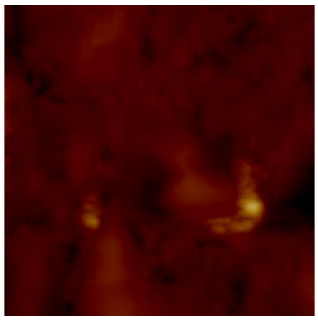

After 125 Wear Scans

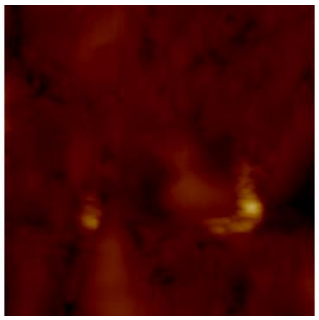

0.55wt% ZDDP Tribofilm – 0.005mN – On a pad

After 0 Wear Scans

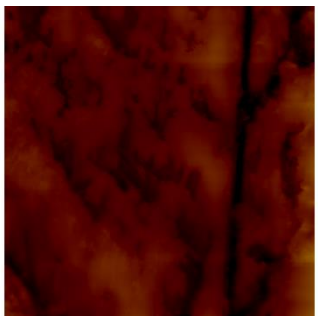

After 5 Wear Scans

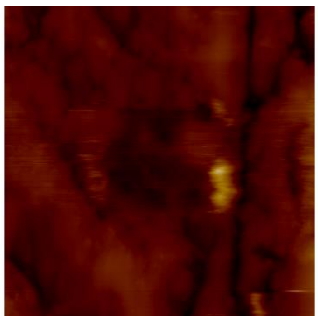

After 10 Wear Scans

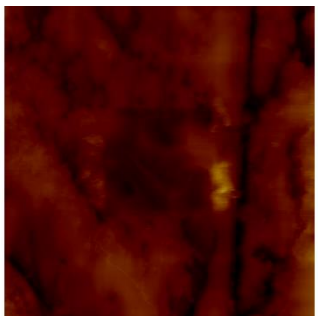

After 15 Wear Scans

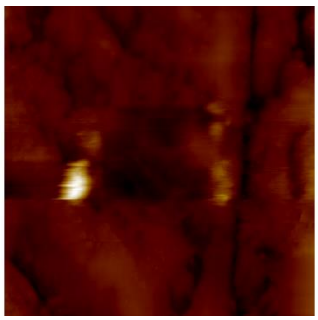

After 20 Wear Scans

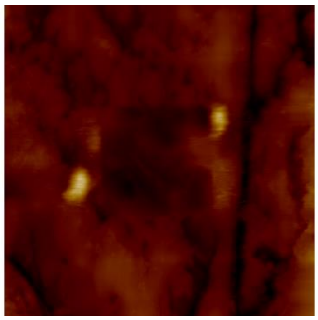

After 25 Wear Scans

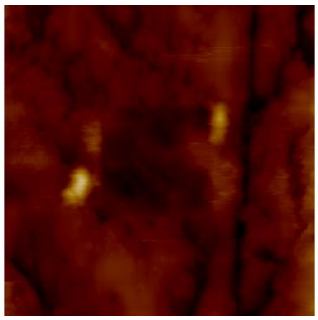

After 30 Wear Scans

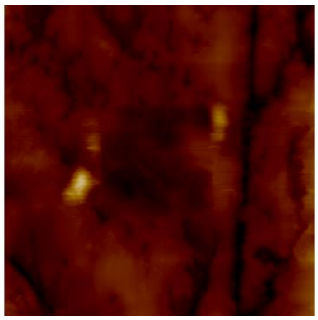

After 35 Wear Scans

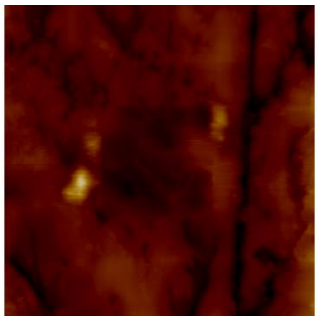

After 40 Wear Scans

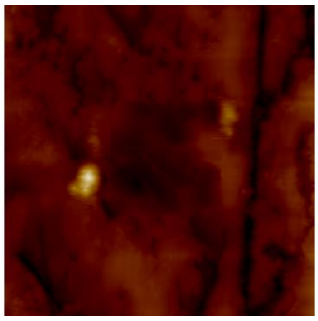

After 45 Wear Scans

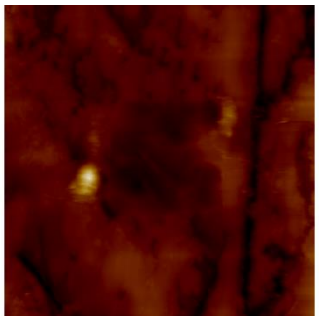

After 50 Wear Scans

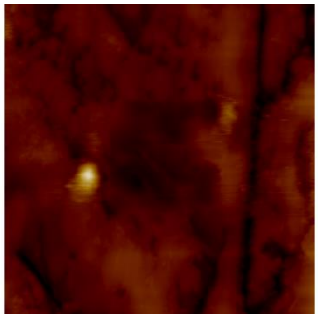

After 56 Wear Scans

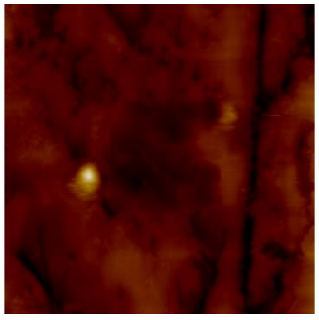

After 60 Wear Scans

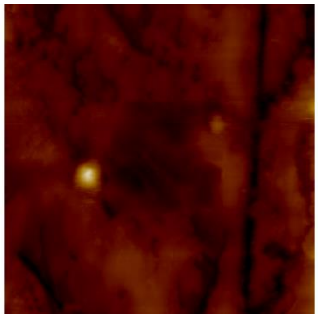

After 70 Wear Scans

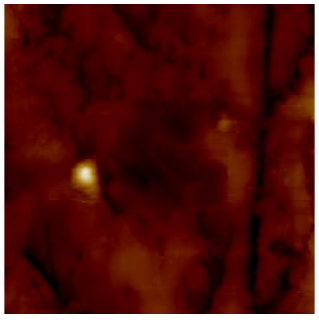

After 80 Wear Scans

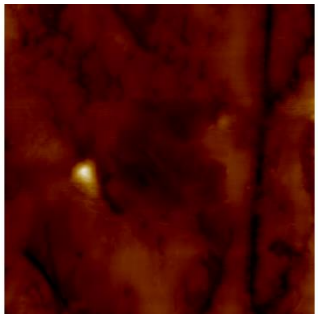

After 90 Wear Scans

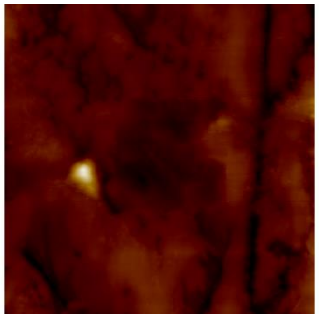

After 100 Wear Scans

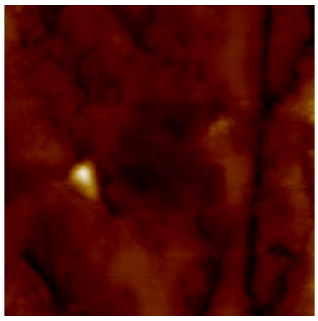

After 110 Wear Scans

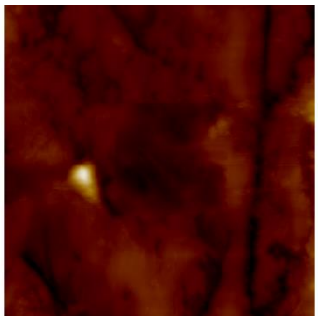

After 120 Wear Scans

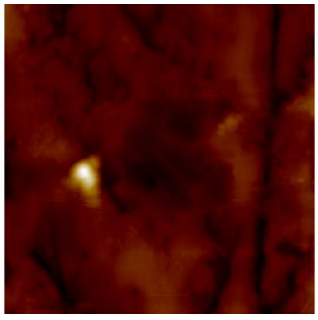

After 130 Wear Scans

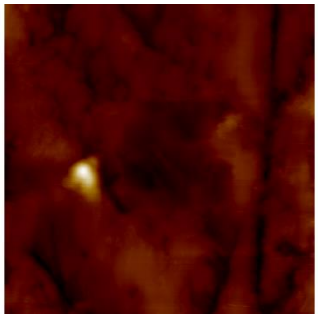

After 140 Wear Scans

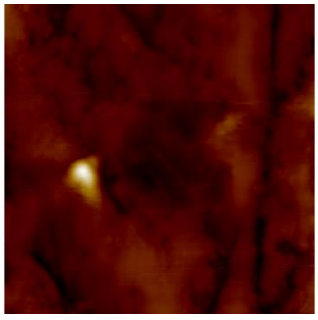

After 150 Wear Scans

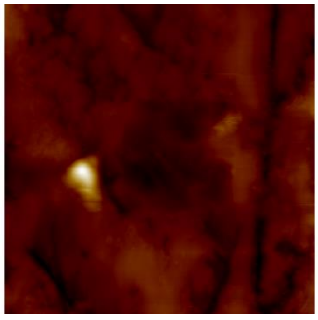

After 160 Wear Scans

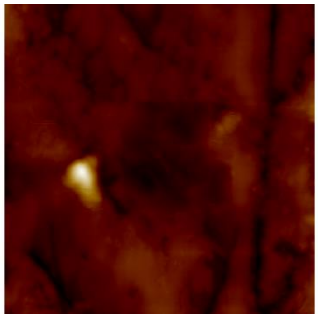

After 170 Wear Scans

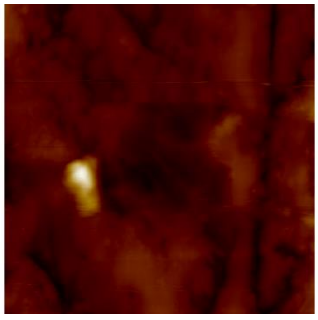

After 180 Wear Scans

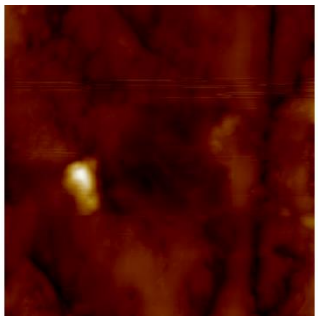

After 190 Wear Scans

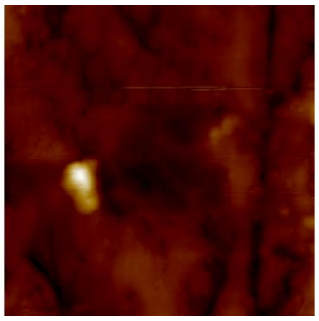

After 200 Wear Scans

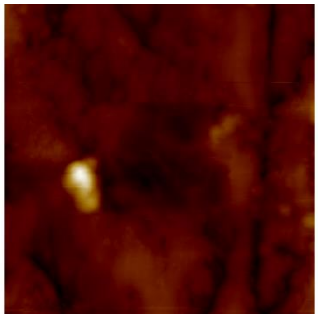

After 210 Wear Scans

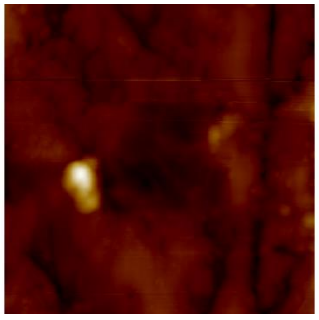

After 220 Wear Scans

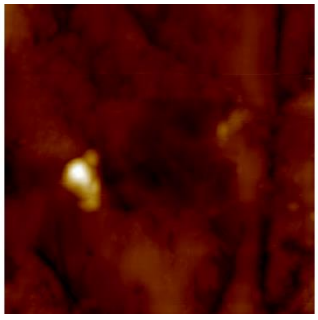

After 230 Wear Scans

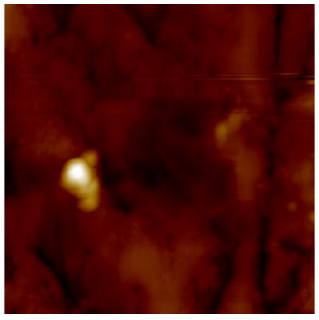

After 240 Wear Scans

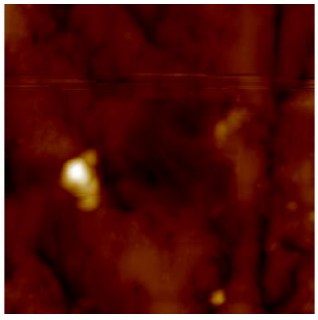

After 250 Wear Scans

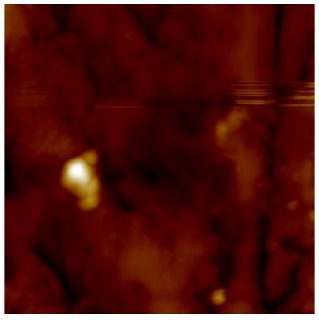

0.55wt% ZDDP Tribofilm – 0.005mN – On the edge of a pad

After 0 Wear Scans

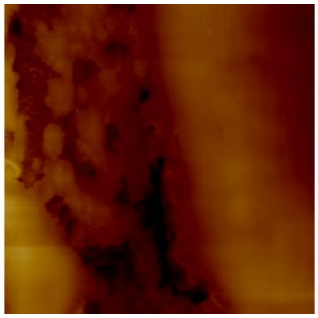

After 5 Wear Scans

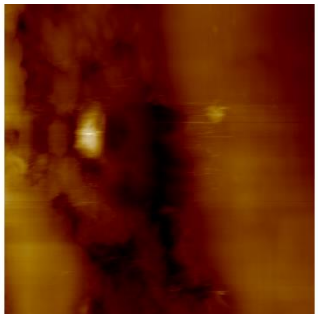

After 10 Wear Scans

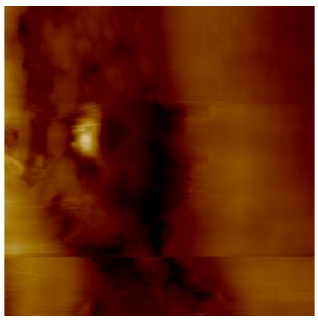

After 15 Wear Scans

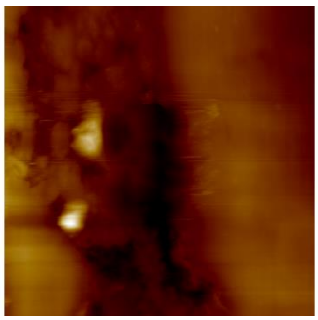

After 20 Wear Scans

After 25 Wear Scans

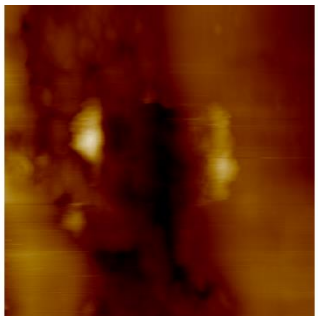

After 30 Wear Scans

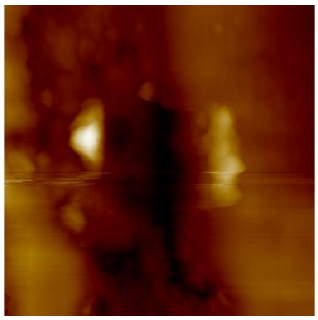

After 35 Wear Scans

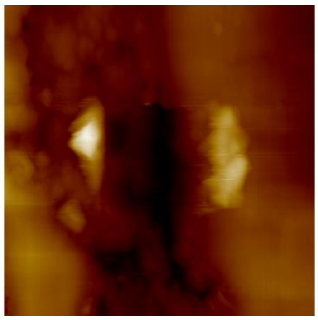

After 40 Wear Scans

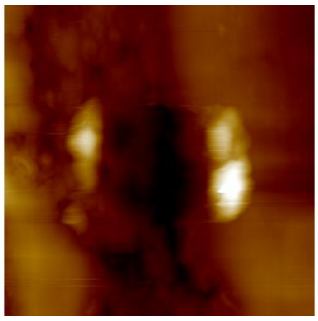

After 45 Wear Scans

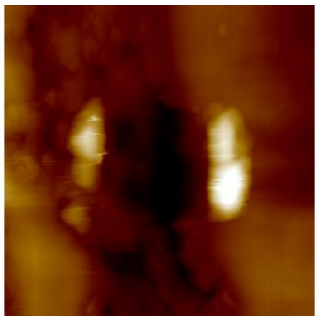

After 50 Wear Scans

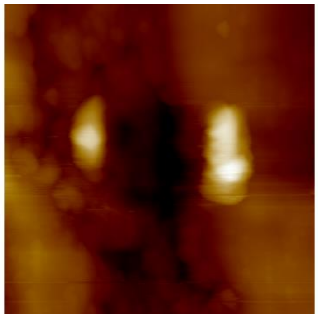

After 55 Wear Scans

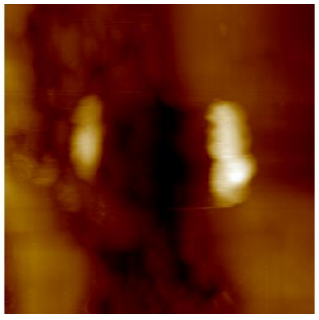

After 60 Wear Scans

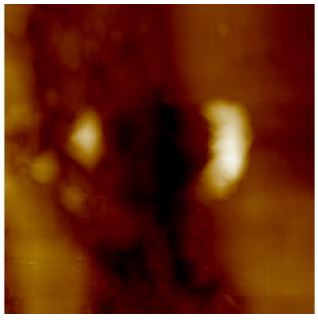

After 70 Wear Scans

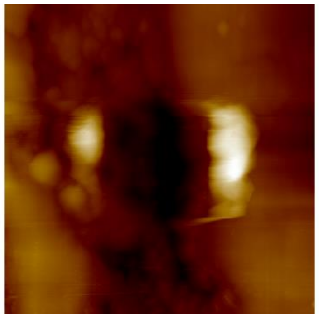

After 80 Wear Scans

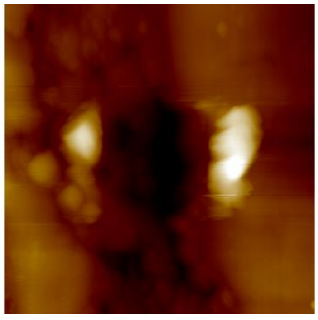

After 90 Wear Scans

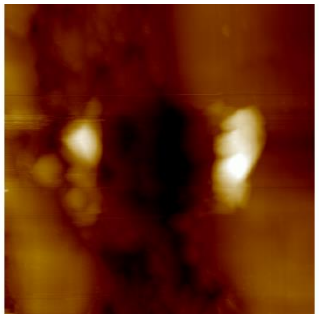

After 100 Wear Scans

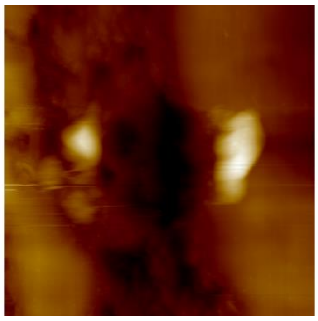

After 110 Wear Scans

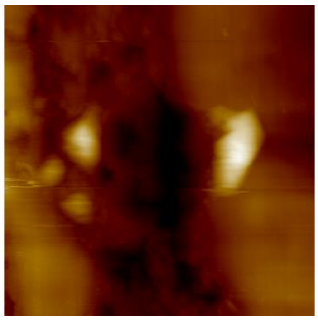

After 120 Wear Scans

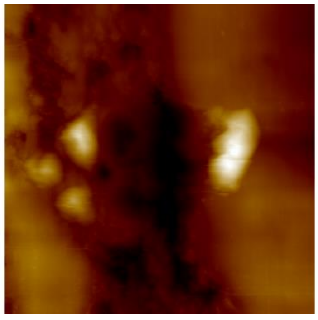

After 130 Wear Scans

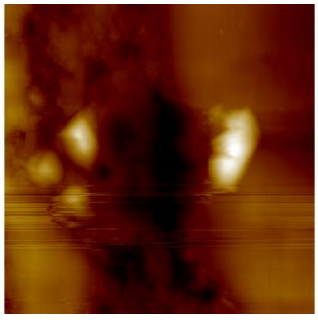

After 140 Wear Scans

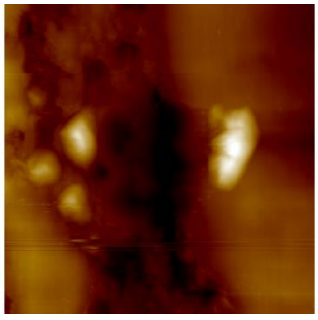

After 150 Wear Scans

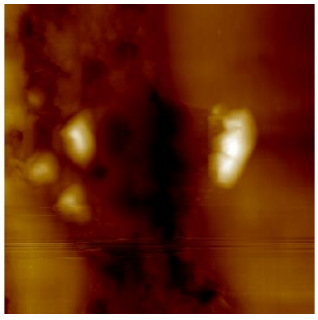

After 160 Wear Scans

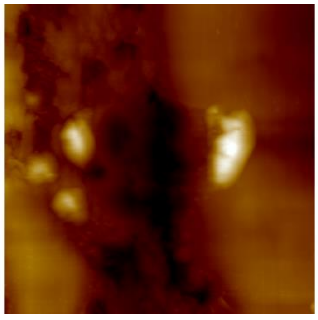

After 170 Wear Scans

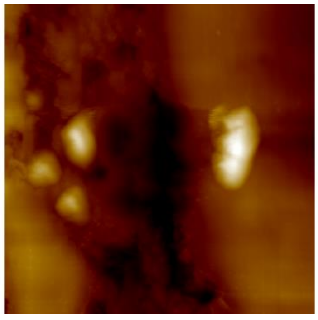

After 180 Wear Scans

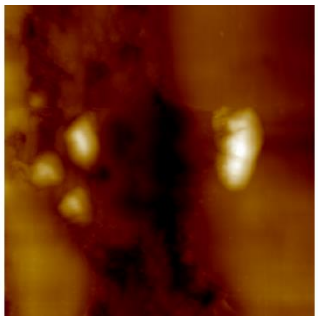

After 190 Wear Scans

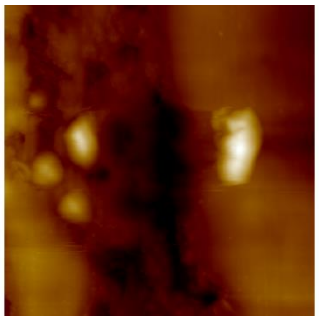

After 200 Wear Scans

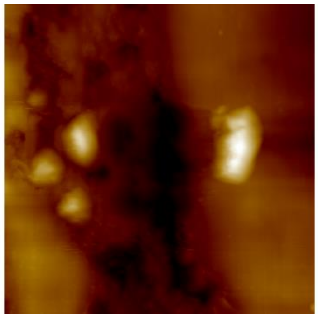

After 210 Wear Scans

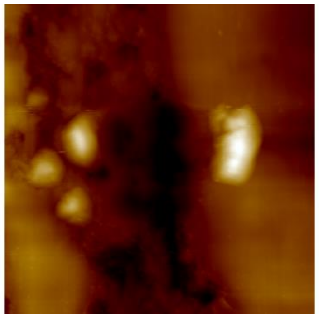

After 220 Wear Scans

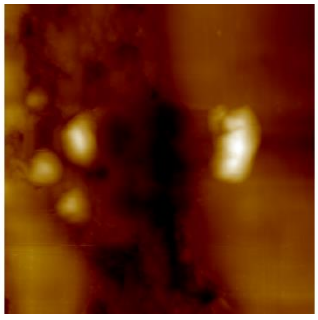

After 230 Wear Scans

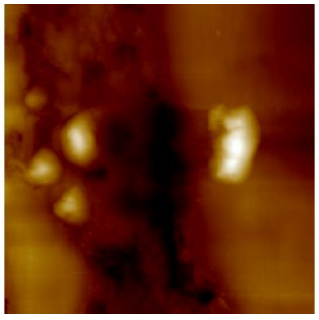

After 240 Wear Scans

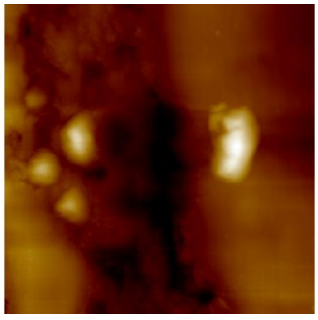

After 250 Wear Scans

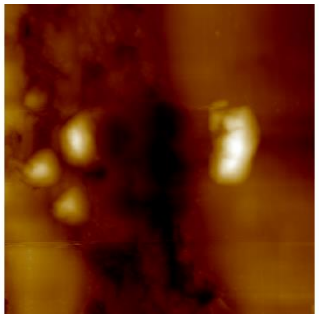

0.55wt% ZDDP Tribofilm – 0.005mN – Between pads

After 0 Wear Scans

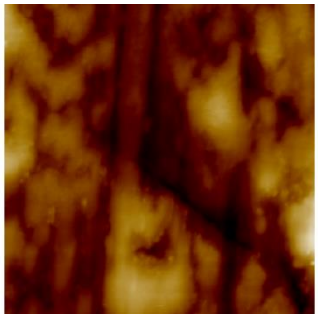

After 5 Wear Scans

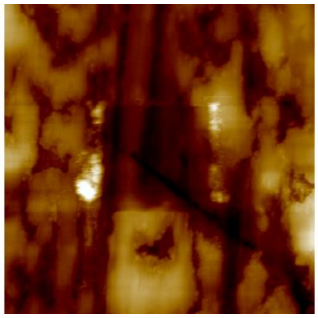

After 10 Wear Scans

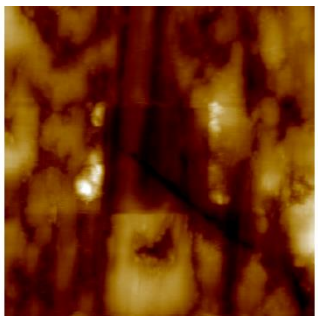

After 15 Wear Scans

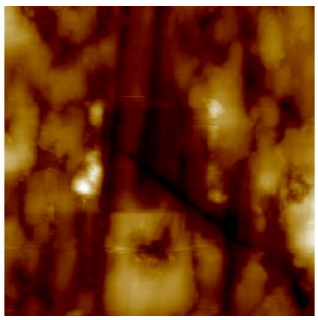

After 20 Wear Scans

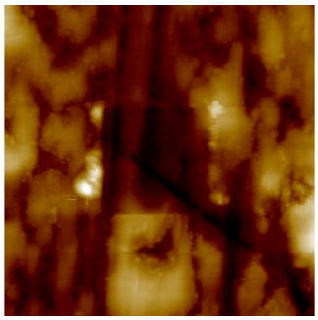

After 25 Wear Scans

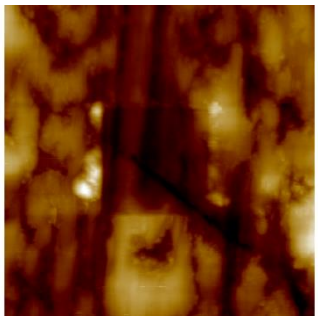

After 30 Wear Scans

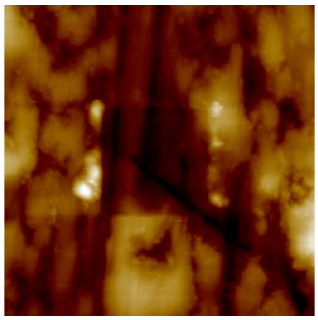

After 35 Wear Scans

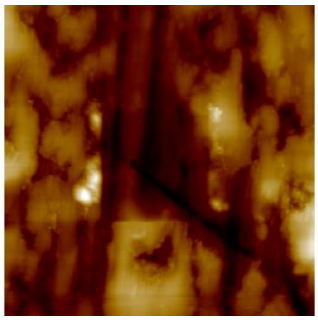

After 40 Wear Scans

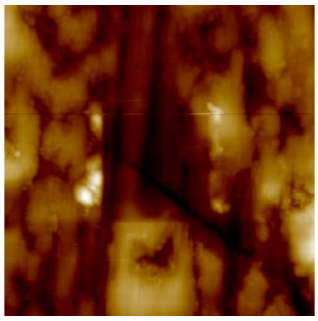

After 45 Wear Scans

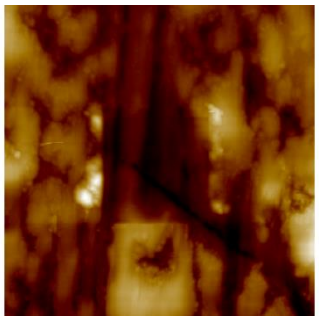

After 50 Wear Scans

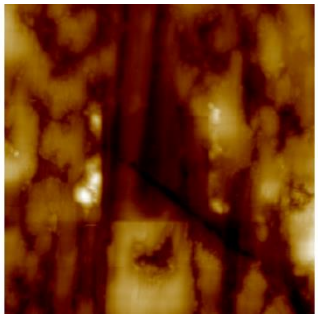

After 55 Wear Scans

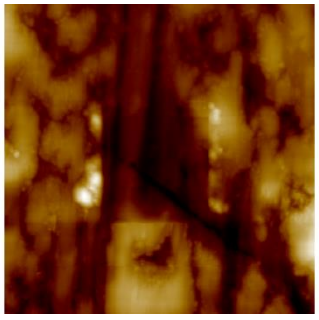

After 60 Wear Scans

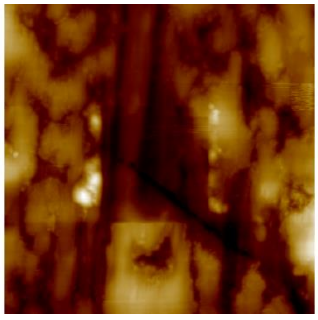

After 70 Wear Scans

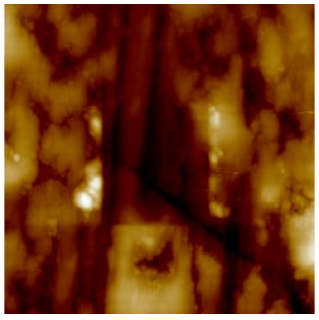

After 80 Wear Scans

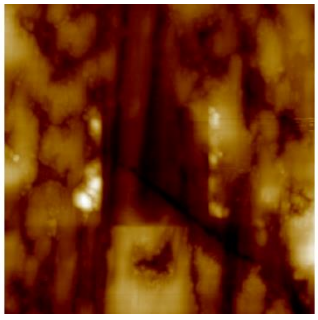

After 90 Wear Scans

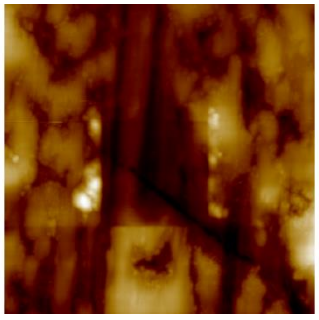

After 100 Wear Scans

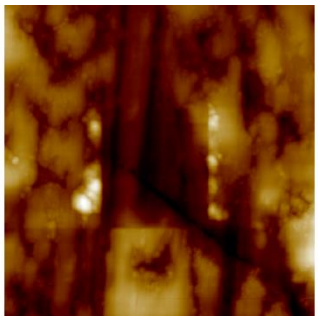

After 110 Wear Scans

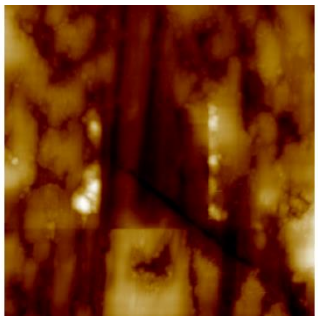

After 120 Wear Scans

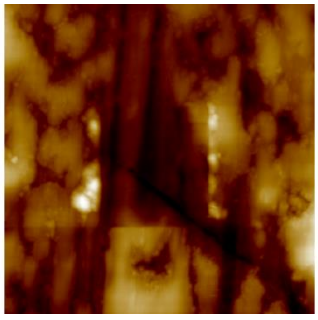

After 130 Wear Scans

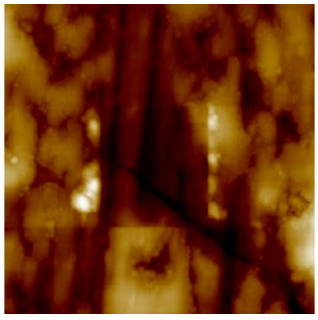

After 140 Wear Scans

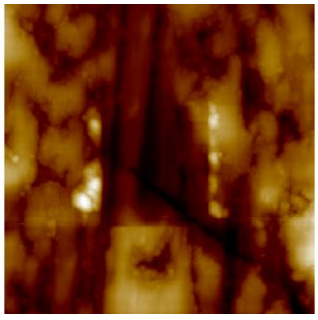

After 150 Wear Scans

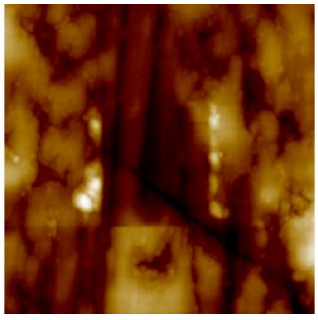

After 160 Wear Scans

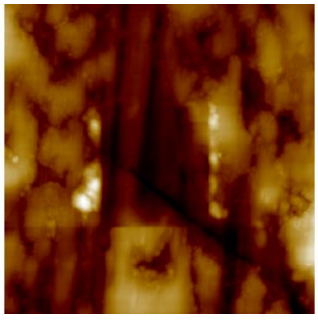

After 170 Wear Scans

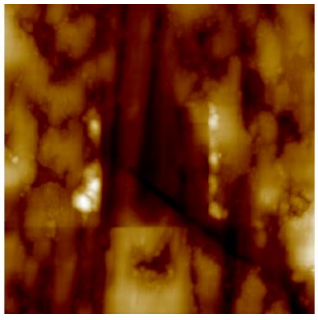

After 180 Wear Scans

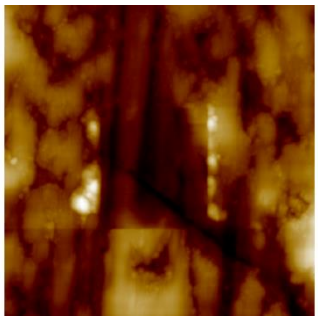

After 190 Wear Scans

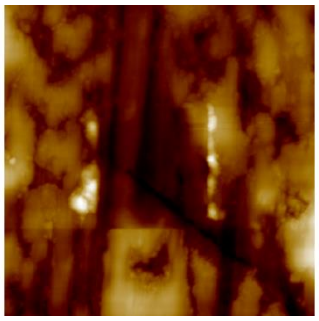

After 200 Wear Scans

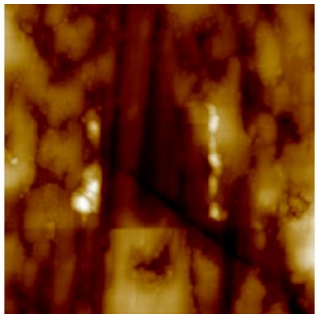

After 210 Wear Scans

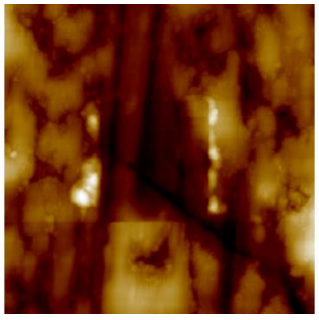

After 220 Wear Scans

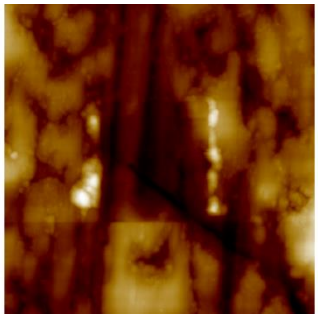

After 230 Wear Scans

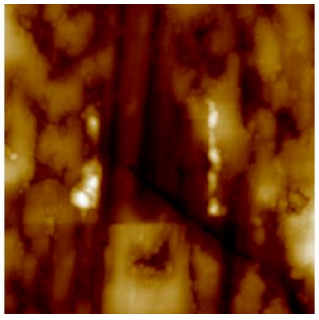

After 240 Wear Scans

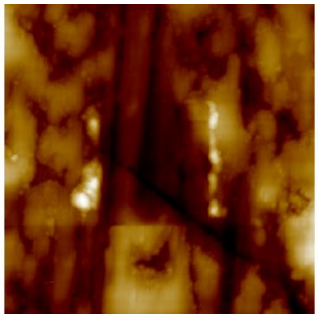

After 250 Wear Scans

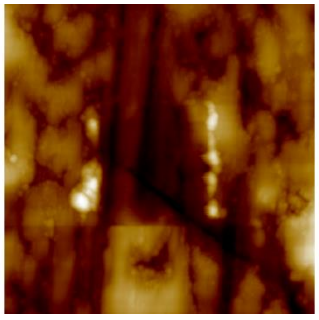

0.55wt% ZDDP Tribofilm – 0.010mN – On a pad

After 0 Wear Scans

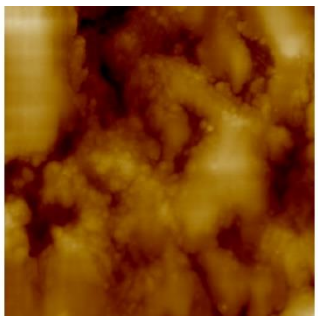

After 5 Wear Scans

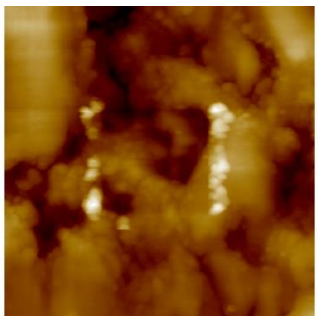

After 10 Wear Scans

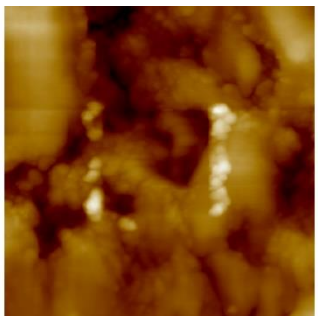

After 15 Wear Scans

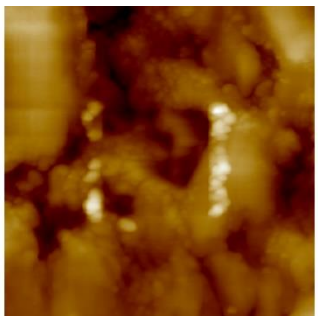

After 20 Wear Scans

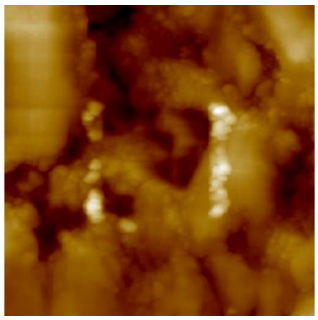

After 25 Wear Scans

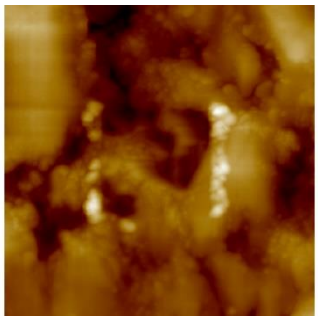

After 30 Wear Scans

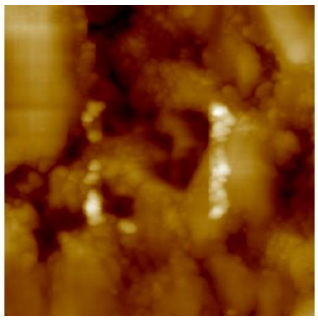

After 35 Wear Scans

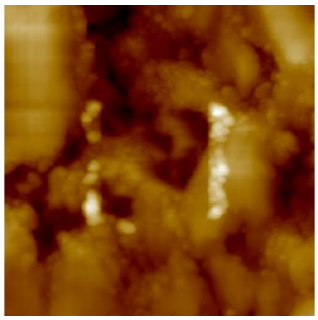

After 40 Wear Scans

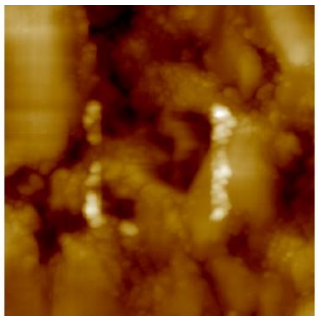

After 45 Wear Scans

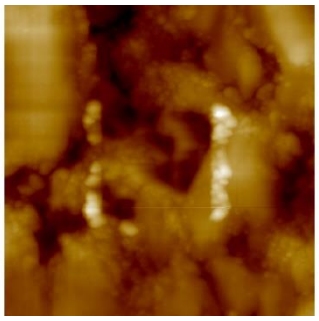

After 50 Wear Scans

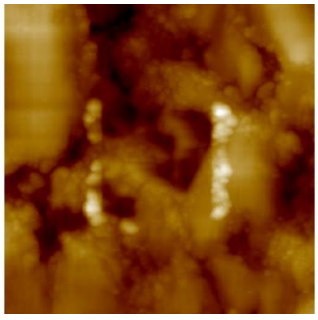

After 55 Wear Scans

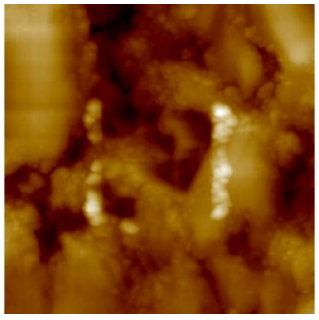

After 60 Wear Scans

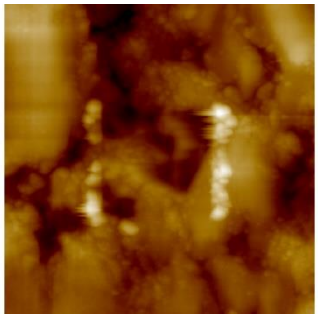

After 70 Wear Scans

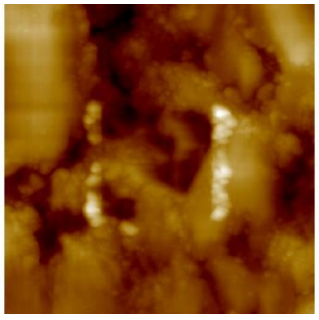

After 80 Wear Scans

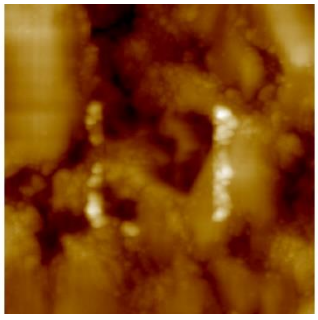

After 90 Wear Scans

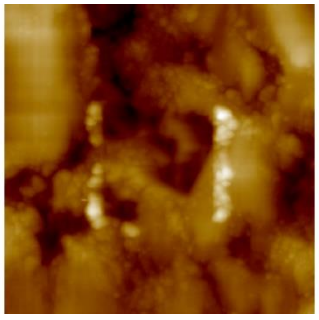

After 100 Wear Scans

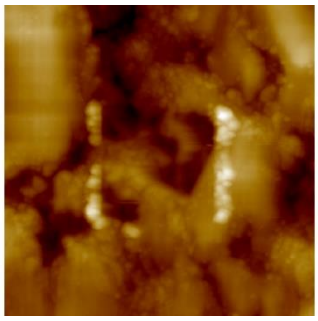

After 110 Wear Scans

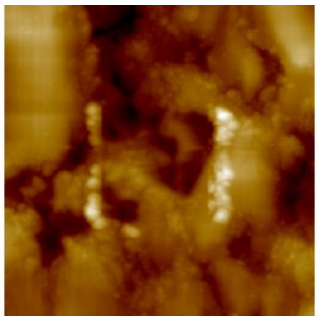

After 120 Wear Scans

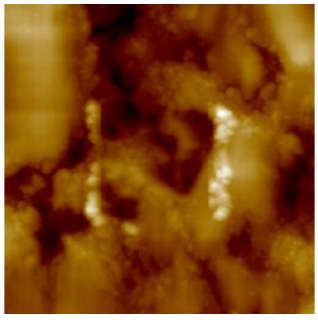

After 130 Wear Scans

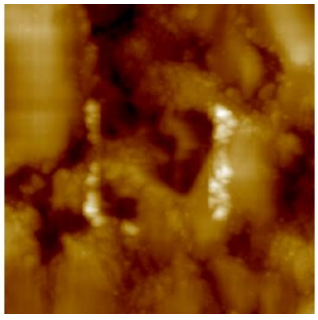

After 140 Wear Scans

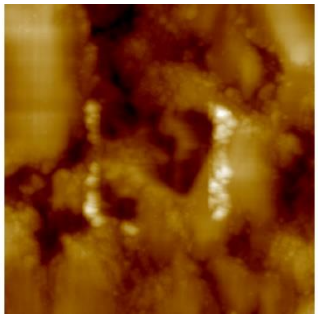

After 150 Wear Scans

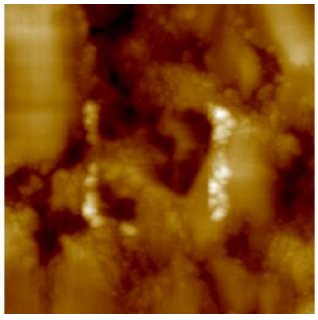

After 160 Wear Scans

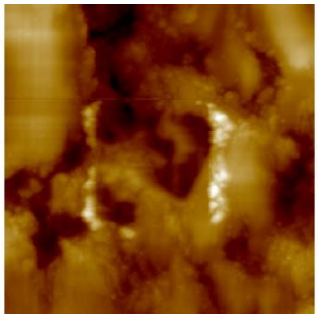

After 170 Wear Scans

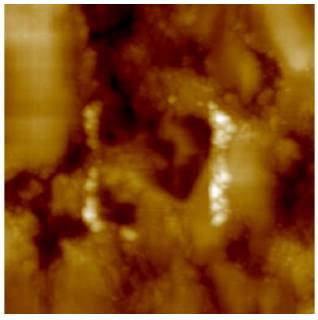

After 180 Wear Scans

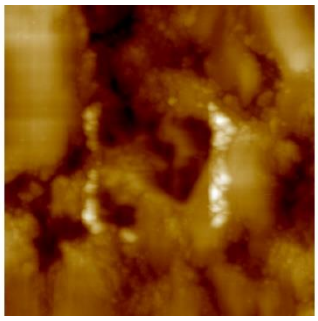

After 190 Wear Scans

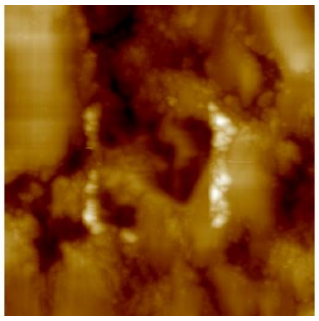

After 200 Wear Scans

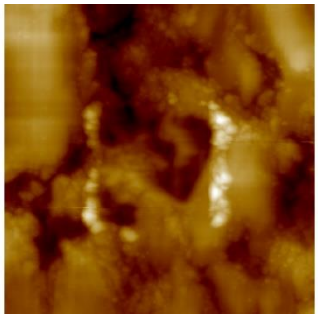

After 210 Wear Scans

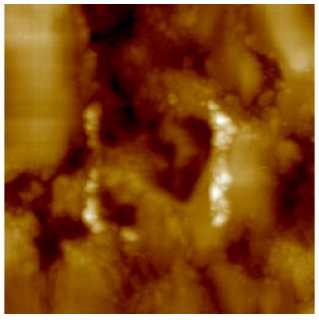

After 220 Wear Scans

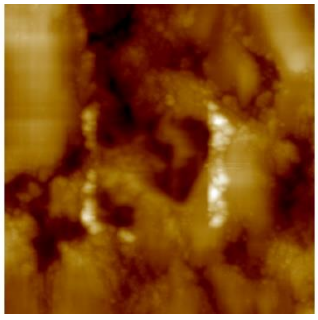

After 230 Wear Scans

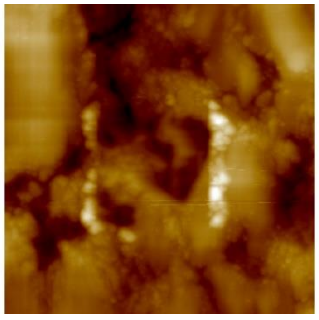

After 240 Wear Scans

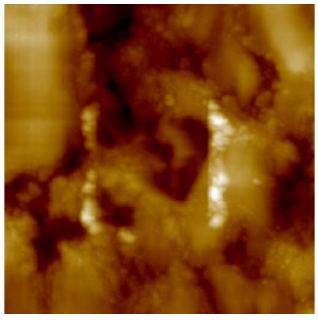

After 250 Wear Scans

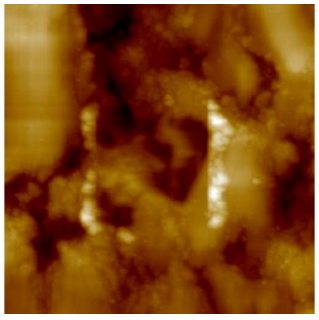

0.55wt% ZDDP Tribofilm – 0.01mN – On a pad film

After 0 Wear Scans

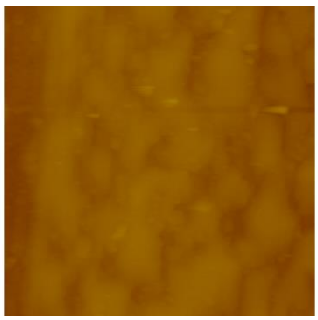

After 5 Wear Scans

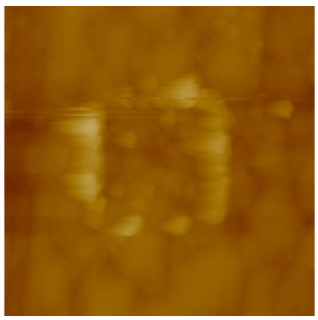

After 10 Wear Scans

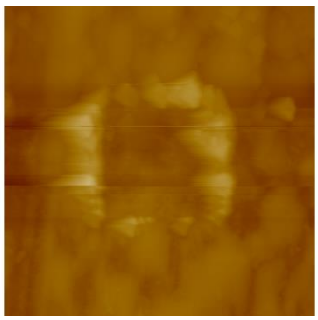

After 15 Wear Scans

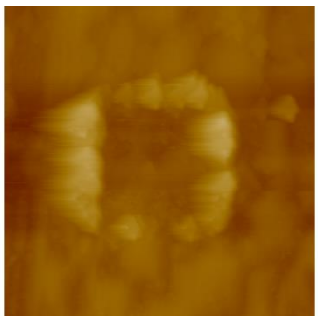

After 20 Wear Scans

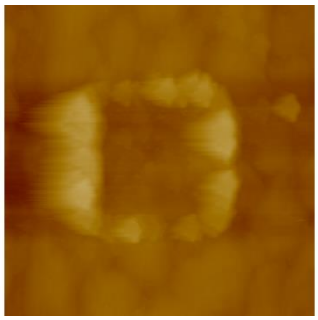

After 25 Wear Scans

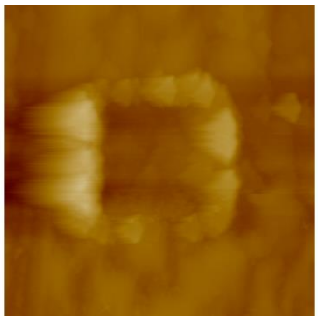

After 30 Wear Scans

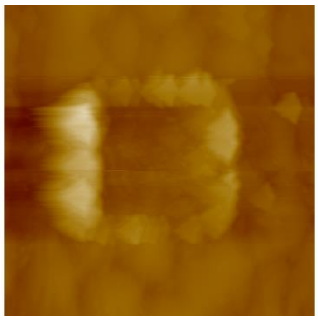

After 35 Wear Scans

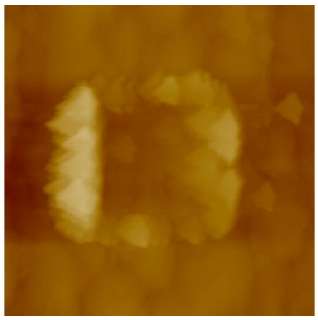

After 40 Wear Scans

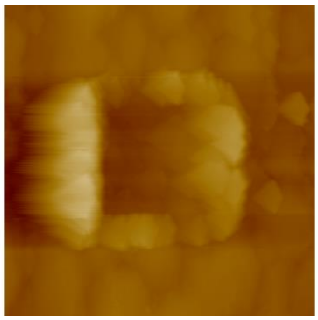

After 45 Wear Scans

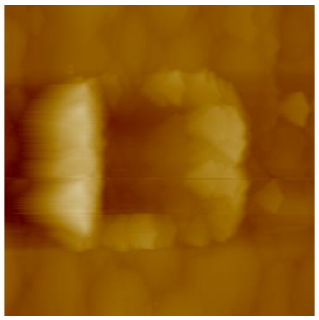

After 50 Wear Scans

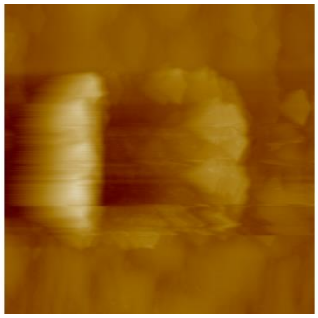

After 55 Wear Scans

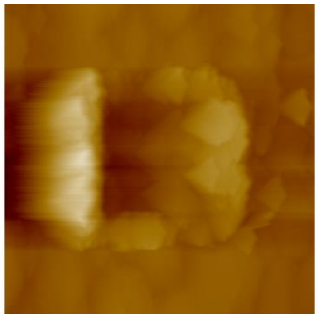

After 60 Wear Scans

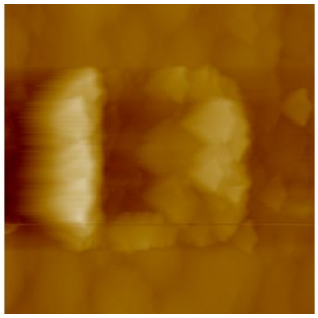

After 70 Wear Scans

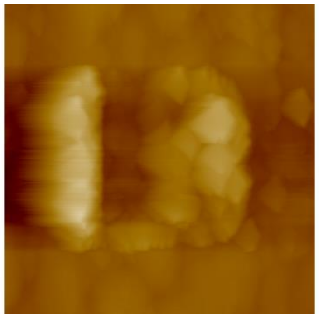

After 80 Wear Scans

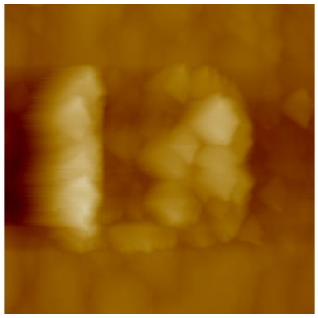

After 90 Wear Scans

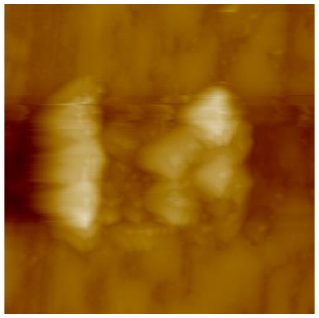

After 100 Wear Scans

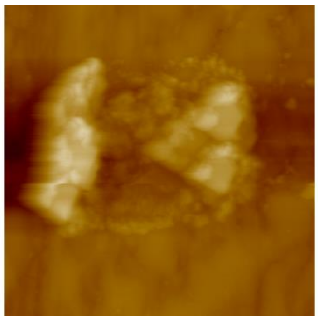

After 110 Wear Scans

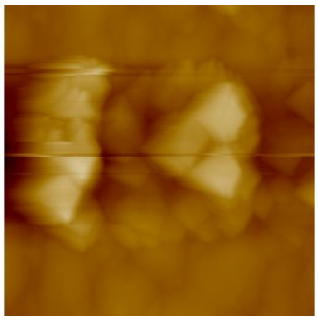

After 120 Wear Scans

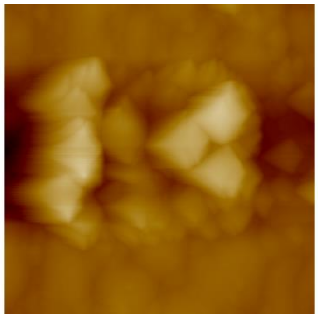

After 130 Wear Scans

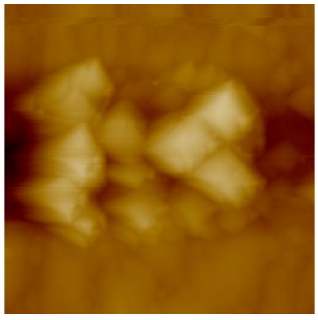

After 140 Wear Scans

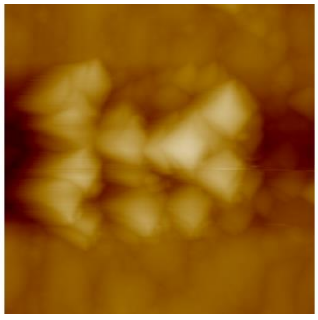

After 150 Wear Scans

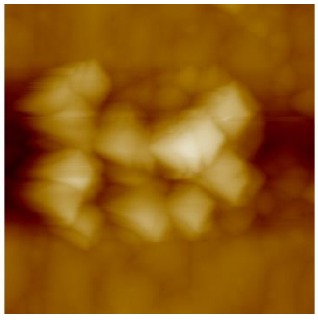

After 160 Wear Scans

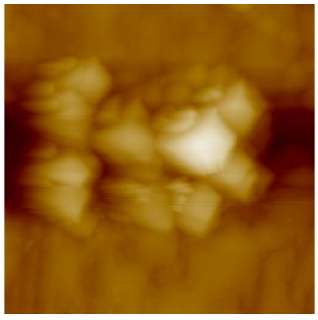

After 170 Wear Scans

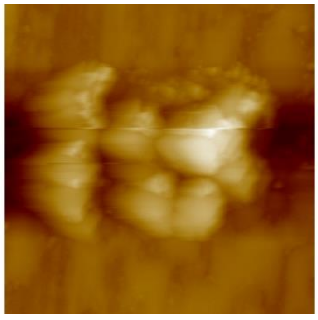

After 180 Wear Scans

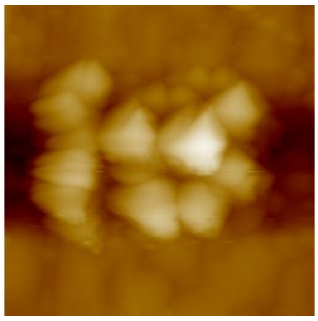

After 190 Wear Scans

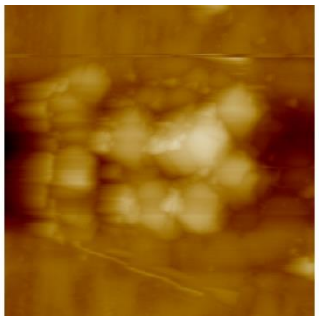

After 200 Wear Scans

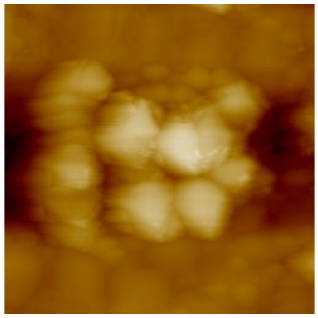

After 210 Wear Scans

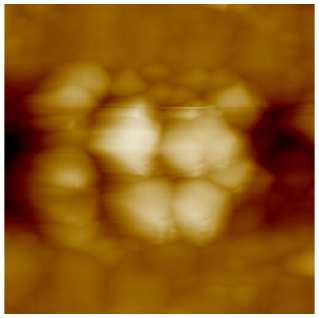

After 220 Wear Scans

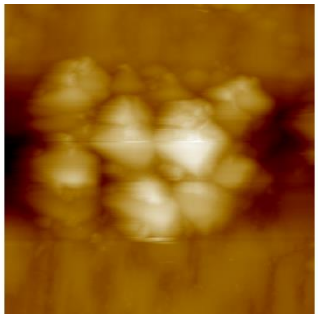

After 230 Wear Scans

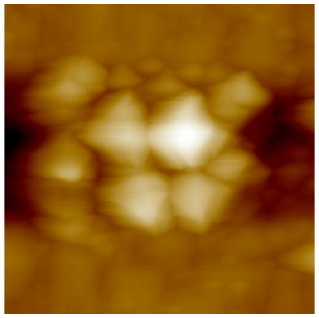

After 240 Wear Scans

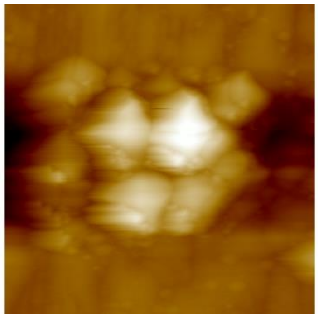

After 250 Wear Scans

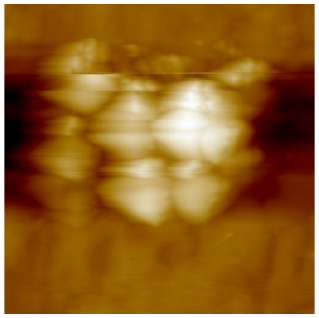

0.55wt% ZDDP Tribofilm – 0.014mN – On a pad

After 0 Wear Scans

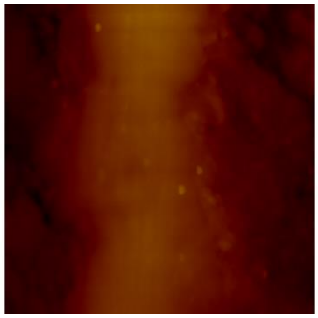

After 5 Wear Scans

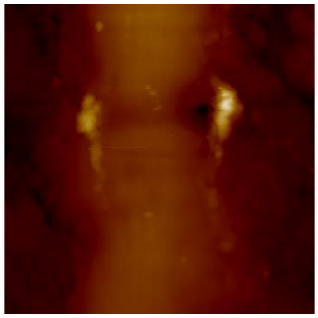

After 10 Wear Scans

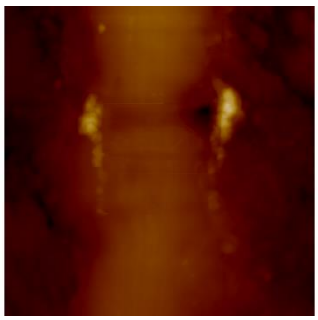

After 15 Wear Scans

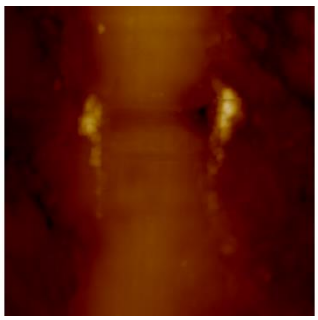

After 20 Wear Scans

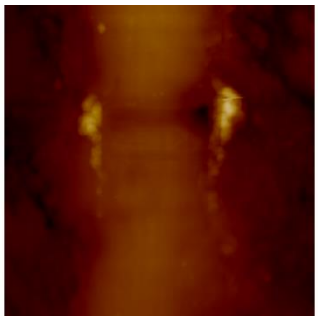

After 25 Wear Scans

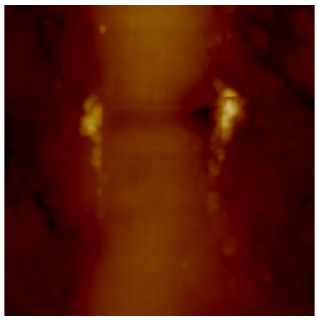

After 30 Wear Scans

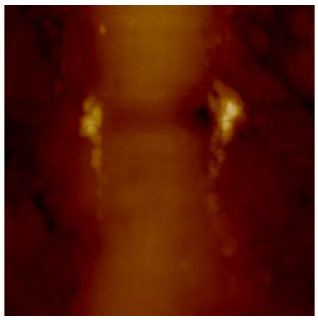

After 35 Wear Scans

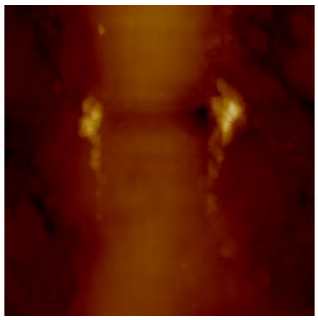

After 40 Wear Scans

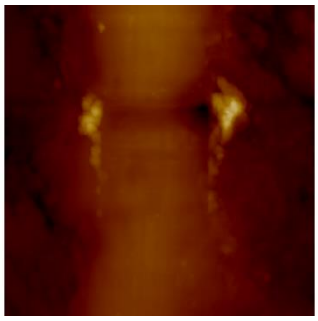

After 45 Wear Scans

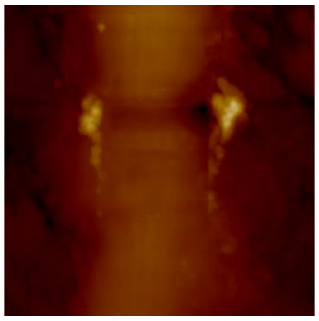

After 50 Wear Scans

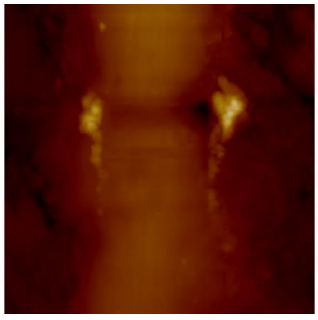

After 55 Wear Scans

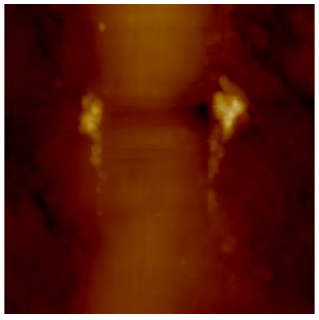

After 60 Wear Scans

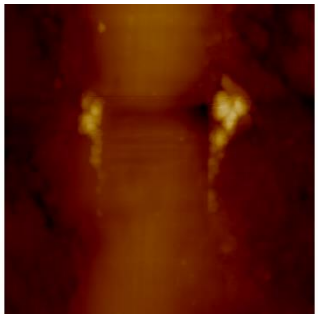

After 70 Wear Scans

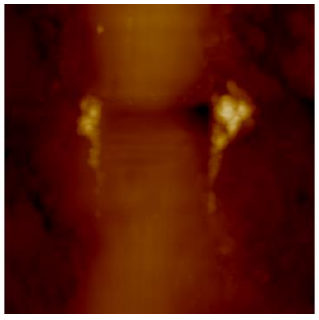

After 80 Wear Scans

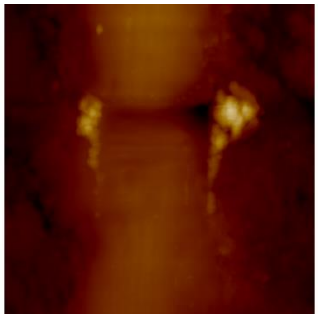

After 90 Wear Scans

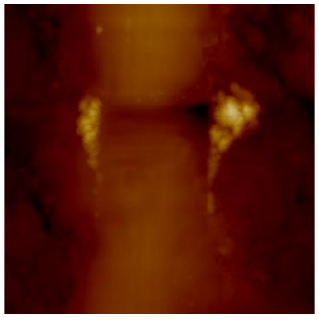

After 100 Wear Scans

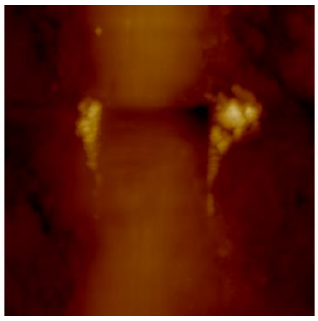

After 110 Wear Scans

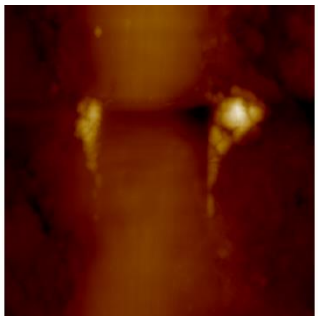

After 120 Wear Scans

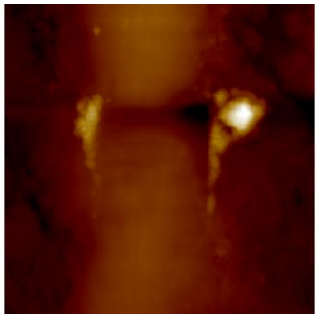

After 130 Wear Scans

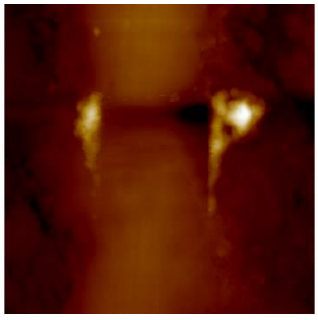

After 140 Wear Scans

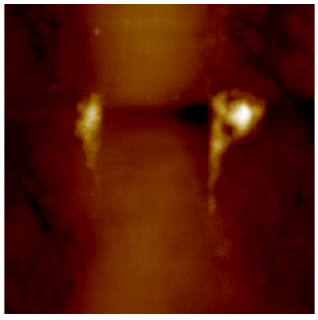

After 150 Wear Scans

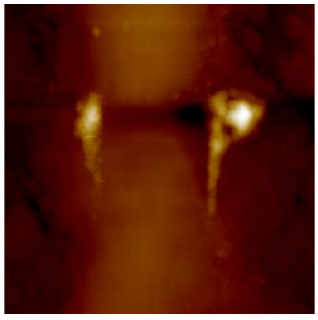

After 160 Wear Scans

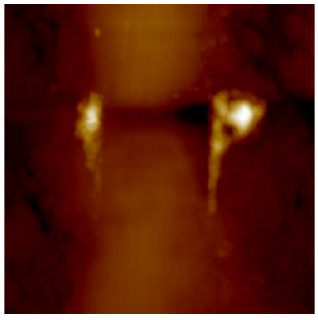

After 170 Wear Scans

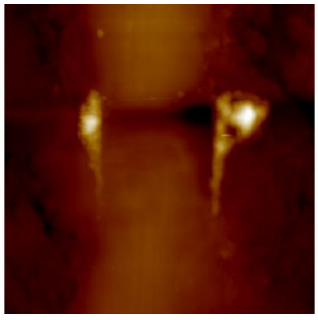

After 180 Wear Scans

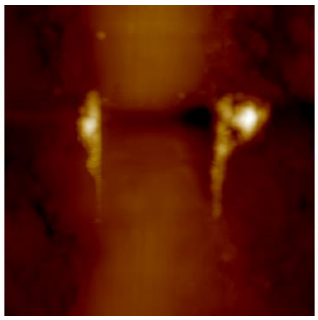

After 190 Wear Scans

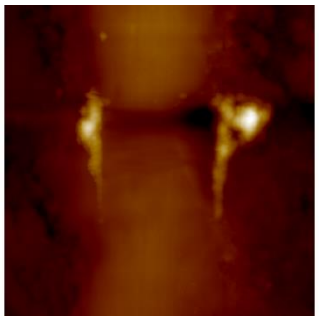

After 200 Wear Scans

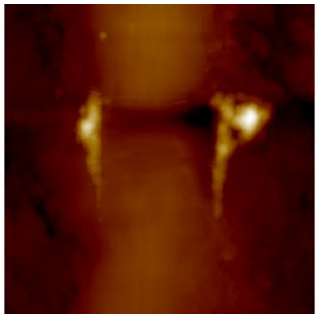

After 210 Wear Scans

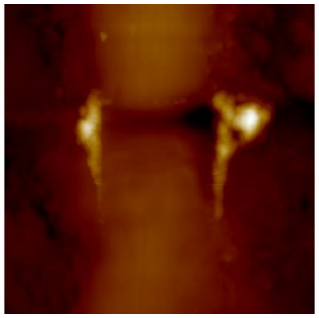

After 220 Wear Scans

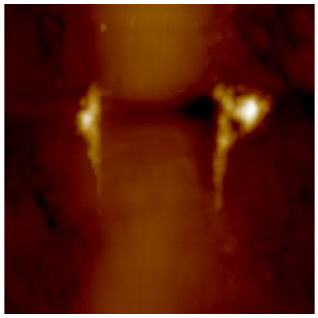

After 231 Wear Scans

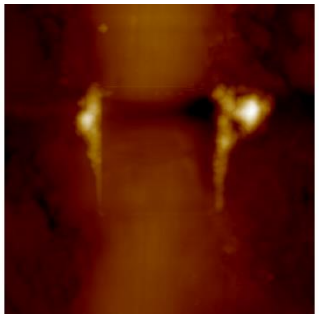

After 240 Wear Scans

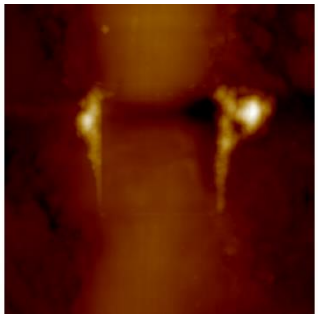

After 250 Wear Scans

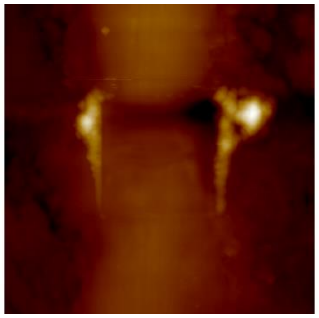

0.55wt% ZDDP Tribofilm – 0.005mN – On a pad film

After 0 Wear Scans

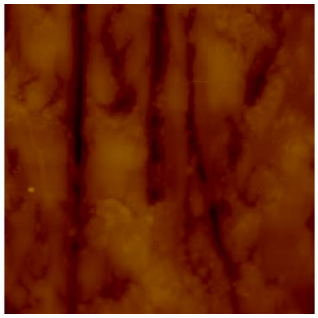

After 5 Wear Scans

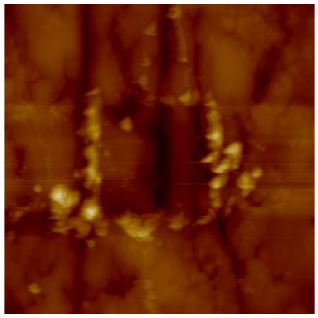

After 10 Wear Scans

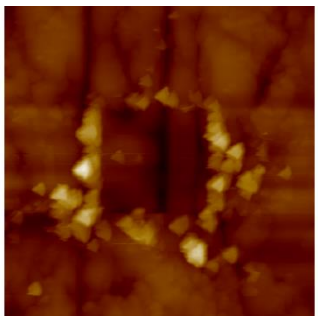

After 15 Wear Scans

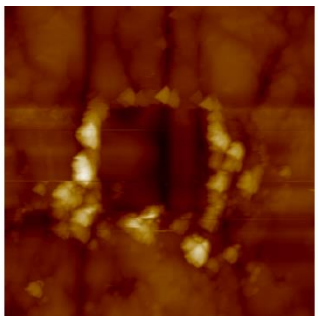

After 20 Wear Scans

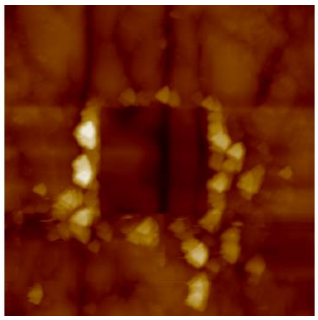

After 25 Wear Scans

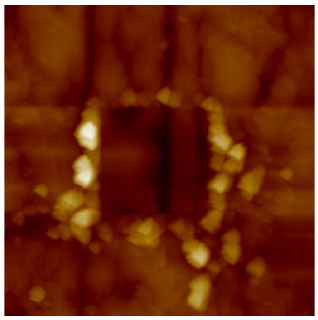

After 30 Wear Scans

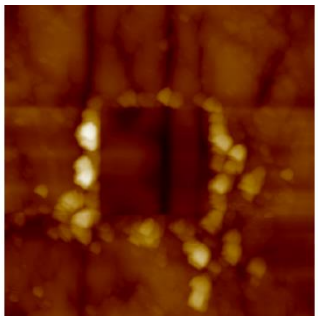

After 35 Wear Scans

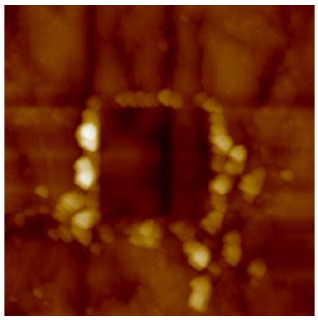

After 40 Wear Scans

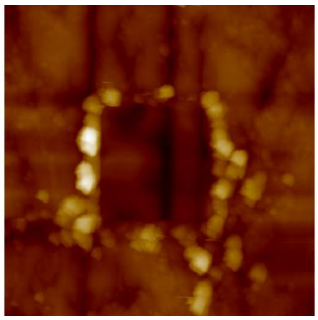

After 45 Wear Scans

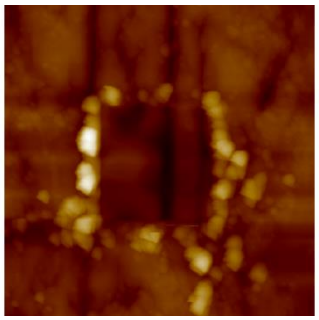

After 50 Wear Scans

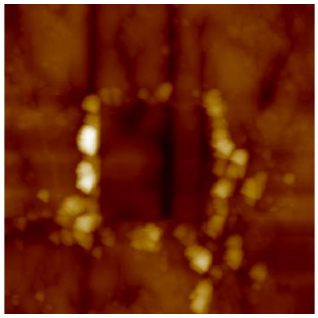

After 55 Wear Scans

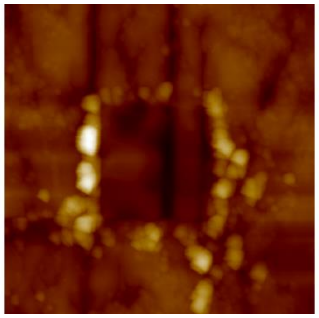

After 60 Wear Scans

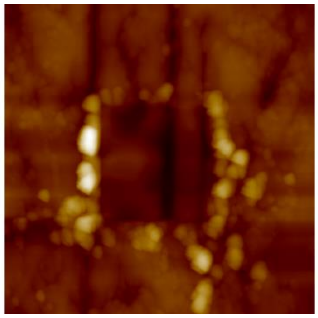

After 70 Wear Scans

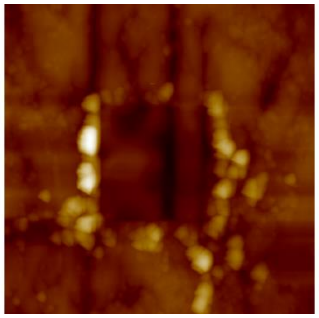

After 80 Wear Scans

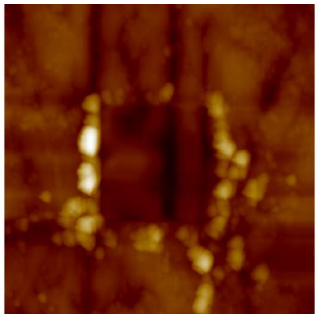

After 90 Wear Scans

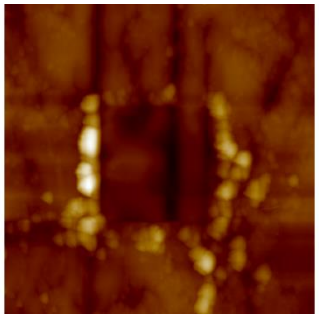

After 100 Wear Scans

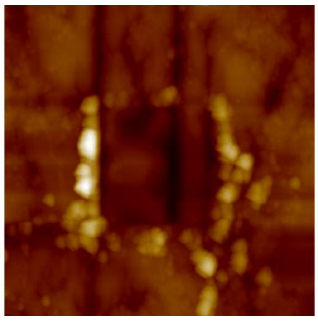

After 110 Wear Scans

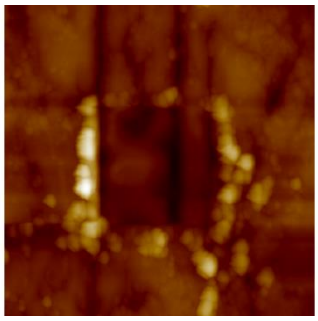

After 120 Wear Scans

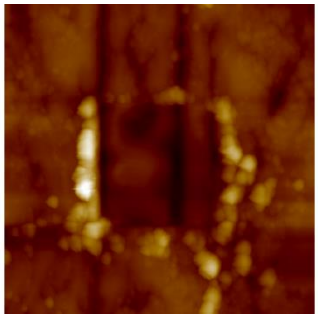

After 130 Wear Scans

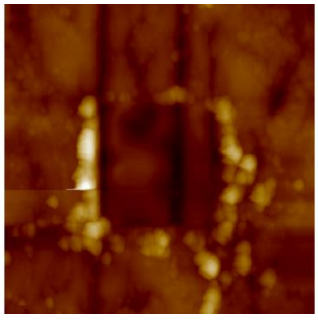

After 140 Wear Scans

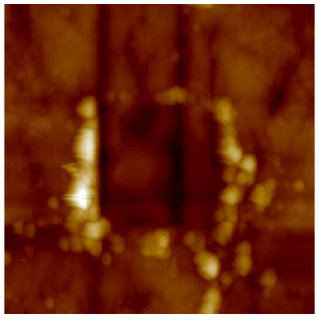

After 150 Wear Scans

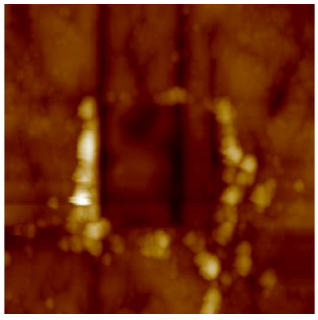

After 160 Wear Scans

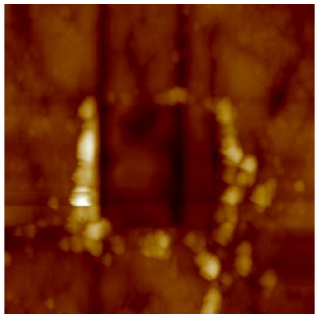

After 170 Wear Scans

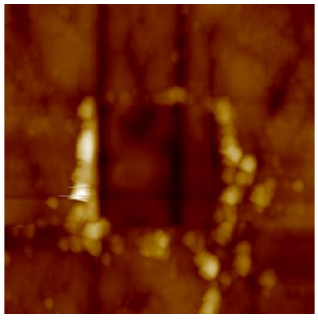

After 180 Wear Scans

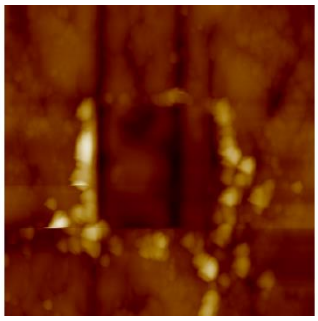

After 190 Wear Scans

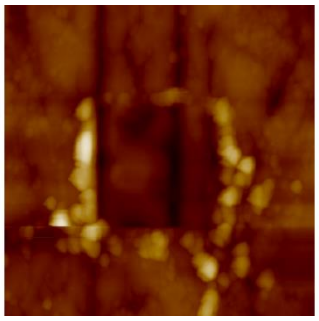

After 200 Wear Scans

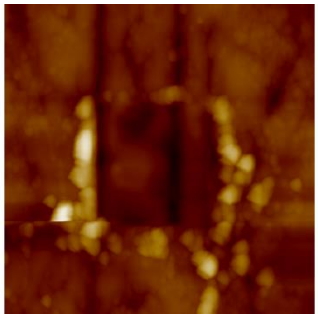

After 210 Wear Scans

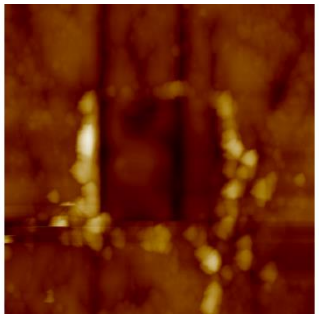

After 220 Wear Scans

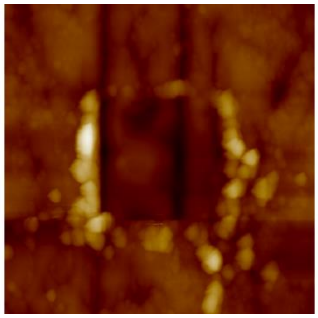

After 230 Wear Scans

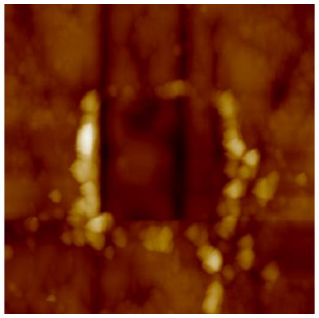

After 240 Wear Scans

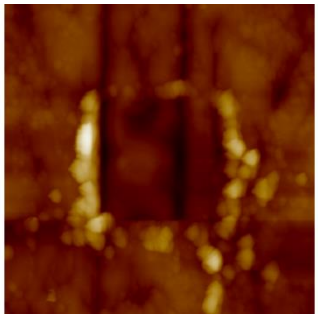

After 250 Wear Scans

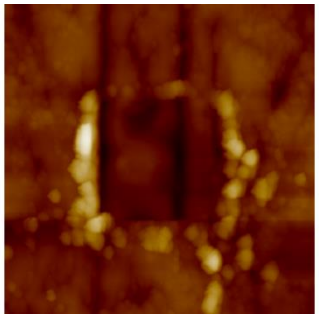

Appendix 4 – Durability Study Contact Scans

0.275wt% ZDDP Tribofilm – 0.005mN load – On a pad

Wear Scan 5

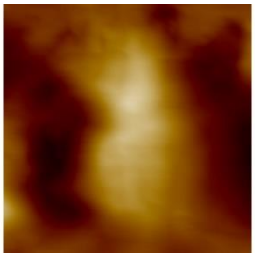

Wear Scan 10

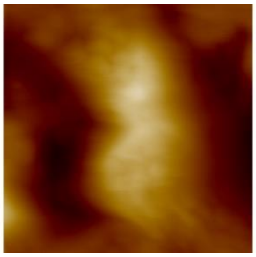

Wear Scan 15

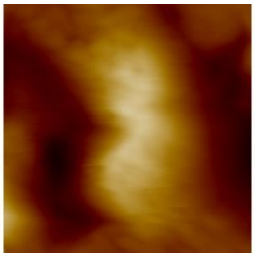

Wear Scan 20

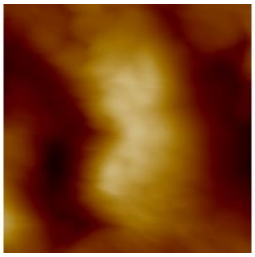

Wear Scan 25

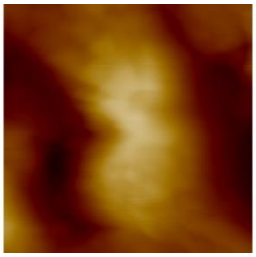

Wear Scan 30

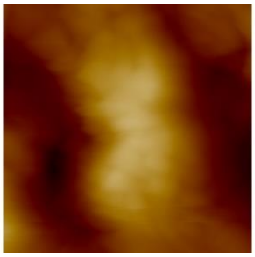

Wear Scan 35

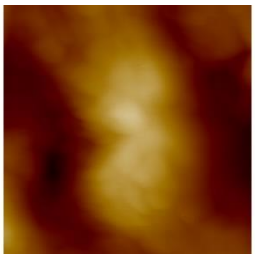

Wear Scan 40

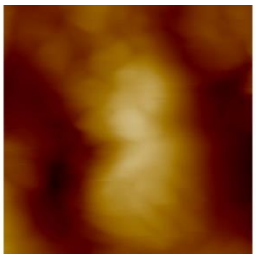

Wear Scan 45

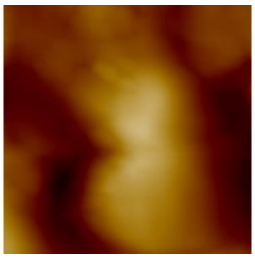

Wear Scan 50

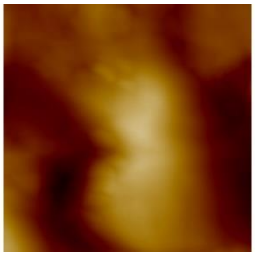

Wear Scan 55

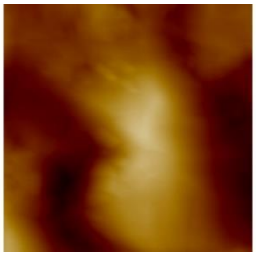

Wear Scan 60

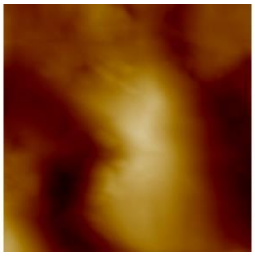

Wear Scan 65

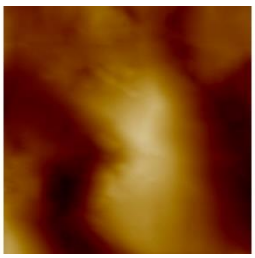

Wear Scan 70

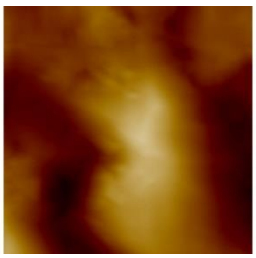

Wear Scan 75

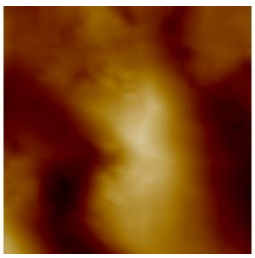

Wear Scan 80

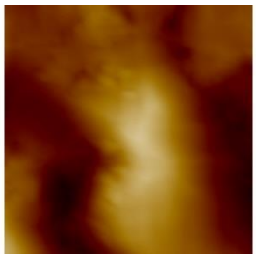

Wear Scan 85

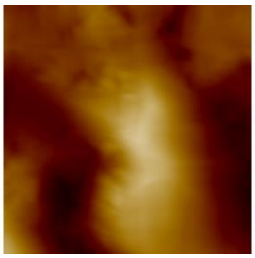

Wear Scan 90

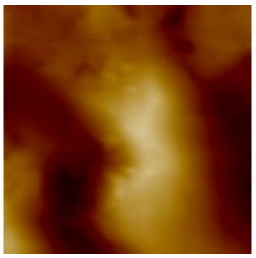

Wear Scan 95

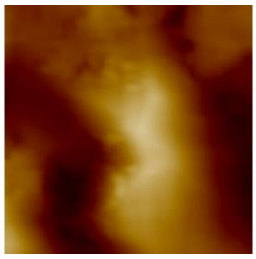

Wear Scan 100

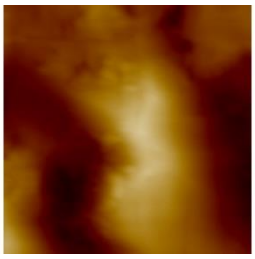

Wear Scan 105

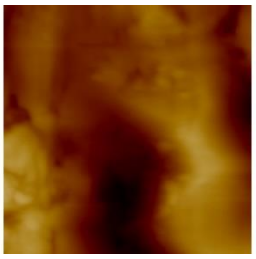

Wear Scan 110

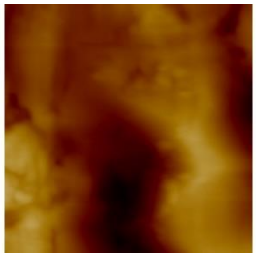

Wear Scan 115

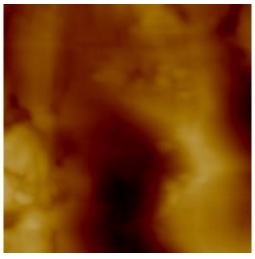

Wear Scan 120

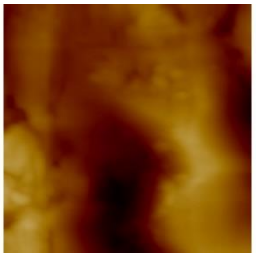

Wear Scan 125

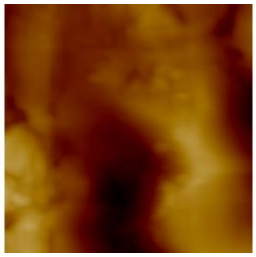

0.275wt% ZDDP Tribofilm – 0.005mN load – Between pads

Wear Scan 5

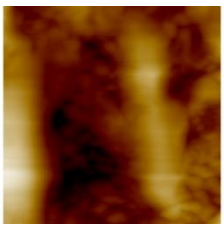

Wear Scan 10

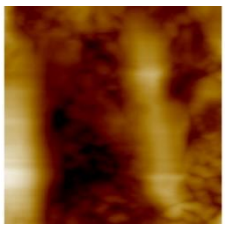

Wear Scan 15

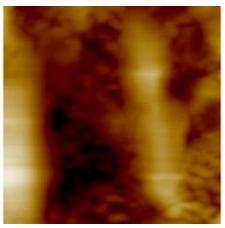

Wear Scan 20

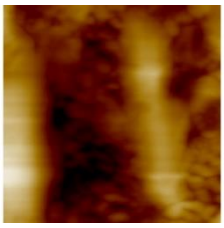

Wear Scan 25

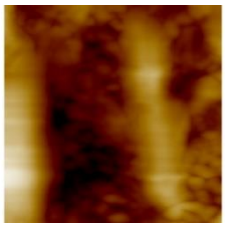

Wear Scan 30

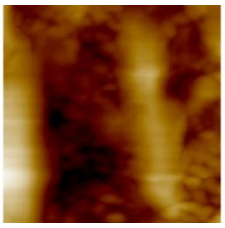

Wear Scan 35

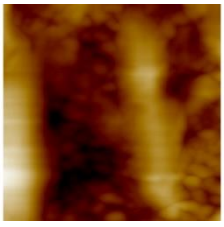

Wear Scan 40

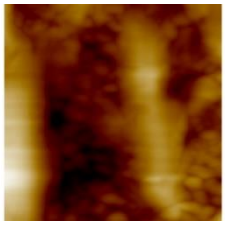

Wear Scan 45

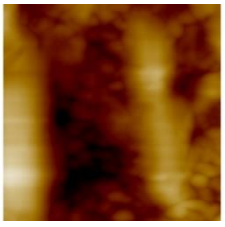

Wear Scan 50

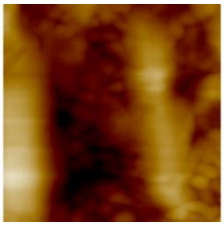

Wear Scan 55

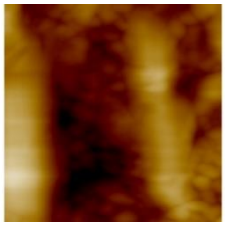

Wear Scan 65

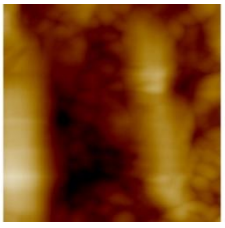

Wear Scan 75

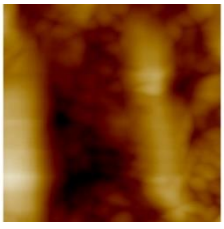

Wear Scan 85

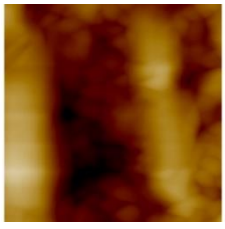

Wear Scan 95

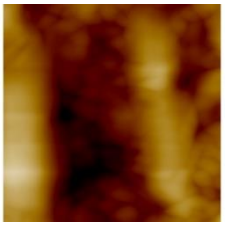

Wear Scan 105

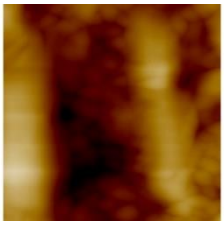

Wear Scan 115

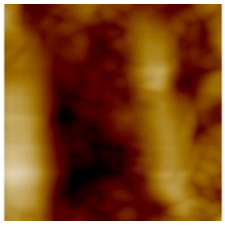

Wear Scan 126

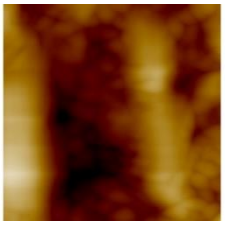

Wear Scan 135

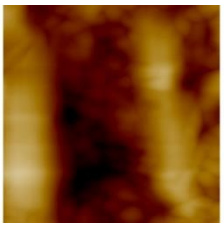

Wear Scan 145

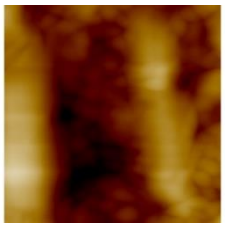

Wear Scan 155

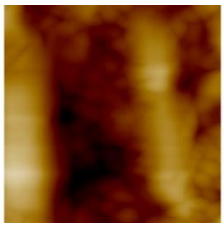

Wear Scan 165

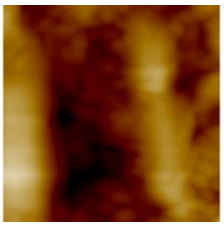

Wear Scan 175

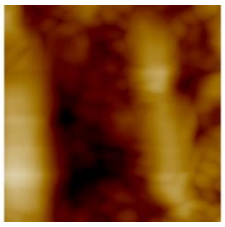

Wear Scan 185

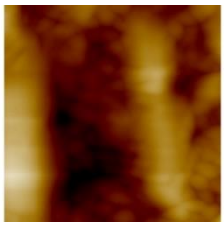

Wear Scan 195

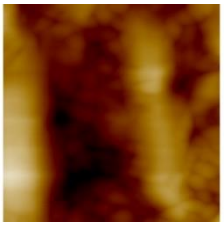

Wear Scan 205

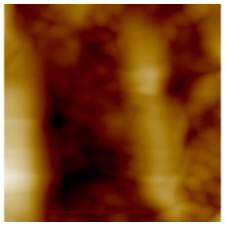

Wear Scan 215

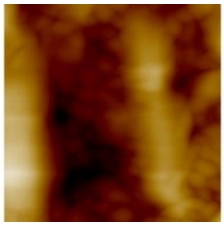

Wear Scan 225

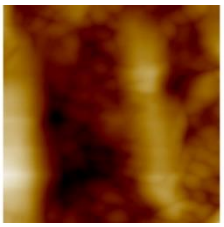

Wear Scan 235

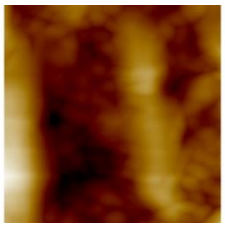

Wear Scan 245

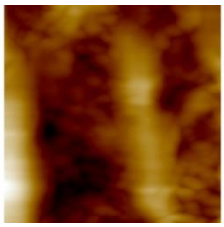

Wear Scan 255

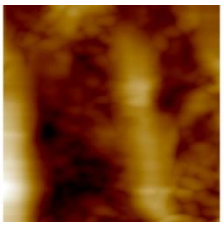

0.275wt% ZDDP Tribofilm – 0.005mN load – On edge of pads

Wear Scan 5

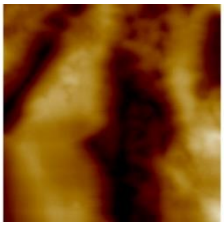

Wear Scan 10

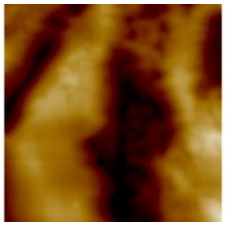

Wear Scan 15

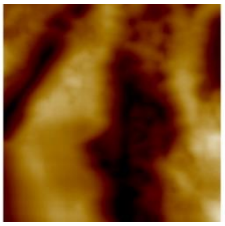

Wear Scan 20

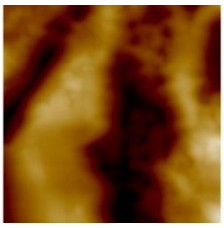

Wear Scan 25

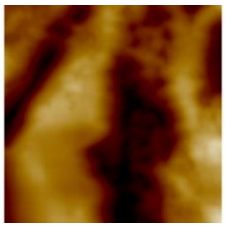

Wear Scan 30

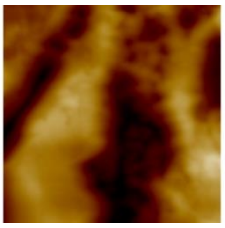

Wear Scan 35

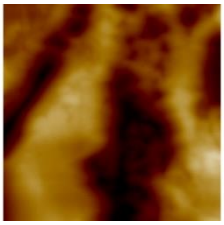

Wear Scan 40

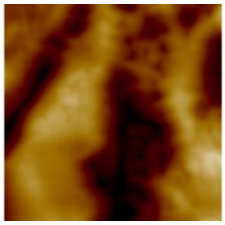

Wear Scan 45

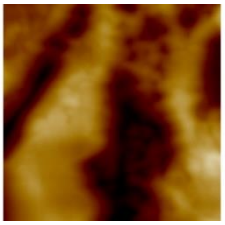

Wear Scan 50

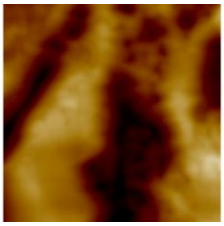

Wear Scan 55

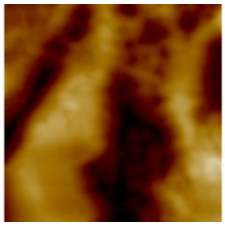

Wear Scan 60

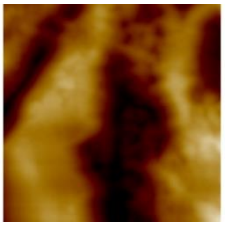

Wear Scan 70

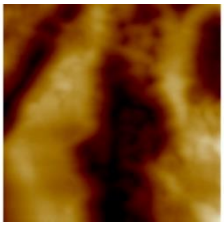

Wear Scan 80

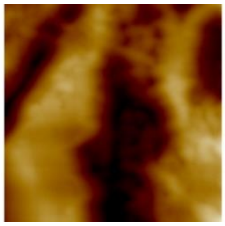

Wear Scan 92

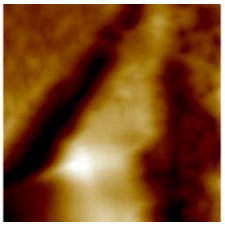

Wear Scan 100

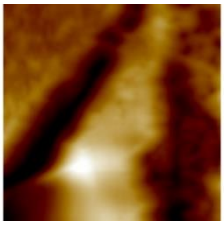

Wear Scan 110

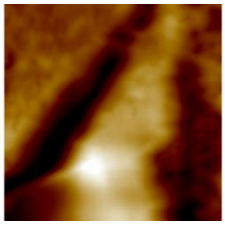

Wear Scan 120

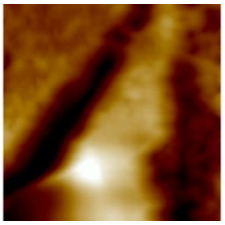

Wear Scan 130

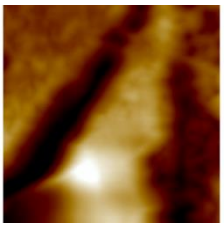

Wear Scan 140

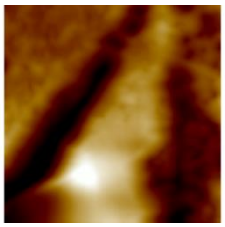

Wear Scan 150

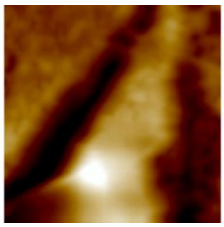

Wear Scan 160

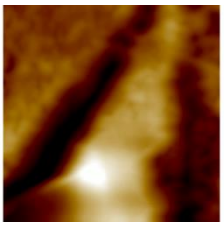

Wear Scan 170

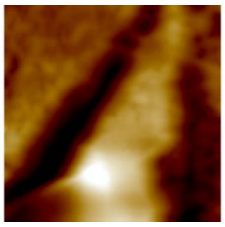

Wear Scan 180

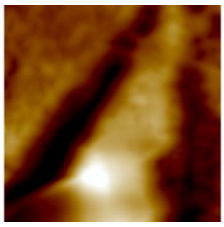

Wear Scan 190

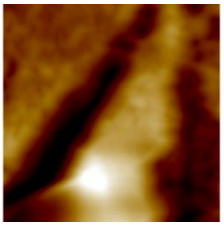

Wear Scan 200

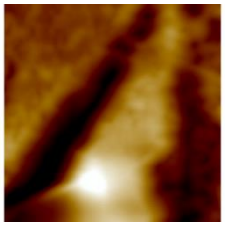

Wear Scan 210

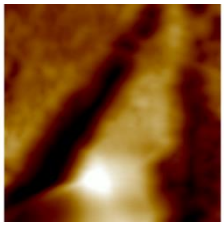

Wear Scan 220

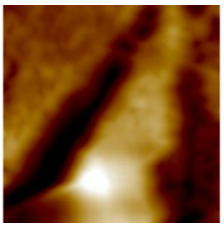

Wear Scan 230

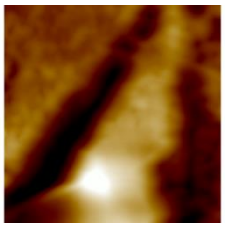

Wear Scan 240

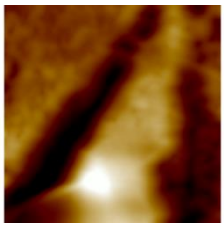

Wear Scan 250

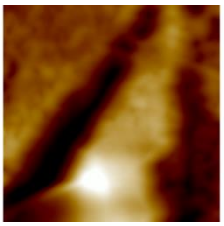

0.55wt% ZDDP Tribofilm – 0.005mN load – On a pad

Wear Scan 5

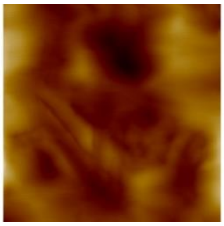

Wear Scan 10

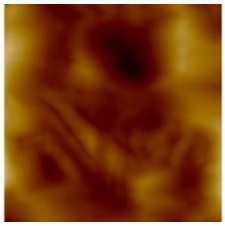

Wear Scan 15

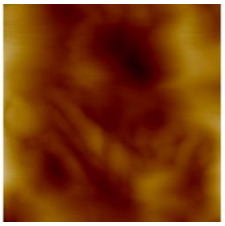

Wear Scan 20

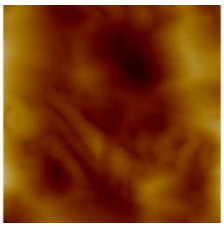

Wear Scan 25

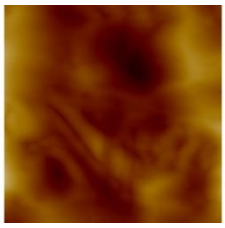

Wear Scan 30

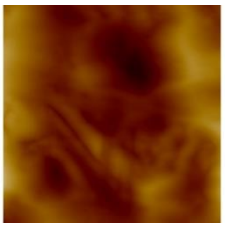

Wear Scan 35

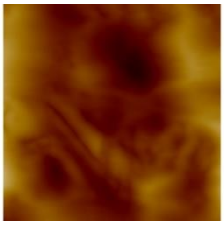

Wear Scan 40

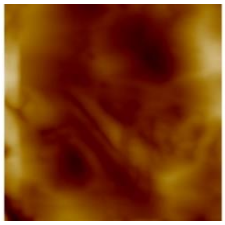

Wear Scan 45

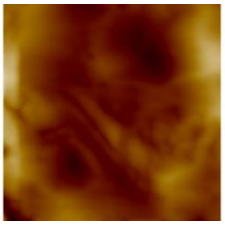

Wear Scan 50

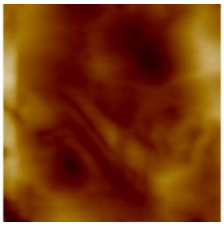

Wear Scan 56

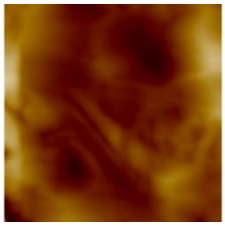

Wear Scan 60

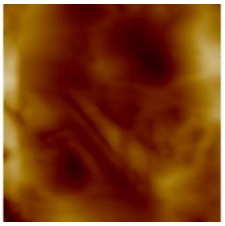

Wear Scan 70

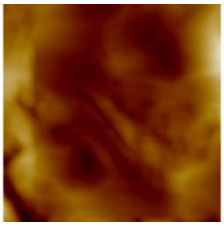

Wear Scan 80

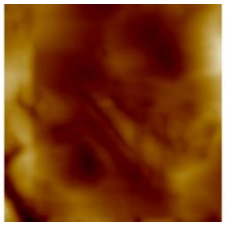

Wear Scan 90

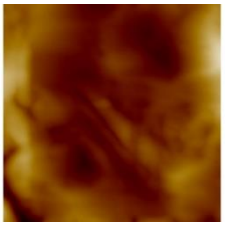

Wear Scan 100

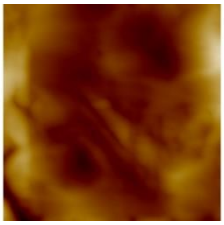

Wear Scan 110

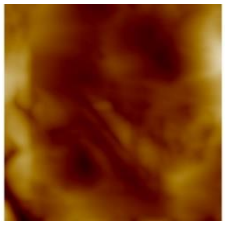

Wear Scan 120

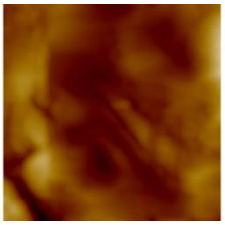

Wear Scan 130

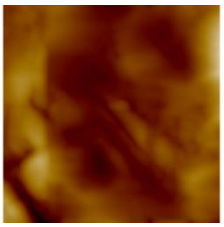

Wear Scan 140

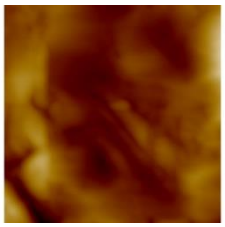

Wear Scan 150

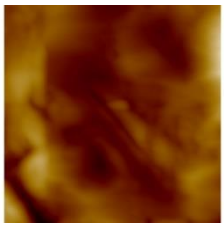

Wear Scan 160

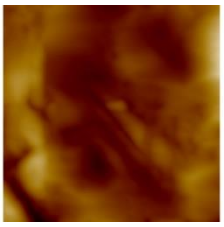

Wear Scan 170

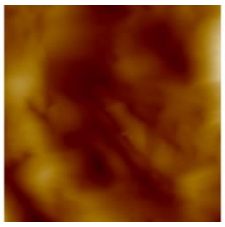

Wear Scan 180

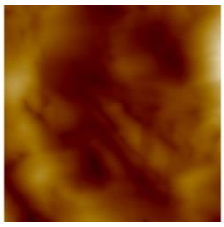

Wear Scan 190

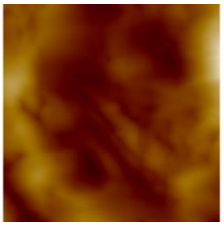

Wear Scan 200

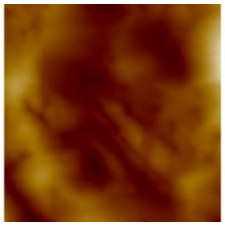

Wear Scan 210

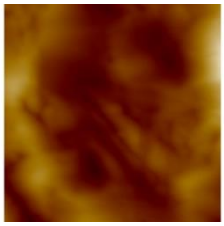

Wear Scan 220

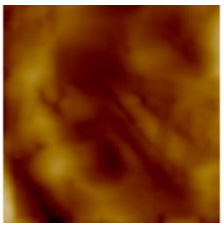

Wear Scan 230

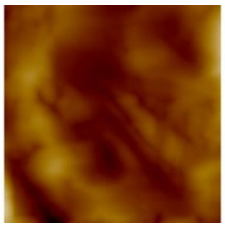

Wear Scan 240

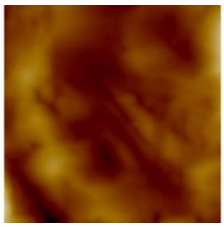

Wear Scan 250

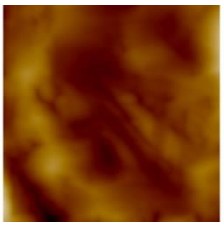

0.55wt% ZDDP Tribofilm – 0.005mN load – On edge of pads

Wear Scan 5

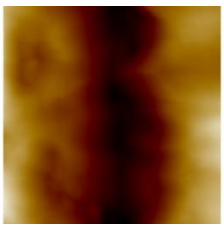

Wear Scan 10

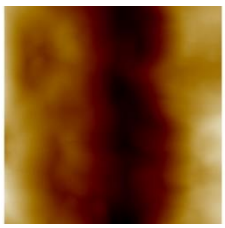

Wear Scan 15

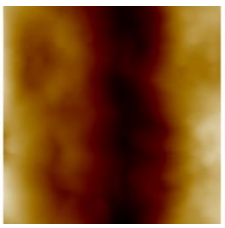

Wear Scan 20

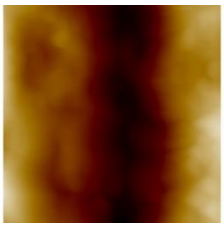

Wear Scan 25

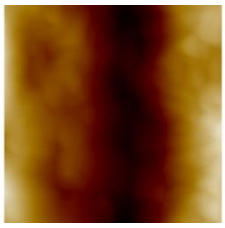

Wear Scan 30

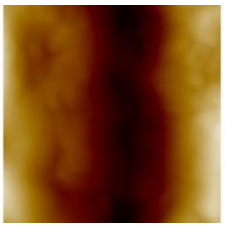

Wear Scan 35

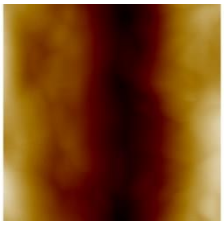

Wear Scan 40

Wear Scan 45

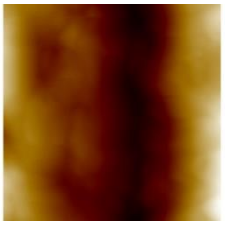

Wear Scan 50

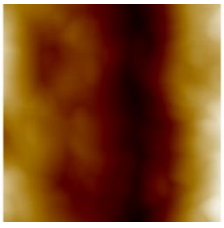

Wear Scan 55

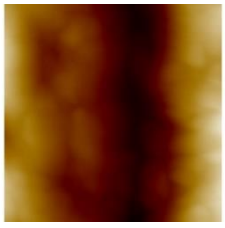

Wear Scan 60

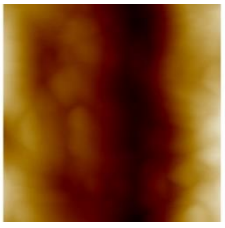

Wear Scan 70

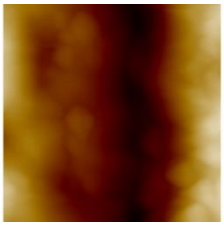

Wear Scan 80

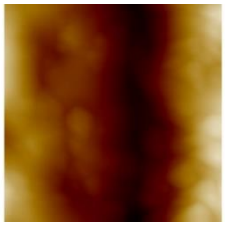

Wear Scan 90

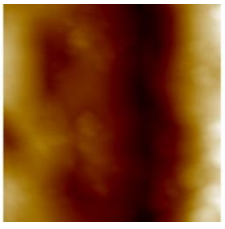

Wear Scan 100

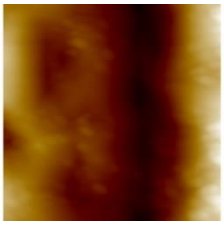

Wear Scan 110

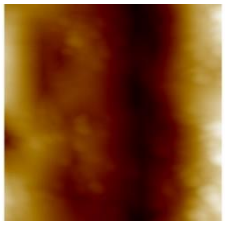

Wear Scan 120

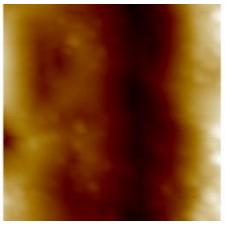

Wear Scan 130

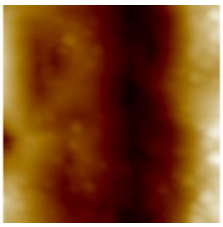

Wear Scan 140

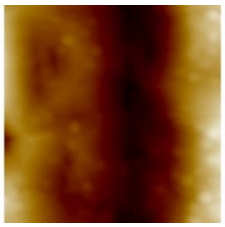

Wear Scan 150

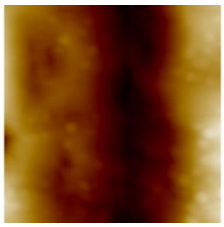

Wear Scan 160

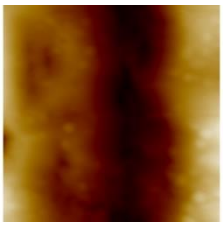

Wear Scan 170

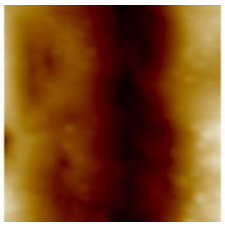

Wear Scan 180

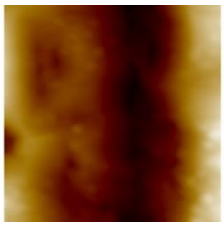

Wear Scan 190

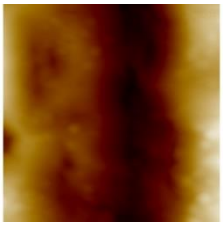

Wear Scan 200

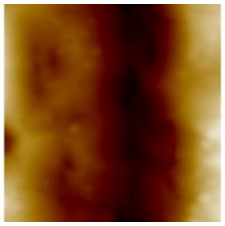

Wear Scan 210

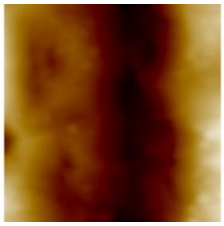

Wear Scan 220

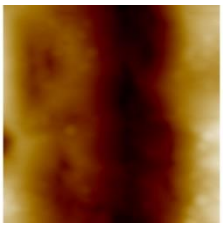

Wear Scan 230

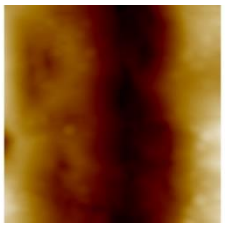

Wear Scan 240

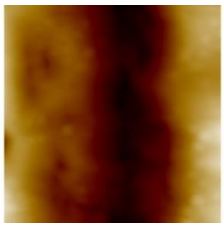

Wear Scan 250

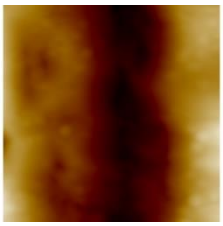

0.55wt% ZDDP Tribofilm – 0.005mN load – Between pads

Wear Scan 5

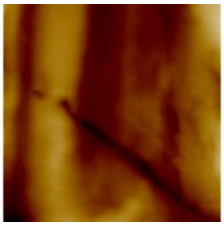

Wear Scan 10

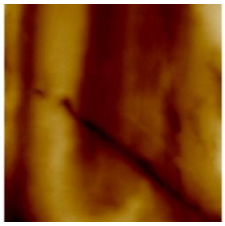

Wear Scan 15

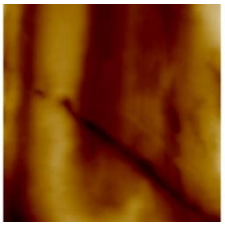

Wear Scan 20

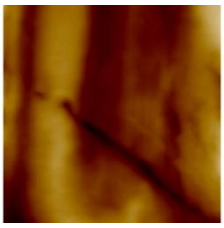

Wear Scan 25

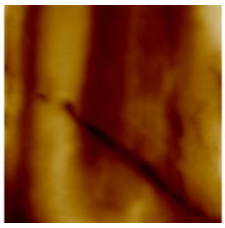

Wear Scan 30

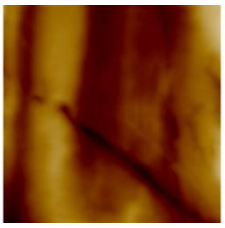

Wear Scan 35

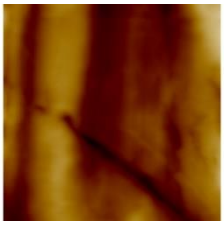

Wear Scan 40

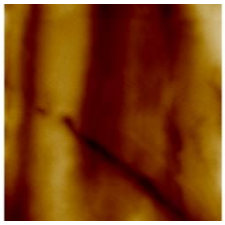

Wear Scan 45

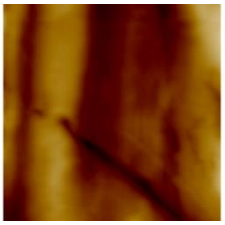

Wear Scan 50

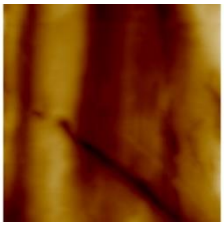

Wear Scan 55

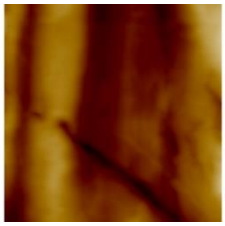

Wear Scan 60

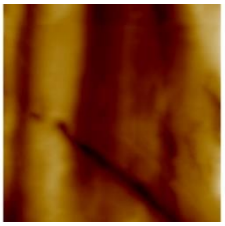

Wear Scan 70

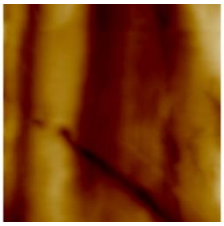

Wear Scan 80

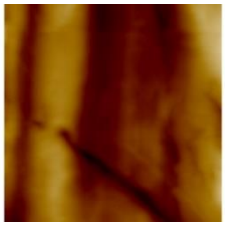

Wear Scan 90

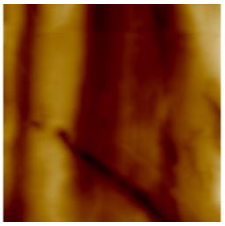

Wear Scan 100

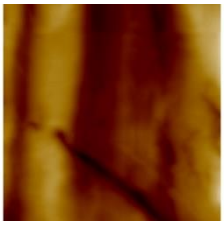

Wear Scan 110

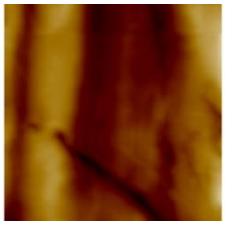

Wear Scan 120

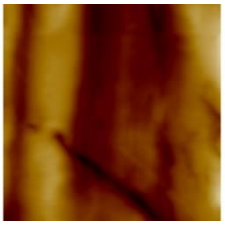

Wear Scan 130

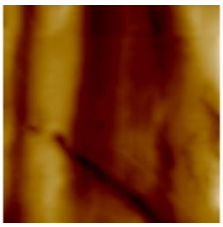

Wear Scan 140

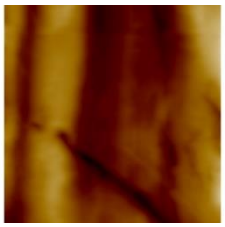

Wear Scan 150

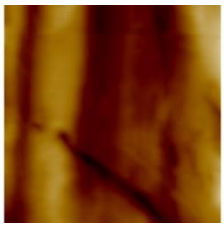

Wear Scan 160

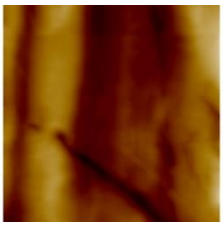

Wear Scan 171

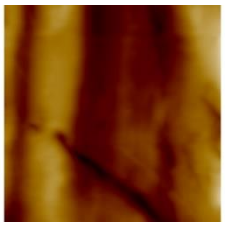

Wear Scan 180

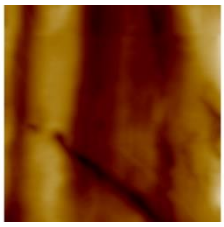

Wear Scan 190

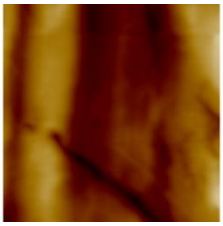

Wear Scan 200

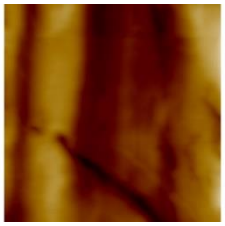

Wear Scan 210

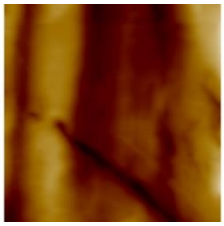

Wear Scan 220

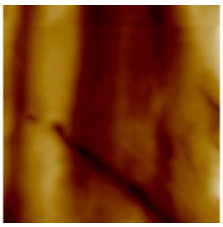

Wear Scan 230

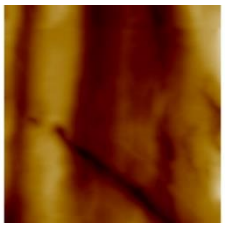

Wear Scan 240

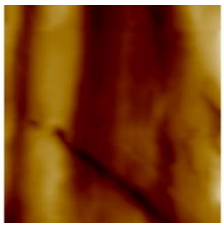

Wear Scan 250

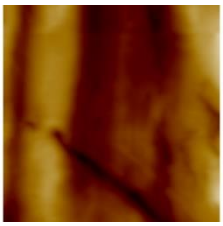

0.55wt% ZDDP Tribofilm – 0.010mN load – Across pads

Wear Scan 5

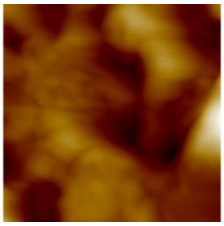

Wear Scan 10

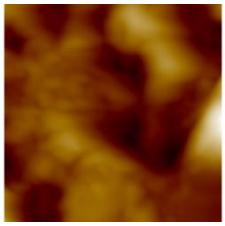

Wear Scan 15

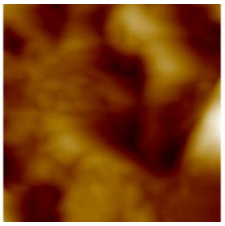

Wear Scan 20

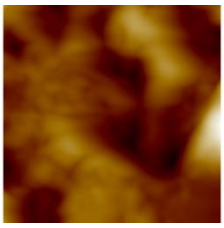

Wear Scan 25

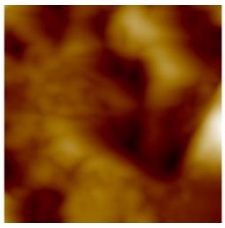

Wear Scan 30

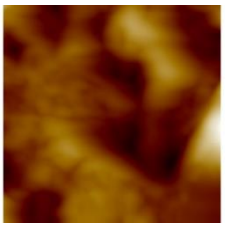

Wear Scan 35

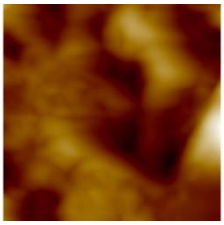

Wear Scan 40

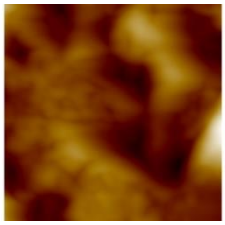

Wear Scan 45

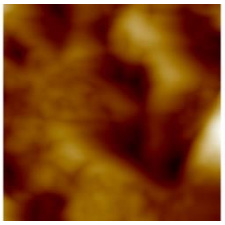

Wear Scan 50

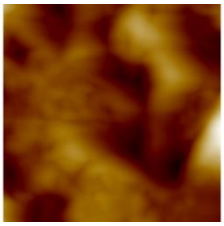

Wear Scan 55

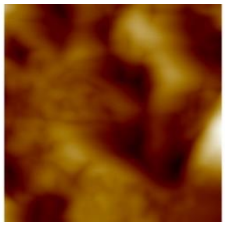

Wear Scan 60

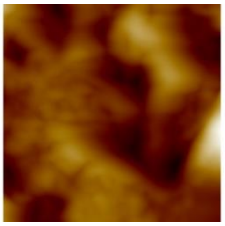

Wear Scan 70

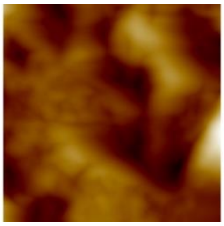

Wear Scan 80

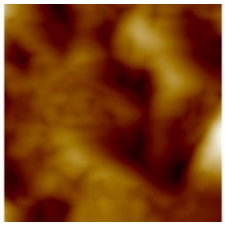

Wear Scan 90

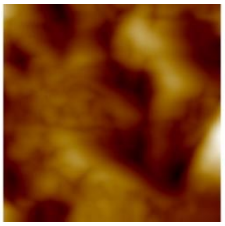

Wear Scan 100

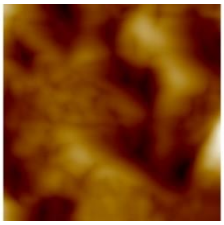

Wear Scan 110

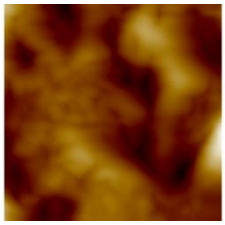

Wear Scan 120

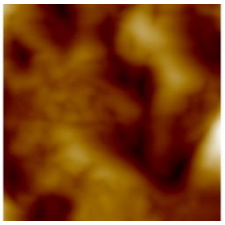

Wear Scan 130

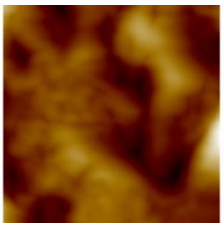

Wear Scan 140

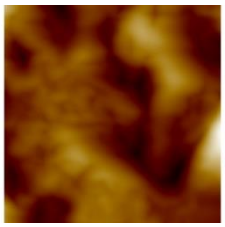

Wear Scan 150

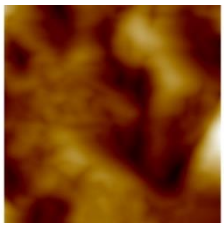

Wear Scan 160

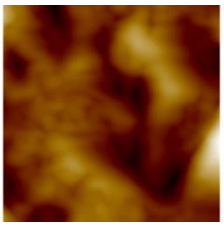

Wear Scan 170

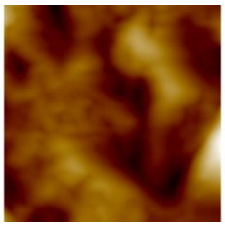

Wear Scan 180

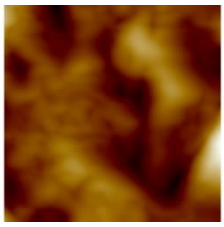

Wear Scan 190

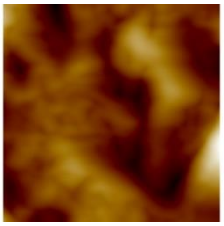

Wear Scan 200

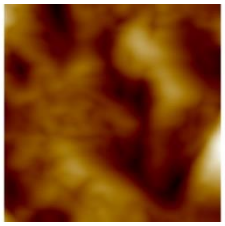

Wear Scan 210

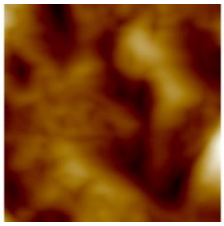

Wear Scan 220

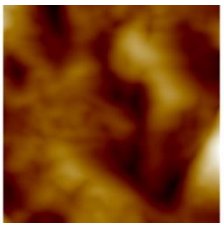

Wear Scan 230

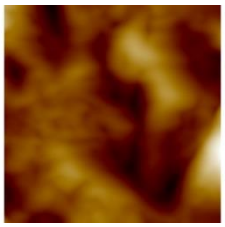

Wear Scan 240

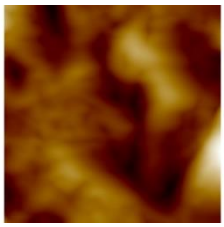

Wear Scan 250

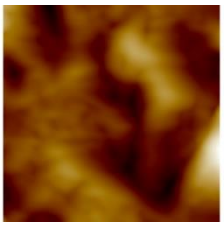

0.55wt% ZDDP Tribofilm – 0.010mN load – On a pad film

Wear Scan 5

Wear Scan 10

Wear Scan 15

Wear Scan 20

Wear Scan 25

Wear Scan 30

Wear Scan 35

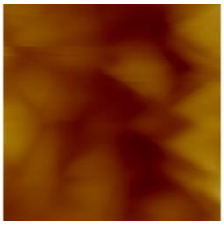

Wear Scan 40

Wear Scan 45

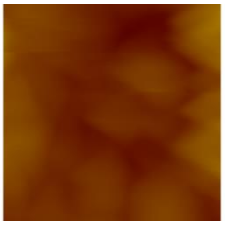

Wear Scan 50

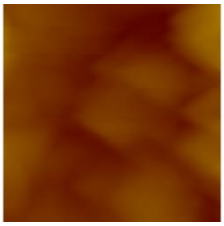

Wear Scan 55

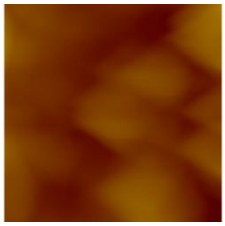

Wear Scan 60

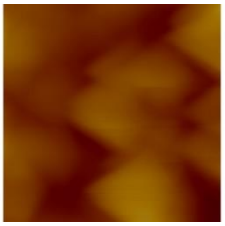

Wear Scan 70

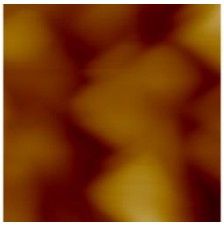

Wear Scan 80

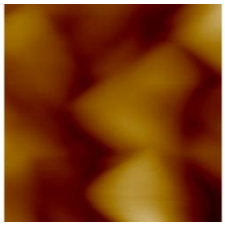

Wear Scan 90

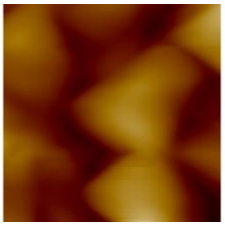

Wear Scan 100

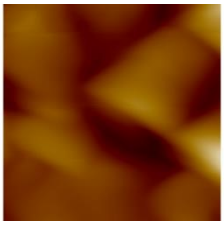

Wear Scan 110

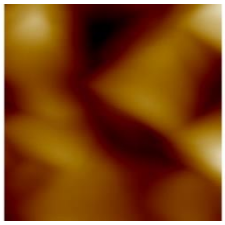

Wear Scan 120

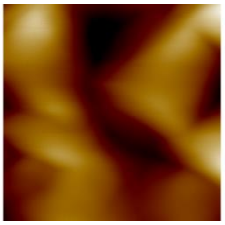

Wear Scan 130

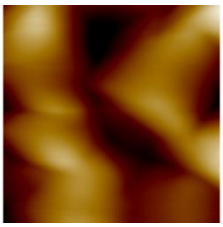

Wear Scan 140

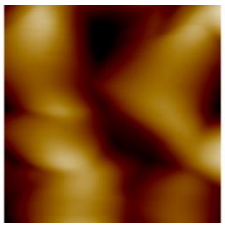

Wear Scan 150

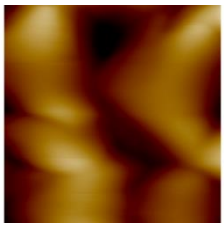

Wear Scan 160

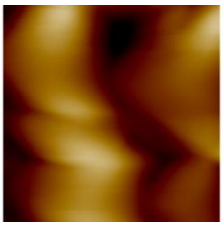

Wear Scan 170

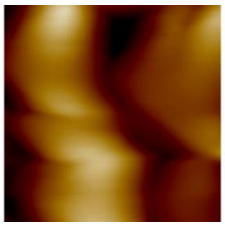

Wear Scan 180

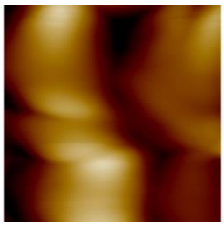

Wear Scan 190

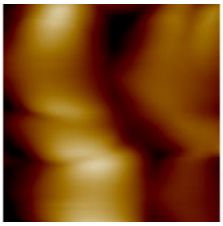

Wear Scan 200

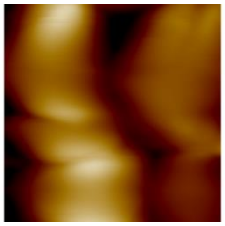

Wear Scan 210

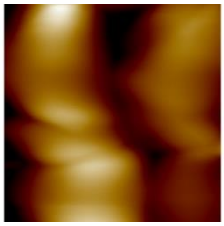

Wear Scan 220

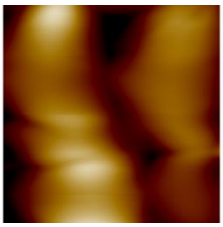

Wear Scan 230

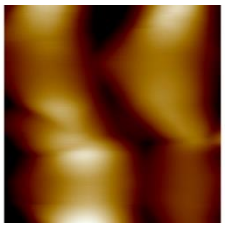

Wear Scan 240

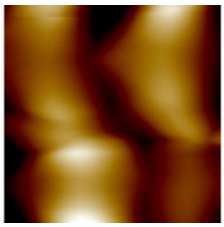

Wear Scan 250

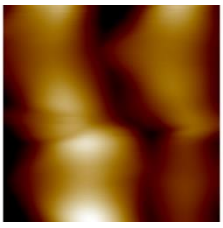

0.55wt% ZDDP Tribofilm – 0.014mN load – On a pad

Wear Scan 5

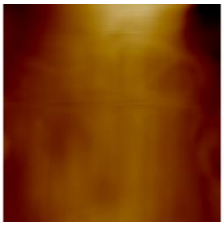

Wear Scan 10

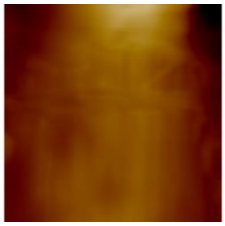

Wear Scan 15

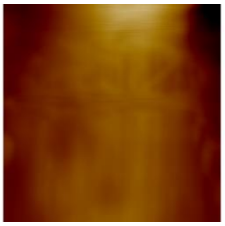

Wear Scan 20

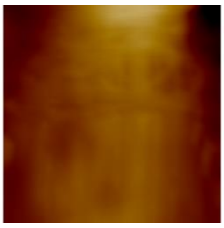

Wear Scan 25

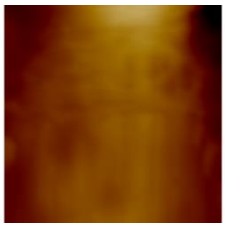

Wear Scan 30

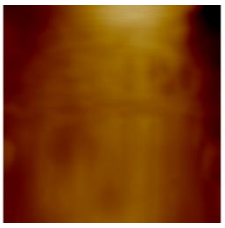

Wear Scan 35

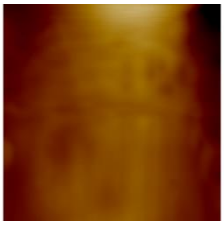

Wear Scan 40

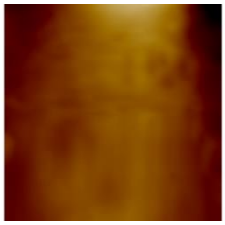

Wear Scan 45

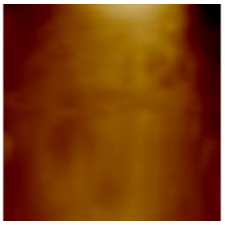

Wear Scan 50

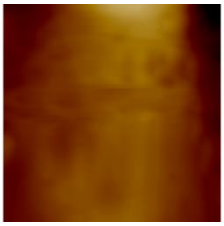

Wear Scan 55

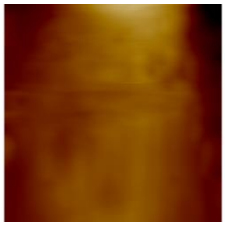

Wear Scan 60

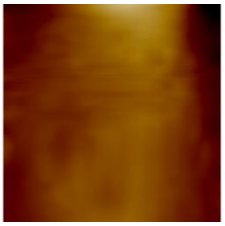

Wear Scan 70

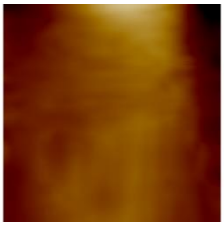

Wear Scan 80

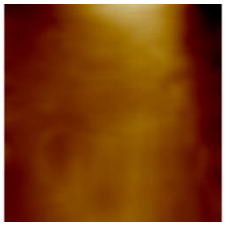

Wear Scan 90

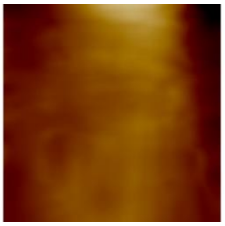

Wear Scan 100

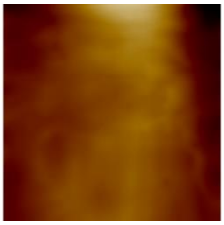

Wear Scan 110

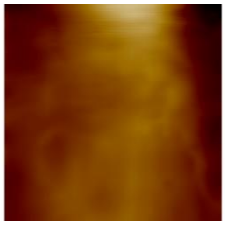

Wear Scan 120

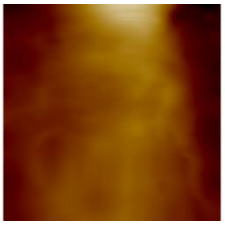

Wear Scan 130

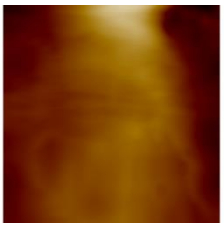

Wear Scan 140

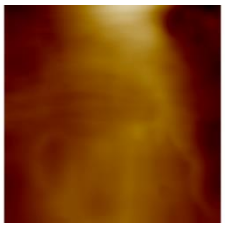

Wear Scan 150

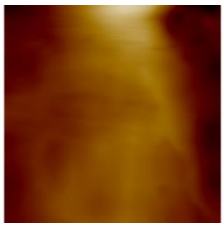

Wear Scan 160

Wear Scan 170

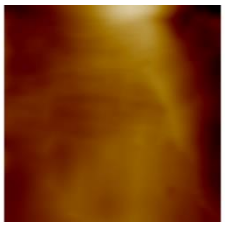

Wear Scan 180

Wear Scan 190

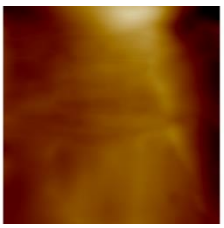

Wear Scan 200

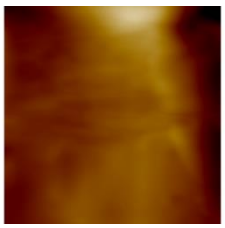

Wear Scan 210

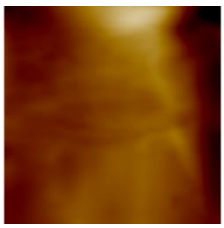

Wear Scan 220

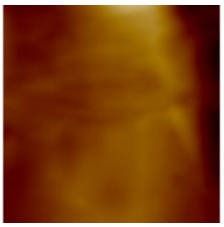

Wear Scan 230

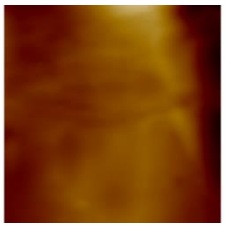

Wear Scan 240

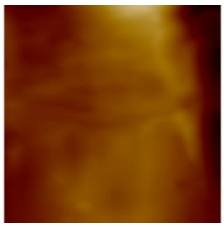

Wear Scan 250

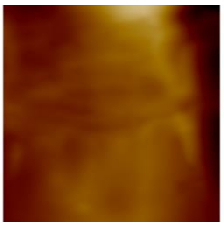

0.55wt% ZDDP Tribofilm – 0.014mN load – On a pad film

Wear Scan 5

Wear Scan 10

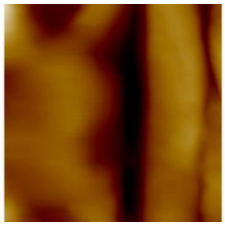

Wear Scan 15

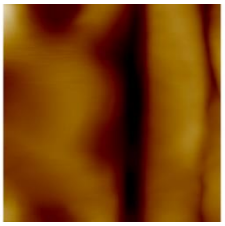

Wear Scan 20

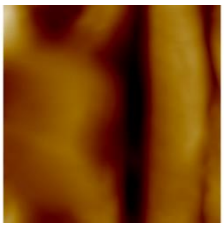

Wear Scan 25

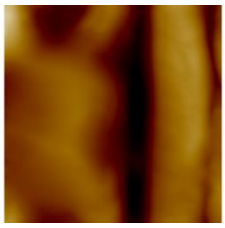

Wear Scan 30

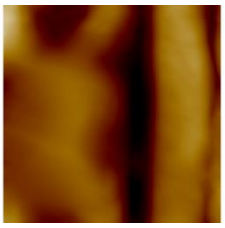

Wear Scan 35

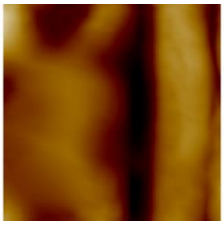

Wear Scan 40

Wear Scan 45

Wear Scan 50

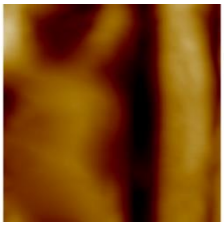

Wear Scan 55

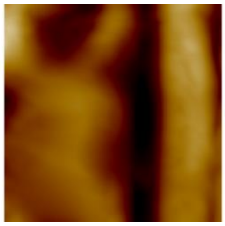

Wear Scan 60

Wear Scan 70

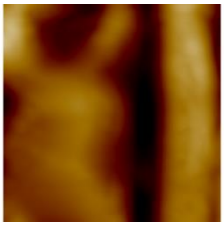

Wear Scan 80

Wear Scan 90

Wear Scan 100

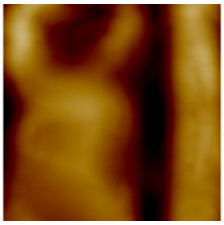

Wear Scan 110

Wear Scan 120

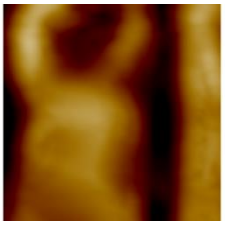

Wear Scan 130

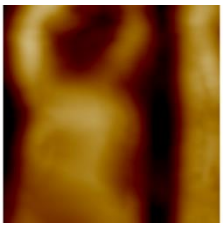

Wear Scan 140

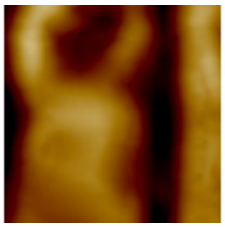

Wear Scan 150

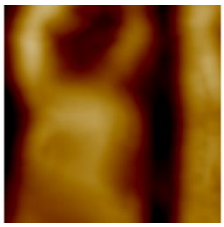

Wear Scan 160

Wear Scan 170

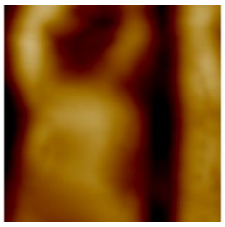

Wear Scan 180

Wear Scan 190

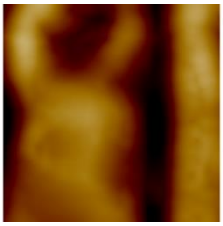

Wear Scan 200

Wear Scan 210

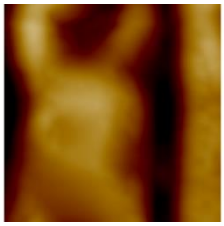

Wear Scan 220

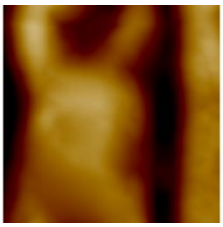

Wear Scan 230

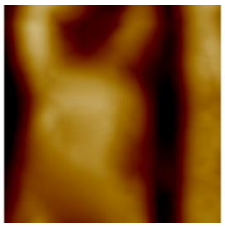

Wear Scan 240

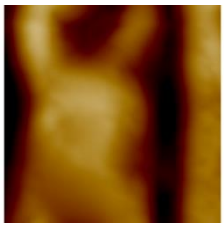

Wear Scan 250